Catalysis of Hydroelementation Reactions using *m*-Terphenyl Complexes

Amy South, MChem (Hons)

Thesis submitted to the University of Nottingham for the degree of Doctor of Philosophy

April 2020

Declaration

The work described in this thesis was carried out at the University of Nottingham between October 2016 and April 2020, under the supervision of Dr Deborah L. Kays. All of the work is my own unless stated to the contrary, and has not previously been submitted for any degrees at this or any other university.

Amy South

Abstract

Herein the synthesis and catalytic properties of low-coordinate *m*-terphenyl transition metal complexes are reported. Previous work in the group has shown that these complexes act as precatalysts for the cyclotrimerisation and hydrophosphination of isocyanates. This project builds on this work and aims to expand the scope of these precatalysts.

The diaryl complexes M(2,6-$Mes_2C_6H_3)_2$ (M = Fe, Co, Zn) are shown to catalyse the hydroamination of isocyanates forming urea derivatives. The use of aromatic isocyanates results in a formal diinsertion of the isocyanate into the N–H bond affording biuret derivatives. These products can be selectively formed by tuning the reaction conditions; performing the reaction in THF solvent results in the exclusive formation of the urea and the use of an excess of the isocyanate results in the exclusive formation of the biuret. The use of diisopropylamine resulted in the tri- and tetrainsertion of the isocyanate into the N–H bond. The hydrophosphination of carbodiimides to form phosphaguanidines, was also investigated. This transformation required higher temperatures compared to the catalysis with isocyanates and the diinsertion of the carbodiimide is only observed with very low conversions. Stoichiometric reactions and catalyst poisoning tests were carried out in order to investigate the mechanism of the catalysis.

The complexes M(2,6-$Mes_2C_6H_3)_2$ are precatalysts for the hydroboration of isocyanates and carbodiimides. The monohydroboration product was shown to be the major product for all the substrates although small amounts of the dihydroboration product were observed with the aromatic isocyanates. The use of ^{t}BuNCO resulted in the hydrodeoxygenation of the isocyanate forming ^{t}BuN(BPin)CH_3 and $O(BPin)_2$.

A series of transition metal complexes containing an *m*-terphenyl ligand and the bidentate ligand TMEDA, with the form M(2,6-$Mes_2C_6H_3$)X(tmeda) (M = Mn, X = Br ; M = Fe, X = Cl; M = Co, X = Br; M = Zn, X = Cl) were synthesised. The DPPE and DME analogues for

M = Fe were also isolated. These complexes were characterised by X-ray crystallography, NMR spectroscopy and the magnetic moments were measured using Evans method.

The reduction of Mn(2,6-$Mes_2C_6H_3$)Br(tmeda) with KC_8 was attempted but resulted in the formation of the dimer [(tmeda)MnBr(μ-Br)]$_2$. Attempts to abstract the halide ligand with halide abstracting agents were unsuccessful. A salt metathesis reaction was carried out between and Na[N($SiMe_3$)$_2$] which afforded Zn(2,6-$Mes_2C_6H_3$)[N($SiMe_3$)$_2$] and Zn[N($SiMe_3$)$_2$]$_2$.

Acknowledgements

First and foremost, I would like to thank Dr Debbie Kays for giving me the opportunity to do this project in her group and for all her support and guidance throughout my PhD. Particular thanks must also go to Dr Ana Geer for her invaluable advice throughout the past four years (even when moving to a different continent). Your incredible knowledge and support have been crucial to this thesis.

Thanks goes to Dr William Lewis and Dr Stephen Argent for their assistance with crystallography, Mr Shazad Aslam and Mr Kevin Butler for their help with NMR measurements, Dr Huw Williams for his help with DOSY experiments, Dr Stephen Davies for his help with UV-vis spectroscopy and Dr Mick Cooper, Mr Ben Pointer-Gleadhill and NMSF Swansea for MS measurements.

Thanks must also go to all members of the Kays group past and present for all the support they have given me and for making this time so enjoyable. In particular to Toby for his help with the ligand synthesis at the beginning of my PhD and to Helen for passing on all her terphenyl and catalysis wisdom. I am also grateful to Rob for all the support and advice he has given me and to Charlotte for immediately making me feel welcome and to both of them for their friendship during my PhD. My thanks also goes to my project students Aaron Insley and Jake Williams for their hard work and dedication.

Finally, I would like to thank my family for their unwavering support throughout the last four years.

Table of Contents

List of Abbreviations 12

Chapter 1: Introduction

1.1 Low-Coordinate Transition Metal Complexes 14

1.2 *m*-Terphenyl Complexes 16

1.3 Low-Coordinate Transition Metal Catalysts 18

1.4 Hydroelementation Reactions 25

1.5 Catalysis with *m*-Terphenyl Complexes 27

1.6 Aims 31

1.7 References 32

Chapter 2: Hydroamination and Hydrophosphination of Heterocumulenes

2.1 Introduction 39

2.2 Aims 42

2.3 Results and Discussion 42

2.3.1 Synthesis of *m*-Terphenyl Complexes 42

2.3.2 Hydroamination of Isocyanates 43

2.3.2.1 Hydroamination of Isocyanates with Diphenylamine 43

2.3.2.2 Recycling the Catalyst 48

2.3.2.3 Reaction Monitoring 49

2.3.2.4 Hydroamination of Isocyanates in THF 50

2.3.2.5 Hydroamination of Isocyanates with Different Amines 51

2.3.2.6 Hydroamination of Isocyanates in the Presence of Additives 55

2.3.2.7 Stoichiometric Studies 57

2.3.2.8 Isolation of Ureas and Biurets 60

2.3.2.9 Scale-Up Reactions 61

2.3.2.10 Hydroamination of Isocyanates Catalysed by **4** and **5** 62

2.3.3 Hydroamination of Other Substrates 63

2.3.4 Hydrophosphination of Carbodiimides 64

2.3.4.1 Iron Catalysed Hydrophosphination of Carbodiimides 65

2.3.4.2 Poisoning Experiments 69
2.3.4.3 Scale-Up Reactions 70
2.3.4.4 Stoichiometric Studies 70
2.3.4.5 Cobalt Catalysed Hydrophosphination of Carbodiimides 72
2.4 Conclusions 72
2.5 Experimental Procedures 73
2.5.1 Synthesis of Precatalysts 74
2.5.2 Catalytic Hydroamination of Isocyanates 74
2.5.2.1 Standard Procedure for the Catalytic Hydroamination of Isocyanates 74
2.5.2.2 Standard Procedure for *in situ* NMR Reaction Monitoring for the Catalytic Hydroamination of Isocyanates 74
2.5.2.3 Catalytic Hydroamination of Isocyanates in THF 74
2.5.2.4 Scaled-up Catalytic Hydroamination of Isocyanates 75
2.5.2.5 Stoichiometric NMR Spectroscopy 75
2.5.2.6 Stoichiometric IR Spectroscopy 75
2.5.2.7 Stoichiometric UV-Vis Spectroscopy 76
2.5.2.8 Catalytic Hydroamination of Isocyanates in the Presence of NEt_3·HCl 76
2.5.2.9 Catalytic Hydroamination of Isocyanates in the Presence of Hg(0) 76
2.5.2.10 Catalytic Hydroamination of Isocyanates in the Presence of CS_2 76
2.5.2.11 Catalytic Hydroamination of Isocyanates in the Presence of $PPhMe_2$ 77
2.5.2.12 Catalytic Hydroamination of Isocyanates in the Presence of Cumene 77
2.5.2.13 Synthesis and Characterisation of Ureas 77
2.5.2.14 Procedure for *in situ* Formation of **7g**, **8g** and **9g** 85
2.5.3 Catalytic Hydrophosphination of Carbodiimides 86
1.5.3.1 Standard Procedure for the Catalytic Hydrophosphination of Carbodiimides 86
2.5.3.2 Catalytic Hydrophosphination of Carbodiimides in the Presence of NEt_3·HCl 86
2.5.3.3 Catalytic Hydrophosphination of Carbodiimides in the Presence of Hg(0) ... 86
2.5.3.4 Catalytic Hydrophosphination of Carbodiimides in the Presence of CS_2 87

2.5.3.5 Catalytic Hydrophosphination of Carbodiimides in the Presence of 1,4-Cyclohexadiene 87
2.5.3.6 Scaled-up Catalytic Hydrophosphination of Carbodiimides 87
2.5.3.7 Stoichiometric NMR 87
2.5.4 Synthesis of *N*,*N*′-Diphenylcarbodiimide **11** 88
2.5.5 Characterisation of Phosphaguanidines 88
2.5.5.1 $Ph_2PC(=NCy)NH(Cy)$ **12a** 88
2.5.5.2 $Ph_2PC(=N^iPr)NH(^iPr)$ **12b** 89
2.5.5.3 $Ph_2PC(=NPh)NH(Ph)$ **12c** 89
2.5.5.4 $Ph_2PC(=NEt)NH(^tBu)$ **12d** 90
2.6 References 90
Chapter 3: Hydroboration of Heterocumulenes
3.1 Introduction 97
3.1.1 Catalytic Hydroboration 97
3.1.2 Hydroboration of Heterocumulenes 99
3.2 Aims 101
3.3 Results and Discussion 102
3.3.1 Iron Catalysed Hydroboration of Isocyanates 102
3.3.1.1 Initial Investigations 102
3.3.1.2 Aromatic Isocyanates 109
3.3.1.3 Aliphatic Isocyanates 111
3.3.1.4 Stoichiometric Studies 119
3.3.1.5 Posioning experiments 121
3.3.1.6 Scale-Up Reactions 122
3.3.2 Cobalt and Zinc Catalysed Hydroboration of Isocyanates 122
3.3.3 Catalytic Hydroboration of Carbodiimides 125
3.4 Conclusions 127
3.5 Experimental Procedures 128
3.5.1 Catalytic Hydroboration of Isocyanates 128

3.5.1.1 Iron Catalysed Hydroboration of PhNCO 128
3.5.1.2 Standard Procedure for Iron Catalysed Hydroboration of Isocyanates 129
3.5.1.3 Standard Procedure for Cobalt Catalysed Hydroboration of Isocyanates ... 129
3.5.1.4 Standard Procedure for Zinc Catalysed Hydroboration of Isocyanates 129
3.5.1.5 Hydroboration of Isocyanates with 1 mol% catalyst loading 129
3.5.1.6 Scaled-Up Catalytic Hydroboration of Isocyanates 130
3.5.1.7 Stoichiometric NMR Studies 130
3.5.1.8 Catalytic Hydroboration of Isocyanates in the Presence of Hg(0) 130
3.5.1.9 Catalytic Hydroboration of Isocyanates in the Presence of CS_2 130
3.5.1.10 Catalytic Hydroboration of Isocyanates in the Presence of 1,4-Cyclohexadiene 131
3.5.2 Catalytic Hydroboration of Carbodiimides 131
3.5.3 Characterisation of Hydroboration Products 131
3.5.3.1 PhN(BPin)C(=O)H **15a** 131
3.5.3.2 3,5-$(OMe)_2C_6H_3$N(BPin)C(=O)H **15b** 132
3.5.3.3 4-BrC_6H_4N(BPin)C(=O)H **15c** 132
3.5.3.4 *p*-TolN(BPin)C(=O)H **15d** 133
3.5.3.5 ^{n}PrN(BPin)C(=O)H **15e** 133
3.5.3.6 ^{n}HexN(BPin)C(=O)H **15f** 134
3.5.3.7 HC(=O)N(BPin)$(CH_2)_6$N(BPin)C(=O)H **15g** 134
3.5.3.8 ^{i}PrN(BPin)C(=O)H **15h** 135
3.5.3.9 CyN(BPin)C(=O)H **15i** 135
3.5.3.10 ^{t}BuN(BPin)C(=O)H **15j** 135
3.5.3.11 ^{t}BuN(BPin)CH_3 **20** 136
3.5.3.12 $O(BPin)_2$ **21** 136
3.5.3.13 CyN=CHN(BPin)Cy **22** 136
3.6 References 137
Chapter 4: Synthesis and Reactivity of *m*-Terphenyl Complexes Containing Bidentate Ligands

4.1 Introduction 141
4.2 Aims 148
4.3 Results and Discussion 149
4.3.1 Diphosphines 149
4.3.2 TMEDA 152
4.3.3 DME 157
4.3.4 Magnetic Measurements 163
4.3.5 Reactivity of TMEDA complexes 164
4.3.5.1 Reduction and Halide Abstraction 164
4.3.5.2 Metathesis Reactions 165
4.4 Conclusions 168
4.5 Experimental Procedures 170
4.5.1 $[ZnCl_2(dppe)]_n$ **23** 170
4.5.2 Fe(2,6-$Mes_2C_6H_3$)Cl(dppe) **25** 170
4.5.3 Mn(2,6-$Mes_2C_6H_3$)Br(tmeda) **26a** 170
4.5.4 Fe(2,6-$Mes_2C_6H_3$)Cl(tmeda) **26b** 171
4.5.5 Co(2,6-$Mes_2C_6H_3$)Br(tmeda) **26c** 171
4.5.6 Zn(2,6-$Mes_2C_6H_3$)Cl(tmeda) **26d** 172
4.5.7 $ZnCl_2$(tmeda) **28** 172
4.5.8 Fe(2,6-$Mes_2C_6H_3$)Cl(dme) **29b** 173
4.5.9 Zn(2,6-$Mes_2C_6H_3$)Cl(dme) **29d** 173
4.5.10 Synthesis of **30** 174
4.5.11 Reduction with KC_8 174
4.5.12 Metathesis Reaction 174
4.5.13 Evans Method 175
4.6 References 175

Chapter 5: Global Conclusions

5.1 Global Conclusions 182
5.2 References 184

Chapter 6: General Experimental

6.1 General Experimental Procedures 186

6.1.1 Manipulation of Air Sensitive Compounds 186

6.1.2 Preparation of Solvents and Reagents 186

6.2 Physical Measurements 186

6.2.1 NMR Spectroscopy 186

6.2.2 DOSY 187

6.2.3 Mass Spectrometry 187

6.2.4 Infrared Spectroscopy 187

6.2.5 UV-Vis Spectroscopy 188

6.2.6 X-Ray Crystallography 188

6.3 References 188

Appendices

Crystallographic Data 191

List of Abbreviations

Ad	1-Adamantyl
APCI	Atmospheric-pressure chemical ionization
Ar	Aryl
BAr^F_4	Tetrakis[3,5-bis(trifluoromethyl)phenyl]borate
9-BBN	9-Borabicyclo[3.3.1]nonane
br	broad (NMR)
^{n}Bu	*normal*-Butyl
^{t}Bu	*tert*-Butyl
Cat	Catecholato
Cp*	Pentamethylcyclopentadienyl
Cy	Cyclohexyl
d	doublet (NMR)
DPBZ	1,2-Bis(diphenylphosphino)benzene
DCC	*N*,*N*'-Dicyclohexylcarbodiimide
DIC	*N*,*N*'-Diisopropylcarbodiimide
Dipp	2,6-Diisopropylphenyl
DME	1,2-Dimethoxyethane
DMBZ	1,2-Bis(dimethylphosphino)benzene
DMPE	1,2-Bis(dimethylphosphino)ethane
DOSY	Diffusion ordered spectroscopy
DPPE	1,2-Bis(diphenylphosphino)ethane
DPPM	1,1-Bis(diphenylphosphino)methane
DPPP	1,3-Bis(diphenylphosphino)propane
DTBPE	1,2-bis(di-tert-butylphosphino)ethane)
ESI	Electrospray ionisation
Et	Ethyl
h	hour
^{n}Hx	*normal*-Hexyl
i	*ipso*
IR	Infrared
m	multiplet
Me	Methyl
Mes	Mesityl, 2,4,6-trimethylphenyl
Mes*	2,4,6-tri-*tert*-butylphenyl
MS	Mass spectrometry
Naph	Naphthyl
NMR	Nuclear magnetic resonance
m	*meta*
o	*ortho*
p	*para*
Ph	Phenyl
Pin	Pinacolato
^{n}Pr	*n*-Propyl
^{i}Pr	*iso*-Propyl
IPr	1,3-bis(2,6-Dipp)imidazol-2-ylidene
R	Any alkyl or aromatic
s	singlet (NMR)
t	triplet (NMR)
THF	Tetrahydrofuran
TMEDA	Tetramethylethylenediamine
Tmp	2,4,5-trimethylphenyl
TMS	Tetramethylsilane
Tol	Tolyl
Trip	2,4,6-Triisopropylphenyl
UV-Vis	Ultraviolet-Visible
2,6-Xyl	2,6-Xylyl, 2,6-dimethylphenyl

Chapter 1

Introduction

1.1 Low-Coordinate Transition Metal Complexes

Low-coordinate transition metal complexes often display unusual structures such as metal-metal bonding.[1] They have electronically unsaturated metal centres and open valence orbitals and so have the potential for substitution or addition reactions at the metal centre with small molecules,[2,3] which leads to applications in the catalysis of organic transformations. Many low-coordinate complexes also have interesting magnetic properties and exhibit single molecule magnet characteristics.[4,5] These magnetic properties arise due to the linear geometry of many low-coordinate complexes. The ligands lie on the z-axis and so d orbitals of the metal in the xy plane do not interact with the ligands and magnetic moments from unpaired electrons in these orbitals are unquenched which results in high values of magnetic susceptibility. Despite these promising properties, low-coordinate transition metal complexes have not been well investigated due to challenges with their stabilisation and isolation.[1] Often the unsaturated metal complex will form aggregates or extended lattices with ligands acting as bridging ligands to increase the coordination number at the metal centre.[6] Low-coordinate complexes can be kinetically stabilised by sterically demanding ligands which impede the coordination of further ligands. The difficulty involved in the synthesis of these bulky ligands has prevented the study of low-coordinate complexes.[7] These complexes are also generally extremely air and moisture sensitive due to their available coordination sites and so must be handled in an inert atmosphere.

The first two-coordinate transition metal complex to be crystallographically characterised was not reported until 1985. This was the dialkyl Mn(II) complex $Mn(C(SiMe_3)_3)_2$ which contains two *σ* Mn–C bonds with a linear C–Mn–C bond angle (Figure 1). It was synthesised *via* a metathesis reaction between $LiC(SiMe_3)_3$ and $MnCl_2$.[8] The bulky tris(trimethylsilyl)methyl ligands interlock and prevent any further coordination to the metal centre, stabilising the low coordination number.

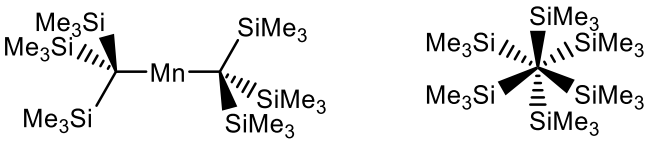


Figure 1. Molecular structure of $Mn(C(SiMe_3)_3)_2$ and side-on view showing interlocking ligands.[8]

Most early examples of metal complexes contained either M–O or M–N bonds and complexes containing M–C bonds were not observed.[9] This was previously thought to be due to the M–C bond being weaker than M–O or M–N bonds, so M–C bond containing complexes were inherently less stable and as a result more difficult to isolate.[10] However it was later shown that the M–C bonds in transition metal alkyl complexes are relatively strong, and the instability of these complexes results from the decomposition of the alkyl *via β*-hydride elimination. This is a decomposition route that is not commonly seen in main group alkyl complexes.[11] This means that alkyl groups that contain no *β*-hydrogens form more stable transition metal complexes.[12] This can also be achieved by using bulky ligands to protect the metal centre and prevent elimination as is seen in $Mn(C(SiMe_3)_3)_2$.[8]

In comparison with low-coordinate alkyl complexes, low-coordinate aryl complexes are much rarer due to the propensity for biphenyl formation and metal reduction.[9] This issue in the synthesis of aryl metal complexes is thought to be due to the abstraction of an *ortho*-H on the phenyl group.[11] This means that *ortho* substituted aryl groups can form more stable complexes. Use of less sterically demanding aryl ligands leads to oligomerisation of complexes.[13–15] An example of this is the trimeric complex $[Mn_3Mes_6]$, which consists of four bridging aryl groups bonded to two Mn atoms and two terminal aryl groups (Figure 2a).[15] The first two-coordinate metal complexes containing an aryl ligand were synthesised in 1995. This was the complex $MMes^*_2$ (M = Fe, Mn) (Figure 2b).[16,17] Both complexes contain a $C_{(ipso)}$–M–$C_{(ipso)}$ bond angle of *ca.* 160°. This distorted linear geometry is due to weak interactions between the metal centre and one of the C–H bonds of the *ortho* bound CH_3 groups.

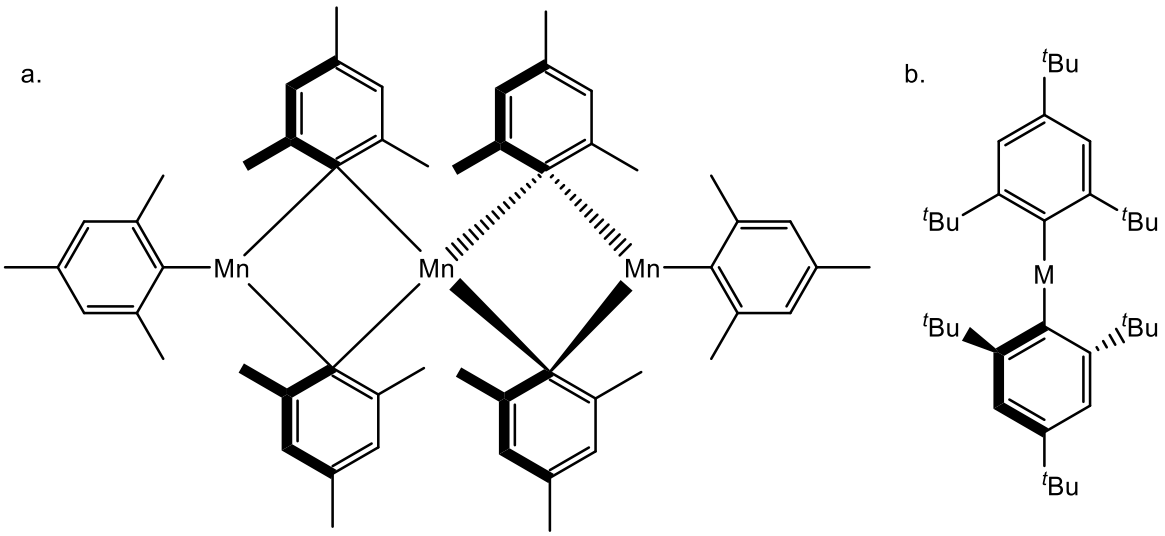


Figure 2. Molecular structure of a. $[Mn_3Mes_6]$[15] and b. $MMes^*_2$ (M = Fe, Mn).[16,17]

1.2 *m*-Terphenyl Complexes

Low-coordinate transition metal aryl complexes can be stabilised with a wide variety of bulky ligands.[7] One example of these is the *m*-terphenyl ligand which has the molecular formula 2,6-$Ar_2C_6H_3^-$ (Figure 3).[18] The two aryl flanking groups are in the *ortho*-position on the central aryl ring and the ligand forms a σ M–C bond with the metal centre. The properties of the *m*-terphenyl ligand can be tuned by the addition of different substituents to the ligand.[9] The substituents on the central aryl ring can be changed to vary the electronic and steric properties and the substituents on the flanking groups can change the steric effect of the ligand.[19]

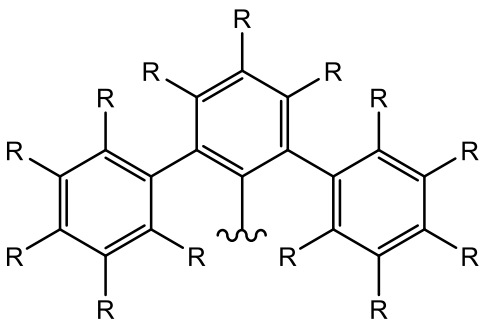


Figure 3. Molecular structure of an *m*-terphenyl ligand (R = alkyl or aromatic).

The first *m*-terphenyl open shell transition metal complex synthesised was [2,6-$Mes_2C_6H_3Co(\mu_2$-Br)THF]$_2$ (Figure 4a), which was reported by Power *et al*. in 1996.[20] Open shell complexes are generally less stable than their closed shell counterparts and so the synthesis is more challenging. This complex was synthesised by the reaction between the Grignard reagent [2,6-$Mes_2C_6H_3Mg(\mu_2$-Br)THF]$_2$ and $CoCl_2$ which resulted in the bromide bridged complex. In 2007 Kays *et al.* reported the synthesis of the homoleptic diaryl complex M(2,6-$Mes_2C_6H_3)_2$ (M = Mn, Fe, Co) *via* the salt metathesis reaction between a metal halide and the lithium salt [2,6-$Mes_2C_6H_3Li]_2$ in a mixture of toluene and THF (Figure 4b).[18]

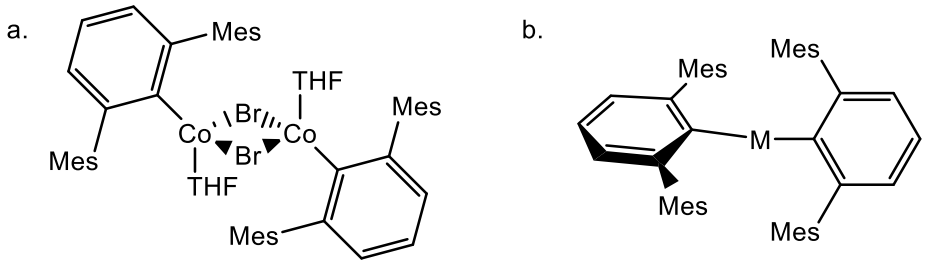


Figure 4. Molecular structure of a. [2,6-$Mes_2C_6H_3Co(\mu_2$-Br)THF]$_2$ and b. M(2,6-$Mes_2C_6H_3)_2$ (M = Mn, Fe, Co).[18,20]

The bulky *m*-terphenyl ligand can aid the isolation of complexes with interesting structures. In 2005 Power and co-workers reported the synthesis of (2,6-$Dipp_2C_6H_3$)Cr–Cr(2,6-$Dipp_2C_6H_3$) which contains an unprecedented Cr–Cr quintuple bond arising from the interaction between five orbitals on each metal centre, synthesised by the reduction of (2,6-$Dipp_2C_6H_3$)CrCl with KC_8 (Figure 5).[21] The quintuple bond is formed by the two Cr(I) metal centres and is made up of a σ, 2 π and 2 δ bonds, resulting in a very short bond length of 1.8351(4) Å.

The R groups on the *meta*-position on the central aryl ring can affect the steric bulk of the ligand; increasing the bulk of these R groups can force the flanking groups closer to the metal centre. This was shown by Power in 2007 with the synthesis of (2,6-$Trip_2$-3,5-$^i Pr_2$-C_6H)Cr(THF). The 2,6-$Trip_2$-3,5-$^i Pr_2$-C_6H^- ligand contains ^{i}Pr groups on the 3- and 5-positions of the central aryl ring. This steric bulk prevents the formation of a Cr–Cr bond

which is observed when using the less bulky ligand 2,6-$Dipp_2C_6H_3^-$ and instead the monomeric two-coordinate complex is formed when (2,6-$Trip_2$-3,5-$^iPr_2$-C_6H)CrCl is reduced with KC_8 in THF (Figure 6).[19,22]

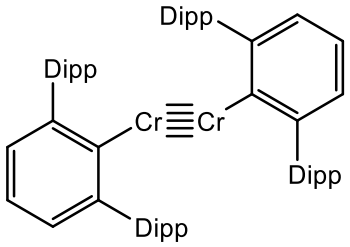


Figure 5. Molecular structure of (2,6-$Dipp_2C_6H_3$)Cr–Cr(2,6-$Dipp_2C_6H_3$) containing a Cr–Cr quintuple bond.[21]

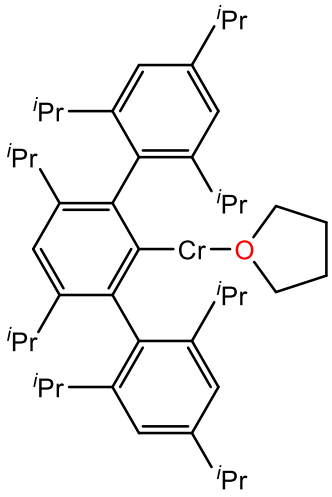


Figure 6. Molecular structure of (2,6-$Trip_2$-3,5-$^iPr_2$-C_6H)Cr(THF).[19,22]

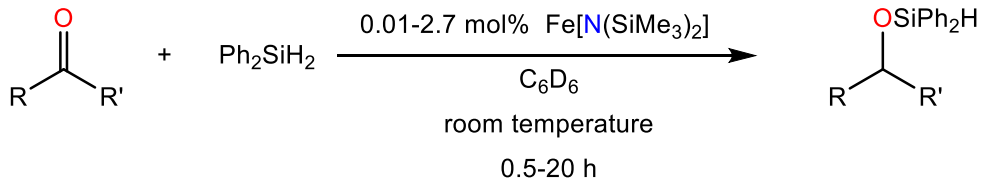
1.3 Low-Coordinate Transition Metal Catalysts

Low coordinate complexes can catalyse a wide range of different reactions due to their electron deficiency and unsaturated metal centre, which can lead to substitution or addition reactions. This area has not been extensively explored and the catalysts that have been reported have mostly only undergone preliminary studies and the reaction scope is

limited. There is a need for greater research in this area in order to understand the mechanistic processes behind these reactions and to improve the scope of the catalysts.

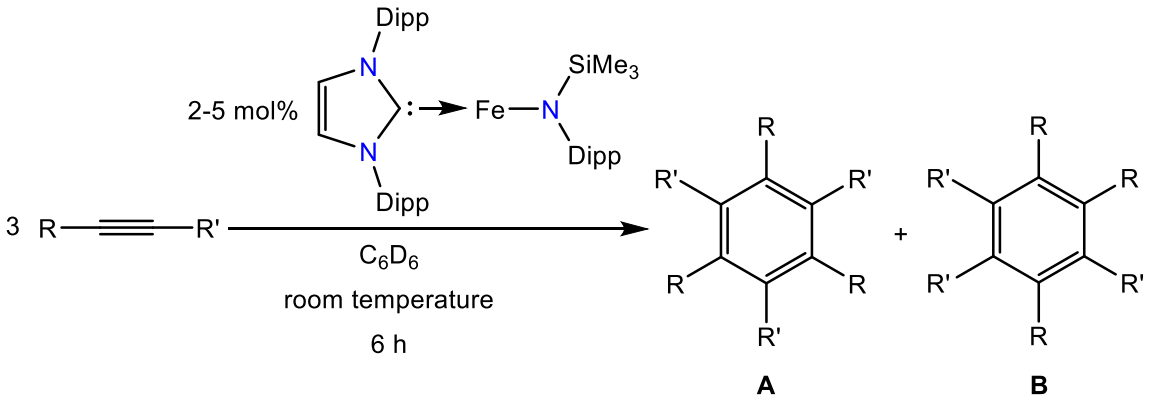
This thesis will focus on transition metal catalysts. These are used for many different reactions but they generally contain precious metals from the 'platinum group' (ruthenium, rhodium, palladium, osmium, iridium and platinum).[23,24] There is a growing shift towards the use of earth abundant metals with a particular focus on iron complexes which have been shown to catalyse a number of reactions that were previously only reported to be catalysed by precious metal catalysts.[25–28] There are a number of reasons for this interest in these metals of which the most evident is the availability and low cost of iron and other earth abundant metals compared to rare metals.[25] The platinum group metals are also typically toxic whereas iron complexes are usually non-toxic.[29] This is particularly important in pharmaceutical applications where separation of toxic metals is vital. The substitution with a non-toxic metal can mean efficient separation of the catalyst is no longer required and production is much cheaper.[24] Low-coordinate complexes containing the earth abundant first row transition metals in particular, have the potential to act as efficient inexpensive catalysts. However, there are very few examples of these complexes used as catalysts in the literature. This section aims to illustrate these examples.

Iron is the most common metal utilised in low coordinate transition metal catalysts due to its ability to adopt a range of different oxidation states and facilitate electron transfers.[27] The simple two-coordinate Fe(II) complex $Fe[N(SiMe_3)_2]$, reported by Tilley *et al*. in 2010 was shown to catalyse the hydrosilylation of aldehydes and ketones (Scheme 1).[30] Catalyst loadings as low as 0.01 mol% were able to reach 98% conversions after 17 h. This catalyst is one of the most active iron catalysts for the hydrosilylation of carbonyl compounds and shows high tolerance towards functional groups such as amines, halides and nitriles. The catalyst was also shown to proceed under solvent-free conditions with the hydrosilylation of acetophenone reaching 98% conversion after 0.5 h.



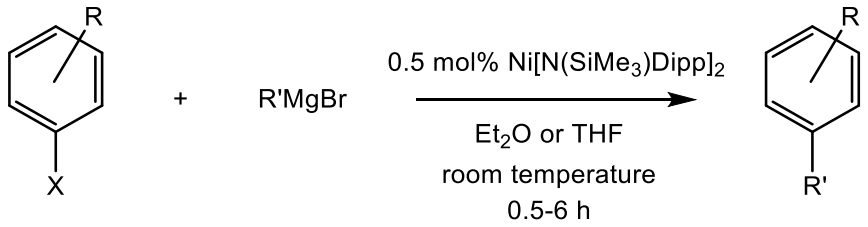
Scheme 1. Hydrosilylation of carbonyl compounds catalysed by $Fe[N(SiMe_3)_2]$.[30]

Tilley and co-workers also reported the two-coordinate Fe(I) complex IPr–Fe–N(SiMe$_3$)Dipp which was shown to catalyse the cyclotrimerisation of alkynes (Scheme 2).[31] This reaction is typically catalysed by rhodium complexes.[32–36] These reactions normally proceed *via* the formation of a metalocyclopentadiene which leads to a formal two election oxidation at the metal centre.[32] This process is thought to be difficult for iron complexes so there are very few iron catalysts for this reaction.[37,38] The Fe(I) complex was shown to catalyse the cyclotrimerisation of both symmetric and asymmetric alkynes at room temperature.[30] A mixture of two different isomers is produced. When asymmetric alkynes were used, the formation of linkage isomers of the type **A** is favoured when R is larger than R'. Only alkyl and aromatic R groups (R/R' = Ph, ^{i}Pr, Me, H) were shown to be compatible with this catalyst. No cyclotrimerization was observed for bis(trimethylsilyl)acetylene R = R' = SiMe$_3$) or dimethylacetylenedicarboxylate (R = R' = C(O)OMe).



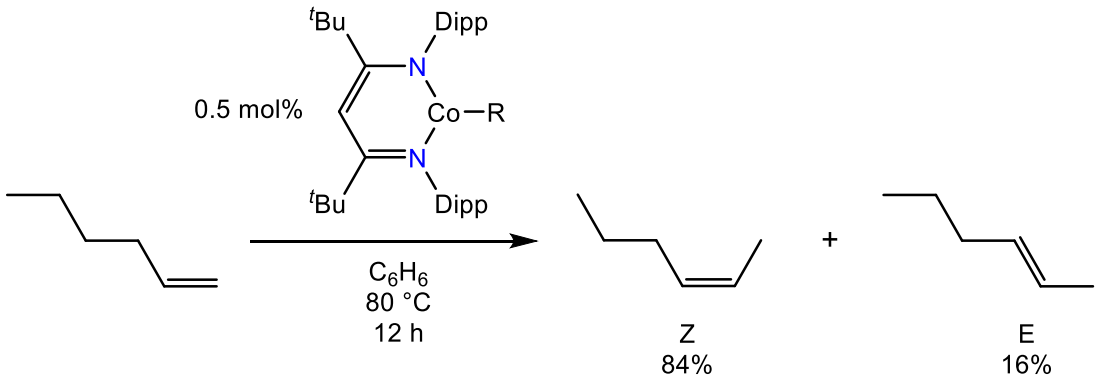
Scheme 2. Cyclotrimerisation of an alkyne catalysed by IPr–Fe–N(SiMe$_3$)Dipp (R = aromatic or alkyl). A mixture of isomer A and B is formed and the major product is dictated by the R group.[31]

Tilley *et al*. also utilised the $N(SiMe_3)Dipp$ ligand in the Ni(II) two-coordinate complex $Ni[N(SiMe_3)Dipp]_2$ which catalyses both the hydrosilylation of alkenes[39] and the cross-coupling reaction between a Grignard reagent and an aryl halide (Scheme 3).[40] The catalyst is effective for the cross-coupling with aryl bromides and iodides as well as the more challenging aryl chlorides although unactivated alkyl halides only showed trace product formation. The use of EtMgBr as the Grignard reagent resulted in a lower yield (30 %) compared to MeMgBr (74 %). This was attributed to *β*-hydride elimination and the formation of ethylene.[41] A mechanism was proposed with the initial coordination of the Grignard reagent to the Ni(II) complex to form an anionic Ni(II)-alkyl complex. This complex then reduces the aryl halide with the formation of an organic radical and a Ni(III) complex. The organic radical then combines with the Grignard reagent to give the cross-coupled product. This one electron oxidation of Ni(II) to Ni(III) has been previously observed for this complex on the addition of an aryl halide.[40]



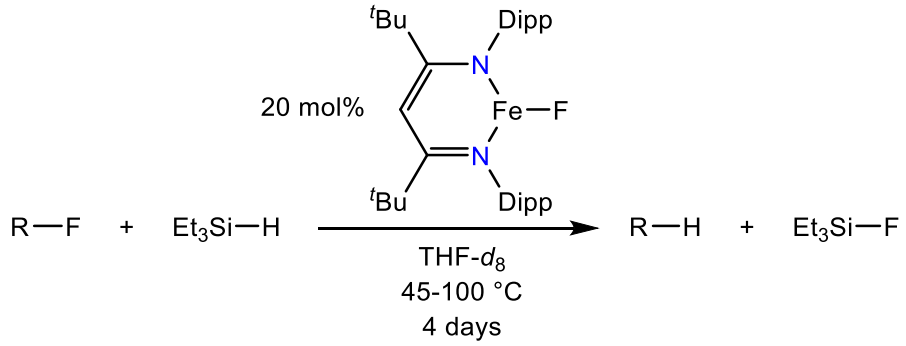
Scheme 3. Cross-coupling between an aryl halide and a Grignard reagent catalysed by $Ni[N(SiMe_3)Dipp]_2$ (R/R' = alkyl or aromatic).[40]

Another common ligand used to stabilise low-coordinate complexes is the *β*-diketiminate ligand. This has been used in a range of different three-coordinate complexes. Holland *et. al.* have reported the catalytic isomerisation of alkenes using a Co(II) *β*-diketiminate complex (Scheme 4).[42] The catalyst facilitates the isomerism of a 1-alkene to a 2-alkene and shows a tolerance for silanes and ethers. With most traditional catalysts, the more stable *E* isomer is formed[43] but the use of this catalyst favours the formation of the less stable *Z* isomer. This is due to the steric bulk of the ligand disfavouring the formation of the *E* isomer.[42]



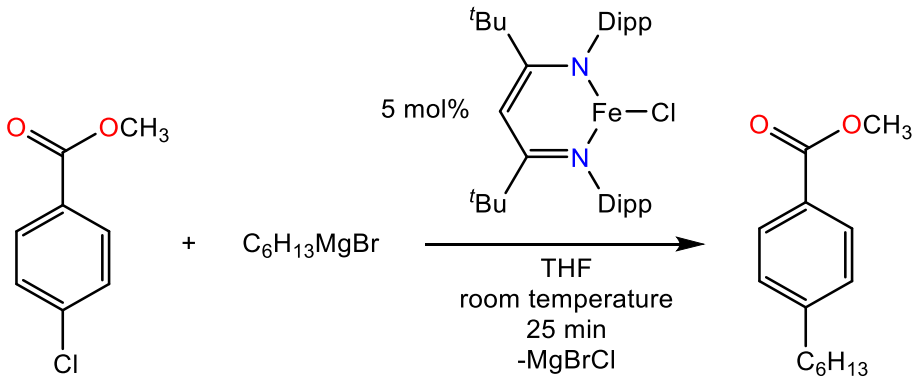
Scheme 4. Isomerisation of 1-hexene with a Co(II) catalyst (R = *n*-hexyl).[42]

Also reported by Holland *et. al.* is an Fe(II) fluoride complex with the structure L$^{t\text{Bu}}$FeF (where L = *β*-diketiminate) which has been shown to act as a catalyst in the hydrodefluorination of both fluoroolefins and fluoroaromatics by activation of the C–F bond (Scheme 5).[44] In the presence of the catalyst in THF, the fluorocarbon and triethylsilane are heated to 45–100 °C depending on the fluorocarbon. This results in the fluorine atom being transferred to the silicon to form a Si–F bond. The complex activates the C–F bond to catalyse the reaction. This reaction only proceeds for sp^2 C–F bonds and aliphatic C–F bonds are not active for this catalyst. Aromatic groups containing functional groups, underwent hydrodefluorination at the position *para* to the most electron withdrawing substituent. The reaction is extremely selective and undergoes monohydrodefluorination with >98% selectivity.



Scheme 5. Catalytic hydrodefluorination of fluoroolefins and fluoroaromatics with an Fe(II) catalyst (R = aromatic or olefin).[44]

A similar complex, L$^{t\text{Bu}}$FeCl was shown to catalyse the cross-coupling of an aryl halide and a Grignard reagent (Scheme 6).[45] When the solvent is THF, the yield is just 45% after 25 min whereas with the addition of *N*-methylpyrrolidone as a co-solvent with THF, the yield increases to 69%. This is proposed to be due to the *N*-methylpyrrolidone coordinating to the metal centre and stabilising the active species.



Scheme 6. Catalytic cross-coupling of an aryl halide and a Grignard reagent with an Fe(II) catalyst.[45]

Webster *et al.* have also reported a three-coordinate Fe(II) *β*-diketiminate catalyst (Figure 7) for a range of different reactions including dehydrocoupling,[46,47] transfer hydrogenation,[48] hydroboration[49] and hydrophosphination.[50,51] This shows the range of applications that are possible with low-coordinate catalysts.

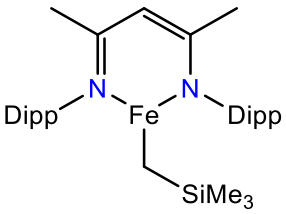
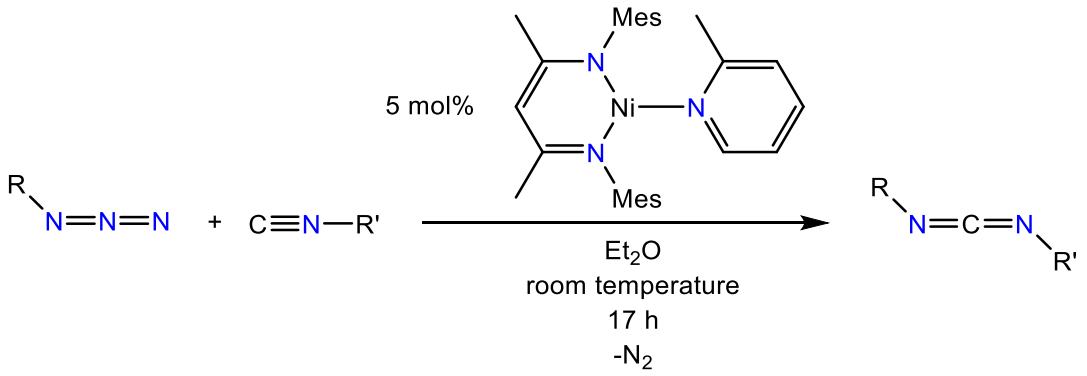


Figure 7. Molecular structure of Fe(II) *β*-diketiminate complex utilised in a range of reactions.[46–51]

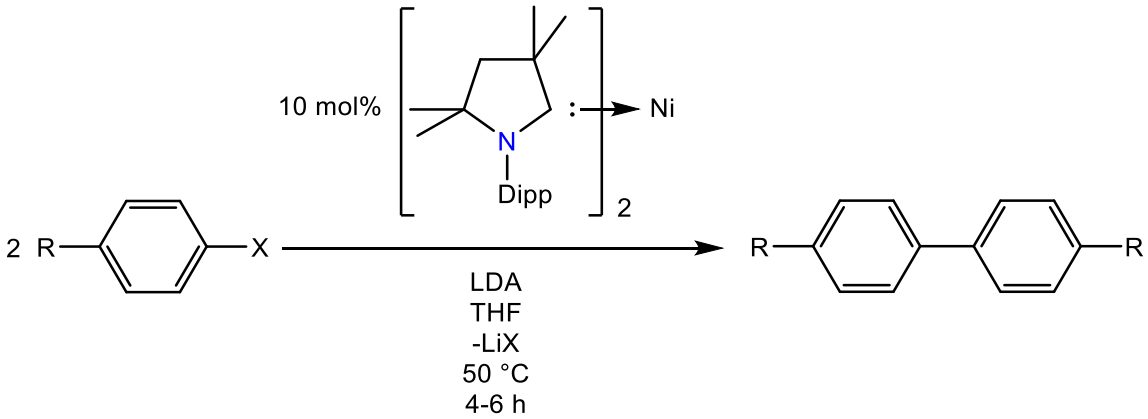
Although they are not as common as iron there are some examples of low coordinate nickel catalysts. The Ni(I) *β*-diketiminate complex reported by Warren *et al*. in 2013 catalyses the nitrene transfer to isocyanides resulting in a carbodiimide (Scheme 7).[52] The

reaction between aromatic azides and ^{t}BuNC showed high conversions (79–99%) after just 30 min at room temperature. The more electron poor isocyanide (2,6-Xyl)NC showed lower yields (46–84%) and significantly lower yields for the more sterically hindered azides such as $MesN_3$ (3%).



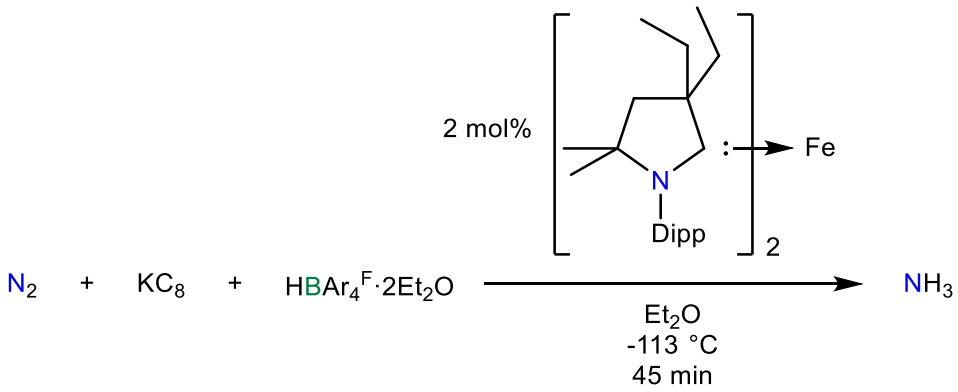
Scheme 7. Catalytic nitrene transfer to isocyanide mediated by Ni(I) complex (R = aromatic or alkyl; R′ = ^{t}Bu or 2,6-Xyl).[52]

A two-coordinate Ni(0) complex was also shown to catalyse the homocoupling of aryl halides.[53] The complex is stabilised by two cyclic (alkyl)(amino)carbene (cAAC) ligands. The reactions reached 55–91% yield after 4–6 h at 50 °C. The use of $Ni(NHC)_2$ (NHC = $C[N(2,4\text{-Dipp})(CH)]_2$) led to the yield dropping to 10–12%. This is attributed to the more electrophilic nature of the cAAC compared to the NHC.



Scheme 8. Catalytic homocoupling of aryl halides mediated by $Ni(cAAC)_2$ (R = H, Me, OMe; X = F, Cl).[53]

The similar Fe(0) complex $Fe(cAAC)_2$ was shown to catalyse the reduction of N_2 to NH_3.[54] In the presence of KC_8 and $HBAr^F_4{\cdot}2Et_2O$, N_2 is reduced to NH_3 with a yield of 3.0 ± 0.7 equivalents of NH_3 per Fe metal centre at −113 °C (Scheme 9). As the temperature increases, the yield decreases with only 0.4 ± 0.2 equivalents of NH_3 per Fe metal centre at 23 °C. This behaviour is due to the fixation of N_2 at the metal centre which occurs at −95 °C and only trace amounts of N_2 fixation is recorded above this temperature.[54]



Scheme 9. Catalytic reduction of N_2 to NH_3 with $Fe(cAAC)_2$.[54]

This section demonstrates the range of different reactions that low coordinate complexes are able to catalyse. This thesis focusses on the catalysis of hydroelementation reactions. Some examples of hydroelementation reactions were discussed above (hydrosilylation,[30,39] hydroboration[49] and hydrophsphination[50,51]) and this class of reaction will be explored further in the following section.

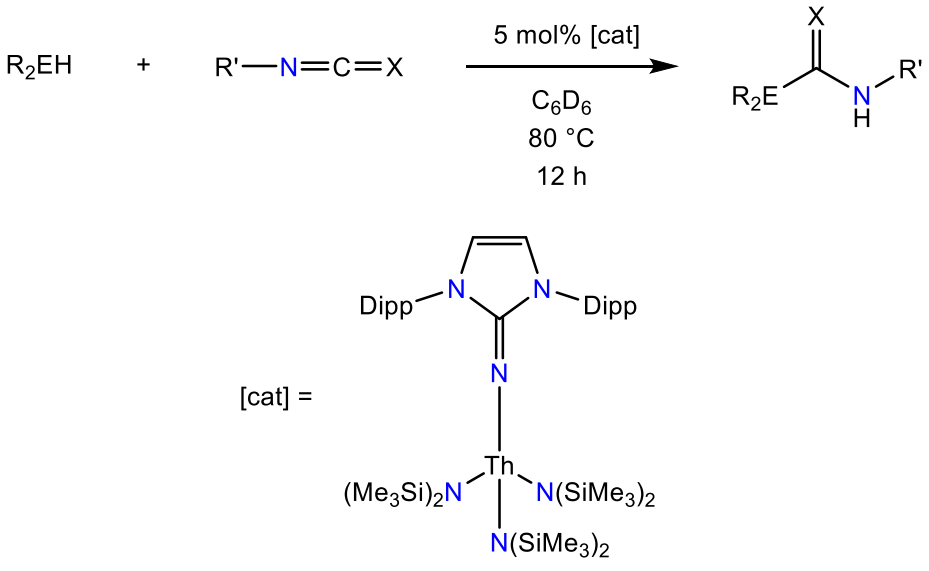
1.4 Hydroelementation Reactions

Hydroelementation reactions are the addition of an E–H bond (E = N, S, P, Si, O etc.) across an unsaturated substrate, and are an atom economical method to synthesise many different organic molecules.[55] The hydroelementation of carbon-carbon multiple bonds such as alkenes and alkynes has been extensively reported[55–63] whereas the hydroelementation of other unsaturated substrates is less common in the literature.

Catalysts for the hydroelementation of heterocumulenes have mostly been limited to group 2[64–73] and f-block[74–81] metals with very few transition metal examples[82–84] which are limited

to titanium or zinc complexes so there is a need for inexpensive catalysts from earth-abundant metals for these reactions.[23] Often catalysts for hydroelementation reactions have issues such as oligomerisation and polymerisation of the heterocumulene (particularly for isocyanates).[85–88] Many catalysts also have issues with functional group and heteroatom tolerance[65,84] or have limited substrate scope.[67,72,83]

In 2015 Eisen and Tamm *et. al.* reported the catalytic hydroamination, hydrophosphination and hydrothiolation of carbodiimides, isocyanates and isothiocyanates catalysed by the imidazolin-2-iminato thorium(IV) complex (Scheme 10).[74] This catalyst has also since been used for the hydroboration of carbodiimides.[76] This is an unprecedented example of a very wide substrate scope for hydroelementation reactions as well as the first reported actinide catalyst for these reactions. The reactions in most cases reach >90% conversion after 12 h at 80 °C and the catalyst shows good tolerance towards silicon, nitrogen and sulfur heteroatoms. Another similar actinide complex containing a benzimidazolin-2-iminato ligand was also shown to catalyse the hydroelementation of heterocumulenes with a wide range of substrates.[76,79–81] This is a promising result for the development of catalysts for hydroelementation reactions.



Scheme 10. Catalytic hydroelementation of heterocumulenes (R/R' = alkyl or aromatic; E = N, P, S; X = O, S, NR').[74]

There are no other examples with quite as wide a range as this actinide catalyst, however the group 2 *β*-diketiminato catalysts first reported by Hill *et al*. in 2008 (Figure 8) have been reported to catalyse the hydroamination[66,67], hydrophosphination,[70] hydroboration[71,72] and hydroacetylenation[69] of isocyanates and carbodiimides.

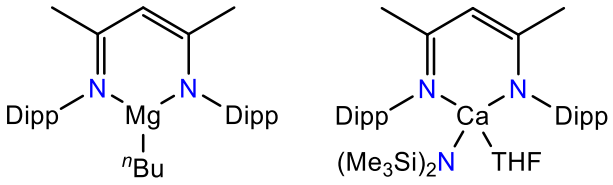
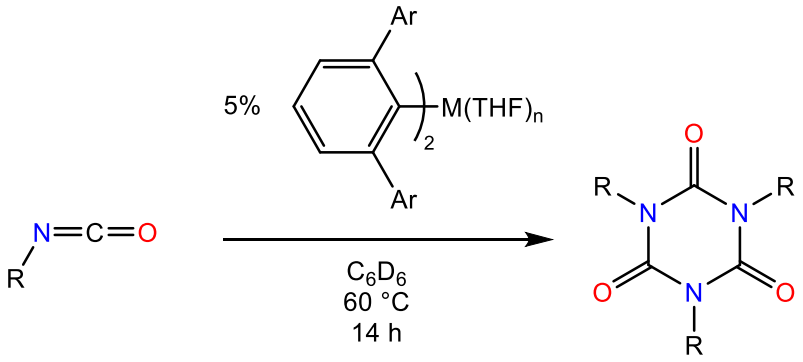


Figure 8. Group 2 *β*-diketiminato catalysts for hydroelementation reactions.[66,67,69–72]

Although there are a handful of examples of catalysts for hydroelemenation reactions there is clearly the need for the development of transition metal catalysts with a wider substrate scope. More detailed discussions of the catalysis of the hydroamination, hydrophosphination and hydroboration of heterocumulenes are presented in later chapters.

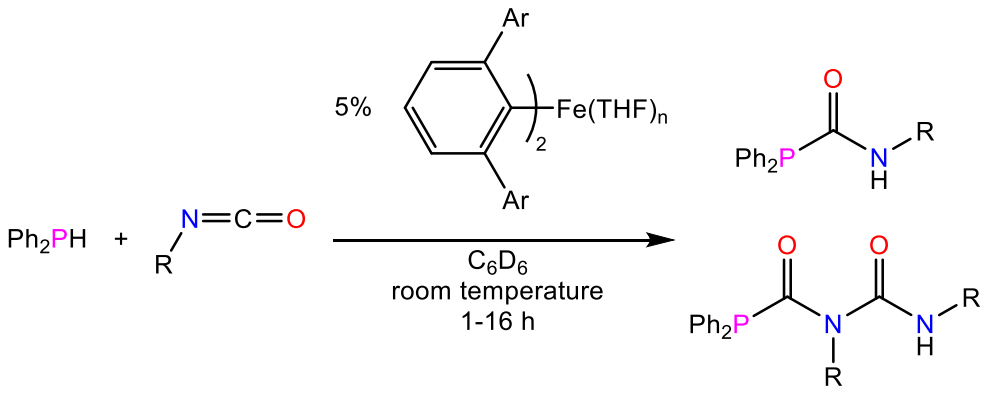
1.5 Catalysis with *m*-Terphenyl Complexes

Previous work in the Kays group has shown that the diaryl transition metal *m*-terphenyl complexes $M(2,6\text{-}Ar_2C_6H_3)_2(THF)_n$ (M = Mn, Fe; Ar = Mes n = 0; Ar = Tmp, n = 1) can be used to catalyse the cyclotrimerisation of isocyanates to form isocyanurates (Scheme 11).[89] Cyclotrimerisation was observed with primary isocyanates such as ethyl isocyanate but was not observed with secondary or tertiary isocyanates. This selectivity towards only primary isocyanates made these complexes an attractive catalyst for the hydrophosphination of isocyanates as a common issue with catalysts for this reaction is the competing cyclotrimerisation of the isocyanate.[65]

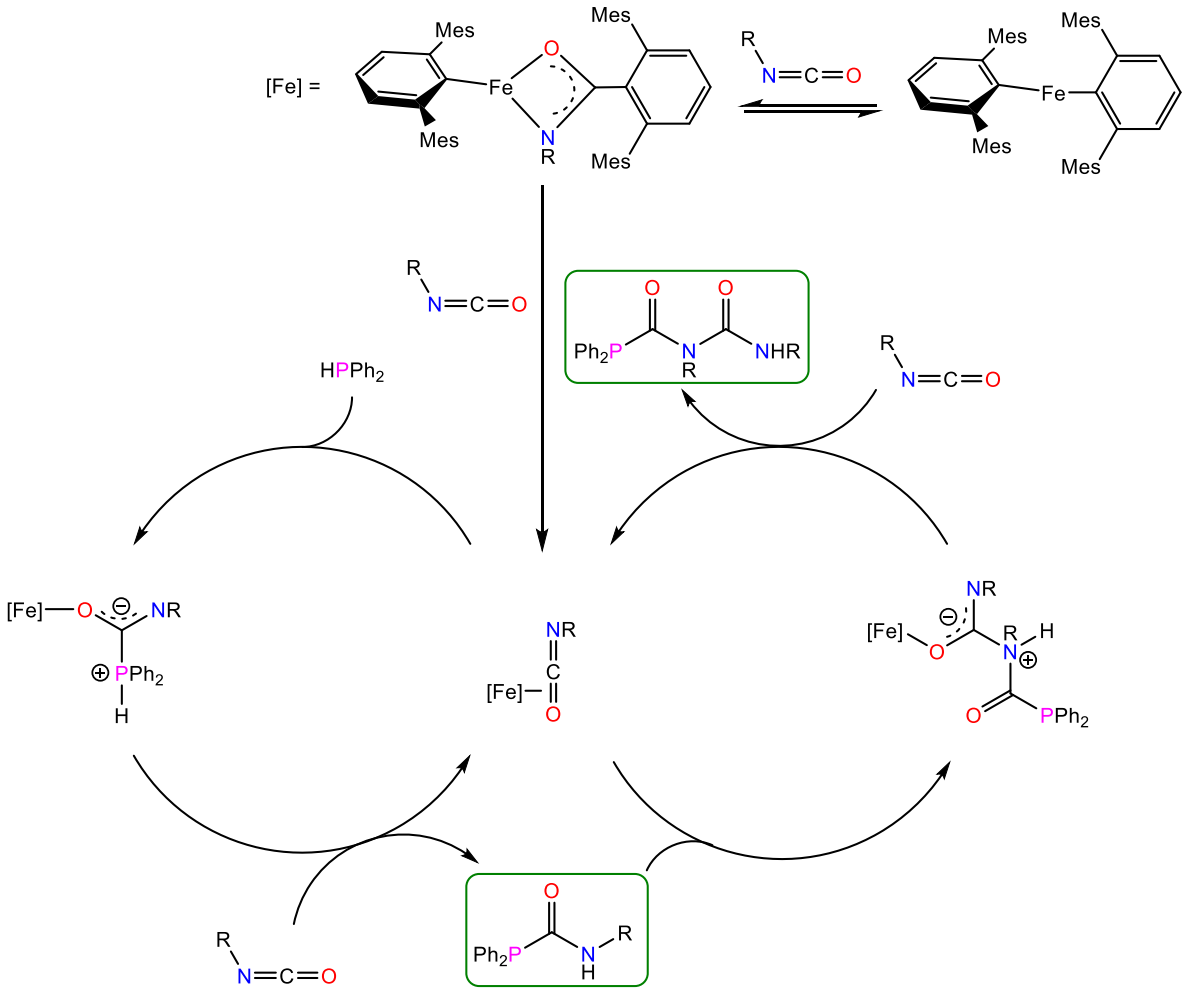


Scheme 11. Cyclotrimerisation of isocyanates catalysed by $M(2,6\text{-}Ar_2C_6H_3)_2(THF)_n$ (M = Mn, Fe; Ar = Mes n = 0; Ar = Tmp, n = 1).[89]

The hydrophosphination of isocyanates can be catalysed by $Fe(2,6\text{-}Mes_2C_6H_3)_2$ and $Fe(2,6\text{-}Tmp_2C_6H_3)_2(THF)$.[90] This catalysis resulted in the unprecedented diinsertion of the isocyanate into the P–H bond of the phosphine (Scheme 12) leading to the formation of phosphinodicarboxamides, a new family of organic compounds. These compounds have potential applications as ligands in metal complexes due to the presence of both hard and soft donors.[91] This allows the ligand to bind to many different metals with different coordination modes. These properties could also lead to applications as building blocks in supramolecular chemistry. The two catalytic products can be selectively formed by tuning the reaction conditions; the use of isocyanates with less sterically demanding aromatic R groups afforded the diinsertion product preferentially, whereas isocyanates featuring larger alkyl R groups formed the monoinsertion product exclusively. Performing the reaction in THF results in the formation of the monoinsertion product exclusively whereas performing the reaction in the presence of a weak acid results in the exclusive formation of the diinsertion product. The proposed mechanism involves the Fe(II) metal centre acting as a Lewis acid with the isocyanate molecule first coordinating to the metal centre and the diphenylphosphine then attacking the isocyanate forming a P–C bond (Scheme 13). The monoinsertion product is then displaced from the metal centre by the coordination of a new isocyanate molecule.

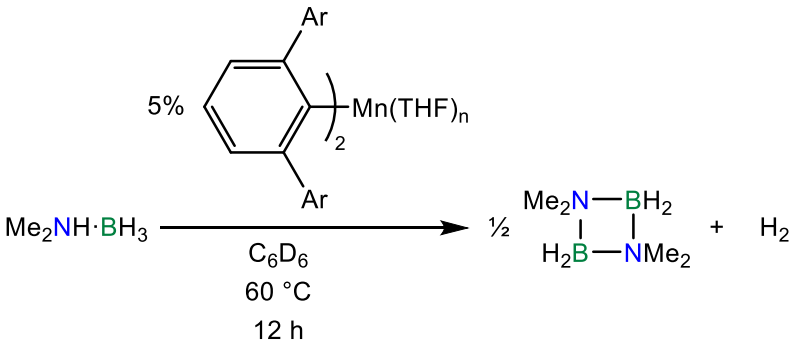


Scheme 12. Hydrophosphination of isocyanates catalysed by Fe(2,6-$Ar_2C_6H_3)_2(THF)_n$ (Ar = Mes, n = 0; Ar = Tmp, n = 1).[90]



Scheme 13. Proposed mechanism for the hydrophosphination of isocyanates catalysed by Fe(2,6-$Mes_2C_6H_3)_2$.[90]

The manganese *m*-terphenyl complexes Mn(2,6-(2,6-Xyl)$_2$C$_6$H$_3$)$_2$, Mn(2,6-Mes$_2$C$_6$H$_3$)$_2$ and Mn(2,6-Tmp$_2$C$_6$H$_3$)$_2$(THF) were shown to catalyse the dehydrocoupling of dimethylamine-borane (Me$_2$NH·BH$_3$).[92] The reaction reached over 94% conversion after 12 h at 60 °C (Scheme 14). A change in the *m*-terphenyl ligand was found to influence the mechanism of the reaction. The two-coordinate complexes underwent a homogeneous mechanism whereas the three-coordinate Tmp complex underwent a heterogeneous mechanism. A darkening of the solution was observed with the Tmp complex which is often an indicator of nanoparticle formation. This was investigated with the use of transmission electron microscopy (TEM) and scanning transmission electron microscopy (STEM) which confirmed the formation of Mn nanoparticles with a diameter of ~10 nm. It is postulated that this difference in mechanism is due to the steric differences between the three ligands. The lower steric demands of the Tmp substituted ligand make the metal centre more susceptible to reduction and the formation of nanoparticles which catalysed the reaction.[92]



Scheme 14. Dehydrocoupling of dimethylamine-borane catalysed by Mn(2,6-Ar$_2$C$_6$H$_3$)$_2$(THF)$_n$ (Ar = 2,6-Xyl, n = 0; Ar = Mes, n = 0; Ar = Tmp, n = 1).[92]

These results show the potential for diaryl *m*-terphenyl complexes to act as efficient catalysts for a range of different organic transformations.

1.6 Aims

The aim of this work was to investigate the ability of *m*-terphenyl complexes to act as precatalysts for organic transformations. *m*-Terphenyl complexes have been shown to undergo reactions with small molecules such as O_2, CO and NH_3 and act as precatalysts for the cyclotrimerisation and hydrophosphination of isocyanates. Based on this work we hypothesised that these complexes would have potential applications as catalysts for the hydroamination of isocyanates to produce urea derivatives as the reaction would be expected to proceed following a similar mechanism to that observed for the hydrophosphination of isocyanates. The aim of this thesis was to build on this and to further the scope of the catalysts to the hydroelementation of heterocumulenes, focussing on the ability of the catalyst to facilitate the diinsertion of the heterocumulene.

The diaryl *m*-terphenyl complexes M(2,6-$Mes_2C_6H_3)_2$ (M = Fe, Co, Zn) were investigated for their ability to act as precatalysts for the hydroamination, hydrophosphination and hydroboration of heterocumulenes. An investigation into the ability of the precatalysts to facilitate the multiple insertions of the heterocumulene was undertaken as a method to synthesise previously unexplored organic molecules. A range of different substrates were utilised, and the mechanism of the catalysis was investigated using stoichiometric reactions and poisoning experiments. The effect of the metal centre in the precatalyst was also investigated.

In an effort to further explore the versatility of the *m*-terphenyl ligand and their potential applications in catalysis, the synthesis and characterisation of a family of four-coordinate *m*-terphenyl complexes containing the bidentate ligands DPPE, TMEDA and DME was undertaken. The effect of altering both the metal centre and the bidentate ligand employed was investigated to give an insight into how the different sterics of the ligands influences the formation of the complexes. Investigations into the magnetic properties and the reactivity of these complexes towards reduction and halide abstraction was then explored in an effort to synthesise a three-coordinate complex containing an *m*-terphenyl ligand, a bidentate ligand and a halide.

1.7 References

1 P. P. Power, *Chem. Rev.*, 2012, **112**, 3482–3507.

2 C. Ni, H. Lei and P. P. Power, *Organometallics*, 2010, **29**, 1988–1991.

3 C. Ni and P. P. Power, *Chem. Commun.*, 2009, 5543–5545.

4 W. M. Reiff, A. M. LaPointe and E. H. Witten, *J. Am. Chem. Soc.*, 2004, **126**, 10206–10207.

5 W. M. Reiff, C. E. Schulz, M. Whangbo, J. I. Seo, Y. S. Lee, G. R. Potratz, C. W. Spicer and G. S. Girolami, *J. Am. Chem. Soc.*, 2009, **131**, 404–405.

6 L. Andrews, *Chem. Soc. Rev.*, 2004, **33**, 123–132.

7 P. P. Power, *J. Organomet. Chem.*, 2004, **689**, 3904–3919.

8 N. H. Buttrus, C. Eaborn, P. B. Hitchcock, J. D. Smith and A. C. Sullivan, *J. Chem. Soc., Chem. Commun.*, 1985, 1380–1381.

9 D. L. Kays, *Dalton Trans.*, 2011, **40**, 769–778.

10 H. H. Jaffé and G. O. Doak, *J. Chem. Phys.*, 1953, **21**, 196–200.

11 R. R. Schrock and G. W. Parshall, *Chem. Rev.*, 1976, **76**, 243–268.

12 M. R. Collier, M. F. Lappert and R. Pearce, *J. Chem. Soc., Dalton Trans.*, 1973, 445–451.

13 R. Fischer, H. Görls, M. Friedrich and M. Westerhausen, *J. Organomet. Chem.*, 2009, **694**, 1107–1111.

14 S. Gambarotta, C. Floriani, A. Chiesivilla and C. Guastini, *J. Chem. Soc. Chem. Commun.*, 1983, **20**, 1128–1129.

15 E. Solari, F. Musso, E. Gallo, C. Floriani, N. Re, A. Chiesi-Villa and C. Rizzoli, *Organometallics*, 1995, **14**, 2265–2276.

16 W. Seidel, H. Muller and H. Gorls, *Angew. Chem. Int. Ed. English*, 1995, **34**, 325–327.

17 R. J. Wehmschulte and P. P. Power, *Organometallics*, 1995, **14**, 3264–3267.

18 D. L. Kays and A. R. Cowley, *Chem. Commun.*, 2007, 1053–1055.

19 R. Wolf, C. Ni, T. Nguyen, M. Brynda, G. J. Long, A. D. Sutton, R. C. Fischer, J. C.

Fettinger, M. Hellman, L. Pu and P. P. Power, *Inorg. Chem.*, 2007, **46**, 11277–11290.

20 J. J. Ellison and P. P. Power, *J. Organomet. Chem.*, 1996, **526**, 263–267.

21 T. Nguyen, A. D. Sutton, M. Brynda, J. C. Fettinger, G. J. Long and P. P. Power, *Science*, 2005, **310**, 844–847.

22 R. Wolf, M. Brynda, C. Ni, G. J. Long and P. P. Power, *J. Am. Chem. Soc.*, 2007, **129**, 6076–6077.

23 P. L. Holland, *Acc. Chem. Res.*, 2015, **48**, 1696–1702.

24 P. B. Kettler, *Org. Process Res. Dev.*, 2003, **7**, 342–354.

25 S. Enthaler, K. Junge and M. Beller, *Angew. Chem. Int. Ed.*, 2008, **47**, 3317–3321.

26 B. D. Sherry and A. Fürstner, *Acc. Chem. Res.*, 2008, **41**, 1500–1511.

27 I. Bauer and H. J. Knölker, *Chem. Rev.*, 2015, **115**, 3170–3387.

28 B. Su, Z. C. Cao and Z. J. Shi, *Acc. Chem. Res.*, 2015, **48**, 886–896.

29 S. R. McWhinney, R. M. Goldberg and H. L. McLeod, *Mol. Cancer Ther.*, 2009, **8**, 10–16.

30 J. Yang and T. D. Tilley, *Angew. Chem. Int. Ed.*, 2010, **49**, 10186–10188.

31 M. I. Lipschutz, T. Chantarojsiri, Y. Dong and T. D. Tilley, *J. Am. Chem. Soc.*, 2015, **137**, 6366–6372.

32 Ò. Torres, M. Fernàndez, À. Díaz-Jiménez, A. Pla-Quintana, A. Roglans and M. Solà, *Organometallics*, 2019, **38**, 2853–2862.

33 M. Saito, M. Nakada, T. Kuwabara, R. Owada, S. Furukawa, R. Narayanan, M. Abe, M. Hada, K. Tanaka and Y. Yamamoto, *Organometallics*, 2019, **38**, 3099–3103.

34 S. Nishigaki, Y. Shibata, A. Nakajima, H. Okajima, Y. Masumoto, T. Osawa, A. Muranaka, H. Sugiyama, A. Horikawa, H. Uekusa, H. Koshino, M. Uchiyama, A. Sakamoto and K. Tanaka, *J. Am. Chem. Soc.*, 2019, **141**, 14955–14960.

35 H. Uchimura, J. ichi Ito, S. Iwasa and H. Nishiyama, *J. Organomet. Chem.*, 2007, **692**, 481–486.

36 Y. Hoshino, Y. Shibata and K. Tanaka, *Adv. Synth. Catal.*, 2014, **356**, 1577–1585.

37 M. I. Lipschutz, X. Yang, R. Chatterjee and T. D. Tilley, *J. Am. Chem. Soc.*, 2013,

135, 15298–15301.

38 C. Gunnar Werncke, P. C. Bunting, C. Duhayon, J. R. Long, S. Bontemps and S. Sabo-Etienne, *Angew. Chem. Int. Ed.*, 2015, **54**, 245–248.

39 M. I. Lipschutz and T. D. Tilley, *Chem. Commun.*, 2012, **48**, 7146–7148.

40 M. I. Lipschutz and T. D. Tilley, *Angew. Chem. Int. Ed.*, 2014, **53**, 7290–7294.

41 L. C. Liang, P. S. Chien, J. M. Lin, M. H. Huang, Y. L. Huang and J. H. Liao, *Organometallics*, 2006, **25**, 1399–1411.

42 C. Chen, T. R. Dugan, W. W. Brennessel, D. J. Weix and P. L. Holland, *J. Am. Chem. Soc.*, 2014, **136**, 945–955.

43 A. Scarso, M. Colladon, P. Sgarbossa, C. Santo, R. A. Michelin and G. Strukul, *Organometallics*, 2010, **29**, 1487–1497.

44 J. Vela, J. M. Smith, Y. Yu, N. A. Ketterer, C. J. Flaschenriem, R. J. Lachicotte and P. L. Holland, *J. Am. Chem. Soc.*, 2005, **127**, 7857–7870.

45 K. Ding, F. Zannat, J. C. Morris, W. W. Brennessel and P. L. Holland, *J. Organomet. Chem.*, 2009, **694**, 4204–4208.

46 N. T. Coles, M. F. Mahon and R. L. Webster, *Organometallics*, 2017, **36**, 2262–2268.

47 A. K. King, A. Buchard, M. F. Mahon and R. L. Webster, *Chem. Eur. J.*, 2015, **21**, 15960–15963.

48 M. Espinal-Viguri, S. E. Neale, N. T. Coles, S. A. MacGregor and R. L. Webster, *J. Am. Chem. Soc.*, 2019, **141**, 572–582.

49 M. Espinal-Viguri, C. R. Woof and R. L. Webster, *Chem. Eur. J.*, 2016, **22**, 11605–11608.

50 M. Espinal-Viguri, A. K. King, J. P. Lowe, M. F. Mahon and R. L. Webster, *ACS Catal.*, 2016, **6**, 7892–7897.

51 A. K. King, K. J. Gallagher, M. F. Mahon and R. L. Webster, *Chem. Eur. J.*, 2017, **23**, 9039–9043.

52 S. Wiese, M. J. B. Aguila, E. Kogut and T. H. Warren, *Organometallics*, 2013, **32**, 2300–2308.

53 K. C. Mondal, P. P. Samuel, Y. Li, H. W. Roesky, S. Roy, L. Ackermann, N. S. Sidhu,

G. M. Sheldrick, E. Carl, S. Demeshko, S. De, P. Parameswaran, L. Ungur, L. F. Chibotaru and D. M. Andrada, *Eur. J. Inorg. Chem.*, 2014, 818–823.

54 G. Ung and J. C. Peters, *Angew. Chem. Int. Ed.*, 2015, **54**, 532–535.

55 X. Zeng, *Chem. Rev.*, 2013, **113**, 6864–6900.

56 G. Zhang, J. Wu, M. Wang, H. Zeng, J. Cheng, M. C. Neary and S. Zheng, *European J. Org. Chem.*, 2017, 5814–5818.

57 G. Lu, R. Y. Liu, Y. Yang, C. Fang, D. S. Lambrecht, S. L. Buchwald and P. Liu, *J. Am. Chem. Soc.*, 2017, **139**, 16548–16555.

58 A. J. Musacchio, B. C. Lainhart, X. Zhang, S. G. Naguib, T. C. Sherwood and R. R. Knowles, *Science*, 2017, **355**, 727–730.

59 A. G. Nair, R. T. McBurney, M. R. D. Gatus, S. C. Binding and B. A. Messerle, *Inorg. Chem.*, 2017, **56**, 12067–12075.

60 T. E. Müller, K. C. Hultzsch, M. Yus, F. Foubelo and M. Tada, *Chem. Rev.*, 2008, **108**, 3795–3892.

61 A. Bismuto, S. P. Thomas and M. J. Cowley, *Angew. Chem. Int. Ed.*, 2016, **55**, 15356–15359.

62 J. P. W. Stelmach, C. A. Bange and R. Waterman, *Dalton Trans.*, 2016, **45**, 6204–6209.

63 G. Wu, U. Chakraborty and A. Jacobi von Wangelin, *Chem. Commun.*, 2018, **54**, 12322–12325.

64 M. De Tullio, A. Hernán-Gómez, Z. Livingstone, W. Clegg, A. R. Kennedy, R. W. Harrington, A. Antiñolo, A. Martínez, F. Carrillo-Hermosilla, E. Hevia, A. Hernan-Gomez, Z. Livingstone, W. Clegg, A. R. Kennedy, R. W. Harrington, A. Antinolo, A. Martinez, F. Carrillo-Hermosilla and E. Hevia, *Chem. Eur. J.*, 2016, **22**, 17646–17656.

65 A. Hernan-Gomez, T. D. Bradley, A. R. Kennedy, Z. Livingstone, S. D. Robertson and E. Hevia, *Chem. Commun.*, 2013, **49**, 8659–8661.

66 J. R. Lachs, A. G. M. Barrett, M. R. Crimmin, G. Kociok-Köhn, M. S. Hill, M. F. Mahon and P. A. Procopiou, *Eur. J. Inorg. Chem.*, 2008, **2008**, 4173–4179.

67 A. G. M. Barrett, T. C. Boorman, M. R. Crimmin, M. S. Hill, G. Kociok-Kohn and P. A. Procopiou, *Chem. Commun.*, 2008, 5206–5208.

68 M. R. Crimmin, A. G. M. Barrett, M. S. Hill, P. B. Hitchcock and P. A. Procopiou, *Organometallics*, 2007, **26**, 2953–2956.

69 M. Arrowsmith, M. R. Crimmin, M. S. Hill, S. L. Lomas, M. S. Heng, P. B. Hitchcock and G. Kociok-Köhn, *Dalton Trans.*, 2014, **43**, 14249–14256.

70 M. R. Crimmin, A. G. M. Barrett, M. S. Hill, P. B. Hitchcock and P. A. Procopiou, *Organometallics*, 2008, **27**, 497–499.

71 C. Weetman, M. S. Hill and M. F. Mahon, *Chem. Eur. J.*, 2016, **22**, 7158–7162.

72 Y. Yang, M. D. Anker, J. Fang, M. F. Mahon, L. Maron, C. Weetman and M. S. Hill, *Chem. Sci.*, 2017, **8**, 3529–3537.

73 D. Mukherjee, S. Shirase, T. P. Spaniol, K. Mashima and J. Okuda, *Chem. Commun.*, 2016, **52**, 13155–13158.

74 I. S. R. Karmel, M. Tamm and M. S. Eisen, *Angew. Chem. Int. Ed.*, 2015, **54**, 12422–12425.

75 J. Tu, W. Li, M. Xue, Y. Zhang and Q. Shen, *Dalton Trans.*, 2013, **42**, 5890–5901.

76 H. Liu, K. Kulbitski, M. Tamm and M. S. Eisen, *Chem. Eur. J.*, 2018, **24**, 5738–5742.

77 A. C. Behrle and J. A. R. R. Schmidt, *Organometallics*, 2013, **32**, 1141–1149.

78 H. Liu, N. Fridman, M. Tamm and M. S. Eisen, *Organometallics*, 2017, **36**, 3896–3903.

79 H. Liu, M. Khononov, N. Fridman, M. Tamm and M. S. Eisen, *Inorg. Chem.*, 2017, **56**, 3153–3157.

80 R. J. Batrice, C. E. Kefalidis, L. Maron and M. S. Eisen, *J. Am. Chem. Soc.*, 2016, **138**, 2114–2117.

81 H. Liu, M. Khononov, N. Fridman, M. Tamm and M. S. Eisen, *Inorg. Chem.*, 2017, **56**, 3153–3157.

82 A. Harinath, K. Bano, S. Ahmed and T. K. Panda, *Phosphorus. Sulfur. Silicon Relat. Elem.*, 2018, **193**, 23–32.

83 K. Naktode, S. Das, J. Bhattacharjee, H. P. Nayek and T. K. Panda, *Inorg. Chem.*,

2016, **55**, 1142–1153.

84 J. Bhattacharjee, S. Das, R. K. Kottalanka and T. K. Panda, *Dalton Trans.*, 2016, **45**, 17824–17832.

85 T. E. Patten and B. M. Novak, *J. Am. Chem. Soc.*, 1991, **113**, 5065–5066.

86 T. E. Patten and B. M. Novak, *J. Am. Chem. Soc.*, 1996, **118**, 1906–1916.

87 S. M. Hoff and B. M. Novak, *Macromolecules*, 1993, **26**, 4067–4069.

88 N. Fukuwatari, H. Sugimoto and S. Inoue, *Macromol. Rapid Commun.*, 1996, **17**, 1–7.

89 H. R. Sharpe, A. M. Geer, H. E. L. Williams, T. J. Blundell, W. Lewis, A. J. Blake and D. L. Kays, *Chem. Commun.*, 2017, **53**, 937–940.

90 H. R. Sharpe, A. M. Geer, W. Lewis, A. J. Blake and D. L. Kays, *Angew. Chem. Int. Ed.*, 2017, **56**, 4845–4848.

91 P. Štěpnika, *Chem. Soc. Rev.*, 2012, **41**, 4273–4305.

92 H. R. Sharpe, A. M. Geer, T. J. Blundell, F. R. Hastings, M. W. Fay, G. A. Rance, W. Lewis, A. J. Blake and D. L. Kays, *Catal. Sci. Technol.*, 2018, **8**, 229–235.

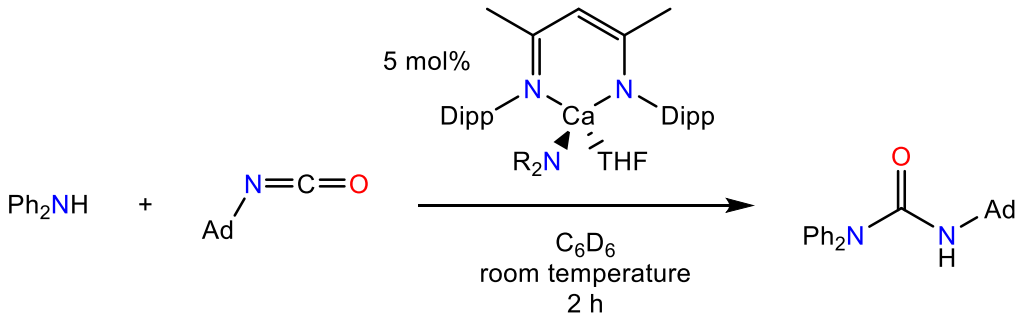
Chapter 2

Hydroamination and Hydrophosphination of Heterocumulenes

2.1 Introduction

Urea derivatives are essential in a wide range of biological systems and have many applications in medicinal,[1–3] materials,[4–7] agricultural[8] and synthetic chemistry.[9] Despite this wide range of applications there are few reported methods to synthesise ureas. Some methods include the catalytic reduction of nitro compounds by CO,[10] the dehydrogenative coupling of formamides and amines,[11] the carbonylation of amines with CO_2,[12] and the oxidative carbonylation of amines with CO.[13] These all require either the presence of catalysts containing rare metals such as palladium and rhodium or stoichiometric amounts of other reagents.

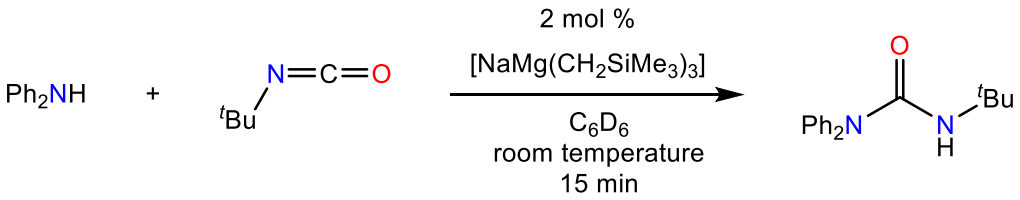
The hydroamination of isocyanates can be used as an atom economical alternative method to synthesise urea derivatives.[14–17] Hydroamination is the formation of a C–N bond by the addition of the N–H bond of an amine to an unsaturated bond in an organic molecule.[18] The catalytic hydroamination of alkenes and alkynes to form C–N bonds has been widely studied,[18,19] however there are few reported examples of the catalytic hydroamination of isocyanates. The hydroamination of isocyanates generally requires high temperatures and long reaction times to overcome the high kinetic barriers and is limited to the use of nucleophilic amines.[2] The use of a catalyst could widen the scope of the reaction and lead to much milder reaction conditions. There are a few examples of the catalytic hydroamination of isocyanates, however these are limited to Group 2,[14,15] titanium,[16,17] zinc[20] and actinide[21,22] complexes.



Scheme 1. Hydroamination of 1-adamantyl isocyanate by diphenyl amine mediated by [(DippNC(Me)CHC(Me)NDipp)Ca(NR_2)(THF)] (R=$SiMe_3$, Ph).[14]

The calcium complex [(DippNC(Me)CHC(Me)NDipp)Ca(NR_2)(THF)] (R = $SiMe_3$, Ph) was shown to catalyse the hydroamination of 1-adamantyl isocyanate and 2,6-diisopropylphenyl isocyanate with diphenylamine (Scheme 1).[14] It was found that using the barium analogue resulted in the formation of an insoluble polymeric amide or ureido side products resulting in a lower catalytic activity. This was proposed to be due to the increased ionic radius of barium compared to calcium which makes the reaction less selective.[14]

Hevia *et al.* reported a sodium magnesiate catalyst for the hydroamination of isocyanates (Scheme 2).[15] This was shown to catalyse the hydroamination of *tert*-butyl isocyanate with diphenylamine. An intermediate was isolated in which the amine was coordinated to the magnesium metal centre and the sodium interacts with two of the phenyl groups from the amine. The isocyanate then inserts into the Mg–N bond and forms a tris(ureido) complex. This complex also catalyses the cyclotrimerisation of less bulky isocyanates which competes with the hydroamination reaction.



Scheme 2. Hydroamination of isocyanates mediated by [$NaMg(CH_2SiMe_3)_3$].[15]

There are very few examples of the transition metal catalysed hydroamination of isocyanates and these are limited to the titanium and zinc complexes reported by Panda *et al*. (Figure 1).[16,17,20] The imidazoline-2-iminato titanium complex [($Im^{Dipp}N$)Ti(NMe_2)$_3$] catalyses the hydroamination of phenyl isocyanate with a range of different aromatic and aliphatic amines.[17] The reaction between phenyl isocyanate and aromatic amines gave high yields of over 90% however 1-fluoroaniline gave a much lower yield of 54%. Secondary amines were found to give higher yields than primary amines due to the inductive effect of the additional alkyl groups. Panda *et al.* also reported the use of a

bis(phosphinoselenoic amide) supported titanium complex to catalyse the hydroamination of isocyanates as well as isothiocyanates and carbodiimides.[16]

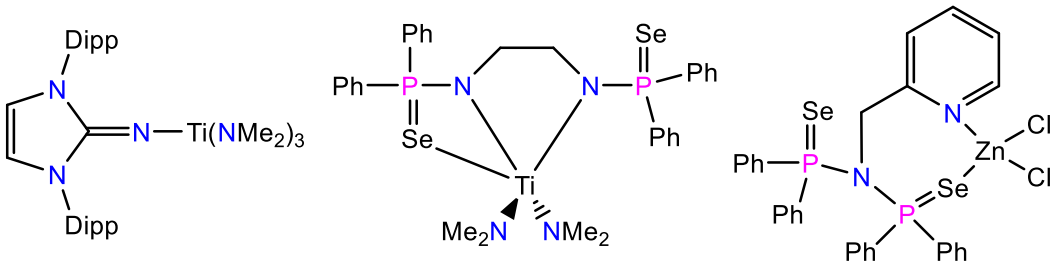
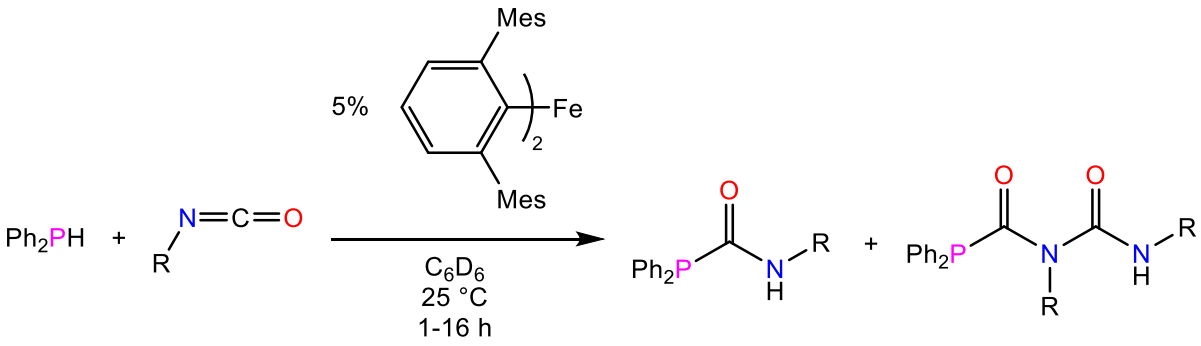


Figure 1. Molecular structure of transition metal catalysts for hydroamination of isocyanates.[16,17,20]

The catalysts that have been discussed so far are able to produce urea derivatives whereas the synthesis of biuret derivatives, obtained from the diinsertion of the isocyanate into the N–H bond, is much more challenging as ureas are much less reactive than amines due to the presence of the electron-withdrawing carbonyl group.[23] These species with multiple urea moieties have a high capacity for hydrogen bonding which is useful for the design of foldamers,[24,25] self-assembly[26,27] and molecular recognition.[28,29] They can also be used as ligands in coordination chemistry.[30–32] Despite these potential applications, there are very few reported syntheses for biurets. Biurets can been synthesised from the pyrolysis of ureas[33] or catalytically from substituted ureas with an organotin compound.[34] More recently, thionyl chloride and chlorosulfonic acid were shown to catalyse the formation of biurets from ureas although a high temperature of 145 °C was still required.[35] There are no examples in the literature of the direct transformation of amines to biuret derivatives.

Previous work in the Kays group has shown that diaryl *m*-terphenyl complex Fe(2,6-$Mes_2C_6H_3$)$_2$ can be used as a catalyst for the hydrophosphination of isocyanates.[36] This reaction results in an unusual double insertion of the isocyanate in to the P–H bond of the phosphine, resulting in the formation of a new class of organophosphorus compounds (Scheme 3).[36] This chapter aims to build on this work and expand the use of this catalyst to more hydroelemenation reactions.



Scheme 3. Hydrophosphination of isocyanates catalysed by Fe(2,6-$Mes_2C_6H_3)_2$.[36]

2.2 Aims

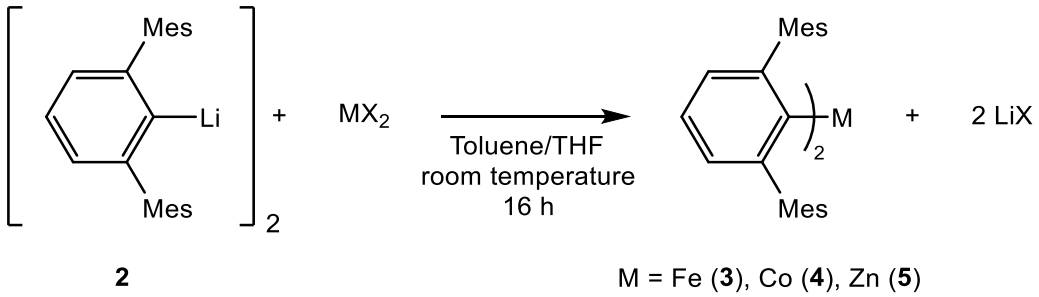
The aim of this work was to outline the synthesis of low-coordinate first row transition metal complexes using the bulky *m*-terphenyl ligand, and the investigation of their use as precatalysts for hydroamination and hydrophosphination of heterocumulenes. This work aimed to investigate whether multiple insertions of the isocyanate were possible (following the previously reported hydrophosphination of isocyanates) as a method to synthesise biurets. The direct transformation of amines to biuret derivatives had not been previously reported. The selectivity of the catalysis was investigated by altering the solvent and stoichiometry of the reaction and a range of different substrates was used to investigate the scope of the catalysts. The effect of the metal centre in the precatalyst was also investigated. Stoichiometric reactions and poisoning experiments were used to probe the mechanism of this catalysis.

2.3 Results and Discussion

2.3.1 Synthesis of *m*-Terphenyl Complexes

The *m*-terphenyl preligand 2,6-$Mes_2C_6H_3I$ (**1**) and the lithium salt [2,6-$Mes_2C_6H_3Li]_2$ (**2**) were synthesised according to literature methods.[38,39] The metal complexes M(2,6-$Mes_2C_6H_3)_2$ (M = Fe (**3**), Co (**4**), Zn (**5**)) were synthesised using a salt metathesis reaction that was first reported by Kays *et al.* in 2007.[40] The lithium salt **2** was reacted with the appropriate metal halide ($FeCl_2{\cdot}THF_{1.5}$, $CoBr_2$(DME) or $ZnCl_2$) in a mixture of toluene and THF and stirred overnight at room temperature (Scheme 4). The solvent was removed *in*

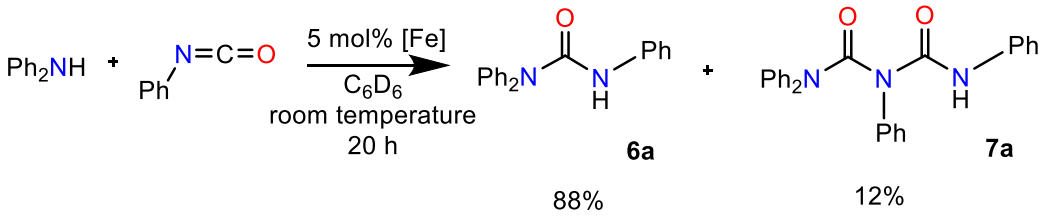
vacuo and the product was then extracted into hexane and crystallised from a saturated solution at −30 °C. This gave yields of 60–70%. The complexes were characterised using ^{1}H NMR spectroscopy which matched the reported literature data.[40,41]



Scheme 4. Synthesis of the metal complexes **3**–**5** (MX_2 = $FeCl_2{\cdot}THF_{1.5}$ (**3**), $CoBr_2$(DME) (**4**), $ZnCl_2$ (**5**)).

2.3.2 Hydroamination of Isocyanates

2.3.2.1 Hydroamination of Isocyanates with Diphenylamine



Scheme 5. Hydroamination of phenyl isocyanate with diphenylamine catalysed by **3** ([Fe] = **3**).

Initially diphenylamine was chosen to allow a direct comparison with diphenylphosphine which was used in the hydrophosphination of isocyanates with **3** and to allow the investigation of the diinsertion of the isocyanate to synthesise a biuret.[36] Table 1 shows the hydroamination of isocyanates with diphenylamine in the absence of a catalyst. There are only very small conversions with the reaction between diphenylamine and these isocyanates even when heated to 60 °C or after 10 days at room temperature.

Table 1. Hydroamination of isocyanates with diphenylamine in the absence of a catalyst.[a]

Entry	RNCO	Ph_2NH:R'NCO	Time	T (°C)	Conversion (%)[b]
1	Ph	1:1	24 h	60	5
2	3,5-$(MeO)_2C_6H_3$	1:1	10 days	25	7
3	4-BrC_6H_4	1:1	10 days	25	7

[a] Reaction conditions: 0.6 mL of C_6D_6. [b] Determined by ^{1}H NMR spectroscopy.

An NMR scale reaction was carried out between Ph_2NH and PhNCO with a catalyst loading of 5 mol% and a 1:1 ratio of Ph_2NH:PhNCO. A solution of 10 mg of **3** in 0.6 mL C_6D_6 was made up in a Young's NMR tube. The amine and isocyanate were then added to this solution. The reaction was monitored by ^{1}H NMR spectroscopy (Figure 2), which showed that the reaction reached 93% conversion after 20 h (Table 1, Entry 1). There was a small colour change from bright yellow to dark yellow. Initially, the N–H peak of the amine was at 5.02 ppm; this shifts downfield after 2 h to 5.41 ppm and decreases in size over time. After 20 h the peak has shifted to 5.57 ppm and becomes very small. This is accompanied by the appearance of two new peaks at 10.70 ppm and 6.37 ppm, which increase in size over time, and correspond to two new N–H signals. The conversion of the reaction was calculated from the integration of the N–H peak of the amine starting material compared with the N–H peak of the products using TMS as an internal standard.

These two new peaks can be assigned to the urea **6a** (6.37 ppm) and the biuret **7a** (10.70 ppm). The two products are obtained in a relative ratio of 88:12 with the major product being **6a**, and the minor product being **7a** (Scheme 5). The reaction only reaches 93% conversion with respect to the amine, which can be explained by the fact that a small amount of the biuret is formed which consumes two isocyanate molecules. This means that some of them are not available to add to a new amine molecule so some of the amine is left unreacted.

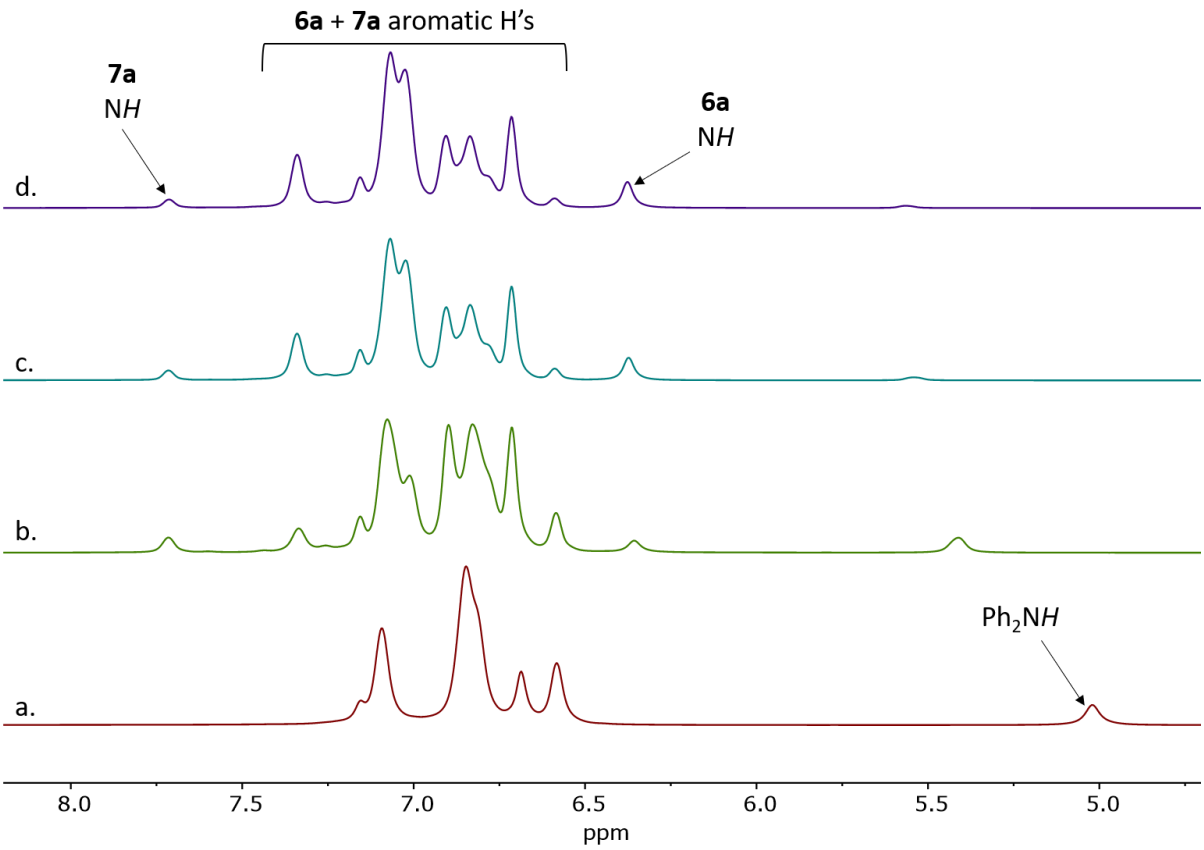


Figure 2. ^{1}H NMR spectra of reaction between Ph_2NH and PhNCO in the presence of 5 mol% **3** in C_6D_6 at 25 °C: a) Immediately after the substrates are added, b) 2 h, c) 12 h and d) 24 h.

The main focus of interest is the biuret **7a**, as this second insertion of the isocyanate has not been previously reported for the hydroamination of isocyanates. In an attempt to selectively form **7a**, a higher ratio of 1:2 Ph_2NH:PhNCO was used. This increased the formation of **7a** from 12% to 44%. Increasing the ratio even further to 1:5 Ph_2NH:PhNCO resulted in 71% conversion to **7a**. Heating this reaction to 60 °C led to completion in 4 h and increases the selectivity with 90% conversion to **7a** (Table 2, Entries 2–4).

In order to explore the scope of the reaction with aromatic isocyanates, both electron donating and electron withdrawing groups were used (Table 2, Entries 5–10). The reaction between Ph_2NH and 3,5-$(MeO)_2C_6H_3NCO$ with a 1:1 ratio resulted in the exclusive formation of the urea **6b**. When a 1:2 ratio was used the biuret **7b** was also observed (59%), and with the use of a 1:5 ratio **7b** is formed exclusively. The reaction reaches

completion after just 2 h at 60 °C (Table 2, Entries 5–7) which is slightly faster than the reaction with PhNCO.

Table 2. Catalytic hydroamination of isocyanates with diphenylamine mediated by **3**.[a]

Entry	RNCO	Ph_2NH: RNCO	T (°C)	t (h)	Conversion (%)[b]	**6**:**7**[b]
1	Ph	1:1	25	20	93	88:12
2	Ph	1:2	25	20	100	56:44
3	Ph	1:5	25	20	100	29:71
4	Ph	1:5	60	4	100	10:90
5	3,5-$(MeO)_2C_6H_3$	1:1	25	24	92	100:0
6	3,5-$(MeO)_2C_6H_3$	1:2	60	17	100	41:59
7	3,5-$(MeO)_2C_6H_3$	1:5	60	2	80	0:100
8	4-BrC_6H_4	1:1	25	96	80	100:0
9	4-BrC_6H_4	1:2	60	4	100	57:43
10	4-BrC_6H_4	1:5	60	4	100	2:98
11	^{i}Pr	1:1	60	4	96	100:0
12	^{t}Bu	1:1	25	3	92	100:0

[a] Reaction conditions: 10 mg of **3** (5 mol%), 0.6 mL of C_6D_6. [b] Determined by ^{1}H NMR spectroscopy using either 1,3,5-trimethoxybenzene or TMS as an internal standard.

When 4-BrC_6H_4NCO was used, the reaction was significantly slower at 25 °C, however full conversion was achieved after 4 h at 60 °C. As with the previous isocyanates, reactions with 4-BrC_6H_4NCO in a 1:5 ratio of Ph_2NH:RNCO showed enhanced selectivity for the diinsertion product **7c** (98%) (Table 2, Entries 8–10). This slower reaction at 25 °C is likely due to the electron withdrawing effect of the Br group which makes the isocyanate less activated.

When reactions containing excess isocyanate were left over several days, cyclotrimerisation of the unreacted isocyanates to isocyanurates was observed. This cyclotrimerisation reaction has been previously reported to be catalysed by Lewis bases,[42] and is therefore presumably catalysed by either the Ph_2NH substrate or the resulting urea products. This reaction is much slower than the desired hydroamination of isocyanates so is not observed on the timescale of the reaction monitoring, however most attempts to crystallise the reaction products resulted in the crystallisation of the isocyanurate (**10**) due to the lower solubility of the isocyanurate compared to the urea derivatives (Figure 3).

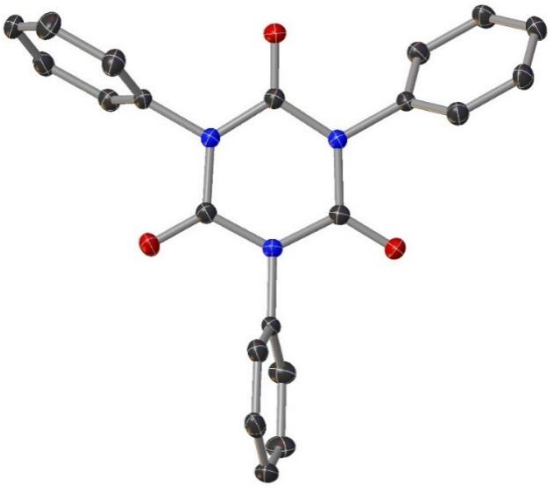


Figure 3. Crystal structure of **10**, with anisotropic displacement ellipsoids set at 50% probability. Hydrogen atoms and solvent molecule omitted for clarity (black = carbon, blue = nitrogen, red = oxygen).

It has been previously reported that for primary aliphatic isocyanate substrates, a competing cyclotrimerisation of the isocyanate affording isocyanurates is observed with **3**.[37] For this reason the secondary and tertiary aliphatic isocyanates ^{i}PrNCO and ^{t}BuNCO were focussed on in this study. For both isocyanates, the monoinsertion product (**6d** and **6f** respectively) is exclusively formed (Table 2, entries 11 and 12). There was no evidence for the formation of the diinsertion product, which is similar to that observed with the hydrophosphination of isocyanates catalysed by **3**.[36] This can be explained by the differences in sterics; the aromatic groups are more planar and rigid and are able to undergo multiple insertions, whereas the aliphatic groups are bulkier, preventing the

second insertion of the isocyanate into the N–H bond. The ^{1}H NMR spectra for the reaction between Ph_2NH and ^{t}BuNCO is shown in Figure 4. The peaks for the ^{t}Bu groups for both the amine and product are sharp singlets. The peak for ^{t}BuNCO appears at 1.05 ppm and the product peak appears at 1.35 ppm which can be observed appearing in the spectra almost immediately. The product N–H peak appears at 4.50 ppm as a broad singlet.

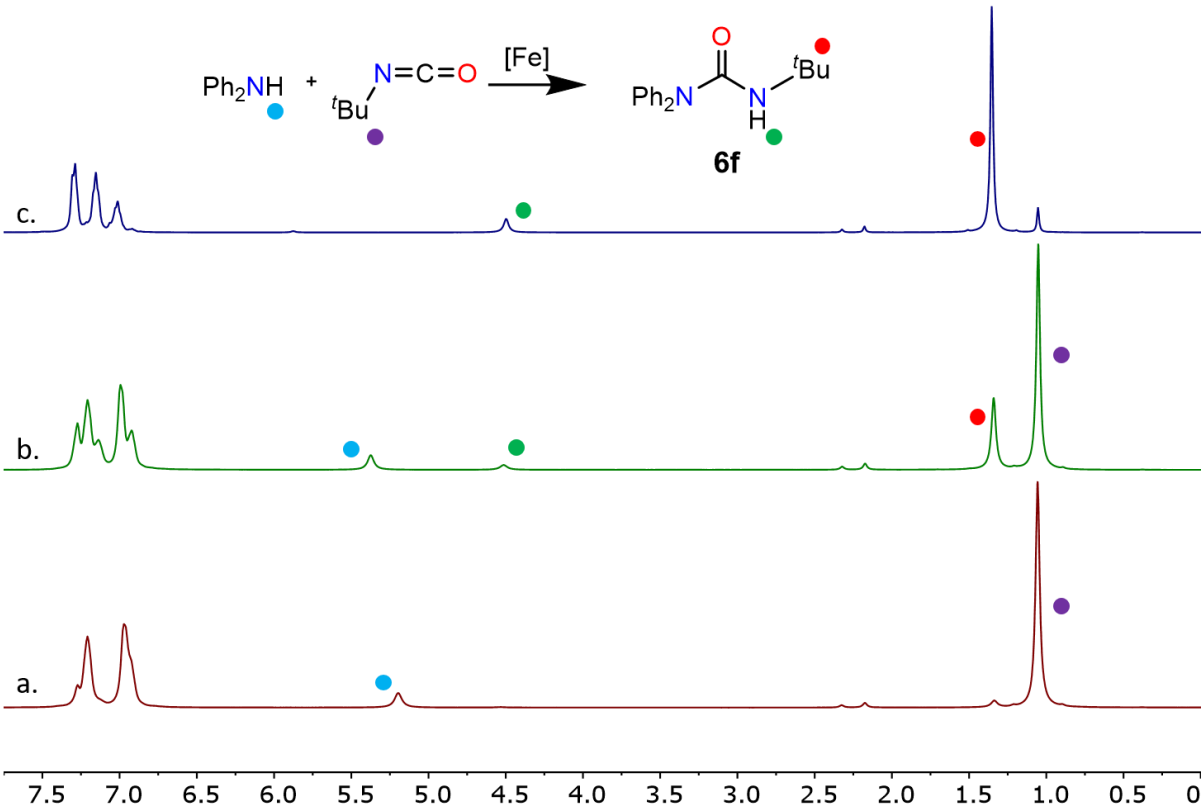


Figure 4. ^{1}H NMR spectra of reaction between Ph_2NH and ^{t}BuNCO in the presence of 5 mol% **3** in C_6D_6 at 25 °C: a) Immediately after the substrates are added, b) 5 h, c) 24 h.

2.3.2.2 Recycling the Catalyst

In order to test whether catalyst **3** could be recycled, a second loading of Ph_2NH and PhNCO was added to the NMR tube after the reaction had reached completion with a 1:1 Ph_2NH:PhNCO ratio. This resulted in the N*H* peak at 5.02 ppm becoming visible again in the ^{1}H NMR spectrum. This peak then gradually shifts downfield to 5.96 ppm after 20 h, as was observed previously and decreased in size indicating that the amine was being

consumed again. After 20 h the reaction had reached 80% conversion which is slightly lower than the first reaction which could indicate that the catalyst has partially decomposed. The product peaks are observed at 6.37 ppm (**6a**) and 10.70 ppm (**7a**). The ratio of the two products **6a**:**7a** is 85:15 which is similar to the ratio observed for the initial reaction (Table 2, Entry 1). This indicates that the catalyst is able to be recycled although separation of the catalyst from the products proved challenging (*vide infra* section 2.3.2.8).

2.3.2.3 Reaction Monitoring

The reaction between Ph_2NH and PhNCO (1:1) in C_6D_6 catalysed by **3** was monitored *in situ* by ^1H NMR spectroscopy in order to see how the conversion changed over time. The reaction was carried out in a similar way as previously described but the reaction was immediately frozen at −78 °C once all the reagents were added. This was to minimise the conversion before the NMR tube reached the spectrometer. The reaction was then allowed to warm to room temperature and the reaction was monitored by ^1H NMR spectroscopy for 22 h. The conversion of **6a** and **7a** was determined by integration of the N–H peaks (with TMS as an internal standard) and then plotted against time (Figure 5). As was previously stated the reaction reaches 93% conversion after 20 h. The first measurement was taken at 0.5 h and the conversion was at only 0.1%. Between 0 and 2 h the ratio of the two products **6a** and **7a** is approximately 50:50, however after this time the formation of **7a** reaches a plateau and the formation of **6a** continues to increase. This is due to the ratio of the starting materials being 1:1 so the formation of the biuret **7a** is not favoured, particularly as less of the isocyanate is available later in the reaction. After 20 h the ratio of **6a**:**7a** is 88:12.

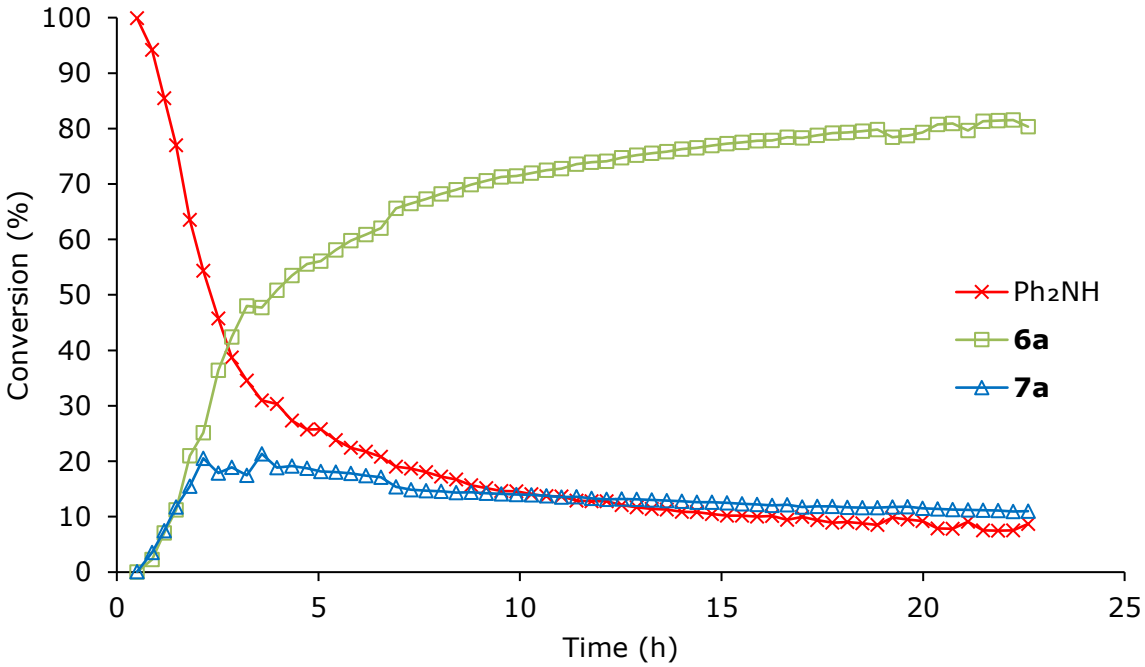
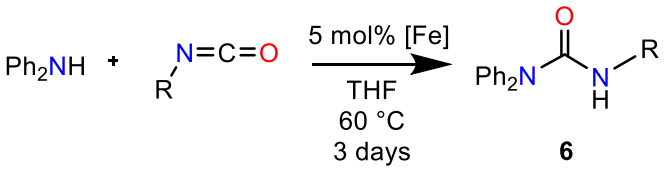


Figure 5. A graph showing conversion (%) *vs.* time (h) for the hydroamination of PhNCO with Ph_2NH in the presence of 5 mol% of **3** in C_6D_6 at 25 °C, as determined by ^1H NMR spectroscopy.

2.3.2.4 Hydroamination of Isocyanates in THF

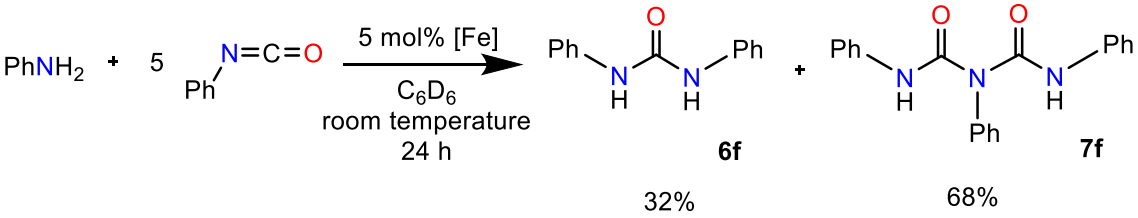
In order to investigate the effect of the solvent on the reaction, the solvent was changed from C_6D_6 to the more polar solvent THF. The reaction was carried out as before in a Young's NMR tube. Once the reaction had finished the solvent was removed *in vacuo* and then C_6D_6 was added to the resulting mixture and the ^1H NMR spectra was collected. The reaction with THF takes much longer to reach completion than the reaction in C_6D_6; 3 days at 60 °C compared to 20 h at room temperature. Similarly to the hydrophosphination of aromatic isocyanates with precatalyst **3**,[36] changing the solvent from C_6D_6 to THF results in the exclusive formation of the monoinsertion products **6a**–**6c** (Scheme 6). This exclusive formation of the urea and the longer reaction time suggests that the THF is coordinating to the catalyst, both preventing the second insertion of the isocyanate and slowing the reaction.



Scheme 6. Hydroamination of aromatic isocyanates in THF (R = Ph (**6a**), 3,5-$(OMe)_2C_6H_3$ (**6b**), 4-BrC_6H_4 (**6c**); [Fe] = **3**).

2.3.2.5 Hydroamination of Isocyanates with Different Amines

In order to increase the scope of the catalysis, two other amines were investigated. Diisopropyl amine and aniline were used to compare how an alkyl amine and a primary amine would influence the reaction. These amines react with PhNCO to give the ureas **6f** and **6g** respectively without the need for a catalyst. The reaction in the presence of **3** was undertaken in order to investigate whether **3** catalyses the diinsertion of the isocyanate. The reaction between $PhNH_2$ and PhNCO was carried out in the presence of 5 mol% **3** in C_6D_6 at room temperature with a 1:5 $PhNH_2$:PhNCO ratio (Scheme 7). After 24 h the reaction reached 100% conversion, which is a similar reaction time to Ph_2NH (Table 3, Entry 1). The biuret **7f** is the major product (68%) indicating that the presence of **3** results in the diinsertion of the isocyanate.



Scheme 7. Hydroamination of phenyl isocyanate with $PhNH_2$ catalysed by **3** ([Fe] = **3**).

Table 3. Catalytic hydroamination of isocyanates with aniline and diisopropylamine mediated by **3**.[a]

Entry	RR'NH	RR'NH: PhNCO	t (h)	Conversion (%)[b]	**6**:**7**:**8**:**9**[b]
1	$PhNH_2$	1:5	24	100	32:68:0:0
2	$^{i}Pr_2NH$	1:2	0.1	100	0:87:13:0
3	$^{i}Pr_2NH$	1:3	0.1	100	0:46:47:7
4	$^{i}Pr_2NH$	1:5	0.1	100	0:25:54:21

[a] Reaction conditions: 10 mg of **3** (5 mol%), 0.6 mL of C_6D_6 at 25 °C. [b] Determined by ^{1}H NMR spectroscopy.

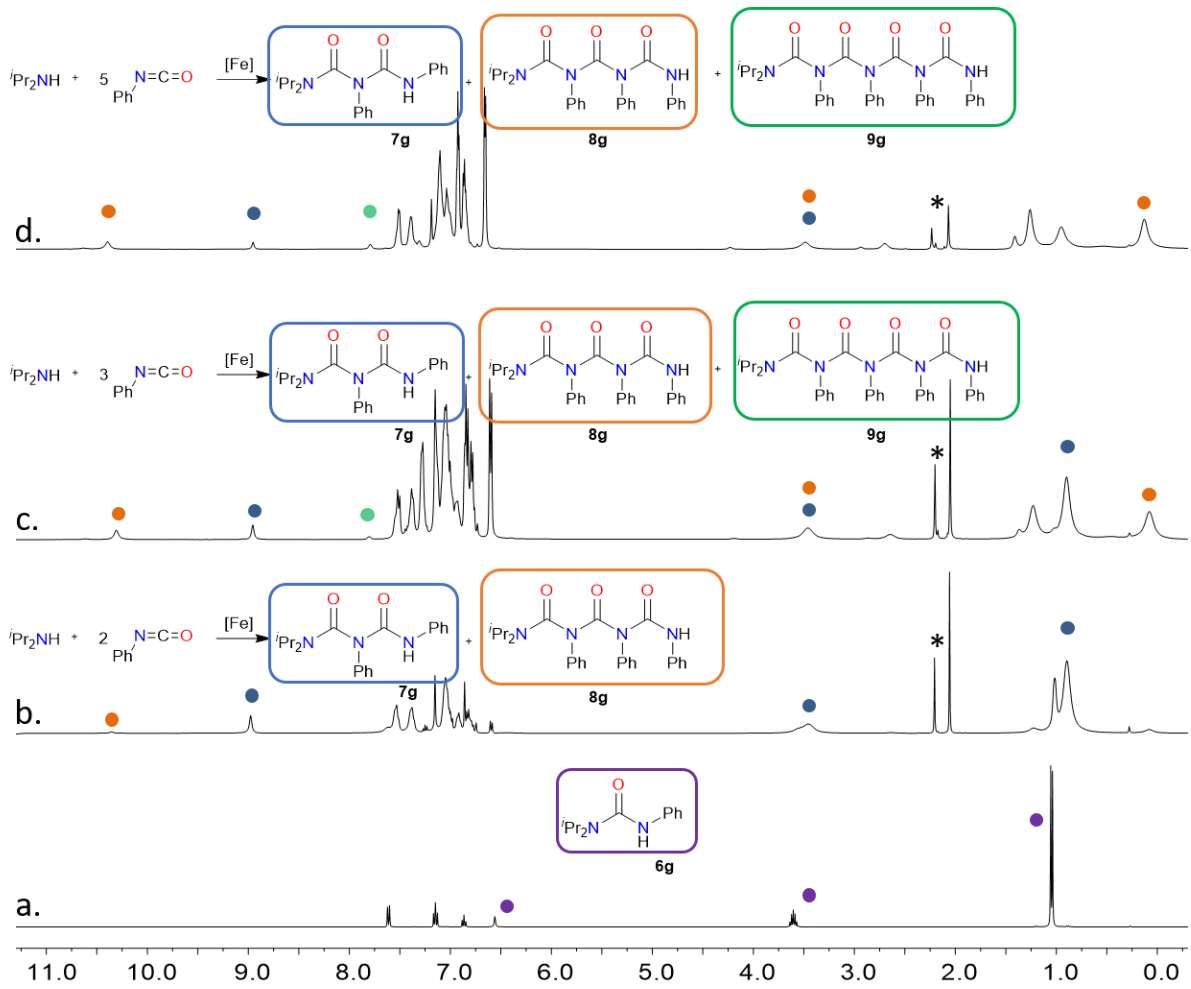


Figure 6. ^{1}H NMR spectra of reactions between $^{i}Pr_2NH$ and PhNCO in the presence of **3** in C_6D_6 at 25 °C ([Fe] = **3**): a) without catalyst, $^{i}Pr_2NH$:PhNCO 1:1, 1 h at 25 °C in C_6D_6; b) $^{i}Pr_2NH$:PhNCO 1:2, 10 min with 5 mol% of **3** at 25 °C in C_6D_6; c) $^{i}Pr_2NH$:PhNCO 1:3, 10 min at 25 °C with 5 mol% of **3** at 25 °C in C_6D_6; d. $^{i}Pr_2NH$:PhNCO 1:5, 10 min at 25 °C with 5 mol% of **3** at 25 °C in C_6D_6) (* indicates Mes peaks from 2,6-$Mes_2C_6H_3$ ligand).

In the absence of a catalyst, the reaction between $^{i}Pr_2NH$ and PhNCO affords the urea **6g** at 25 °C in 10 min. However, in the presence of 5 mol% of **3**, **6g** is not observed. Instead, the diinsertion product **7g** is the major product. There is also another small N–H peak at 10.36 ppm which was identified as the triuret **8g**. When the ratio of $^{i}Pr_2NH$:PhNCO ratio is increased to 1:3 the tetrauret (**9g**) is also observed at 7.76 ppm and increasing the $^{i}Pr_2NH$:PhNCO ratio even further to 1:5 increases the ratio of the tetrainsertion product formed. These products were identified by ^{1}H, $^{13}C\{^{1}H\}$ and DOSY NMR spectroscopy and mass spectrometry (Figure 6). The DOSY NMR spectra were used to assign the different peaks in the ^{1}H NMR spectrum. DOSY NMR spectroscopy is used to identify different components in a mixture according to the diffusion coefficient.[43,44] The hydrodynamic radius can be calculated from the diffusion coefficient using the Stokes-Einstein equation:

$$D = \frac{k_b T}{6\pi\eta r}$$

where,

D = Diffusion coefficient

k_B = Boltzmann constant

T = temperature

$\boldsymbol{\eta}$ = dynamic viscosity of solvent

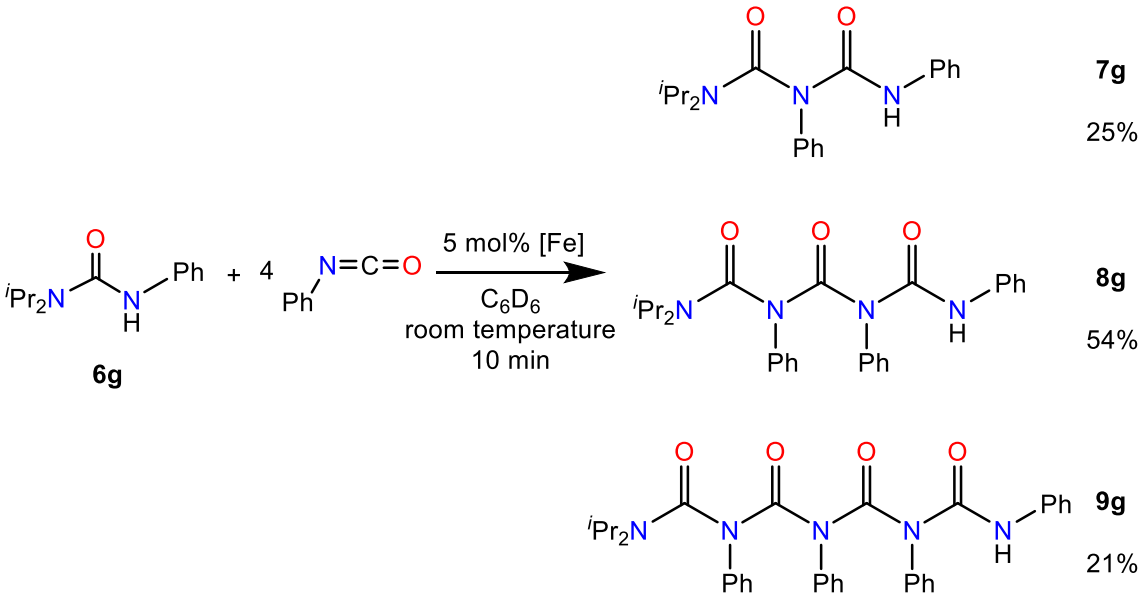
r = hydrodynamic radius

Table 4 shows the measured diffusion coefficient and the calculated hydrodynamic radius for each N–H peak in the DOSY NMR spectra. The hydrodynamic radius will increase as the chain length increases so the peaks could be assigned from the hydrodynamic radius. This meant that the ratios of the products could be calculated (Table 3, Entries 2–4).

Table 4. Diffusion coefficients obtained from DOSY NMR spectroscopy in C_6D_6 (25 °C).

Substrate	Chemical Shift of N*H* (ppm)	Diffusion Coefficient (m^2s^{-1})	Hydrodynamic Radius (m)
6g	6.22	$8.60x10^{-10}$	$4.21x10^{-10}$
7g	9.03	$4.99x10^{-10}$	$7.26x10^{-10}$
8g	10.36	$4.53x10^{-10}$	$7.99x10^{-10}$
9g	7.76	$4.25x10^{-10}$	$8.52x10^{-10}$

The reaction was also carried out using the urea **6g** as the starting material instead of the amine, with a 1:4 **6g**:PhNCO ratio (Scheme 8). The reaction reached 100% conversion to the polyinsertion products in 10 min at room temperature with a similar product distribution to the 1:5 reaction between $^{i}Pr_2NH$ and PhNCO. Efforts to separate these products were unsuccessful (see section 2.3.2.9).



Scheme 8. Hydroamination of PhNCO with **6g** in the presence of **3** ([Fe] = **3**).

There are very few reported synthetic routes to these compounds in the literature and they generally require high temperatures and pressures.[45–47] The synthesis of these molecules under such mild conditions is promising for the future development of species

with multiple amide functionalities. These molecules have many potential applications in natural products,[48] drugs[49,50] and polymers.[51–53]

2.3.2.6 Hydroamination of Isocyanates in the Presence of Additives

The catalysis was conducted in the presence of different additives (Table 5). It has been previously reported that the addition of a weak acid such as NEt_3·HCl, results in the selective formation of the diinsertion product for the hydrophosphination of isocyanates with **3**.[36] In order to see if this was also observed for the hydroamination of isocyanates, an NMR-scale reaction between Ph_2NH and PhNCO (1:2) in the presence of **3** (5 mol%) and NEt_3·HCl in C_6D_6 was carried out. The reaction proceeded at a similar rate to that without the weak acid present, and the ratio of **6**:**7** was 54:46 compared with 56:44 without the weak acid (Table 2, Entry 2 and Table 5, Entry 1). This indicates that the addition of a weak acid has very little effect on the product distribution. The formation of the diinsertion product in the hydrophosphination of isocyanates is hydrophosphination followed by the hydroamination of the monoinsertion product. The addition of the weak acid favours this second step leading to the selective formation of the diinsertion product. However with the hydroamination of isocyanates, the formation of the diinsertion product is hydroamination followed by a second hydroamination so the weak acid does not favour one step over another and the product distribution does not change.

In order to determine whether the catalysis was heterogeneous or homogeneous, a poisoning experiment[54,55] was carried out using Hg(0) (Table 5, Entry 2). The Hg(0) drop test indicates whether the catalysis proceeds *via* a homogeneous or heterogeneous mechanism, as Hg(0) has been shown to selectively poison heterogeneous catalysts because Hg(0) forms an amalgam and inhibits the reaction.[54,55] The Hg(0) drop test is not conclusive for iron as Hg(0) does not always form an amalgam with iron however there are some reported examples where this does happen.[56,57] CS_2 can be used as an alternative to Hg(0).[55,58] This is a small ligand which can coordinate to the metal and poison the catalyst. If the reaction is heterogeneous then only a fraction of the active sites

are available on the surface of the particles. If the reaction is slowed with only 0.1 equivalents of the ligand with respect to the catalyst this suggests that all the active sites have been blocked and it is a heterogeneous catalysis whereas a homogeneous catalyst would only be inhibited with at least 1 equivalent of CS_2. The phosphine $PPhMe_2$ can be used in a similar way to CS_2.[59] In all of these poisoning experiments, the reaction reached similar conversions to those without the poison, which suggests that the catalysis is proceeding through a homogeneous pathway (Table 5, entry 2–4). No visible metal precipitate or darkening of the solution was observed during the reaction, which further supports a homogeneous mechanism.

Table 5. Catalytic hydroamination of isocyanates mediated by **3** in the presence of additives.[a]

Entry	RNCO	Ph_2NH: RNCO	Additive	T (°C)	t (h)	Conversion (%)[b]	**6**:**7**[b]	Amount of Additive
1	Ph	1:2	NEt_3·HCl	25	24	84	54:46	0.146 mmol
2	Ph	1:1	Hg(0)	25	20	85	90:10	*ca*. 1 drop
3	^{t}Bu	1:1	CS_2	25	5	90	100:0	0.001 mmol
4	^{t}Bu	1:1	$PPhMe_2$	25	3	93	100:0	0.007 mmol
5	Ph	1:1	Cumene	25	6	83	78:22	0.073 mmol

[a] Reaction conditions: 10 mg of **3** (5 mol%), 0.6 mL of C_6D_6. [b] Determined by ^{1}H NMR spectroscopy.

The catalysis was also performed in the presence of cumene, which can act as a radical trap (Table 5, Entry 5).[60] A longer reaction time would indicate that the catalysis undergoes a radical mechanism. The addition of cumene does not affect the reaction time, suggesting that the reaction does not proceed *via* a radical mechanism.

2.3.2.7 Stoichiometric Studies

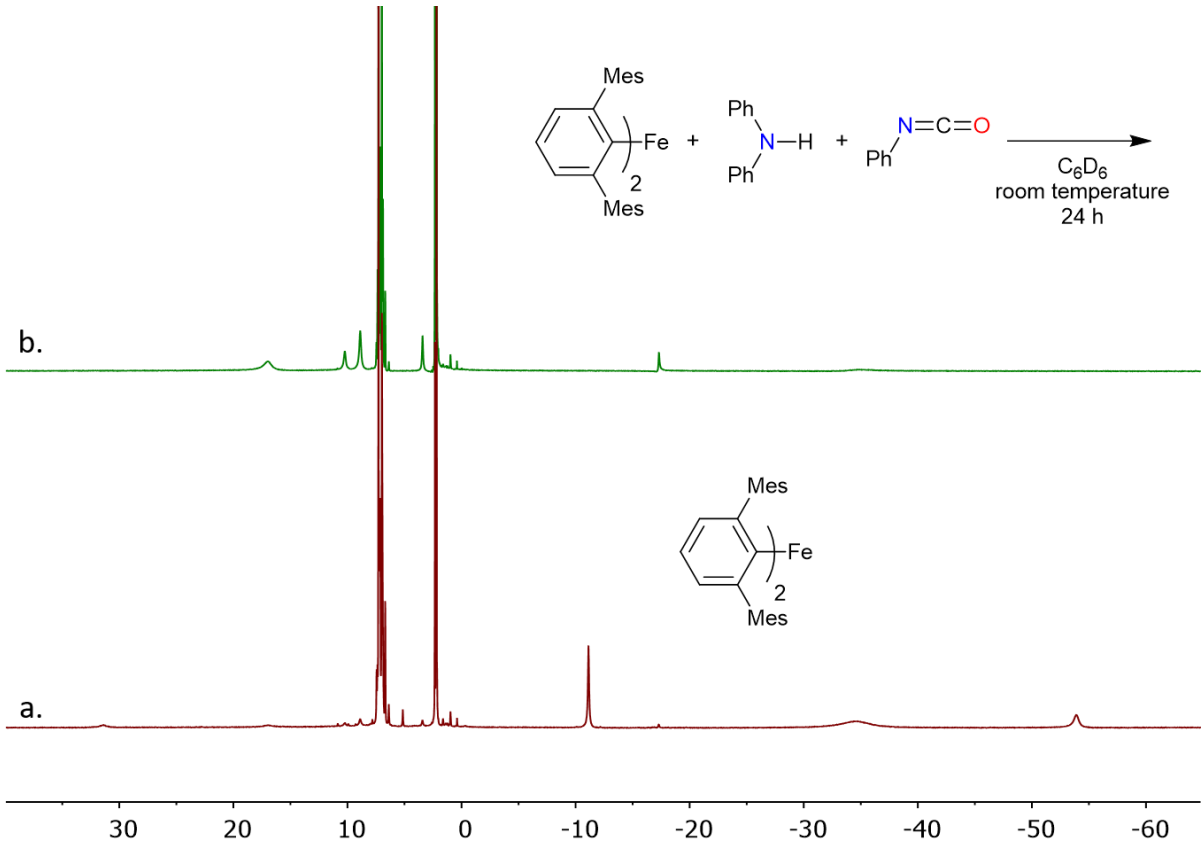


Figure 7. ^{1}H NMR spectra of stoichiometric reaction between **3** and Ph_2NH and PhNCO in C_6D_6; a) Before substrates added, b) After 24 h at room temperature.

The poisoning experiments discussed previously indicate that the reaction is homogeneous. In order to further investigate the mechanism of this catalysis, a stoichiometric reaction between **3**, Ph_2NH and PhNCO was performed on an NMR scale. A 1:1:2 ratio of **3**:Ph_2NH:PhNCO was dissolved in C_6D_6. This reaction resulted in a colour change from a bright to pale yellow solution. In the ^{1}H NMR spectrum, the paramagnetically-shifted peaks for **3** at 31, –11, –35 and –54 ppm were no longer present and new peaks were observed at –17, 8, 10 and 17 ppm, indicating that **3** had transformed into a new paramagnetic species, possibly the active catalyst (Figure 7). This change is not observed when either Ph_2NH or PhNCO alone is added to **3**. The same peaks were also observed when the urea **6a** is added to **3** suggesting that it could be relating to the urea coordinating to the iron centre. One possible mechanism for hydroamination reactions is

via the formation of a metal amide.[61,62] This would result in the formation of protonated ligand and no protonated *m*-terphenyl ligand was observed in these stoichiometric NMR spectra or in the reaction monitoring NMR spectra so this mechanism was discounted.

An attempt was made to characterise this reaction mixture using mass spectrometry, however only the precatalyst **3** and protonated ligand were identified. Attempts to crystallise this compound from saturated solutions of hexane, toluene or C_6D_6 at either room temperature or –30 °C were also unsuccessful.

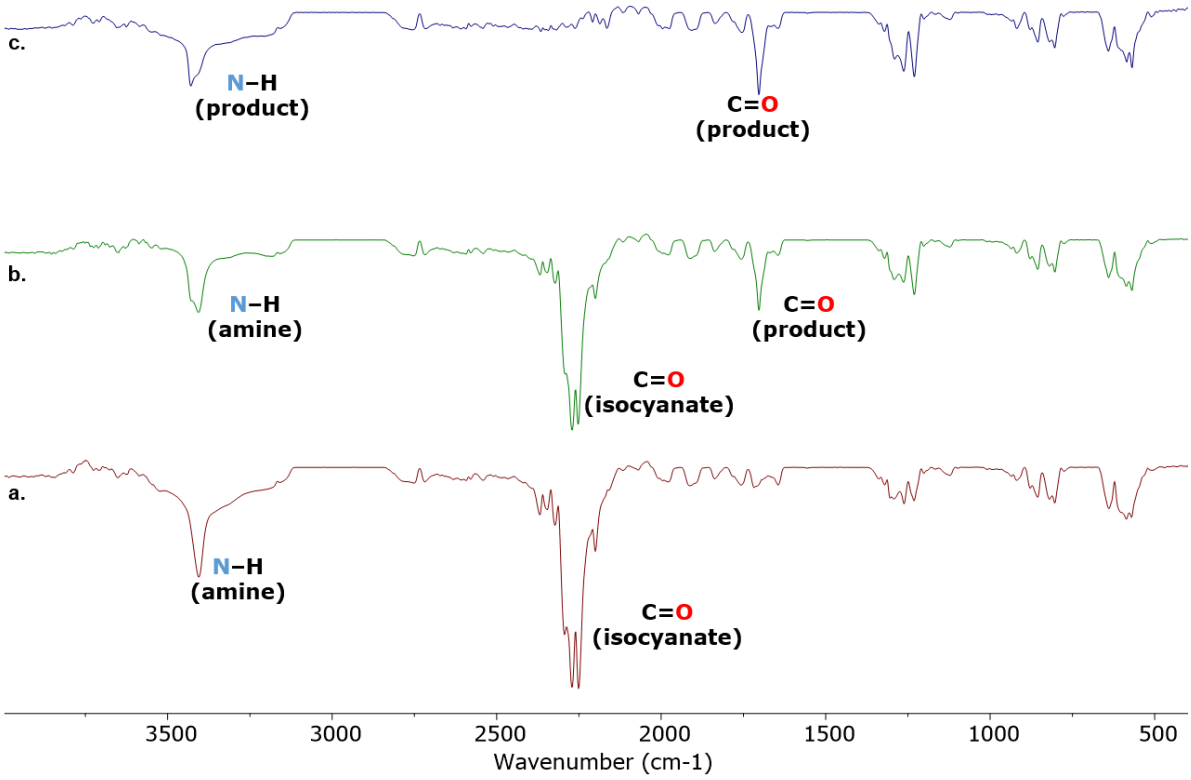


Figure 8. IR spectra of stoichiometric reaction between **3**, Ph_2NH and PhNCO in toluene; a) 15 min, b) 2 h, c) 18 h.

A stoichiometric reaction was also carried out on a larger scale in toluene. Aliquots were taken and the IR spectra of the solution was measured. Monitoring this reaction by IR spectroscopy revealed the loss of N–H and C=O stretches from the substrates, and the formation of a new C=O stretch at 1702 cm^{-1} for the new urea product (Figure 8). No iron-containing species was identified.

This stoichiometric reaction was also analysed by UV-vis spectroscopy. The UV-vis spectrum of a solution containing **3**, Ph_2NH and PhNCO showed a very strong absorbance between 300 and 400 nm with shoulders at λ_{max} = 356, 368 and 380 nm and another peak at 410 nm (Figure 9). This was not a significant change to the UV-vis spectrum of **3**.[40] This is likely because the UV-vis transitions are dominated by the aromatic *m*-terphenyl ligands meaning that any change to the iron species is not shown.

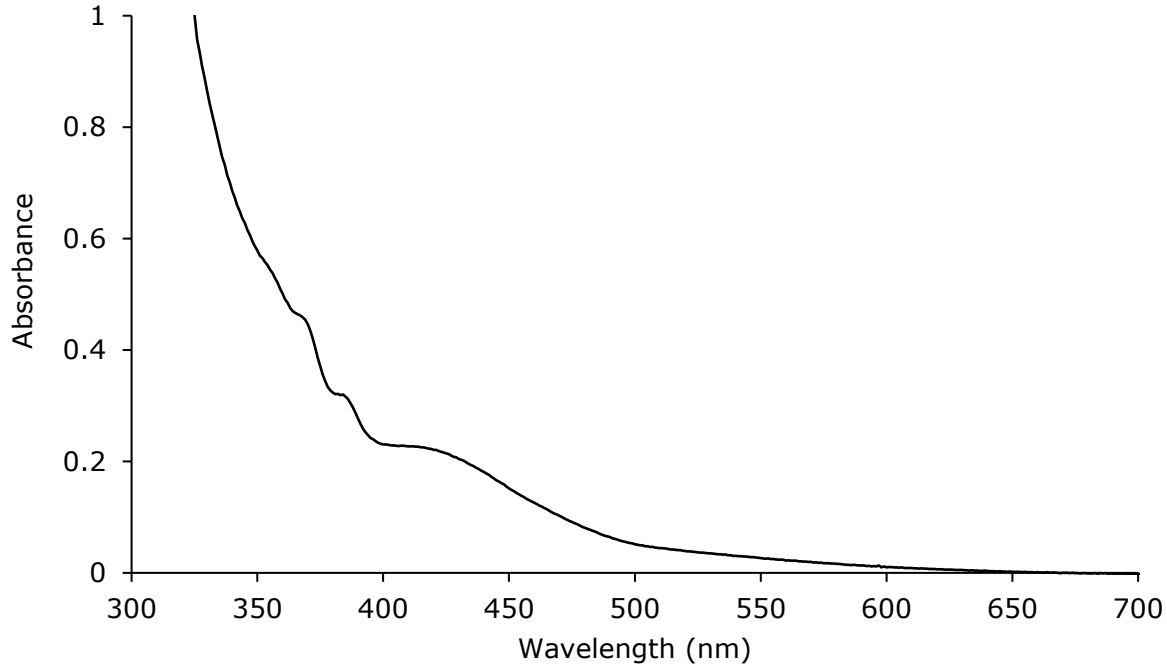
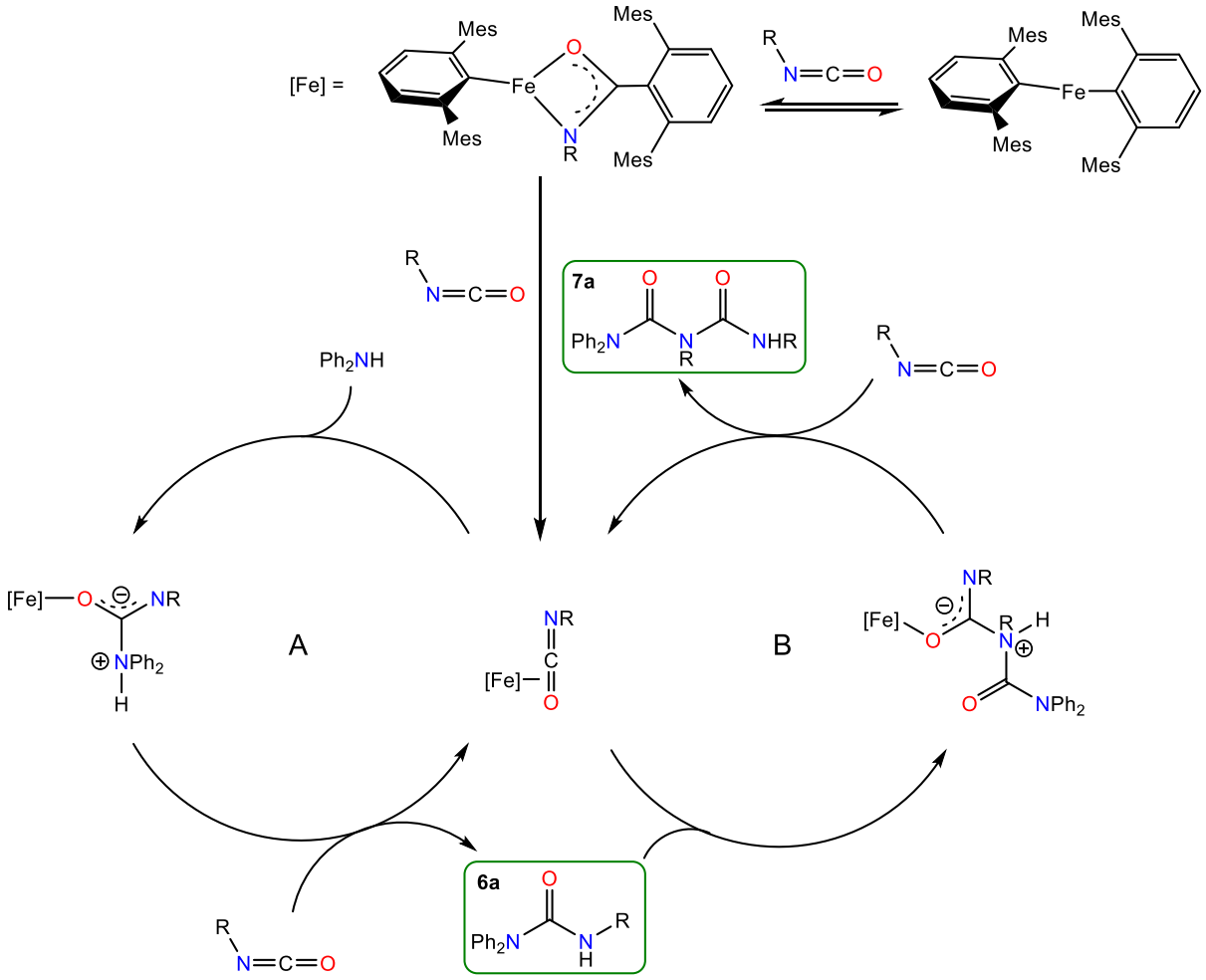


Figure 9. UV-vis spectrum of the stoichiometric reaction between **3**, Ph_2NH and PhNCO in hexane.

These investigations were not conclusive in identifying an active species for this reaction, however the catalysis has very similar characteristics to the previously reported hydrophosphination of isocyanates.[36] and so a similar mechanism can be envisioned for the hydroamination of isocyanates (Scheme 9). The isocyanate is first coordinated to the metal centre and the amine undergoes a nucleophilic attack on the isocyanate. There is then a 1,3-proton shift and the urea product is displaced by a new isocyanate molecule coordinating to the metal centre. The urea can then enter cycle B by undergoing a nucleophilic attack and another 1,3-proton shift to form the biuret. The multiple insertions

of the isocyanate that are observed with the use of diisopropylamine can be envisioned to take place with further cycles.



Scheme 9. Proposed mechanism for the hydroamination of isocyanates catalysed by **3**.

2.3.2.8 Isolation of Ureas and Biurets

The separation of the catalyst from the urea and biuret products proved challenging. Initially attempts were made to isolate the products from the NMR scale reactions. This was done by removing the solvent *in vacuo* and then extracting into small amounts (<5 mL) of either toluene or hexane. These solutions were then stored at –30 °C and a white precipitate formed which was found to be the urea or biuret. This was mostly successful although the yields were very low in most cases for the ureas **6a**–**e** (23–55%) and particularly for the biurets **7b** (14%) and **7c** (16%). This is due to the higher solubility

of the catalyst compared to the urea and biuret in most organic solvents so small impurities of the catalyst were often carried through and only small amounts of the desired product goes into the solution. An alternative method of purification using a silica plug was used in the scale up reactions and is discussed in the next section.

2.3.2.9 Scale-Up Reactions

A scaled-up reaction was carried out in toluene. 50 mg of **3** (5 mol%) was used compared with 10 mg for the NMR scale reactions. PhNCO was added to a solution of **3** and Ph_2NH in toluene and then stirred at room temperature (1:5 Ph_2NH:PhNCO). Aliquots were taken and the ^1H NMR spectrum was measured every hour to measure the conversion. The reaction reached completion after 3 hours and the solvent was removed *in vacuo* to give a brown oily solid. The product was opened to air (resulting in the decomposition of the catalyst) and extracted into CH_2Cl_2 to remove any iron oxides. The crude product was then passed through a silica plug with CH_2Cl_2/hexane (25:75) to remove any impurities (primarily protonated *m*-terphenyl ligand). The product was then removed from the silica with acetone. This resulted in the isolation of the biuret **7a** in a 77% yield. An attempt was made to crystallise this sample from the slow evaporation of toluene over several weeks. This instead resulted in the crystallisation of the isocyanurate **10** suggesting that the biuret is not stable in solution over long periods of time and eventually decomposes giving the isocyanate which then undergoes cyclotrimerisation to the isocyanurate.

A scale up reaction was also carried out in THF using 30 mg of **3** (5 mol%). PhNCO was added to a solution of **3** and Ph_2NH in THF (1:1 Ph_2NH:PhNCO). The reaction mixture was heated to 60 °C for 3 days. The product was then isolated using a similar method as for above resulting in a 61% yield of **6a**.

This method using a silica plug was successful in separating the product from any iron species and protonated *m*-terphenyl ligand, however it does have some disadvantages. The main disadvantage is that it requires exposing the reaction mixture to air which causes the catalyst to decompose. This means that the catalyst is not be able to be recycled which

would be useful for future applications. This method is also not useful for reactions where multiple urea/biuret derivatives are formed (*e.g.* the reactions between $^{i}Pr_2NH$ and PhNCO) as all of the products would remain on the silica and would all come off with the acetone wash so it would remain a mixture of products.

2.3.2.10 Hydroamination of Isocyanates Catalysed by 4 and 5

In order to investigate the effect of the metal centre on the catalysis, the reaction between Ph_2NH and PhNCO was carried out in the presence of $Co(2,6\text{-}Mes_2C_6H_3)_2$ (**4**) with a catalyst loading of 5 mol% (Table 6, Entry 1). After 2 h there was a colour change from dark red to turquoise and some black precipitate had formed, which may be due to the decomposition of the catalyst with concomitant formation of Co(0). The ^{1}H NMR spectrum showed that a small peak had appeared at 10.77 ppm which is the N–H peak of the biuret **7a** (20%) but the major product was **6a** (80%). The ratio of the two products was similar to that observed for **3**. The reaction only had a conversion of 79% after more than a week, which is likely due to the decomposition of the catalyst.

Table 6. Hydroamination of isocyanates catalysed by **4** or **5**.[a]

Entry	Catalyst	RNCO	Ph_2NH: RNCO	T (°C)	t	Conversion (%)[b]	**6**:**7**[b]
1	**4**	Ph	1:1	25	8 days	79	80:20
2	**5**	Ph	1:1	60	17 h	36	86:14

[a] Reaction conditions: 10 mg of **4** or **5** (5 mol%), 0.6 mL of C_6D_6. [b] Determined by ^{1}H NMR spectroscopy using TMS as an internal standard.

The potential of $Zn(2,6\text{-}Mes_2C_6H_3)_2$ (**5**) as a catalyst was also investigated with the same method as above (Table 6, Entry 2). No difference was seen in the ^{1}H NMR spectrum at room temperature after 4 h. However, after heating to 60 °C for 17 h, a small peak at 10.78 ppm appears indicating the formation of the biuret product. The N–H peak of the

diphenylamine starting material shifts downfield from 5.02 ppm to 5.36 ppm. This peak is still quite large with a conversion of only 36% suggesting that the reaction occurs very slowly even at this higher temperature. This suggests that the catalysis is not simply Lewis acid catalysed.[63] This was also confirmed when the reaction was carried out in the presence of $FeCl_2$. No reaction was observed suggesting that the *m*-terphenyl ligand does play some role in the catalysis as if the reaction was purely Lewis acid catalysed then $FeCl_2$ would also catalyse the reaction. The slower reaction with the Zn(II) complex is likely due to the full d^{10} orbital which makes it less activated compared to the d^6 Fe(II) complex.

2.3.3 Hydroamination of Other Substrates

In order to expand on the scope of the catalyst other substrates were investigated. Both isothiocyanates (R–N=C=S) and carbodiimdes (R–N=C=N–R) were chosen as other catalysts for the hydroamination of isocyanates have been shown to also catalyse reactions with these substrates.[16,22] When both Ph_2NH and PhNCS were added to a Young's NMR tube containing a solution of **3** (5 mol%) in C_6D_6, no change to the ^1H NMR spectrum was observed indicating that no reaction has taken place (Table 7, Entry 1). A black solid was observed in the yellow reaction solution after 1 h. This is also observed when PhNCS is added on its own to **3**. This suggests that the PhNCS is reacting with the catalyst, with likely reduction of Fe(II) to Fe(0).

Table 7. Hydroamination of heterocumulenes mediated by **3**.[a]

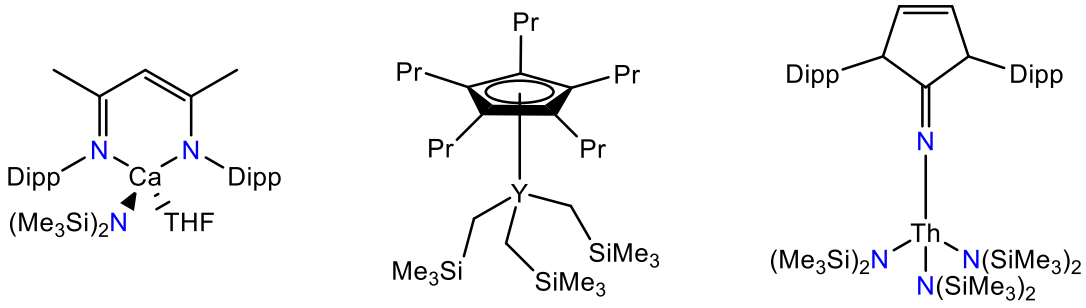
Entry	R_2NH	Heterocumulene	Time (h)	T (°C)	Conversion (%)[b]
1	Ph	PhNCS	48	60	0
2	Ph	PhNCNPh	48	60	0

[a] Reaction conditions: 10 mg of **3** (5 mol%), 0.6 mL of C_6D_6. [b] Determined by ^1H NMR spectroscopy.

The carbodiimide PhNCNPh was also used however no reaction was observed even after heating to 60 °C, although it was observed *via* ^{1}H NMR spectroscopy that the catalyst still remained intact and did not decompose (Table 7, Entry 2). This lack of reactivity compared to that observed for the analogous isocyanate reactions is likely due to carbodiimides being less reactive compared to isocyanates. This has been observed previously in the literature.[17]

2.3.4 Hydrophosphination of Carbodiimides

Although this catalyst was not successful for the hydroamination of carbodiimides, the catalyst was also investigated for the hydrophosphination of carbodiimides. This reaction is used to synthesise phosphaguanidines which are used as building blocks for ligands in transition metal complexes.[64–66] There are few examples of catalysts for this reaction in the literature and these are limited to s-block and f-block metals (Figure 10).[21,67–69] In all cases, only the monoinsertion of the carbodiimide takes place. The diinsertion of the carbodiimides is not observed.

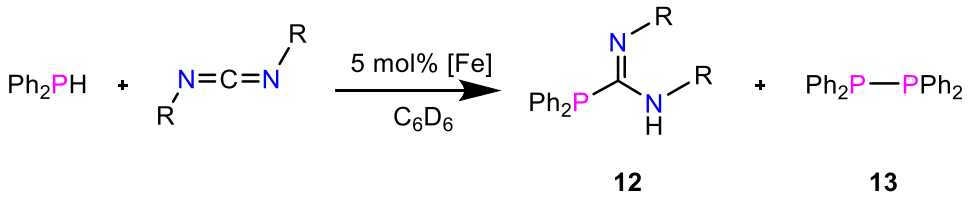


Hill, **2008** Zhang, **2015** Eisen, **2015**

Figure 10. Examples of catalysts for the hydrophosphination of carbodiimides.[21,67,68]

2.3.4.1 Iron Catalysed Hydrophosphination of Carbodiimides

There are very few commercially available carbodiimides. *N*,*N*'-dicyclohexylcarbodiimide (DCC, CyNCNCy) and *N*,*N*'-diisopropylcarbodiimide (DIC, ^{i}PrNCN^{i}Pr) are the two most widely available options and are both used in organic synthesis.[70,71] Initially, CyNCNCy was used to test the suitability of catalyst **3** for the hydrophosphination of isocyanates. A control reaction between Ph_2PH and CyNCNCy was carried out in the absence of a catalyst and no change in the ^{31}P NMR spectra is observed after heating to 60 °C for 24 h, indicating that this reaction does not proceed in the absence of a catalyst. An NMR scale reaction was carried out in C_6D_6 with 5 mol% of **3**. The reaction was monitored by ^{1}H and ^{31}P NMR spectroscopy (Figure 11). The reaction solution gradually turns from bright yellow to a very dark orange-brown colour. The Ph_2PH has a broad peak in the $^{31}P\{^{1}H\}$ NMR spectrum at –38.8 ppm. After 2 h two new peaks at –18.2 ppm and –15.0 ppm appeared with a ratio of 98:2. The minor peak at –15.0 ppm can be assigned to the dehydrocoupling product $Ph_2P–PPh_2$ which is a common side product in these reactions.[36] The major peak at –18.2 ppm corresponds to the phosphaguanidine **12a** which is formed from the monoinsertion of the carbodiimide into the P–H bond (Scheme 10).[72] No diinsertion reaction was observed. This is consistent with the previously reported hydrophosphination of CyNCO with **3**.[36] An attempt was made to form the diinsertion product by increasing the ratio to 1:2 and 1:5 Ph_2PH:CyNCNCy but this had no effect on the ratio of products formed (Table 8, Entries 2–3).



Scheme 10. Catalytic hydrophosphination of RNCNR using Ph_2PH (1:1) mediated by **3** in C_6D_6 (R = Cy (**12a**), ^{i}Pr (**12b**), Ph (**12c**)); ([Fe] = **3**).

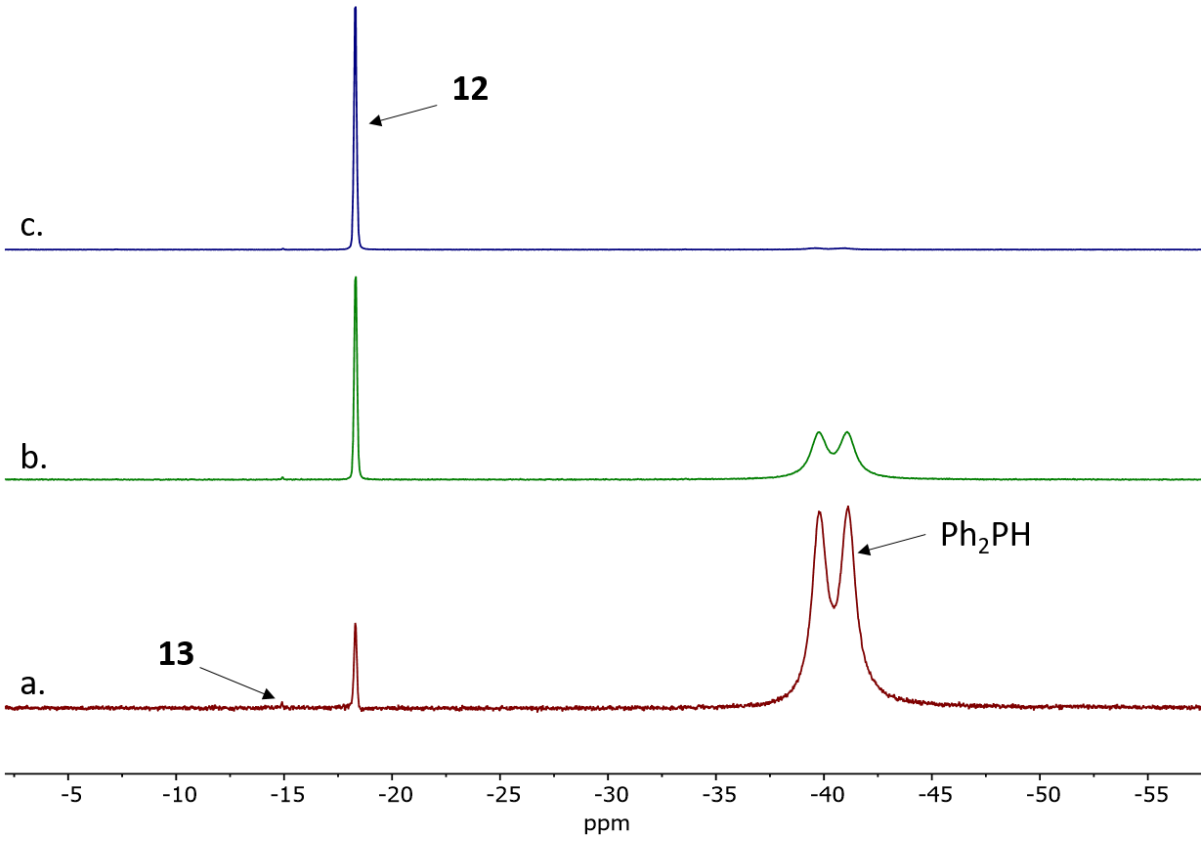


Figure 11. ^{31}P NMR spectra of the hydrophosphination of CyNCNCy with Ph_2PH (1:1) mediated by **3** (5 mol%) in C_6D_6 at room temperature; a) 30 min, b) 3 h, c) 20 h.

Table 8. Hydrophosphination of carbodiimides catalysed by **3**.

Entry	RNCNR	Ph_2PH: RNCNR	T (°C)	t (h)	Conversion (%)[b]	**12**:**13**[b]
1	Cy	1:1	25	20	95	98:2
2	Cy	1:2	25	20	100	98:2
3	Cy	1:5	25	24	97	98:2
4	^{i}Pr	1:1	60	3	97	99:1
5	Ph	1:1	60	18	100	99:1
6	Ph	1:2	60	24	85	77:1:22[c]
7	^{t}Bu Et	1:1	60	24	96	95:5

[a] Reaction conditions: 10 mg of **3** (5 mol%), 0.6 mL of C_6D_6. [b] Determined by ^{31}P NMR spectroscopy. [c] Other unidentified peaks.

The analogous reaction using ^{i}PrNCN^{i}Pr as a substrate reached 97% conversion after just 3 h at 60 °C (Table 8, Entry 4). The $^{31}P\{^{1}H\}$ NMR spectrum had a new peak at −18.6 ppm which corresponds to the analogous monoinsertion of the carbodiimide (**12b**) that was observed with CyNCNCy.

In order to investigate if the diinisertion reaction that is observed with isocyanates would occur with carbodiimides, an aromatic carbodiimide, PhNCNPh (**11**), was chosen as the substrate in order to provide a direct comparison with the PhNCO reaction. PhNCNPh was synthesised by reducing *N*,*N'*-diphenylthiourea using HgO.[73]

The hydrophosphination of PhNCNPh was performed in a Young's NMR tube in the presence of **3** (5 mol%) in C_6D_6 solution with a 1:1 Ph_2PH:PhNCNPh ratio (Table 8, Entry 5). The reaction reached 100% conversion after 18 h at 60 °C. The major product (99%) was observed in the ^{31}P NMR spectrum at −11.4 ppm and was assigned as the phosphaguanidine **12c**.[72] The only other peak in the ^{31}P NMR spectrum is at −15 ppm which is $Ph_2P–PPh_2$. This is in contrast to the catalysis with isocyanates where even with a 1:1 ratio, a third peak was observed for the product resulting from the diinsertion of the isocyanate into the P–H bond.[36] This is likely to be less favoured for the carbodiimide due to the steric bulk of the second R group.

The reaction with PhNCNPh was repeated using a 1:2 Ph_2PH:PhNCNPh ratio to probe if any diinsertion of the carbodiimide occurs (Table 8, Entry 6). This reaction reached 85% conversion after 24 h at 60 °C, and the major product remained **12c** (77%) at −11.4 ppm, but this was accompanied by the formation of multiple new peaks in the ^{31}P NMR spectrum (Figure 12). There is a peak at 42.8 ppm which is in the region where phosphine oxides are generally observed, however this chemical shift does not correspond to diphenylphosphine oxide or the oxide of **12c**. There are also four new peaks between –1 and 7 ppm which is the region where the phosphaguanidine products from the analogous diinsertion reactions for isocyanates are observed,[36] so it is possible that one of these peaks results from the diinsertion of the carbodiimide. These peaks are all singlets in the ^{31}P NMR spectrum, indicating no coupling between the phosphorus atoms and protons. As the peaks corresponding to these products are so small in the ^{1}H and ^{13}C NMR spectra and

are likely overlapping with the much larger peaks for **12c** it was not possible to identify the structures to which they corresponded. Mass spectrometric investigation of the reaction mixture revealed the presence of a peak corresponding to $C_{38}H_{32}N_4OP$ which is the $[M+H]^+$ ion for the possible diinsertion product (**14**, Figure 13). Although there is some evidence for the diinsertion for the carbodiimides, it appears that these species are only formed in very small quantities.

As for the hydrophosphination of isocyanates, which favours the formation of the diinsertion product in the presence of a weak acid,[36] the analogous reaction with PhNCNPh was repeated in the presence of NEt_3·HCl. However this did not significantly change the ratio of the peaks.

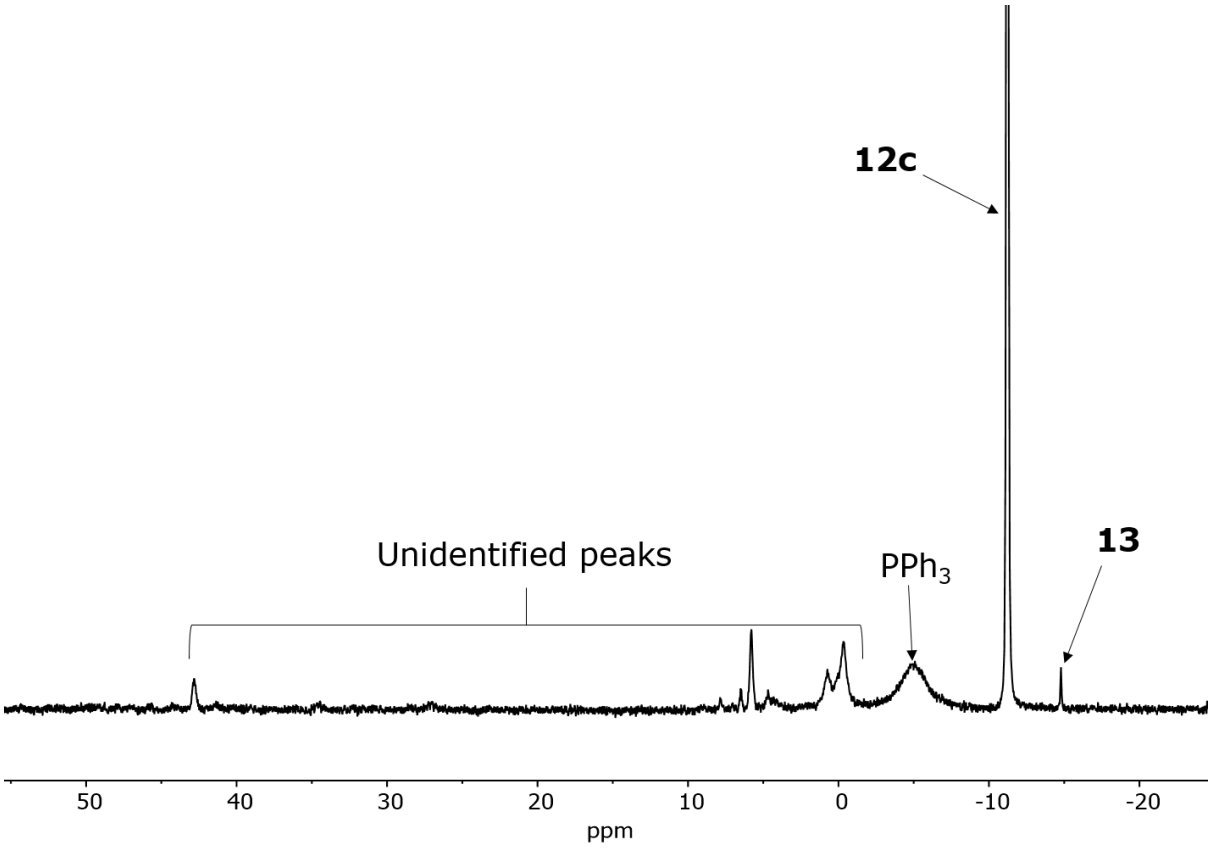
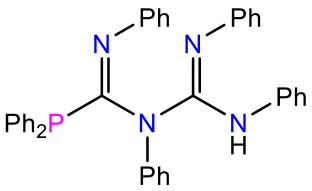


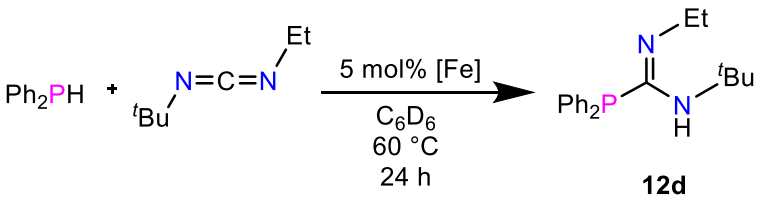
Figure 12. ^{31}P NMR spectrum of catalytic hydrophosphination of PhNCNPh with Ph_2PH mediated by **3** in C_6D_6 after 24 h at 60 °C with PPh_3 as an internal standard.



14

Figure 13. Molecular structure of a potential diinsertion product (**14**).

The asymmetric carbodiimide ^{t}BuNCNEt was used as a substrate (Table 8, Entry 7). The reaction reached 96% conversion after 24 h. Only one new product peak was formed in the ^{31}P NMR spectrum, indicating that the reaction was very selective. This product was identified as **12d** by ^{1}H and ^{31}P NMR spectroscopy (Scheme 11).[74] Use of COSY NMR spectroscopy confirmed that the product was **12d**, as shown by the coupling of the ^{t}Bu and N*H* protons. This selectivity is likely due to the bulky ^{t}Bu group being too sterically demanding to allow close proximity to the PPh_2 group and this is the most thermodynamically stable product.



12d

Scheme 11. Hydrophosphination of ^{t}BuNCNEt catalysed by **3** in C_6D_6 ([Fe] = **3**).

2.3.4.2 Poisoning Experiments

In order to determine whether the catalysis was heterogeneous or homogeneous, poisoning experiments were carried out using Hg(0) as well as CS_2 using a similar method to that used in the hydroamination reactions in Section 2.3.2.6.[54,55] The reaction with Hg(0) and CS_2 both reached similar conversion after 24 h to the reaction without the presence of an additive (Table 9, Entries 1–2). This provides evidence towards a homogeneous mechanism for this reaction.

The reaction was also carried out in the presence of 1,4-cyclohexadiene which acts as a radical trap (Table 9, Entry 3). This did not inhibit the reaction indicating that the catalysis does not proceed *via* a radical mechanism.

Table 9. Catalytic hydrophosphination of carbodiimides in the presence of **3** with additives.

Entry	Additive	T (°C)	t (h)	Conversion (%)[b]	**12**:**13**[b]
1	Hg(0)	25	24	85	99:1
2	CS_2	25	24	85	99:1
3	1,4-cyclohexadiene	25	24	81	99:1

[a] Reaction conditions: 10 mg of **3** (5 mol%), 0.6 mL of C_6D_6, 1:1 Ph_2PH:CyNCNCy.

[b] Determined by ^{31}P NMR spectroscopy.

2.3.4.3 Scale-Up Reactions

The reaction between Ph_2PH and CyNCNCy was repeated on a larger scale in toluene with 30 mg of **3** (5 mol%). The reaction was heated to 60 °C for 24 h, and subsequently the solvent was removed *in vacuo* and the resulting brown oil was extracted into hexane. This resulted in the isolation of **12a** as a pale-yellow powder in a yield of 30%. This low yield (compared with the 97% conversion) can be explained by the low solubility of **12a** in hexane. Most of the product was likely left behind in the reaction mixture. Other solvents such as toluene were also used but this resulted in small amounts of the catalyst being dissolved into the solvent, leading to the isolation of impure product.

2.3.4.4 Stoichiometric Studies

A stoichiometric hydrophosphination reaction was carried out in a similar way to the hydroamination reaction. The precatalyst **3**, Ph_2PH and CyNCNCy in a 1:1:1 ratio were dissolved in C_6D_6 in a Young's NMR tube and kept at room temperature. The ^1H and ^{31}P NMR spectra were measured immediately after adding the substrates and after 1 h, 20 h and 48 h. The presence of the paramagnetic iron complex means that the peaks are

broadened and can be difficult to observe in a ^{31}P NMR spectrum as they may be hidden by the background noise in the spectrum. However, a peak at –18.3 ppm was observed in the ^{31}P NMR spectrum after monitoring the reaction for 20 h, which was assigned to **12a**. The peaks corresponding to **12a** are also present in the ^{1}H NMR spectrum. The peaks corresponding to **3** at 31, –11, –35 and –54 ppm are present for the whole reaction and no new paramagnetically-shifted peaks are observed so this reaction did not give any insight into the identity of the active species in the catalysis.

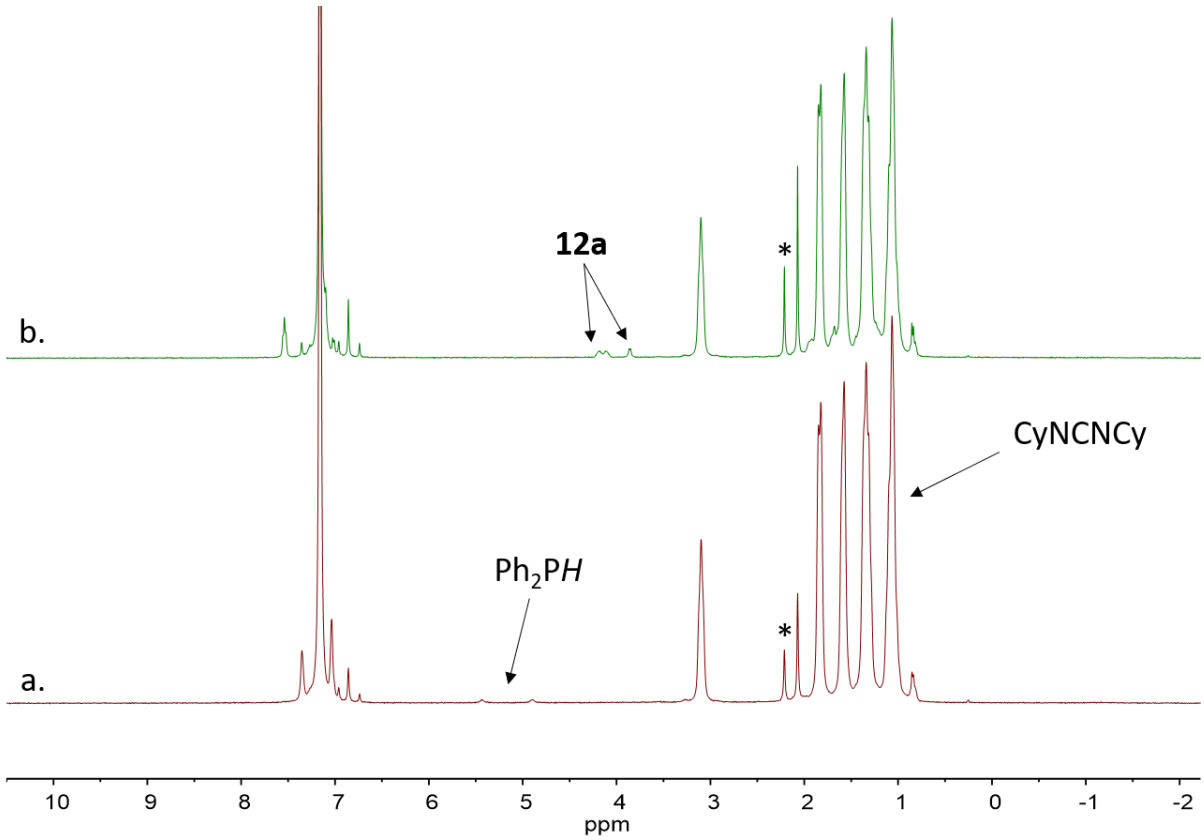
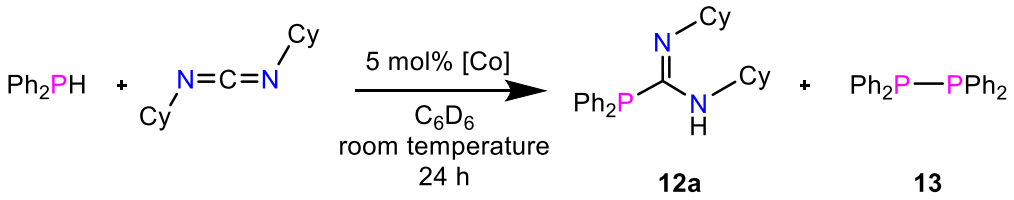


Figure 14. ^{1}H NMR spectra of the stoichiometric reaction between **3**, Ph_2PH and CyNCNCy in C_6D_6; a) Immediately after substrates added, b) After 48 h at room temperature (* indicates Mes peaks from 2,6-$Mes_2C_6H_3$ ligand).

2.3.4.5 Cobalt Catalysed Hydrophosphination of Carbodiimides

The reaction between Ph_2PH and CyNCNCy was also tested with the Co(II) complex **4** (Scheme 12). The reaction was performed on an NMR scale and followed by ^{31}P NMR spectroscopy as detailed previously. After 24 h at room temperature the reaction had reached 38% conversion, which is much lower than the analogous reaction with **3**. This is similar to the trend observed for the hydroamination reactions in the presence of **4** and confirms that **3** is a much more efficient catalyst than **4**. The ^{31}P NMR spectrum shows the same two new peaks that were previously observed for the monoinsertion product **12a** at –18.3 ppm and the dehydrocoupled product **13** at –15 ppm. A higher ratio of **13** is formed (23%) than for **3** which is likely due to the longer reaction time.



Scheme 12. Catalytic hydrophosphination of CyNCNCy using Ph_2PH (1:1) mediated by **4** in C_6D_6 ([Co] = **4**).

2.4 Conclusions

The Fe(II) complex **3** acts as an effective precatalyst for both the hydroamination of isocyanates and the hydrophosphination of carbodiimides under mild conditions. The hydroamination reaction was shown to be analogous to the previously reported hydrophosphination of isocyanates.[36] The Co(II) and Zn(II) complexes **4** and **5** produced the same products as **3** but they had much lower conversions and were not explored further.

Biuret derivatives were able to be synthesised through the use of the aromatic isocyanates which led to the diinsertion of the isocyanate into the N–H bond. This product could be selectively formed by increasing the ratio of R_2NH:R'NCO to 1:5. This was extended further

with the use of diisopropylamine, which resulted in the formation of triuret and tetrauret products from the tri- and tetrainsertion of the isocyanate. This showed the first reported example of the direct transformation of amines to biurets and longer chain urea derivatives. These species with multiple urea moieties have a high capacity for hydrogen bonding which leads to applications in self-assembly and as ligands in coordination chemistry.

This diinsertion reaction is not as favoured in the hydrophosphination of carbodiimides due to the use of the bulkier substrates and the diinsertion product was only tentatively identified through mass spectrometry. This could be explored further with a wider range of carbodiimides.

Mechanistic studies were undertaken through the use of poisoning experiments which indicated that the catalysis is homogeneous and not radical catalysed. Stoichiometric studies were also undertaken and were monitored by both NMR and IR spectroscopy and these indicate that **3** transforms into a new iron species which is likely the active species, however the nature of this species was not determined as attempts to isolate and crystallise the species were unsuccessful. Further mechanistic investigations could be carried out with the diamagnetic Zn(II) complex **5** as the longer reaction times could lead to an intermediate species that could be identified through NMR spectroscopy.

This chapter shows the promising potential of the diaryl *m*-terphenyl complexes to act as precatalysts for hydroelementation reactions and their unusual ability to synthesise species with multiple insertions of the heterocumulene. This catalyst is also the first reported iron catalyst for these reactions.

2.5 Experimental Procedures

See Chapter 6 for general experimental.

2.5.1 Synthesis of Precatalysts

2,6-$Mes_2C_6H_3I$ (**1**), [2,6-$Mes_2C_6H_3Li]_2$ (**2**) and complexes **3**–**5** were synthesised according to literature methods and characterisation matched literature data.[38–41]

2.5.2 Catalytic Hydroamination of Isocyanates

2.5.2.1 Standard Procedure for the Catalytic Hydroamination of Isocyanates

5 mol% of **3** (10.0 mg, 0.0147 mmol) was dissolved in C_6D_6 (0.6 mL) in a Young's NMR tube along with the corresponding isocyanate and amine (1:1, 1:2 or 1:5 of R_2NH:R'NCO). The reaction was either carried out at room temperature or heated to 60 °C and the reaction was monitored by ^{1}H NMR spectroscopy. Conversion was quantified by integration of ^{1}H NMR spectra using either 1,3,5-trimethoxybenzene or TMS as an internal standard and the results can be found in Table 2.

2.5.2.2 Standard Procedure for *in situ* NMR Reaction Monitoring for the Catalytic Hydroamination of Isocyanates

5 mol% of **3** (10.0 mg, 0.0147 mmol) was dissolved in C_6D_6 (0.6 mL) along with Ph_2NH (49 mg, 0.292 mmol) in a Young's NMR tube. The solution was cooled to −30 °C after which the corresponding isocyanate (1:1 of Ph_2NH:RNCO) was added and the sample was cooled to −78 °C to prevent the reaction from initiating. The sample was then transferred to an NMR spectrometer and monitored by ^{1}H NMR spectroscopy at 25 °C. Conversion was quantified by integration of ^{1}H NMR spectra using TMS as an internal standard.

2.5.2.3 Catalytic Hydroamination of Isocyanates in THF

5 mol% of **3** (10.0 mg, 0.0147 mmol) was dissolved in THF (0.6 mL) along with the corresponding isocyanate (0.292 mmol) and Ph_2NH (49 mg, 0.292 mmol) in a Young's

NMR tube. The reaction was heated to 60 °C for 3 days. The solvent was then removed *in vacuo* and the resulting solid was dissolved in C_6D_6. Conversion was quantified by integration of the ^1H NMR spectrum.

2.5.2.4 Scaled-up Catalytic Hydroamination of Isocyanates

In a Schlenk flask 5 mol% of **3** (50.0 mg, 0.0732 mmol), Ph_2NH (247 mg, 1.46 mmol) and PhNCO (796 µL, 7.32 mmol) were dissolved in toluene (5.0 mL) and stirred at room temperature for 3 h. The solvent was removed *in vacuo* and the solid was extracted into CH_2Cl_2 (20 mL). The crude product was first passed through a silica column in CH_2Cl_2/hexane (25/75) and then the isolated product was washed from the silica with acetone (250 mL). (**7a**: 460 mg, 77%).

2.5.2.5 Stoichiometric NMR Spectroscopy

In a Young's NMR tube, the precatalyst **3** (10.0 mg, 0.0146 mmol), Ph_2NH (2.5 mg, 0.0146 mmol) and PhNCO (6.4 µL, 0.0292 mmol) were dissolved in C_6D_6 (0.6 mL). The reaction was carried out at room temperature and was monitored by ^1H NMR spectroscopy using 1,3,5-trimethoxybenzene as an internal standard.

2.5.2.6 Stoichiometric IR Spectroscopy

In a Schlenk flask, the precatalyst **3** (30.0 mg, 0.044 mmol), Ph_2NH (7.4 mg, 0.044 mmol) and PhNCO (4.7 µL, 0.044 mmol) were dissolved in toluene (5.0 mL) and stirred at room temperature for 24 h. Aliquots of 0.3 mL were taken at three intervals throughout the reaction and the IR spectrum of the solution was measured.

2.5.2.7 Stoichiometric UV-Vis Spectroscopy

The precatalyst **3** (15.0 mg, 0.0219 mmol), Ph_2NH (3.7 mg, 0.0219 mmol) and PhNCO (2.4 μL, 0.0219 mmol) were dissolved in hexane (10.0 mL). This was then diluted to give a concentration of 0.439 M. The UV-vis spectrum of this solution was then measured. λ_{max}/nm (ε/$dm^3mol^{-1}cm^{-1}$) = 356 (1.23), 368 (1.04), 380 (0.71), 410 (0.50).

2.5.2.8 Catalytic Hydroamination of Isocyanates in the Presence of NEt_3·HCl

5 mol% of **3** (10.0 mg, 0.0147 mmol) was dissolved in C_6D_6 (0.6 mL) in a Young's NMR tube along with Ph_2NH (49 mg, 0.292 mmol), PhNCO (64 μL, 0.586 mmol) and NEt_3·HCl (20 mg, 0.146 mmol). The reaction was carried out at room temperature and was monitored by ^1H NMR spectroscopy. Conversion was quantified by integration of ^1H NMR spectra using TMS as an internal standard.

2.5.2.9 Catalytic Hydroamination of Isocyanates in the Presence of Hg(0)

5 mol% of **3** (10.0 mg, 0.0147 mmol) was dissolved in C_6D_6 (0.6 mL) in a Young's NMR tube along with Ph_2NH (49 mg, 0.292 mmol) and PhNCO (32 μL, 0.292 mmol). A drop of Hg(0) was then added to the reaction mixture. The reaction was carried out at room temperature and monitored by ^1H NMR spectroscopy. Conversion was quantified by integration of ^1H NMR spectra using TMS as an internal standard.

2.5.2.10 Catalytic Hydroamination of Isocyanates in the Presence of CS_2

5 mol% of **3** (10.0 mg, 0.0147 mmol) was dissolved in C_6D_6 (0.6 mL) in a Young's NMR tube along with Ph_2NH (49 mg, 0.292 mmol), ^{t}BuNCO (28 μL, 0.292 mmol) and CS_2 (0.05 M in toluene, 29 μL, 0.00146 mmol). The reaction was carried out at room temperature

and monitored by ^{1}H NMR spectroscopy. Conversion was quantified by integration of ^{1}H NMR spectra using 1,3,5-trimethoxybenzene as an internal standard.

2.5.2.11 Catalytic Hydroamination of Isocyanates in the Presence of $PPhMe_2$

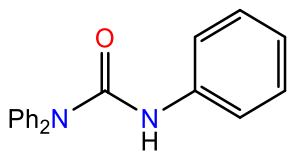
5 mol% of **3** (10.0 mg, 0.0147 mmol) was dissolved in C_6D_6 (0.6 mL) in a Young's NMR tube along with Ph_2NH (49 mg, 0.292 mmol), ^{t}BuNCO (28 µL, 0.292 mmol) and $PPhMe_2$ (1 µL, 0.00702 mmol). The reaction was carried out at room temperature and monitored by ^{1}H NMR spectroscopy. Conversion was quantified by integration of ^{1}H NMR spectra using 1,3,5-trimethoxybenzene as an internal standard.

2.5.2.12 Catalytic Hydroamination of Isocyanates in the Presence of Cumene

5 mol% of **3** (10.0 mg, 0.0147 mmol) was dissolved in C_6D_6 (0.6 mL) in a Young's NMR tube along with Ph_2NH (49 mg, 0.292 mmol), PhNCO (32 µL, 0.292 mmol) and cumene (10 µL, 0.0733 mol). The reaction was carried out at room temperature and monitored by ^{1}H NMR spectroscopy. Conversion was quantified by integration of ^{1}H NMR spectra using TMS as an internal standard.

2.5.2.13 Synthesis and Characterisation of Ureas

2.5.2.13.1 $Ph_2NC(=O)NH(Ph)$ 6a

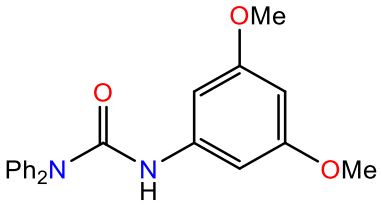


A solution of PhNCO (96 µL, 0.879 mmol) in THF (1 mL) was added to a solution of **3** (30.0 mg, 0.0439 mmol) and Ph_2NH in THF (2 mL) and heated to 60 °C for 3 days. The solvent was removed *in vacuo* and the solid was extracted into CH_2Cl_2 (10 mL). The crude product was first passed through a silica column in CH_2Cl_2 and then the isolated product was

washed from the silica with acetone. The solvent was removed *in vacuo* affording **6a** as a white solid; 153 mg, 61%.

^{1}H NMR (400 MHz, C_6D_6, 25 °C) δ = 7.43 (d, ^{3}J(H,H) = 8.1 Hz, 2H, Ph^{o}), 7.19–7.06 (m, 10H, NPh$_2$^{o,m,p}), 6.99 (t, ^{3}J(H,H) = 7.2 Hz, 2H, Ph^{m}), 6.92 (t, ^{3}J(H,H) = 7.5 Hz, 1H, Ph^{p}), 6.44 (s, 1H, N*H*) ppm. ^{13}C{^{1}H} NMR (101 MHz, C_6D_6, 25 °C) δ = 153.0 (*C*=O), 143.3 (NPh$_2$^{i}), 139.6 (Ph^{i}), 137.6 (NPh$_2$^{o}), 129.6 (NPh$_2$^{m}), 129.2 (NPh$_2$^{p}), 126.3 (Ph^{m}), 123.1 (Ph^{p}), 119.1 (Ph^{o}) ppm. MS (ESI) Expected: 289.1335, found: 289.1333 (err [ppm] = 0.70) [M+H]$^{+}$. Characterisation matched literature data.[75]

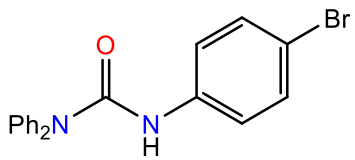
2.5.2.13.2 Ph$_2$NC(=O)NH(3,5-(OMe)$_2$C$_6$H$_3$) 6b



In a Young's NMR tube 5 mol% of **3** (10.0 mg, 0.0146 mmol), Ph$_2$NH (49.0 mg, 0.292 mmol) and 3,5-(OMe)$_2$C$_6$H$_3$NCO (52 mg, 0.292 mmol) were dissolved in THF (0.6 mL) and heated to 60 °C for 3 days. The solvent was removed *in vacuo* and the solid was extracted into toluene (3 × 5 mL) and stored at –30°C overnight resulting in the precipitation of **6b** as a white solid; 49 mg, 48%.

^{1}H NMR (400 MHz, C_6D_6, 25 °C) δ = 7.09 (m, 4H, NPh$_2$^{o}), 7.00 (m, 4H, NPh$_2$^{m}), 6.93 (d, ^{4}J(H,H) = 2.2 Hz, 2H, Ph^{o}), 6.89 (m, 2H, NPh$_2$^{p}), 6.39 (s, 1H, N*H*), 6.35, (t, ^{4}J(H,H) = 2.2 Hz, 1H, Ph^{p}), 3.33 (s, 6H, OC*H*$_3$) ppm. ^{13}C{^{1}H} NMR (101 MHz, C_6D_6, 25 °C) δ = 161.9 (Ph^{m}) 153.1 (*C*=O), 143.2 (NPh$_2$^{i}), 141.5 (Ph^{i}), 129.6 (NPh$_2$^{m}), 127.7 (NPh$_2$^{o}), 126.3 (NPh$_2$^{p}), 97.5 (Ph^{o}), 96.2 (Ph^{p}), 54.9 (O*C*H$_3$) ppm. MS (ESI) Expected: 349.1547, found: 349.1532 (err [ppm] = 4.30) [M+H]$^{+}$.

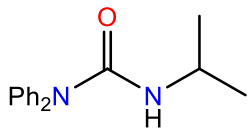
2.5.2.13.3 $Ph_2NC(=O)NH(4\text{-}BrC_6H_4)$ 6c



In a Young's NMR tube 5 mol% of **1** (10.0 mg, 0.0146 mmol), Ph_2NH (49.0 mg, 0.292 mmol) and 4-BrC_6H_4NCO (58 mg, 0.292 mmol) were dissolved in THF (0.6 mL) and heated to 60 °C for 3 days. The solvent was removed *in vacuo* and the solid was extracted into toluene (3 × 5 mL) and stored at –30°C overnight resulting in the precipitation of **6c** as a white solid; 58 mg, 54%.

^{1}H NMR (400 MHz, C_6D_6, 25 °C) δ = 7.15 (m, 2H, Ph^o) 7.13 (m, 2H, Ph^m), 7.07–6.96 (m, 8H, NPh_2^{o+m}), 6.90 (m, 2H, NPh_2^p), 6.11 (s, 1H, N*H*) ppm. ^{13}C{^{1}H} NMR (101 MHz, C_6D_6, 25 °C) δ = 152.6 (*C*=O), 143.1 (NPh_2^i), 138.5 (Ph^i), 132.1 (Ph^m), 129.6 (NPh_2^o), 127.7 (PPh^o), 126.4 (NPh_2^p), 120.7 (NPh_2^m), 115.7 (Ph^p) ppm. MS (ESI) Expected: 367.0441, found: 367.0456 (err [ppm] = 4.30) $[M+H]^+$.

2.5.2.13.4 $Ph_2NC(=O)NH(^iPr)$ 6d

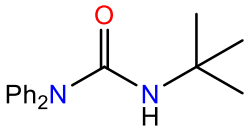


In a Young's NMR tube 5 mol% of **3** (10.0 mg, 0.0146 mmol), Ph_2NH (49.0 mg, 0.292 mmol) and ^{i}PrNCO (29 µL, 0.292 mmol) were dissolved in C_6D_6 (0.6 mL) at room temperature. The solvent was removed *in vacuo* and the solid was extracted into hexane (3 × 5 mL) and stored at –30 °C overnight resulting in the precipitation of **6d** as a white solid; 17 mg, 23%.

^{1}H NMR (400 MHz, C_6D_6, 25 °C) δ = 7.20 (d, ^3J(H,H) = 7.9 Hz, 4H, NPh_2^o), 7.03 (t, ^3J(H,H) = 7.7 Hz, 4H, NPh_2^m), 6.88 (t, ^3J(H,H) = 7.4 Hz, 2H, NPh_2^p), 4.22–4.10 (m, 2H, N*H* + C*H*$(CH_3)_2$), 0.85 (d, ^3J(H,H) = 5.8 Hz, 6H, C*H*$_3$) ppm. ^{13}C{^{1}H} (101 MHz, C_6D_6, 25 °C) δ = 154.6 (*C*=O), 143.7 (Ph^i), 129.0 (NPh_2^m), 127.2 (NPh_2^o), 125.3 (NPh_2^p), 42.4 (*C*H$(CH_3)_2$),

22.5 (*C*CH_3) ppm. MS (ESI) Expected: 255.1492, found: 255.1495 (err [ppm] = 1.40) $[M+H]^+$.

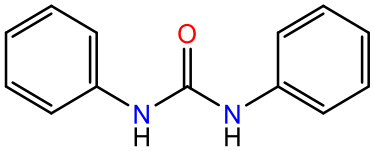
2.5.2.13.5 $Ph_2NC(=O)NH(^tBu)$ 6e



In a Young's NMR tube 5 mol% of **3** (10.0 mg, 0.0146 mmol), Ph_2NH (49.0 mg, 0.292 mmol) and ^{t}BuNCO (0.292 mmol) were dissolved in C_6D_6 (0.6 mL) at room temperature. The solvent was removed *in vacuo* and the solid was extracted into hexane (3 × 5 mL) and stored at –30 °C overnight resulting in the precipitation of **6e** as a white solid; 27 mg, 25%.

^{1}H NMR (400 MHz, C_6D_6, 25 °C) δ = 7.19 (d, ^3J(H,H) = 7.3 Hz, 4H, Ph^o), 7.03 (t, ^3J(H,H) = 7.9 Hz, 4H, Ph^m), 6.88 (t, ^3J(H,H) = 7.4 Hz, 2H, Ph^p), 4.35 (s, 1H, N*H*), 1.25 (s, 9H, C(C*H*$_3$)$_3$) ppm. ^{13}C{^{1}H} (101 MHz, C_6D_6, 25 °C) δ = 154.8 (*C*=O), 144.2 (Ph^i), 129.4 (Ph^m), 127.6 (Ph^o), 125.5 (Ph^p), 51.0 (*C*(CH$_3$)$_3$), 29.2 (C(*C*H$_3$)$_3$) ppm. MS (ESI) Expected: 269.1648, found: 269.1645 (err [ppm] = 1.1) $[M+H]^+$.

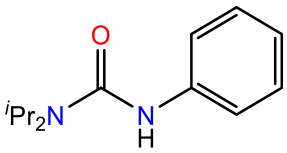
2.5.2.13.6 PhHNC(=O)NH(Ph) 6f



In a Young's NMR tube 5 mol% of **3** (10.0 mg, 0.0146 mmol), $PhNH_2$ (26 µL, 0.292 mmol) and PhNCO (159 µL, 1.46 mmol) were dissolved in C_6D_6 (0.6 mL) at room temperature for 24 h. **6f** and **7f** were obtained as a mixture and conversions were obtained by ^{1}H NMR spectroscopy (**6f**: 32%; **7f**: 68%).

6f: ^{1}H NMR (400 MHz, $CDCl_3$, 25 °C) δ = 7.49 (m, 4H, Ph^{o}), 7.41 (m, 4H, Ph^{m}), 7.33 (d, ^{3}J(H,H) = 3.5 Hz, 2H, Ph^{p}), 6.46 (s, 2H, N*H*) ppm. ^{13}C{^{1}H} NMR (101 MHz, $CDCl_3$, 25 °C) δ = 148.8 (*C*=O), 133.8 (Ph^{i}), 129.5 (Ph^{o}), 128.6 (Ph^{m}), 121.4 (Ph^{p}) ppm. MS (ESI) Expected: 235.0842, found: 235.0846 (err [ppm] = 1.80) $[M+Na]^+$. Characterisation matched literature data.[76]

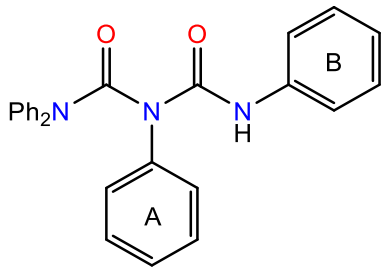
2.5.2.13.7 $^{i}Pr_2NC(=O)NH(Ph)$ 6g



In a Young's NMR tube 5 mol% of **3** (10.0 mg, 0.0146 mmol), $^{i}Pr_2NH$ (41 µL, 0.292 mmol) and PhNCO (32 µL, 0.292 mmol) were dissolved in C_6D_6 (0.6 mL) at room temperature. The solvent was removed *in vacuo* and the solid was extracted into hexane (3 × 5 mL) and stored at −30 °C overnight resulting in the precipitation of **6g** as a white solid; 42 mg, 64%.

^{1}H NMR (400 MHz, $CDCl_3$, 25 °C) δ = 7.39 (m, 2H, Ph^{o}), 7.30 (m, 2H, Ph^{m}) 7.03 (t, ^{3}J(H,H) = 7.3 Hz, 1H, Ph^{p}), 6.22 (s, 1H, N*H*), 4.01 (sep, ^{3}J(H,H) = 6.9 Hz, 2H, C*H*$(CH_3)_2$), 1.35 (d, ^{3}J(H,H) = 6.9 Hz, 12H, CH_3) ppm. ^{13}C{^{1}H} (101 MHz, $CDCl_3$, 25 °C) δ = 154.6 (*C*=O), 139.4 (Ph^{i}), 128.9 (Ph^{m}), 122.6 (Ph^{p}), 119.6 (Ph^{o}), 45.5 (*C*H$(CH_3)_2$), 21.6 (*C*H_3) ppm. MS (ESI) Expected: 221.1648, found: 221.1645 (err [ppm] = 1.60) $[M+H]^+$. Characterisation matched literature data.[75]

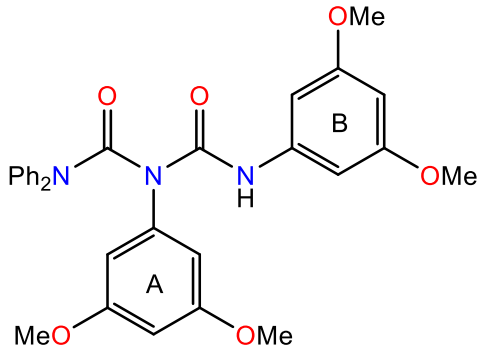
2.5.2.13.8 $Ph_2NC(=O)N(Ph)C(=O)NH(Ph)$ 7a



In a Schlenk flask 5 mol% of **3** (50.0 mg, 0.0732 mmol), Ph_2NH (247 mg, 1.46 mmol) and PhNCO (796 µL, 7.32 mmol) were dissolved in toluene (5.0 mL) and stirred at room temperature for 5 h. The solvent was removed *in vacuo* and the solid was extracted into CH_2Cl_2 (20 mL). The crude product was first passed through a silica column in CH_2Cl_2/hexane (25/75) and then the isolated product was washed from the silica with acetone (250 mL). The solvent was removed *in vacuo* affording **7a** as a white solid; 460 mg, 77%.

^{1}H NMR (400 MHz, C_6D_6, 25 °C) δ = 10.81 (s, 1H, N*H*), 7.84 (m, 2H, Ph^{Bo}) 7.34 (m, 4H, NPh_2^{o}), 7.28–7.07 (m, 9H, NPh_2^{m+p} + Ph^{Bm+Bp}), 7.03–6.85 (m, 5H, Ph^{Ao+m+p}) ppm. ^{13}C{^{1}H} (101 MHz, C_6D_6, 25 °C) δ = 160.2 (*C*=O) 153.1 (*C*=O), 148.7 (NPh_2^{i}), 143.4 (Ph^{Ai}), 139.1 (Ph^{Bi}), 129.6–129.0 (NPh_2^{m+p} + Ph^{Bm+p}), 127.4 (Ph^{Ao}), 126.7 (Ph^{Am}), 126.2 (Ph^{Ap}), 120.0 (Ph^{Bo}), 119.2 (NPh_2^{o}) ppm. MS (ESI) Expected: 408.1707, found: 408.1707 (err [ppm] = 0.00) $[M+H]^+$.

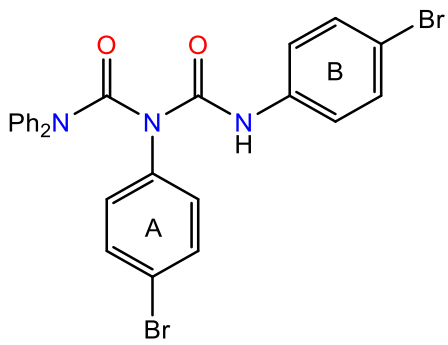
2.5.2.13.9 $Ph_2NC(=O)N(3,5\text{-}(OMe)_2C_6H_3)C(=O)NH(3,5\text{-}(OMe)_2C_6H_3)$ 7b



In a Young's NMR tube 5 mol% of **3** (10.0 mg, 0.0146 mmol), Ph_2NH (49.0 mg, 0.292 mmol) and 3,5-$(OMe)_2C_6H_3NCO$ (262 mg, 1.46 mmol) were dissolved in C_6D_6 (0.6 mL). The solution was heated to 60 °C for 4 hours. The solvent was removed *in vacuo* and the solid was washed with hexane (3 × 5 mL) and stored at –30 °C overnight resulting in the precipitation of **7b** as a white solid; 21 mg, 14%.

^{1}H NMR (400 MHz, C_6D_6, 25 °C) δ = 10.77 (s, 1H, N*H*), 7.24 (d, ^4J(H,H) = 2.3 Hz, 2H, Ph^{Bo}), 6.84–6.79 (m, 8H, NPh_2^{o+m}), 6.41 (m, 1H, Ph^{Bp}), 6.36–6.32 (m, 3H, NPh_2^{p} + Ph^{Ap}), 6.22 (d, ^4J(H,H) = 2.3 Hz, 2H, Ph^{Ao}), 3.32 (s, 6H, OCH_3^B), 3.17 (s, 6H, OCH_3^A) ppm. $^{13}C\{^1H\}$ (101 MHz, C_6D_6, 25 °C) δ = 162.3 (Ph_2NC=O), 162.0 (Ph^{Bm}), 160.6 (Ph^{Am}), 152.0 (HN*C*=O), 143.5 (NPh_2^{i}), 140.9 (Ph^{Bi}), 140.2 (Ph^{Ai}), 129.3 (NPh_2^{o}), 126.9 (NPh_2^{m}), 108.1 (NPh_2^{p}), 107.7 (Ph^{Ao}), 100.5 (Ph^{Ap}), 98.3 (Ph^{Bo}), 97.4 (Ph^{Bp}), 54.9 (OCH_3^B), 54.9 (OCH_3^A) ppm. MS (ESI) Expected: 528.2129, found: 528.2123 $[M+H]^+$ (err [ppm] = 1.20).

2.5.2.13.10 $Ph_2NC(=O)N(4\text{-}BrC_6H_4)C(=O)NH(4\text{-}BrC_6H_4)$ 7c

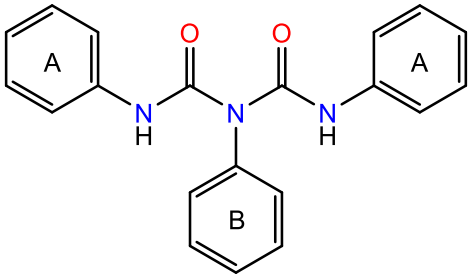


In a Young's NMR tube 5 mol% of **1** (10.0 mg, 0.0146 mmol), Ph_2NH (49.0 mg, 0.292 mmol) and 4-BrC_6H_4NCO (289 mg, 1.46 mmol) were dissolved in C_6D_6 (0.6 mL). The solution was heated to 60 °C for 4 hours. The solvent was removed *in vacuo* and the solid was washed with hexane (3 × 5 mL) and stored at –30 °C overnight resulting in the precipitation of **7c** as a white solid; 26 mg, 16%.

^{1}H NMR (400 MHz, C_6D_6, 25 °C) δ = 10.63 (s, 1H, N*H*), 7.39 (m, 2H, Ph^{Bo}), 7.18 (m, 2H, Ph^{Bm}), 6.95 (m, 4H, NPh_2^{m}), 6.82 (m, 2H, Ph^{Am}), 6.61 (d, ^3J(H,H) = 6.8 Hz, 2H, Ph^{Ao}), 6.50 (m, 2H, NPh_2^{p}), 6.21 (d, ^3J(H,H) = 8.1 Hz, 4H, NPh_2^{o}) ppm. $^{13}C\{^1H\}$ (101 MHz, C_6D_6,

25 °C) δ = 149.5 (*C*=O), 147.8 (*C*=O), 142.6 (NPh_2^{i}), 141.6 (Ph^{Bi}), 139.1 (Ph^{Ai}), 132.3 (NPh_2^{m}), 132.0 (Ph^{Bm}), 130.3 (NPh_2^{p}), 129.0 (Ph^{Am}), 126.3 (Ph^{Ao}), 126.1 (NPh_2^{o}), 121.3 (Ph^{Bo}), 118.6 (Ph^{Ap}) 116.3 (Ph^{Bp}) ppm. MS (ESI) Expected: 563.9917, found: 563.9915 $[M+H]^+$ (err [ppm] = 0.30).

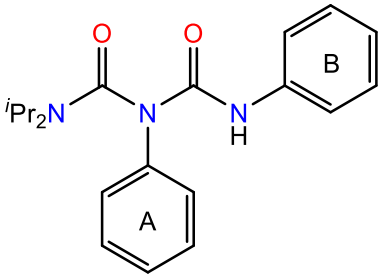
2.5.2.13.11 PhNHC(=O)N(Ph)C(=O)NH(Ph) 7f



In a Young's NMR tube 5 mol% of **3** (10.0 mg, 0.0146 mmol), $PhNH_2$ (26 µL, 0.292 mmol) and PhNCO (159 µL, 1.46 mmol) were dissolved in C_6D_6 (0.6 mL) at room temperature for 24 h. **6f** and **7f** were obtained as a mixture and conversions were obtained by ^{1}H NMR spectroscopy (**6f**: 32%; **7f**: 68%).

7f: ^{1}H NMR (400 MHz, C_6D_6, 25 °C) δ = 8.99 (s, 2H, N*H*), 7.45 (d, ^3J(H,H) = 7.5 Hz, 4H, Ph^{Ao}), 7.06 (m, 4H, Ph^{Am}), 7.01–6.95 (m, 4H, Ph^{Ap} + Ph^{Bo}), 6.87 (m, 2H, Ph^{Bm}), 6.79 (m, 1H, Ph^{Bp}) ppm. $^{13}C\{^1H\}$ (101 MHz, C_6D_6, 25 °C) δ = 152.9 (*C*=O), 138.0 (Ph^{Bi}), 136.9 (Ph^{Ai}), 129.9 (Ph^{Bp}), 129.7 (Ph^{Ap}), 128.9 (Ph^{Am}), 128.1 (Ph^{Bo}), 123.9 (Ph^{Bm}), 129.2 (Ph^{Ao}) ppm. MS (ESI) Expected: 354.1213, found: 354.1199 (err [ppm] = 3.90) $[M+Na]^+$.

2.5.2.13.12 ^{i}Pr$_2$NC(=O)N(Ph)C(=O)NH(Ph) 7g



(See section 2.5.2.14 for synthesis).

^{1}H NMR (400 MHz, C_6D_6, 25 °C) δ = 9.03 (s, 1H, N*H*), 7.58 (m, 2H, Ph^{o}), 7.42 (m, 1H, Ph^{o}), 7.09–6.99 (m, 4H, Ph^{Am} + Ph^{Bm}), 6.91 (m, 1H, Ph^{p}), 6.82 (m, 1H, Ph^{p}), 3.45 (br s, 2H, C*H*(CH_3)$_2$), 0.90 (br s, 12H, C*H*$_3$) ppm. ^{13}C{^{1}H} (101 MHz, C_6D_6, 25 °C) δ = 140.0 (Ph^{i}), 139.3 (Ph^{i}), 129.2 (Ph^{m}), 129.0 (Ph^{m}), 127.8 (Ph^{o}), 126.8 (Ph^{p}), 123.4 (Ph^{p}), 119.9 (Ph^{o}), 21.4 (*C*H(CH_3)$_2$), 19.9 (*C*H_3) ppm. MS (ESI) Expected: 340.2020, found: 340.2010 (err [ppm] = 2.70) $[M+H]^+$.

2.5.2.14 Procedure for *in situ* Formation of 7g, 8g and 9g

In a Young's NMR tube 5 mol% of **3** (10.0 mg, 0.0146 mmol), ^{i}Pr$_2$NH (41 μL, 0.292 mmol) and phenyl isocyanate [64 μL, 0.586 mmol (affording a mixture of **7g** and **8g**); 95 μL, 0.876 mmol (affording a mixture of **7g**, **8g** and **9g**); 159 μL, 1.46 mmol (affording a mixture of **7g**, **8g** and **9g**)] were dissolved in C_6D_6 (0.6 mL). The reaction was performed at room temperature and monitored by ^{1}H NMR spectroscopy. Conversion was quantified by integration of ^{1}H NMR spectra (**7g** 25%, **8g** 54% and **9g** 21%).

Selected spectroscopic data for **8g** and **9g** (observed as a mixture): ^{i}Pr$_2$NC(=O)N(Ph)C(=O)N(Ph)C(=O)NH(Ph) (**8g**): ^{1}H NMR (400 MHz, C_6D_6, 25 °C) δ = 10.36 (s, 1H, N*H*), 7.58–6.51 (m, 15H, Ph), 3.45 (br s, 2H, C*H*(CH_3)$_2$), 0.10 (br s, 12H, C*H*$_3$) ppm. MS (ESI) Expected: 459.2391, found: 459.2395 (err [ppm] = 0.90) $[M+H]^+$. ^{i}Pr$_2$NC(=O)N(Ph)C(=O)N(Ph)C(=O)N(Ph)C(=O)NH(Ph) (**9g**): ^{1}H NMR (400 MHz, C_6D_6, 25 °C) δ = 7.76 (s, 1H, N*H*) ppm. MS (ESI) Expected: 578.2762, found: 578.2777 (err [ppm] = 2.70) $[M+H]^+$.

2.5.3 Catalytic Hydrophosphination of Carbodiimides

2.5.3.1 Standard Procedure for the Catalytic Hydrophosphination of Carbodiimides

5 mol% of **3** (10.0 mg, 0.0147 mmol) was dissolved in C_6D_6 (0.6 mL) in a Young's NMR tube along with Ph_2PH (51 µL, 0.292 mmol) and the corresponding carbodiimide (1:1 or 1:2 of Ph_2NH:RNCNR). The reaction was either carried out at room temperature or heated to 60 °C. The reaction was monitored by ^1H and ^{31}P NMR spectroscopy. Conversion was quantified by integration of ^{31}P NMR spectra with PPh_3 as an internal standard.

2.5.3.2 Catalytic Hydrophosphination of Carbodiimides in the Presence of NEt_3·HCl

5 mol% of **3** (10.0 mg, 0.0147 mmol) was dissolved in C_6D_6 (0.6 mL) in a Young's NMR tube along with Ph_2PH (51 µL, 0.292 mmol), PhNCNPh (114 mg, 0.586 mmol) and NEt_3·HCl (40 mg, 0.292 mmol). The reaction was heated to 60 °C and was monitored by ^1H and ^{31}P NMR spectroscopy. Conversion was quantified by integration of ^{31}P NMR spectra with PPh_3 as an internal standard.

2.5.3.3 Catalytic Hydrophosphination of Carbodiimides in the Presence of Hg(0)

5 mol% of **3** (10.0 mg, 0.0147 mmol) was dissolved in C_6D_6 (0.6 mL) in a Young's NMR tube along with Ph_2PH (51 µL, 0.292 mmol) and CyNCNCy (60 mg, 0.292 mmol). A drop of Hg(0) was then added to the reaction mixture. The reaction was carried out at room temperature and monitored by ^1H and ^{31}P NMR spectroscopy. Conversion was quantified by integration of ^{31}P NMR spectra with PPh_3 as an internal standard.

2.5.3.4 Catalytic Hydrophosphination of Carbodiimides in the Presence of CS_2

5 mol% of **3** (10.0 mg, 0.0147 mmol) was dissolved in C_6D_6 (0.6 mL) in a Young's NMR tube along with Ph_2PH (51 µL, 0.292 mmol), CyNCNCy (60 mg, 0.292 mmol) and CS_2 (0.05 M in toluene, 29 µL, 0.00146 mmol). The reaction was carried out at room temperature and monitored by ^1H and ^{31}P NMR spectroscopy. Conversion was quantified by integration of ^{31}P NMR spectra with PPh_3 as an internal standard.

2.5.3.5 Catalytic Hydrophosphination of Carbodiimides in the Presence of 1,4-Cyclohexadiene

5 mol% of **3** (10.0 mg, 0.0147 mmol) was dissolved in C_6D_6 (0.6 mL) in a Young's NMR tube along with Ph_2PH (51 µL, 0.292 mmol), CyNCNCy (60 mg, 0.292 mmol) and 1,4-cyclohexadiene (6.9 µL, 0.073 mmol). The reaction was heated to 60 °C and was monitored by ^1H and ^{31}P NMR spectroscopy. Conversion was quantified by integration of ^{31}P NMR spectra with PPh_3 as an internal standard.

2.5.3.6 Scaled-up Catalytic Hydrophosphination of Carbodiimides

In a Schlenk flask 5 mol% of **3** (30.0 mg, 0.0439 mmol), Ph_2PH (153 µL, 0.879 mmol) and CyNCNCy (181 mg, 0.879 mmol) were dissolved in toluene (5.0 mL) and stirred at 60 °C for 24 h. The solvent was removed *in vacuo* to give a dark brown oil which was then extracted into hexane (3 × 5 mL). The solvent was removed *in vacuo* to give a pale yellow solid. (**13a**: 102 mg, 30%).

2.5.3.7 Stoichiometric NMR

The precatalyst **3** (10.0 mg, 0.0146 mmol) was dissolved in C_6D_6 (0.6 mL) in a Young's NMR tube along with Ph_2PH (2.5 µL, 0.0146 mmol) and CyNCNCy (3.0 mg, 0.0146 mmol).

The reaction was carried out at room temperature and was monitored by ^{1}H and ^{31}P NMR spectroscopy.

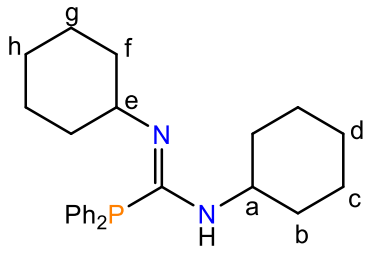
2.5.4 Synthesis of *N*,*N*′-Diphenylcarbodiimide 11

The synthesis of **11** was adapted from that reported by Jiang and co-workers, with minor changes.[73] *N*,*N*′-diphenylthiourea (4 g, 17.5 mmol) and HgO (5.6 g, 25.8 mmol) were dissolved in acetone (20 mL) along with $MgSO_4$ (5.0 g, 42 mmol). The solution was heated to reflux for 1 h. After cooling to room temperature, the black suspension was filtered through Celite® resulting in a colourless solution. The solvent was removed *in vacuo* giving a yellow oil and a colourless solid. This was extracted into CH_2Cl_2 and the solvent was removed *in vacuo* to give a yellow liquid.

Yellow liquid: 2.41 g, 57%. ^{1}H NMR (400 MHz, C_6D_6, 25 °C) δ 7.03 (m, 4H, Ph^{o}), 6.97 (m, 4H, Ph^{m}), 6.86 (m, 2H, Ph^{p}) ppm. $^{13}C\{^{1}H\}$ (101 MHz, C_6D_6, 25 °C) δ 139.0 (N*C*N), 135.7 (Ph^{i}), 129.8 (Ph^{m}), 125.7 (Ph^{o}), 124.6 (Ph^{p}) ppm. IR (ATR) ν = 2110 (C=N) cm^{-1}.

2.5.5 Characterisation of Phosphaguanidines

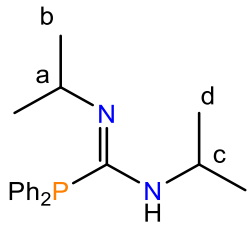
2.5.5.1 $Ph_2PC(=NCy)NH(Cy)$ 12a



^{1}H NMR (400 MHz, C_6D_6, 25 °C) δ = 7.51 (m, 4H, PPh_2^{m}), 7.18–7.02 (m, 6H, PPh_2^{o+p}), 4.15 (m, 1H, C*H*^{a}), 4.09 (m, 1H C*H*^{e}), 3.82 (d, ^{3}J(H,H) = 6.9 Hz, 1H, N*H*), 1.96–1.78 (m, 6H, CH_2^{b+d}), 1.69 (m, 4H, CH_2^{c}), 1.45 (m, 2H, CH_2^{h}), 1.24 (m, 4H, CH_2^{g}), 0.97 (m, 4H, CH_2^{f}) ppm. $^{13}C\{^{1}H\}$ (101 MHz, C_6D_6, 25 °C) δ = 152.3 (d, ^{1}J(C,P) = 31.8 Hz, *C*=N), 135.8 (d, ^{1}J(C,P) = 14.4 Hz, PPh_2^{i}), 134.4 (d, ^{3}J(C,P) = 19.5 Hz, PPh_2^{m}), 129.4 (PPh_2^{p}), 129.1

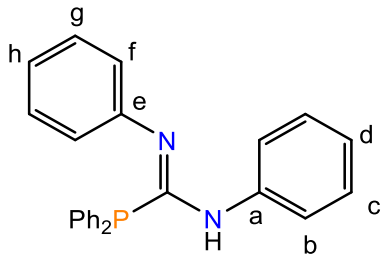
(d, ^{2}J(C,P) = 6.8 Hz, PPh_2^{o}), 60.4 (d, ^{4}J(C,P) = 34.0 Hz, CH^{e}), 49.3 (CH^{a}), 35.8 (CH_2^{d}), 32.7 (CH_2^{b}), 26.4 (CH_2^{h}), 26.3(CH_2^{f}), 25.3(CH_2^{g}), 24.7 (CH_2^{c}). ppm. $^{31}P\{^{1}H\}$ (162 MHz, C_6D_6, 25 °C) δ = −18.3 ppm. MS (ESI) Expected: 393.2454, found: 393.2455 (err [ppm] = 0.30) $[M+H]^+$. Cyclohexyl environments assigned using COSY. Characterisation matched literature data.[74]

2.5.5.2 $Ph_2PC(=N^{i}Pr)NH(^{i}Pr)$ 12b



^{1}H NMR (400 MHz, C_6D_6, 25 °C) δ = 7.46 (m, 4H, Ph^{o}), 7.06 (m, 6H, Ph^{m+p}), 4.38 (br s, 1H, CH^{a}), 4.31 (br s, 1H, CH^{c}), 1.22 (br s, 6H, CH_3^{b}), 0.96 (br s, 6H, CH_3^{d}) ppm. $^{13}C\{^{1}H\}$ NMR (101 MHz, C_6D_6, 25 °C) δ = 152.4 (d, ^{1}J(C,P) = 32.1 Hz, C=N), 135.6 (d, ^{1}J(C,P) = 14.2 Hz, Ph^{i}), 134.3 (d, ^{2}J(C,P) = 19.7 Hz, Ph^{o}), 129.4 (Ph^{p}), 129.1 (d, ^{3}J(C,P) = 6.7 Hz, Ph^{m}), 52.2 (d, ^{4}J(C,P) = 35.2 Hz, $CH^{a,}$), 42.9 (CH^{c}), 25.4 (CH_3^{b}), 22.5 (CH_3^{d}) ppm. $^{31}P\{^{1}H\}$ (162 MHz, C_6D_6, 25 °C) δ = −18.5 ppm. MS (ESI) Expected: 313.1828, found: 313.1845 (err [ppm] = 5.40) $[M+H]^+$. Characterisation matched literature data.[74]

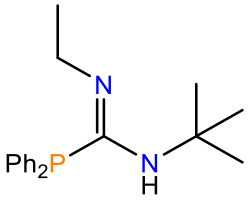
2.5.5.3 $Ph_2PC(=NPh)NH(Ph)$ 12c



^{1}H NMR (400 MHz, C_6D_6, 25 °C) δ = 7.68 (d, ^{3}J(H,H) = 8.0 Hz, 4H, Ph^{b+f}), 7.44–7.28 (m, 6H, PPh_2^{o+p}), 7.13–7.05 (m, 2H, Ph^{d+h}), 7.00 (m, 4H, PPh_2^{m}), 6.91–6.81 (m, 4H, Ph^{c+g}),

6.44 (s, 1H, N*H*) ppm. $^{13}C\{^{1}H\}$ NMR (101 MHz, C_6D_6, 25 °C) δ = 155.3 (*C*=N, ^{1}J(C,P) = 41.0 Hz), 150.8 (PPh_2^{i}, ^{1}J(C,P) = 12.3 Hz), 141.9 (Ph^{e}), 141.0 (PPh_2^{o}), 139.43 (Ph^{a}), 134.4 (PPh_2^{p}), 129.8 (Ph^{b}), 129.3 (Ph^{h}), 129.2 (Ph^{d}), 123.2 (Ph^{g}), 122.9 (Ph^{c}), 122.8 (d, ^{3}J(C,P) = 2.3 Hz, PPh_2^{m}), 119.0 (Ph^{f}) ppm. $^{31}P\{^{1}H\}$ (162 MHz, C_6D_6, 25 °C) δ = –11.3 ppm. MS (ESI) Expected: 381.1515, found: 381.1534 (err [ppm] = 5.00) $[M+H]^+$. Characterisation matched literature data.[72]

2.5.5.4 $Ph_2PC(=NEt)NH(^tBu)$ 12d



^{1}H NMR (400 MHz, C_6D_6, 25 °C) δ = 7.45 (m, 4H, Ph^{m}), 7.10–7.01 (m, 6H, Ph^{o+p}), 3.78–3.70 (m, 3H, CH_2CH_3 + N*H*), 1.32 (s, 9H, CCH_3), 1.27 (t, ^{3}J(H,H) = 7.1 Hz, 3H, CH_2CH_3) ppm. $^{13}C\{^{1}H\}$ (101 MHz, C_6D_6, 25 °C) δ = 153.8 (d, ^{1}J(C,P) = 33.5 Hz *C*=N), 138.0 (d, ^{1}J(C,P) = 12.2 Hz Ph^{i}), 134.4 (Ph^{m}), 129.3 (Ph^{p}), 129.1 (Ph^{o}), 52.2 (CCH_3) 46.8 (d, ^{4}J(C,P) = 36.7 Hz CH_2CH_3), 28.8 (CCH_3), 17.8 (CH_2CH_3) ppm. $^{31}P\{^{1}H\}$ (162 MHz, C_6D_6, 25 °C) δ = –16.1 ppm. MS (ESI) Expected: 131.1828, found: 313.1829 (err [ppm] = 0.10) $[M+H]^+$. Characterisation data matched literature data.[67]

2.6 References

1 T. C. McMorris, R. Chimmani, K. Alisala, M. D. Staake, G. Banda and M. J. Kelner, *J. Med. Chem.*, 2010, **53**, 1109–1116.

2 I. H. Kim, H. J. Tsai, K. Nishi, T. Kasagami, C. Morisseau and B. D. Hammock, *J. Med. Chem.*, 2007, **50**, 5217–5226.

3 E. Ballinger, J. Mosior, T. Hartman, K. Burns-Huang, B. Gold, R. Morris, L. Goullieux, I. Blanc, J. Vaubourgeix, S. Lagrange, L. Fraisse, S. Sans, C. Couturier, E. Bacqué,

K. Rhee, S. M. Scarry, J. Aubé, G. Yang, O. Ouerfelli, D. Schnappinger, T. R. Ioerger, C. A. Engelhart, J. A. McConnell, K. McAulay, A. Fay, C. Roubert, J. Sacchettini and C. Nathan, *Science*, 2019, **363**, 498.

4 J.-U. Kim, R. Davis and R. Zentel, *J. Colloid Interface Sci.*, 2011, **359**, 428–435.

5 B. Lin and R. M. Waymouth, *J. Am. Chem. Soc.*, 2017, **139**, 1645–1652.

6 S. Dawn, S. R. Salpage, B. A. Koscher, A. Bick, A. C. Wibowo, P. J. Pellechia and L. S. Shimizu, *J. Phys. Chem. A*, 2014, **118**, 10563–10574.

7 P. W. Sherwood, *J. Coatings Technol.*, 1982, **54**, 61–65.

8 A. Guan, C. Liu, X. Yang and M. Dekeyser, *Chem. Rev.*, 2014, **114**, 7079–7107.

9 H. A. Bates, N. Condulis and N. L. Stein, *J. Org. Chem.*, 1986, **51**, 2228–2229.

10 A. M. Tafesh and J. Weiguny, *Chem. Rev.*, 1996, **96**, 2035–2052.

11 T. Kondo, S. Kotachi, Y. Tsuji, Y. Watanabe and T. Mitsudo, *Organometallics*, 1997, **16**, 2562–2570.

12 R. Nomura, Y. Hasegawa, M. Ishimoto, T. Toyosaki and H. Matsuda, *J. Org. Chem.*, 1992, **57**, 7339–7342.

13 D. J. Díaz, A. K. Darko and L. McElwee-White, *Eur. J. Org. Chem.*, 2007, 4453–4465.

14 A. G. M. Barrett, T. C. Boorman, M. R. Crimmin, M. S. Hill, G. Kociok-Kohn and P. A. Procopiou, *Chem. Commun.*, 2008, 5206–5208.

15 A. Hernan-Gomez, T. D. Bradley, A. R. Kennedy, Z. Livingstone, S. D. Robertson and E. Hevia, *Chem. Commun.*, 2013, **49**, 8659–8661.

16 J. Bhattacharjee, S. Das, R. K. Kottalanka and T. K. Panda, *Dalton Trans.*, 2016, **45**, 17824–17832.

17 K. Naktode, S. Das, J. Bhattacharjee, H. P. Nayek and T. K. Panda, *Inorg. Chem.*, 2016, **55**, 1142–1153.

18 T. E. Müller, K. C. Hultzsch, M. Yus, F. Foubelo and M. Tada, *Chem. Rev.*, 2008, **108**, 3795–3892.

19 R. Severin and S. Doye, *Chem. Soc. Rev.*, 2003, **32**, 104–114.

20 A. Harinath, K. Bano, S. Ahmed and T. K. Panda, *Phosphorus Sulfur Silicon Relat.*

Elem., 2018, **193**, 23–32.

21 I. S. R. Karmel, M. Tamm and M. S. Eisen, *Angew. Chem. Int. Ed.*, 2015, **54**, 12422–12425.

22 H. Liu, N. Fridman, M. Tamm and M. S. Eisen, *Organometallics*, 2017, **36**, 3896–3903.

23 E. Delebecq, J.-P. Pascault, B. Boutevin and F. Ganachaud, *Chem. Rev.*, 2013, **113**, 80–118.

24 T. Hu, A. L. Connor, D. P. Miller, X. Wang, Q. Pei, R. Liu, L. He, C. Zheng, E. Zurek, Z. L. Lu and B. Gong, *Org. Lett.*, 2017, **19**, 2666–2669.

25 J. L. Hou, X. Bin Shao, G. J. Chen, Y. X. Zhou, X. K. Jiang and Z. T. Li, *J. Am. Chem. Soc.*, 2004, **126**, 12386–12394.

26 T. Moriuchi, T. Tamura and T. Hirao, *J. Am. Chem. Soc.*, 2002, **124**, 9356–9357.

27 A. Kwiatkowski, I. Grela and B. Ośmiałowski, *New J. Chem.*, 2017, **41**, 1073–1081.

28 K. Mroczyńska, M. Kaczorowska, E. Kolehmainen, I. Grubecki, M. Pietrzak and B. Ośmiałowski, *Beilstein J. Org. Chem.*, 2015, **11**, 2105–2116.

29 D.-W. Zhang, X. Zhao, J.-L. Hou and Z.-T. Li, *Chem. Rev.*, 2012, **112**, 5271–5316.

30 J. Lawson and W. T. A. Harrison, *Acta Crystallogr. Sect. E Struct. Reports Online*, 2005, **61**, 525–527.

31 W. T. A. Harrison, *Acta Crystallogr. Sect. C Cryst. Struct. Commun.*, 2008, **64**, 205–208.

32 M. Graf, K. Sünkel, R. Czerwieniec and H.-C. Böttcher, *J. Organomet. Chem.*, 2013, **745**–**746**, 341–346.

33 F. Kurzer, *Chem. Rev.*, 1956, **56**, 95–197.

34 E. Dyer and R. B. Pinkerton, *J. Appl. Polym. Sci.*, 1965, **9**, 1713–1729.

35 D. R. Park, H. Kim, J. C. Jung, M. S. Shin, S. J. Han and I. K. Song, *Korean J. Chem. Eng.*, 2009, **26**, 990–993.

36 H. R. Sharpe, A. M. Geer, W. Lewis, A. J. Blake and D. L. Kays, *Angew. Chem. Int. Ed.*, 2017, **56**, 4845–4848.

37 H. R. Sharpe, A. M. Geer, H. E. L. Williams, T. J. Blundell, W. Lewis, A. J. Blake and

D. L. Kays, *Chem. Commun.*, 2017, **53**, 937–940.

38 A. Saednya and H. Hart, *Synthesis*, 1996, 1455–1458.

39 K. Ruhlandt-Senge, J. J. Ellison, R. J. Wehmschulte, F. Pauer and P. P. Power, *J. Am. Chem. Soc.*, 1993, **115**, 11353–11357.

40 D. L. Kays and A. R. Cowley, *Chem. Commun.*, 2007, 1053–1055.

41 A. Schröder, E. Lork and J. Beckmann, *Main Group Met. Chem.*, 2014, **37**, 155–157.

42 Y. Taguchi, I. Shibuya, T. Tsuchiya and K. Yonemoto, *Bull. Chem. Soc. Jpn.*, 1990, 63, 3486–3489.

43 J. E. Tanner, *J. Chem. Phys.*, 1970, **52**, 2523–2526.

44 P. Groves, *Polym. Chem.*, 2017, **8**, 6700–6708.

45 R. Richter, *Chem. Ber.*, 1968, **101**, 3002–3009.

46 Y. V. Savel'ev, V. A. Khranovskii, V. Y. Veselov, A. P. Grekov and O. A. Savel'eva, *Russ. J. Org. Chem.*, 2003, **39**, 96–98.

47 Y. Okamoto, M. Matsuda, T. Nakano and E. Yashima, *J. Polym. Sci. Part A Polym. Chem.*, 1994, **32**, 309–315.

48 J. Dawlaty, X. Zhang, M. A. Fischbach and J. Clardy, *J. Nat. Prod.*, 2010, **73**, 441–446.

49 B. K. Verlinden, J. Niemand, J. Snyman, S. K. Sharma, R. J. Beattie, P. M. Woster and L. M. Birkholtz, *J. Med. Chem.*, 2011, **54**, 6624–6633.

50 T. A. Wencewicz, *Bioorganic Med. Chem.*, 2016, **24**, 6227–6252.

51 M. Vojdani and R. Giti, *J. Dent. (Shiraz, Iran)*, 2015, **16**, 1–9.

52 D. L. Francisco, L. B. Paiva and W. Aldeia, *Polym. Compos.*, 2019, **40**, 851–870.

53 W. J. Lau, S. Gray, T. Matsuura, D. Emadzadeh, J. Paul Chen and A. F. Ismail, *Water Res.*, 2015, **80**, 306–324.

54 R. H. Crabtree, *Chem. Rev.*, 2012, **112**, 1536–1554.

55 J. A. Widegren and R. G. Finke, *J. Mol. Catal. A Chem.*, 2003, **198**, 317–341.

56 Y. Li, S. Yu, X. Wu, J. Xiao, W. Shen, Z. Dong and J. Gao, *J. Am. Chem. Soc.*, 2014, **136**, 4031–4039.

57 A. M. Träff, M. Janjetovic, L. Ta and G. Hilmersson, *Angew. Chem. Int. Ed.*, 2013, **52**, 12073–12076.

58 B. J. Hornstein, J. D. A. Iii and R. G. Finke, *Inorg. Chem.*, 2002, **41**, 1625–1638.

59 J. F. Sonnenberg and R. H. Morris, *Catal. Sci. Technol.*, 2014, **4**, 3426–3438.

60 K. J. Gallagher and R. L. Webster, *Chem. Commun.*, 2014, **50**, 12109–12111.

61 J. Penafiel, L. Maron and S. Harder, *Angew. Chem. Int. Ed.*, 2015, **54**, 201–206.

62 M. R. Crimmin, I. J. Casely and M. S. Hill, *J. Am. Chem. Soc.*, 2005, **127**, 2042–2043.

63 M. D. Greenhalgh, A. S. Jones and S. P. Thomas, *ChemCatChem*, 2015, **7**, 190–222.

64 R. J. Schwamm, B. M. Day, N. E. Mansfield, W. Knowelden, P. B. Hitchcock and M. P. Coles, *Dalton Trans.*, 2014, **43**, 14302–14314.

65 A. G. M. Barrett, M. R. Crimmin, M. S. Hill, P. B. Hitchcock, S. L. Lomas, M. F. Mahon and P. A. Procopiou, *Dalton Trans.*, 2010, **39**, 7393–7400.

66 F. T. Edelmann, *Chem. Soc. Rev.*, 2012, **41**, 7657–7672.

67 M. R. Crimmin, A. G. M. Barrett, M. S. Hill, P. B. Hitchcock and P. A. Procopiou, *Organometallics*, 2008, **27**, 497–499.

68 W. Ma, L. Xu, W.-X. Zhang and Z. Xi, *New J. Chem.*, 2015, **39**, 7649–7655.

69 V. A. Pollard, A. Young, R. McLellan, A. R. Kennedy, T. Tuttle and R. E. Mulvey, *Angew. Chem. Int. Ed.*, 2019, **58**, 12291–12296.

70 B. Neises and W. Steglich, *Org. Synth.*, 1990, **7**, 93.

71 L. A. Carpino and A. El-Faham, *Tetrahedron*, 1999, **55**, 6813–6830.

72 Y. Zhang, L. Qu, Y. Wang, D. Yuan, Y. Yao and Q. Shen, *Inorg. Chem.*, 2018, **57**, 139–149.

73 C. Jiang, P. J. Young, C. B. Durr, T.F. Spilker, M. H. Chisholm, *Inorg. Chem.*, 2016, **55**, 5836–5844.

74 W.-X. X. Zhang, M. Nishiura and Z. Hou, *Chem. Commun.*, 2006, 3812–3814.

75 S. Lee, H. Matsushita, B. Clapham and K. D. Janda, *Tetrahedron*, 2004, 3439–3443.

76 M. J. Fuchter, C. J. Smith, M. W. S. Tsang, A. Boyer, S. Saubern, J. H. Ryana and

A. B. Holmes, *Chem. Commun.*, 2008, 2152–2154.

Chapter 3

Hydroboration of Heterocumulenes

3.1 Introduction

3.1.1 Catalytic Hydroboration

Hydroboration is the addition of a B–H bond across an unsaturated bond. It is an important reaction in organic chemistry due to its use in forming a variety of organoboron compounds[1] that have applications in organic synthesis to produce a wide range of organic products.[2–5] A common example is in the hydration of alkenes which can be achieved by the hydroboration of the alkene and then subsequent oxidation of the organoboron product.[6] The structures of some commercially available boranes that are frequently used in hydroboration reactions are shown in Figure 1.

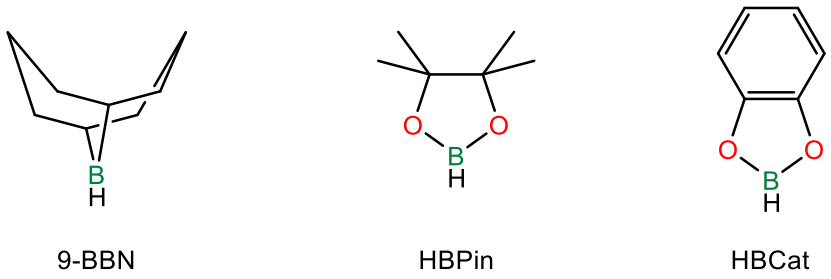
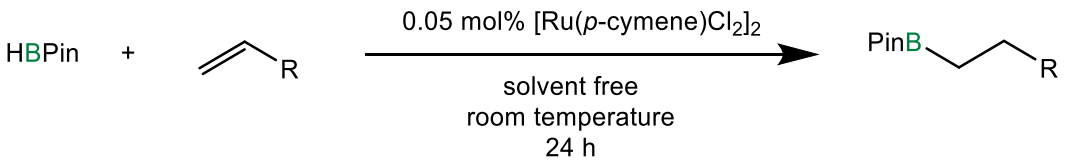


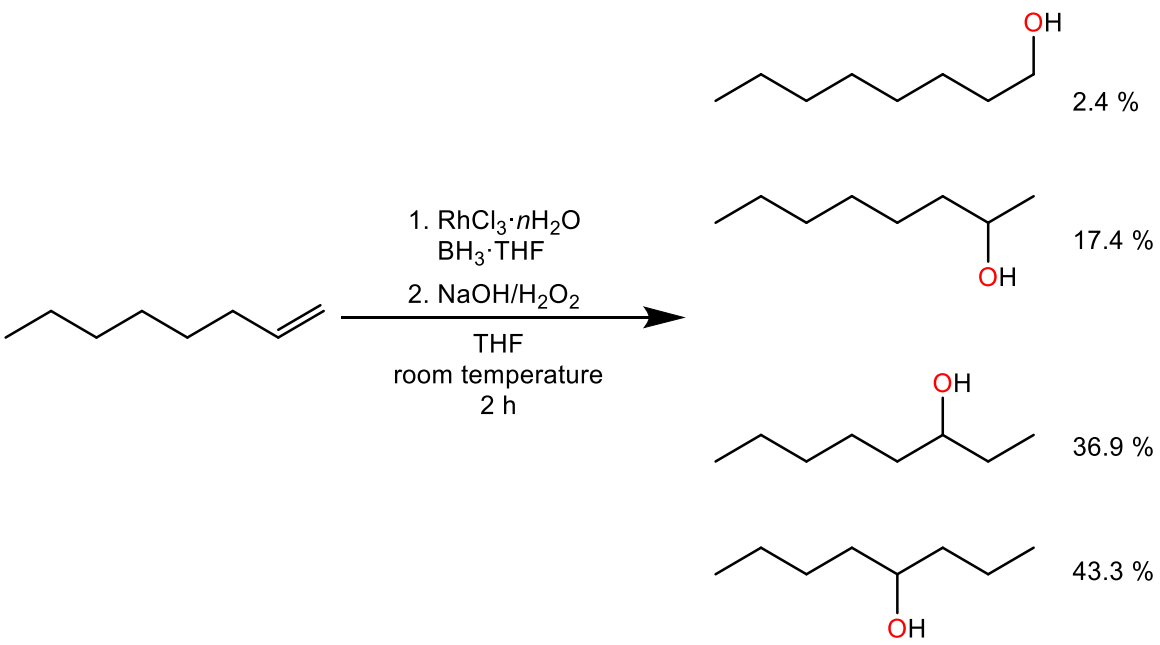
Figure 1. Molecular structure and abbreviations of commonly used boranes.

There are some examples of hydroboration reactions that do not require the use of a catalyst, for example the hydroboration of alkenes using 9-borabicyclo[3.3.1]nonane (9-BBN) has been widely reported.[1,7] Other boranes, such as the more electron deficient pinacolborane (HBPin) and catecholborane (HBCat) often require a catalyst in order to undergo hydroboration under mild conditions.[8–13] A recent example is the hydroboration of alkenes with HBPin catalysed by [Ru(*p*-cymene)Cl_2]$_2$ (Scheme 1).[14]



Scheme 1. Hydroboration of alkenes catalysed by [Ru(*p*-cymene)Cl_2]$_2$.[14]

Some catalysts can control the selectivity of the reaction. One example of this is the hydroboration of 1-octene by BH_3·THF catalysed by $RhCl_3$·$n$$H_2O$.[10] The hydroboration reaction was followed by an oxidation with $NaOH/H_2O_2$, which resulted in only 2.4% conversion to the 1-octanol product, and a much larger conversion to the 3- and 4-octanol products (Scheme 2). This is in comparison to the uncatalysed reaction where 92.8% of the 1-octanol is formed. In the uncatalysed reaction the 'BH_2' moiety is substituted at the least sterically hindered position, but in the catalysed reaction the 'BH_2' group is substituted in the more sterically hindered positions. In the catalysed reaction the isomerisation of the alkene is much faster than the formation of the C–B bond so the more stable isomer is formed and then hydroboration takes place leading to the formation of 3- and 4-octanol.[10]



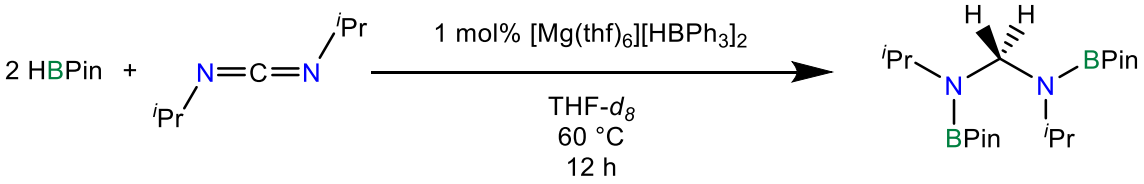
Scheme 2. Catalytic hydroboration of 1-octene followed by oxidation with $NaOH/H_2O_2$.[10]

Traditional catalysts for hydroboration are generally precious metals such as rhodium or ruthenium[15–17] (as illustrated in the previous examples) so there is a need for catalysts from more earth abundant metals due to their lower cost and higher availability.

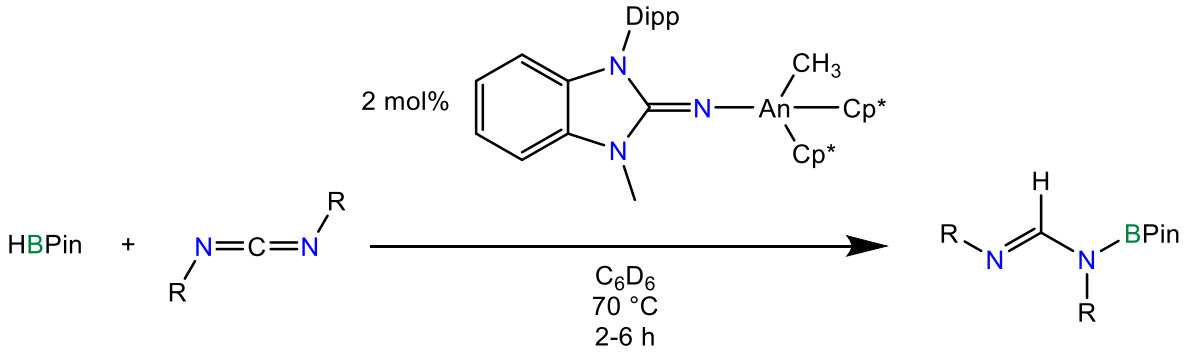
3.1.2 Hydroboration of Heterocumulenes

The hydroboration of substrates such as alkenes[10–20] and ketones[21–23] has been widely investigated but reports of the hydroboration of heterocumulenes such as isocyanates and carbodiimides are limited to magnesium,[24–27] aluminium[28] and f block[29] metals. There have currently been no transition metal catalysts reported.

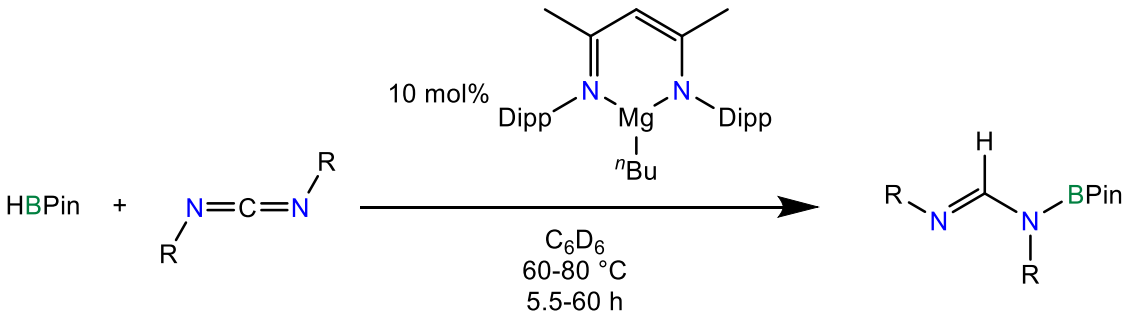
The hydroboration of carbodiimides can result in either the monohydroboration or dihydroboration product where the boron group ends up on either one nitrogen or both nitrogen atoms of the carbodiimide respectively. The use of different catalysts can selectively produce one of these products. For example, the use of $[Mg(thf)_6][HBPh_3]_2$ as a catalyst results in the exclusive formation of the dihydroboration product (Scheme 3),[25] whereas the actinide catalyst reported by Eisen *et al.* exclusively forms the monohydroboration product (Scheme 4).[29] Hill *et al.* also reported a magnesium precatalyst that catalyses the hydroboration of carbodiimides (Scheme 5) which exclusively forms the monohydroboration product.[24]



Scheme 3. Hydroboration of ^{i}PrNCN^{i}Pr with HBPin catalysed by $[Mg(thf)_6][HBPh_3]_2$.[25]

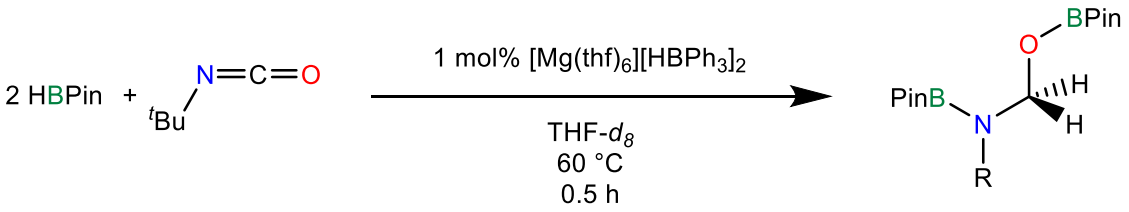


Scheme 4. Hydroboration of carbodiimides with HBPin in the presence of an actinide catalyst (An = U or Th; R = alkyl or aromatic group).[29]



Scheme 5. Hydroboration of carbodiimides with a magnesium catalyst (R = alkyl or aromatic group).[24]

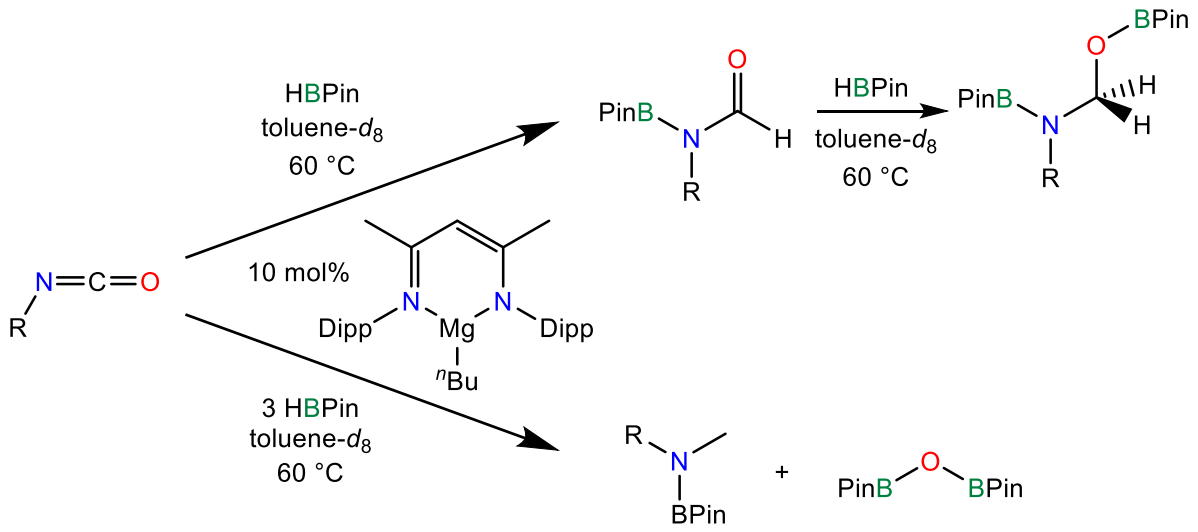
There are only two reported precatalysts for the hydroboration of isocyanates and these are the two magnesium complexes previously reported for the hydroboration of carbodiimides.[25,26] $[Mg(thf)_6][HBPh_3]_2$ was shown to catalyse the hydroboration of ^{t}BuNCO with HBPin. The dihydroboration of the isocyanate at both the nitrogen and oxygen atoms occurs (Scheme 6).[25] The reaction reached completion after 0.5 h at 60 °C.



Scheme 6. Hydroboration of ^{t}BuNCO with HBPin catalysed by $[Mg(thf)_6][HBPh_3]_2$

The magnesium precatalyst reported by Hill *et al.* has a wider substrate scope than $[Mg(thf)_6][HBPh_3]_2$.[26] The products obtained with this precatalyst can be changed through the manipulation of the reaction stoichiometry (Scheme 7). When two equivalents of HBPin were used the dihydroboration of isocyanates at the nitrogen and oxygen atoms occurs. This hydroboration reaction only takes place in significant yields with the aromatic isocyanates MesNCO and DippNCO as substrates. These reactions take place at room temperature and reach 100% conversion after just 15 minutes. The monohydroboration product, where the BPin only adds at the nitrogen atom of the isocyanate is observed as an intermediate for this reaction. When three equivalents of HBPin were used in the

reaction the hydrodeoxygenation of the isocyanate occurs; this reaction involves the cleavage of the C=O bond of the isocyanate and the formation of $O(BPin)_2$. The mechanism for this catalysis involves the sequential addition of the borane to the isocyanate and the hydrodeoxygenation reaction proceeds *via* the formation of the monohydroboration and then dihydroboration products.[26]



Scheme 7. Hydroboration and hydrodeoxygenation of isocyanates with a magnesium catalyst (R = alkyl or aromatic group).[26]

3.2 Aims

The aim of this work was to investigate the use of first row transition metal *m*-terphenyl complexes as precatalysts for the hydroboration of heterocumulenes. The effect of the metal centre on the reaction was investigated. A range of different substrates were used to investigate the effect of the heterocumulene on the catalysis and the mechanism of the catalysis was investigated using stoichiometric reactions and poisoning experiments. This was the first reported example of a transition metal catalyst for this reaction and greatly increases the scope of the reaction compared to the previously reported catalysts.

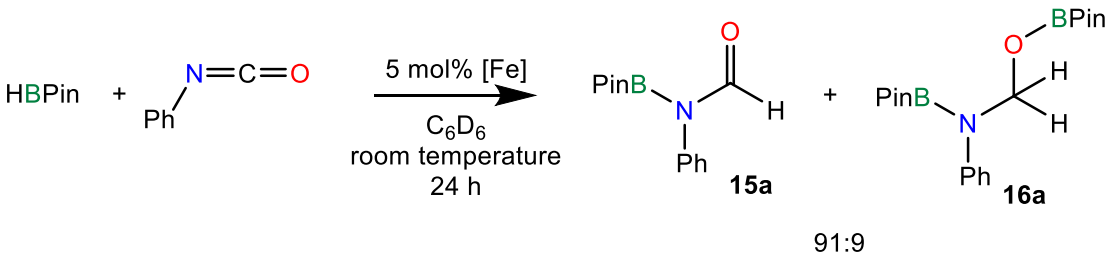
3.3 Results and Discussion

3.3.1 Iron Catalysed Hydroboration of Isocyanates

3.3.1.1 Initial Investigations

Initially, control reactions between HBPin and PhNCO were performed in the absence of a catalyst. No reaction was determined to have occurred at room temperature after 48 h by ^{1}H and ^{11}B NMR spectroscopy. In order to investigate the use of Fe(2,6-$Mes_2C_6H_3)_2$ (**3**) as a precatalyst for this reaction, an NMR scale reaction in C_6D_6 between HBPin and PhNCO (1:1) in the presence of **3** (5 mol%) was carried out (Scheme 8). The hydroboration products (of the formula RN(BPin)C(=O)H and RN(BPin)C(OBPin)H_2) have been reported to decompose with heating so the reaction was carried out at ambient temperature.[26] The reaction was monitored using ^{1}H and ^{11}B NMR spectroscopy (Figure 2), with the initial ^{11}B NMR spectrum displaying a doublet at 28.5 ppm due to the HBPin substrate. After 4 h a new peak in the spectrum at 25.9 ppm is observed and there is a concomitant colour change from a bright yellow to a colourless solution. Measurement of the ^{11}B NMR spectrum at 24 hours shows that this resonance had increased in intensity, and the initial doublet has decreased in size and a second small new peak at 21.9 ppm has grown in with 82% conversion of the HBPin. These two new chemical shifts are in agreement with those observed by Hill *et al.*, suggesting that the use of precatalyst **3** affords the analogous mono- and dihydroboration products.[26] The peak at 25.9 ppm is assigned to N*B*Pin and the peak at 21.9 ppm is assigned to O*B*Pin.[26] In the monohydroboration product there is one NBPin and in the dihydroboration product there is both an NBPin and an OBPin (Scheme 8), the similarity between the two NBPin environments mean that it is difficult to quantify the ratio of these two products from the integration of the ^{11}B NMR spectra (integration of ^{11}B NMR is also often unreliable). However, it was possible to quantify the product ratio using the ^{1}H NMR spectrum, as the monohydroboration C*H* appears at 9.18 ppm and the dihydroboration CH_2 appears at 4.96 ppm.[26] The integration of these peaks confirms the major product as the monohydroboration product (**15a**) and the minor product as the dihydroboration product (**16a**) with a ratio of 91:9 indicating that although

the ratio of HBPin:PhNCO used was 1:1 a small amount of **16a** is formed (Table 2, Entry 1).



Scheme 8. Catalytic hydroboration of PhNCO with HBPin in the presence of **3** (5 mol%) in C_6D_6 at room temperature ([Fe] = **3**).

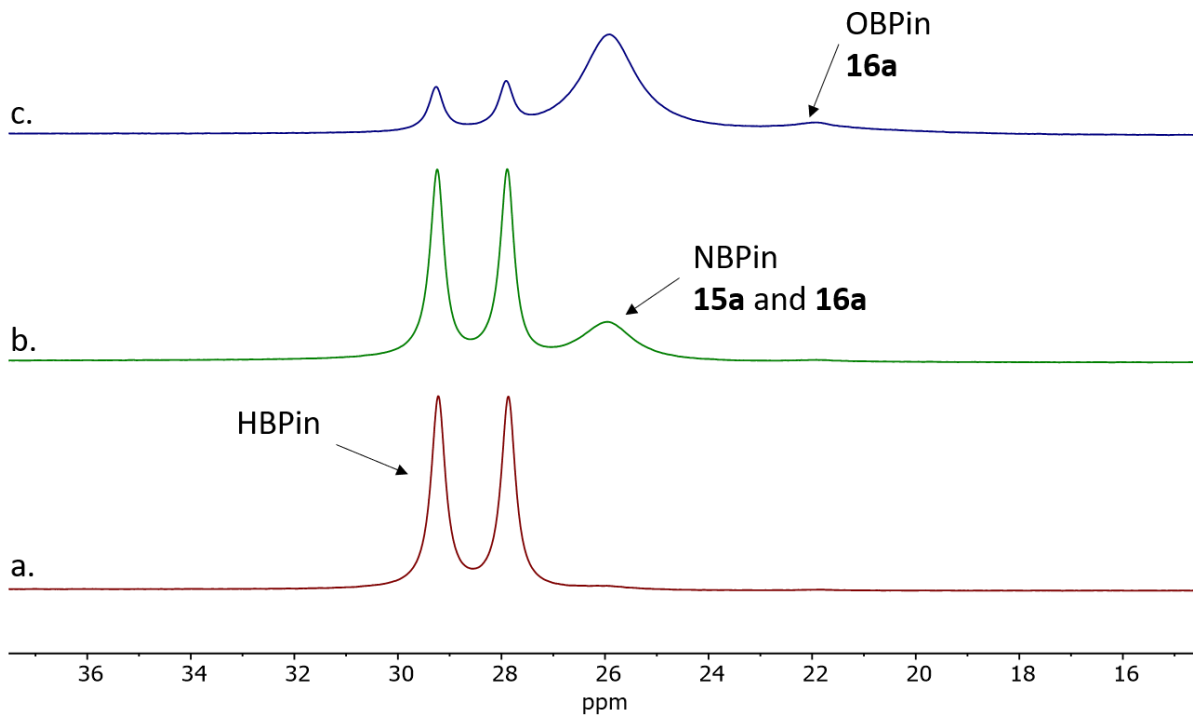


Figure 2. ^{11}B NMR spectra of reaction between HBPin and PhNCO (1:1) in C_6D_6 at 25 °C in the presence of 3 after a) 10 min, b) 4 h, c) 24 h.

Crystals of **15a** suitable for X-ray crystallography were grown from a saturated solution of the compound in C_6D_6 solution at room temperature (Figure 3 and Table 1). The C1–O1 bond length is 1.2149(14) Å and the O3–C7–N1 bond angle is 125.06(11)° which are both

indicative of a carbonyl bond and are similar values to the Dipp-substituted analogue reported by Hill *et al*.[26]

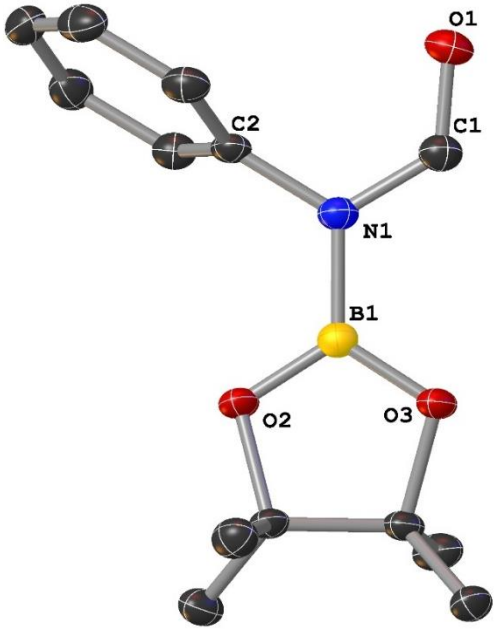
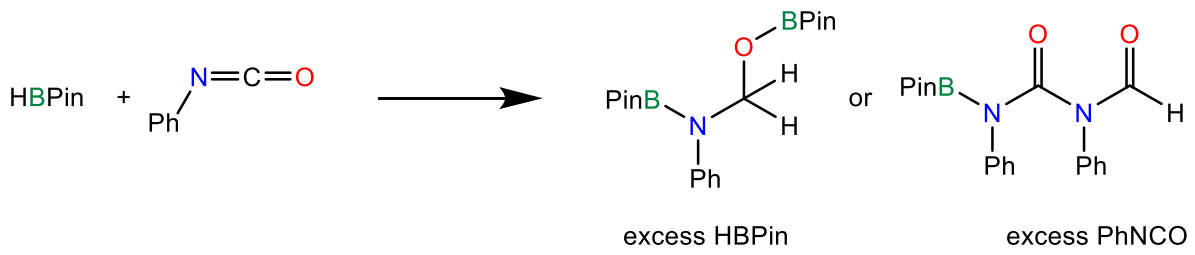


Figure 3. Crystal structure of **15a**, with thermal ellipsoids at 50% probability and hydrogen atoms omitted for clarity (black = carbon, blue = nitrogen, red = oxygen, yellow = boron).

Table 1. Selected bond lengths (Å) and bond angles (°) for **15a**.

	15a
B1–N1	1.4480(15)
C1–O1	1.2149(14)
O1–C1–N1	125.06(11)

The ratio of the substrates was altered in an effort to investigate the effect on the selectivity of the reaction. Increasing the ratio of HBPin could increase the yield of the dihydroboration product **16a** whereas increasing the ratio of PhNCO could result in the diinsertion of the isocyanate which is observed in the hydrophosphination[31] and hydroamination (Chapter 2) of isocyanates with this precatalyst (Scheme 9).



Scheme 9. Proposed structures of products resulting from the dihydroboration of the isocyanate or the diinsertion of the isocyanate.

In an effort to increase the yield of the dihydroboration product **16a**, the reaction was performed with a 2:1 ratio of HBPin:PhNCO (Table 2, Entry 2). This resulted in complete consumption of the isocyanate in just 7 h but little change in the ratio of the products formed, as determined by ^{1}H NMR spectroscopy. The reaction with a 5:1 HBPin:PhNCO ratio was also carried out and it was found that there was no PhNCO present after 5 h, but again the monohydroboration product is favoured (Table 2, Entry 3). This suggests that the catalyst favours the monohydroboration product even when there is an excess of HBPin available. This is different to the magnesium catalyst reported by Hill *et al*. where the dihydroboration is selectively formed and the monohydroboration is only observed as an intermediate.[26] This suggests that this catalyst undergoes a different mechanism to that proposed by Hill and the second hydroboration is disfavoured. Crystals were obtained from the 5:1 C_6D_6 reaction solution and were found to be $[PinBOC(CH_3)_2]_2$ (**17**) (Figure 4). This is from the decomposition of pinacol borane which is also observed by Hill *et al*. in the hydroboration of imines.[30] This is likely a consequence of the large excess of unreacted pinacolborane that was present in the reaction mixture. It has a chemical shift in the ^{11}B NMR spectra at 24.8 ppm. It is not observed during the course of the reaction and the crystals formed after storage of the C_6D_6 solution for a week at room temperature.

Table 2. Catalytic hydroboration of PhNCO with HBPin in C_6D_6 mediated by **3**.[a]

Entry	HBPin:PhNCO	Time (h)	Conversion (%)[b]	**15a**:**16a**[b]
1	1:1	24	82	91:9
2	2:1	7	100	98:2
3	5:1	5	99	98:2
4	1:2	24	100	82:18[c]
5	1:5	0.75	100	82:18[c]

[a] Reaction conditions: 10 mg of **3** (5 mol%), 0.6 mL C_6D_6 at room temperature. [b] Determined by ^{1}H NMR spectroscopy using TMS as an internal standard with respect to limiting reagent. [c] Unidentified product also present.

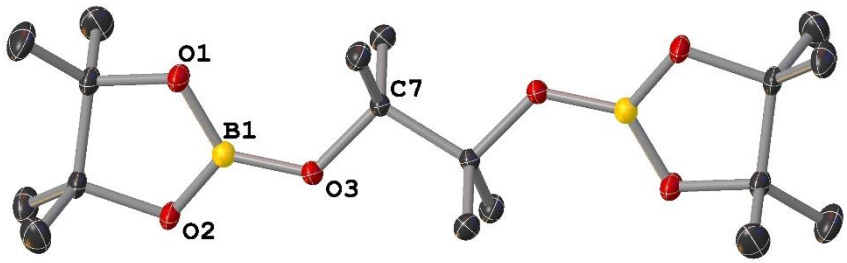


Figure 4. Crystal structure of **17**, with thermal ellipsoids at 50% probability. Hydrogen atoms omitted for clarity (black = carbon, red = oxygen, yellow = boron).

In order to investigate whether the diinsertion of the isocyanate occurs, two reactions with an excess of PhNCO were carried out with HBPin:PhNCO ratios of 1:2 and 1:5 (Table 2, Entries 4 and 5). This resulted in a new unidentified peak in the ^{11}B NMR spectrum at 9.4 ppm, which became larger as the ratio of isocyanate was increased (Figure 5). It was also observed that adding an excess of isocyanate decreased the reaction time needed for the pinacol borane to be fully consumed. When 5 equivalents of phenyl isocyanate are used there is no pinacol borane present after 45 minutes, however, there is still phenyl isocyanate present in the reaction mixture, which continues to react, and the peak at 9.4 ppm (broad singlet indicating that there is no coupling to any protons) in the ^{11}B NMR

spectra increases in size while the other peaks decrease. This is therefore likely to be a BPin group, although it is shifted significantly upfield compared to the OBPin and NBPin groups observed. The ratio of **15a**:**16a** increased from 91:9 (Table 2, Entry 1) to 82:18 (Table 2, Entries 4 and 5) as the ratio of PhNCO is increased. This appears to suggest that the ratio of the dihydroboration product is increasing as the ratio of HBPin decreases, however in the 1:2 and 1:5 reactions there is also another identified product (peak at 9.4 ppm). This means that the overall conversion of **15a** and **16a** in these reactions is smaller than it appears although the exact conversion of the unidentified product cannot be reported without confirmation of the structure.

Attempts were made to crystallise the reaction product for the 1:2 reaction between HBPin and PhNCO, in order to identify the unknown peak in the ^{11}B NMR spectrum. Colourless crystals were grown from hexane diffusion into the C_6D_6 solution. These were found to be **18** (Figure 6). The molecule is made up from four PhNCO fragments and one 'PhNC' fragment. It is a similar structure to the isocyanurate than can result from the cyclotrimerisation of isocyanates.[32] This unusual structure is presumably a result of the excess unreacted isocyanate that was in solution for a long period of time. One explanation for the missing O from the 'PhNC' fragment is the formation of $O(BPin)_2$ similar to the hydrodeoxygenation reaction that occurs with the magnesium catalyst reported by Hill *et al*. as discussed above.[26] This structure does not contain any boron atoms however, so does not explain the extra peak in the ^{11}B NMR spectrum.

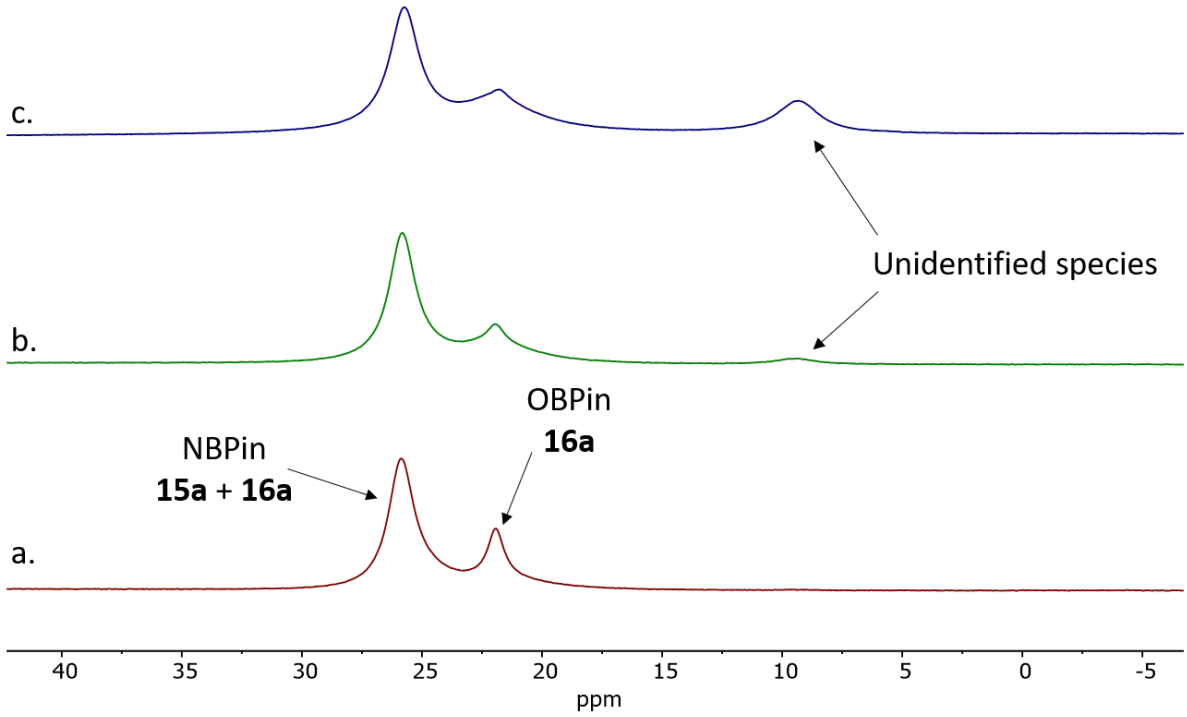


Figure 5. ^{11}B NMR spectra of reaction between HBPin and PhNCO in C_6D_6 in the presence of **3** after 24 h with a HBPin:PhNCO ratio of a) 1:1, b) 1:2 and c) 1:5.

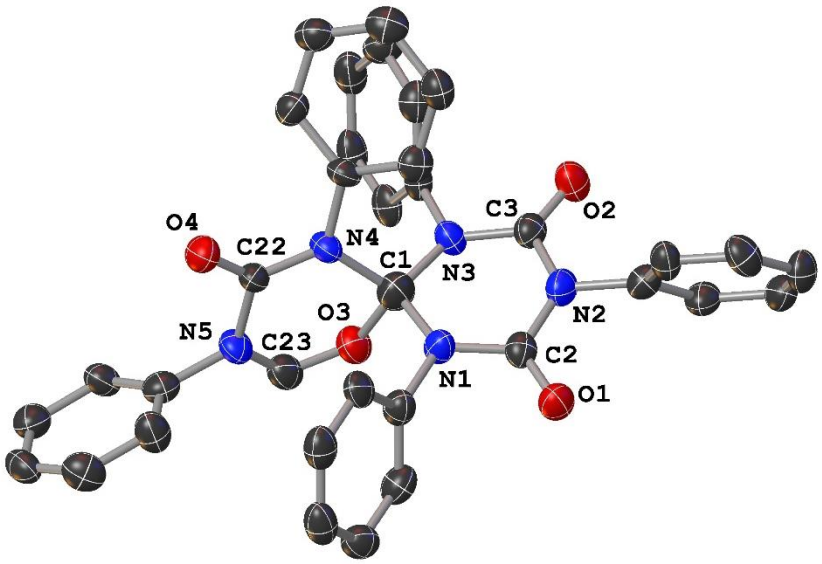


Figure 6. Crystal structure of **18**, with thermal ellipsoids at 50% probability. Hydrogen atoms and solvent molecule omitted for clarity (black = carbon, blue = nitrogen, red = oxygen).

3.3.1.2 Aromatic Isocyanates

The reaction was performed using a range of different aromatic isocyanates including isocyanates containing electron donating and withdrawing groups such as 3,5-$(MeO)_2C_6H_3NCO$ and 4-BrC_6H_4NCO as well as *p*-TolNCO. These all reached over 99% conversion after 24 h, apart from the Br containing isocyanate, which only reached 53% conversion (Table 3). This slower reaction was also observed for the hydroamination of this isocyanate at room temperature. The ratio of **15**:**16** for these isocyanates was similar to the 1:1 reaction between HBPin and PhNCO with the monohydroboration product being the major product and only a very small amount (less than 10%) of the dihydroboration product being formed.

Table 3. Catalytic hydroboration of aromatic isocyanates with HBPin in C_6D_6 at room temperature mediated by **3**.[a]

Entry	RNCO	HBPin:RNCO	Time (h)	Conversion (%)[b]	**15**:**16**[b]
1	3,5-$(MeO)_2C_6H_3$	1:1	24	94	93:7
2	4-BrC_6H_4	1:1	24	53	93:7
3	*p*-Tol	1:1	24	99	90:10

[a] Reaction conditions: 10 mg of **3** (5 mol%), 0.6 mL C_6D_6 at room temperature. [b] Determined by ^{1}H NMR spectroscopy using TMS as an internal standard.

A second peak corresponding to a C(=O)*H* proton at 9.61 ppm is observed in the ^{1}H NMR spectra in the reaction between HBPin and 3,5-$(OMe)_2C_6H_3NCO$ in the presence of **3**. Crystals were grown from a saturated C_6D_6 solution at room temperature. Single crystal X-ray diffraction measurements on these crystals determined them to be the Fe(II) complex **19** (Figure 7).

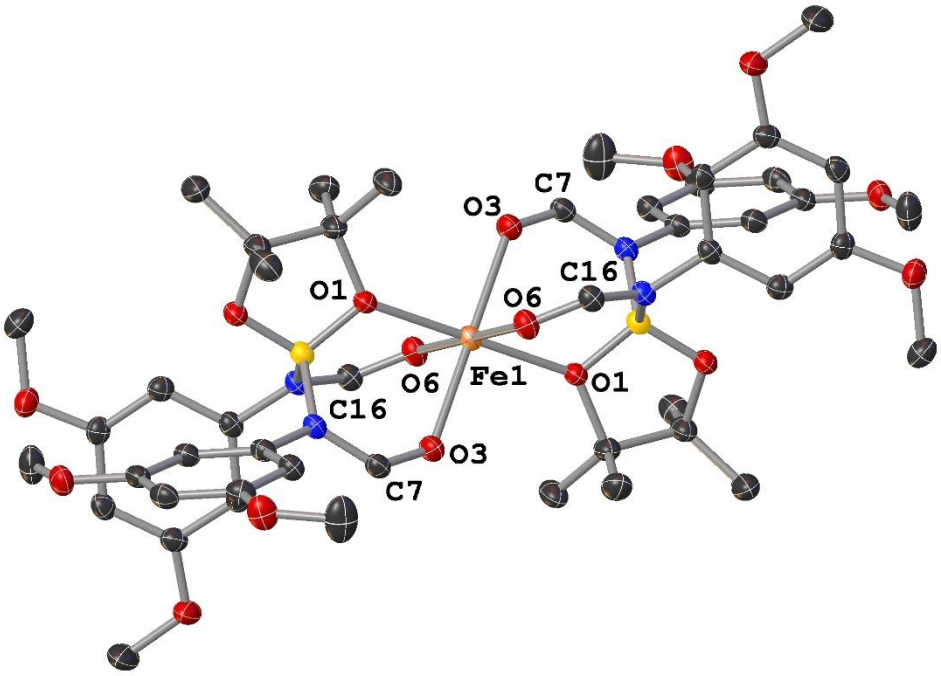


Figure 7. Crystal structure of **19**, with thermal ellipsoids at 50% probability. Hydrogen atoms and solvent molecules omitted for clarity (orange = iron, black = carbon, blue = nitrogen, red = oxygen, yellow = boron).

Table 4. Selected bond lengths (Å) and bond angles (°) for **19**.

	19
Fe1–O1	2.1130(9)
Fe1–O3	2.1666(9)
Fe1–O6	2.0477(9)
O3–C7	1.2448(16)
O6–C16	1.2480(17)
O1–Fe1–O3	95.73(3)
O1–Fe1–O6	84.81(4)
O3–Fe1–O6	88.55(4)

This crystallised in the $P2_1/c$ space group with half a molecule in the asymmetric unit and a benzene solvent molecule. It has a pseudo octahedral geometry around the iron metal

centre (O–Fe–O bond angles range from 84.27(3) to 95.73(3)°) with two tridentate ligands. A similar complex was reported by Kamitani *et al*. which was isolated from a reaction between an Fe(II) complex, KOAc and HBPin (Figure 8b).[33] The ligand for complex **19** is shown in Figure 8a. It is similar to the monohydroboration product **15b**, however with the incorporation of two isocyanate molecules leading to a four-coordinate boron atom. This product may explain the presence of the second carbonyl peak in the ^{1}H NMR spectrum at 9.62 ppm. The ligand is coordinated to the metal *via* the carbonyl oxygen atoms and one of the oxygen atoms in the BPin group. Hill *et al*. have observed a similar compound from the addition of HBPin and DippNCO to the Mg catalyst used for hydroboration (Figure 8c).[26] The O3–C7 and O6–C16 bond lengths are 1.2448(16) and 1.2480(17) Å respectively. These are similar to the C–O bond length (1.262(2) Å) in the complex shown in Figure 8c.[33] The ^{11}B NMR spectrum also exhibits small peaks at 1.1 and 6.7 ppm, which could be a result of this complex. As **19** does not contain any *m*-terphenyl ligands it seems unlikely that this is an intermediate to the catalysis.

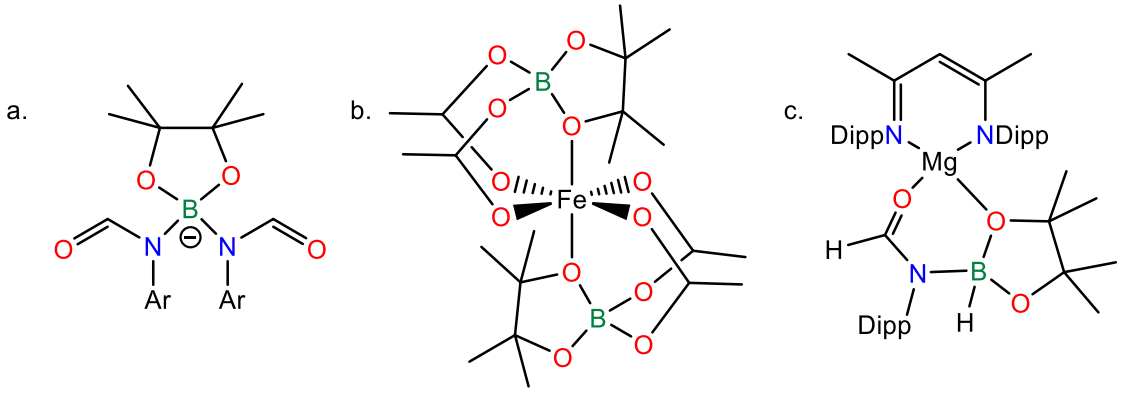


Figure 8. a) Ligand in complex **19** (Ar = 3,5-$(OMe)_2C_6H_3$); b) Molecular structure of a bis(diacetatopinacolylborate) iron complex.[33]; c) Molecular structure of Mg complex containing BPin group.[26]

3.3.1.3 Aliphatic Isocyanates

The reaction was also carried out with a range of alkyl isocyanates. It has previously been reported by the Kays group that **3** catalyses the cyclotrimerisation of primary isocyanates.[32] For this reason *n*-hexyl isocyanate was initially chosen as a primary alkyl

isocyanate as the rate of cyclotrimerisation is much slower than shorter chain alkyl isocyanates.[32] The hydroboration reaction reached completion in less than 15 minutes at room temperature (Table 5, Entry 2). As the cyclotrimerisation reaction takes 14 h at 60 °C, it seems unlikely that any significant cyclotrimerisation occurred in this reaction.[32] This was confirmed as there were no peaks for the cyclotrimer present in the ^{1}H and ^{13}C NMR spectra. The reaction resulted in only one new peak at 26.1 ppm in the ^{11}B NMR spectra indicating that only one new product is formed (Figure 9). This has a similar chemical shift to the peak that was previously assigned to N*B*Pin suggesting that just the monohydroboration product is formed (**15f**). This is supported by the ^{1}H NMR spectra where there is a peak at 8.75 ppm for the C*H* of the monohydroboration product but no peak at ~5 ppm for the CH_2 of the dihydroboration product.

Table 5. Catalytic hydroboration of aliphatic isocyanates with HBPin in C_6D_6 at room temperature mediated by **3**.[a]

Entry	RNCO	HBPin:RNCO	Time (h)	Conversion (%)[b]	**15**:**16**[b]
1	^{n}Pr	1:1	<0.25	100	100:0
2	^{n}Hx	1:1	<0.25	100	100:0
3	^{n}Hx[d]	1:1	24	17	100:0
4	^{n}Hx	2:1	24	100	100:0
5	OCN(CH$_2$)$_6$NCO	2:1	24	100	100:0
6	^{i}Pr	1:1	24	99	100:0
7	Cy	1:1	24	98	100:0
8	^{t}Bu	1:1	48	49	100:0[c]
9	^{t}Bu	3:1	24	100	100:0[c]

[a] Reaction conditions: 10 mg of **3** (5 mol%), 0.6 mL C_6D_6 at room temperature. [b] Determined by ^{1}H NMR spectroscopy using TMS as an internal standard with respect to the limiting reagent. [c] Hydrodeoxygenation products also present. [d] 1 mol% catalyst loading.

As the reaction with ^{n}HxNCO reaction reached completion in such a short amount of time, a reaction with a lower catalyst loading of 1 mol% was carried out (Table 5, Entry 3). After 24 h at room temperature only 17% conversion of the HBPin had occurred showing that lowering the catalyst loading significantly increases the reaction time. The reaction with an increased HBPin:^{n}HxNCO ratio of 2:1 was also carried out but this did not result in any dihydroboration (Table 5, Entry 4).

A shorter chain primary isocyanate was also used, with the 1:1 reaction between HBPin and ^{n}PrNCO in the presence of **3** reaching 100% conversion in under 15 min and again only the monohydroboration product was observed (Table 5, Entry 1). This is a promising result as it widens the range of isocyanates able to be used in this reaction compared with the analogous hydrophosphination[31] and hydroamination (chapter 2) reactions, as the short reaction time means there is no competing cyclotrimerisation with primary isocyanates. This confirms that primary isocyanates selectively form the monohydroboration product. This could be due the higher steric demands of the alkyl isocyanates compared to the aromatic isocyanates or it may be a difference in the electronic effect between the isocyanates.

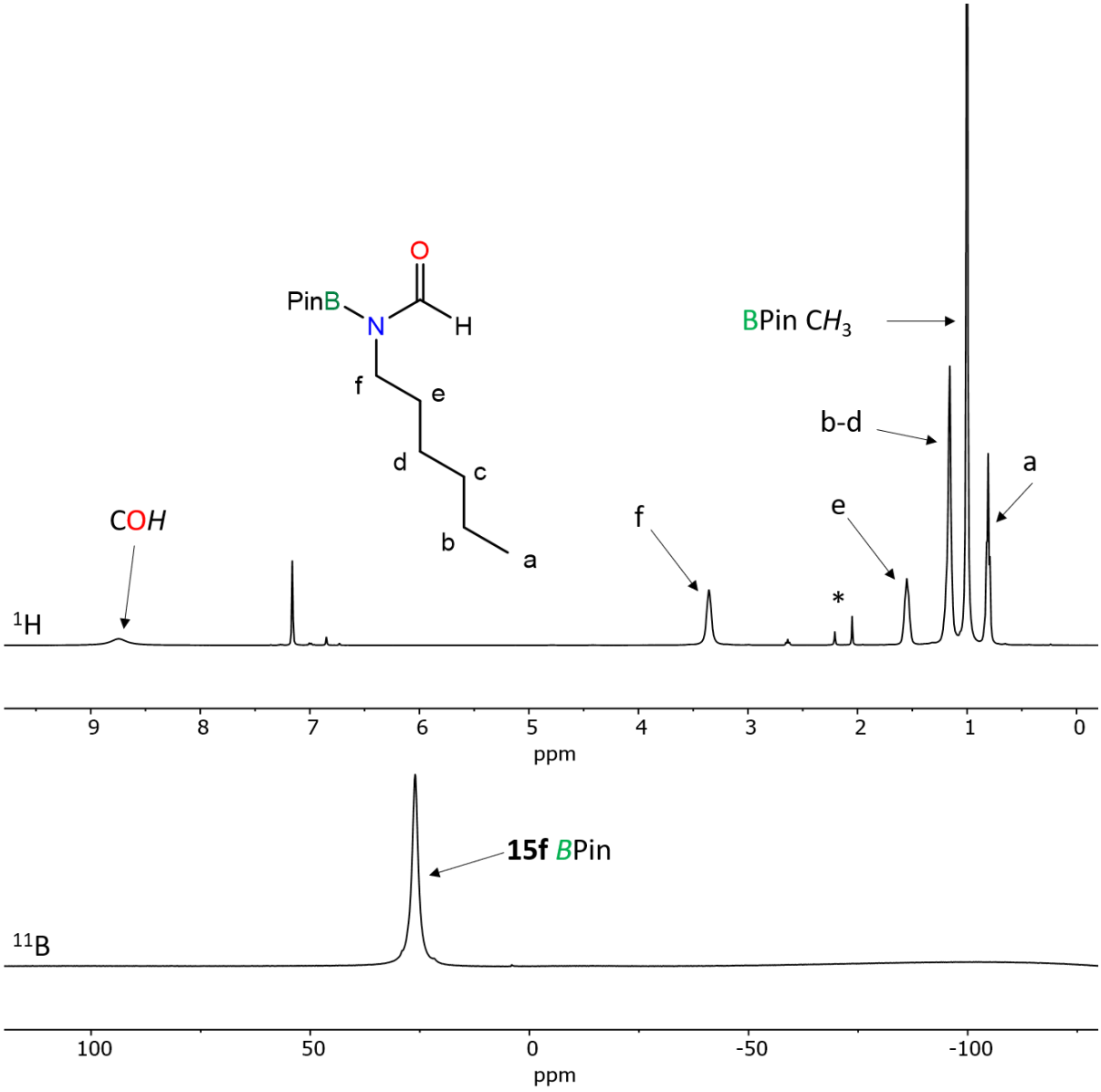
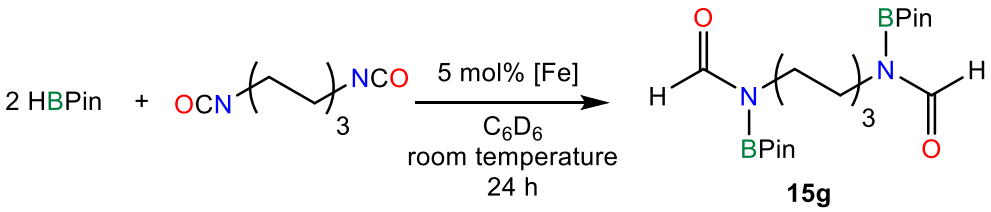


Figure 9. ^{1}H and ^{11}B NMR spectra of reaction between HBPin and ^{n}HxNCO in C_6D_6 in the presence of **3** after 15 min (* indicates Mes peaks from 2,6-$Mes_2C_6H_3$ ligand).

The diisocyanate, 1,6-diisocyanatohexane was also used. This reaction took significantly longer than the other primary isocyanates. The reaction reached completion after 24 h (Table 5, Entry 5) compared to 15 min for ^{n}HxNCO, however still no cyclotrimerisation was observed. Only one new peak was observed in the ^{11}B NMR at 26.1 ppm. The ^{1}H NMR spectrum displayed a new resonance at 8.65 ppm for the C*H* environment in the monohydroboration product **15g** (Scheme 10). Crystals suitable for X-ray diffraction were

grown by the diffusion of hexane into the C_6D_6 reaction solution and identified as **15g** (Figure 10 and Table 6).



Scheme 10. Hydroboration of 1,6-diisocyanatohexane with HBPin in the presence of **3** (5 mol%) in C_6D_6 at room temperature ([Fe] = **3**).

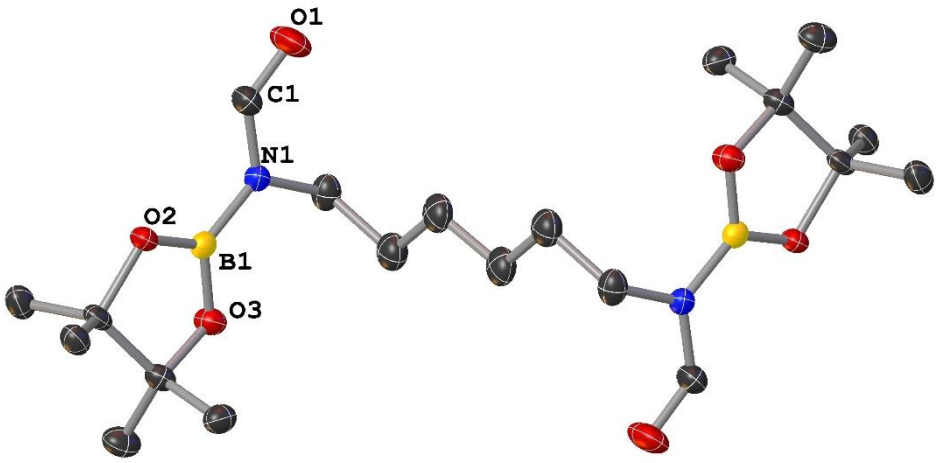


Figure 10. Crystal structure of **15g**, with thermal ellipsoids at 50% probability and hydrogen atoms omitted for clarity (black = carbon, blue = nitrogen, red = oxygen, yellow = boron).

Table 6. Selected bond lengths (Å) and bond angles (°) for **15g**.

	15g
B1–N1	1.440(2)
C1–O1	1.216(2)
O1–C1–N1	124.82(17)

The use of the secondary alkyl isocyanates ^{i}PrNCO and CyNCO demonstrated increased reaction times compared to those for the primary isocyanates. The reactions took 24 h to reach >98% conversion with catalyst loadings of 5 mol% at ambient temperature, and the monohydroboration product was also formed exclusively (Table 5, Entries 6–7). This suggests that sterics play a role in the selectivity of these reactions with the dihydroboration product being more disfavoured with these bulkier alkyl isocyanates compared with the less bulky planar aromatic isocyanates. This reaction selectivity influenced by sterics is similar to the diinsertion of the isocyanate that is observed with the hydrophosphination[31] and hydroamination (Chapter 2) reactions catalysed by **3**.

The tertiary alkyl isocyanate ^{t}BuNCO demonstrated even longer reaction times, and after 48 h there was only 49% consumption of the HBPin with the monohydroboration product (**15j**) being formed (Table 5, Entry 8), according to ^{11}B NMR spectroscopic measurements. However, the monohydroboration product only forms part of the product composition and there are multiple peaks in the ^{11}B NMR spectrum that do not correspond to **15j** (Figure 11). There is a doublet at 28.4 ppm for the HBPin starting material and the NBPin resonance for **15j** is at 26.2 ppm (60%). There are also two large singlets at 24.3 (10%) and 21.7 ppm (30%) and a minor triplet at –4.8 ppm (<1%) with a ^{1}J(B,H) value of 117.9 Hz. The triplet suggests the presence of a 'BH_2' species in the reaction mixture. The lower chemical shift is also indicative of a four-coordinate boron species.[34] The two singlets indicate that there is a significant product or products that are not the monohydroboration product. There is no peak in the ^{1}H NMR spectrum corresponding to the CH_2 in the dihydroboration product, so this is not one of the unidentified resonances in the ^{11}B NMR spectrum. The resonance at 24.3 ppm is assigned to ^{t}BuN(BPin)CH_3 (**20**) (the resonance corresponding to the CH_3 groups was also observed at 2.71 ppm in the ^{1}H NMR spectrum) and the resonance at 21.7 ppm to $O(BPin)_2$ (**21**), when comparing to literature values for these species.[26,35] These products occur from the cleavage of the C=O bond in the isocyanate from the addition of three equivalents of pinacol borane (Scheme 11). Hill *et al.* previously reported this hydrodeoxygenation reaction.[26] This does not occur with any

other isocyanates catalysed by **3**. The ratio of the products was obtained by integration of the BPin signals in the ^{1}H NMR spectrum. After 48 h at room temperature only 10% of the product was **20** but after 2 weeks, the monoinsertion product **15j** had been almost completely consumed and converted to **20**, indicating that the hydrodeoxygenation occurs much slower than the hydroboration reaction. This also suggests that the monohydroboration product is an intermediate of the hydrodeoxygenation reaction. Crystals were grown by diffusion of hexane into the C_6D_6 solution and were found to be $O(BPin)_2$ (**21**) by X-ray diffraction (Figure 12).

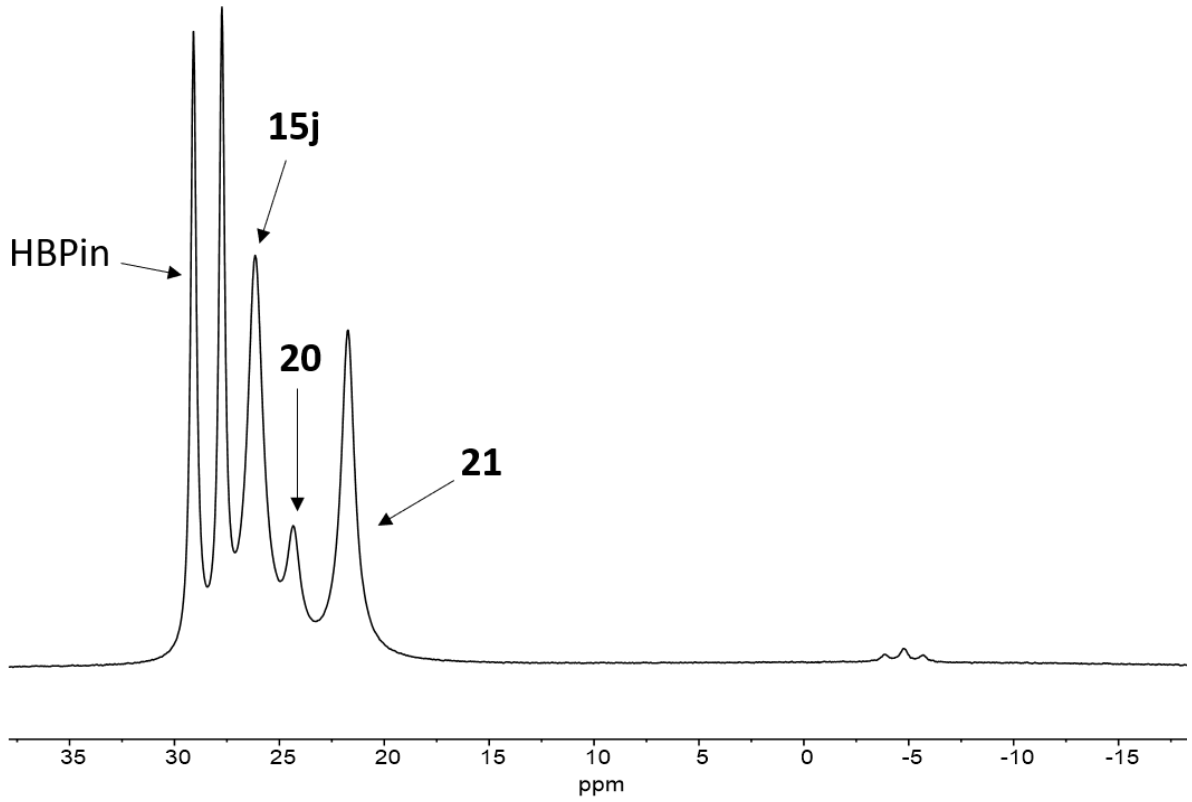
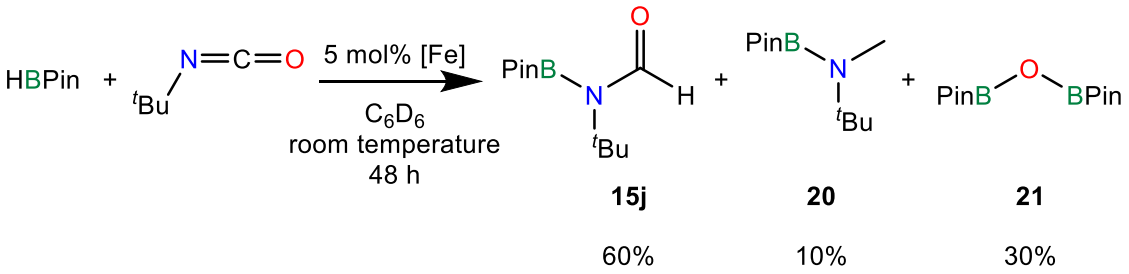


Figure 11. ^{11}B NMR spectrum of reaction between HBPin and ^{t}BuNCO (1:1) in the presence of **3** after 48 h at room temperature.



Scheme 11. Catalytic hydroboration and hydrodeoxygenation of ^{t}BuNCO with HBPin (1:1) in the presence of **3** (5 mol%) in C_6D_6 at room temperature after 48 h. ([Fe] = **3**).

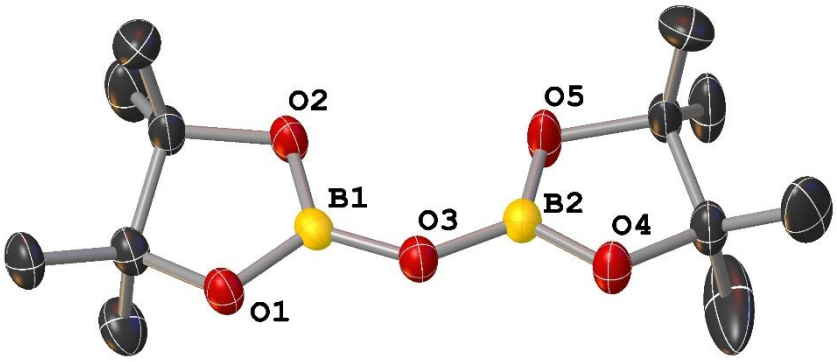


Figure 12. Crystal structure of **21**, with thermal ellipsoids at 50% probability and hydrogen atoms omitted for clarity (black = carbon, red = oxygen, yellow = boron).

A reaction was carried out with a HBPin:^{t}BuNCO ratio of 3:1 in an effort to optimise the yield of **20** (Table 5, Entry 9). After 24 h the ^{t}BuNCO had been fully consumed although there was still HBPin present in the reaction mixture. The major product formed was the monohydroboration product **15j** (96%) and only a small conversion to the hydrodeoxygenation product **20** (4%). The previously observed triplet at –4.8 ppm was also present. This increase in the ratio of HBPin did not increase the yield of **20** so the catalyst appears to favour the hydroboration reaction over the hydrodeoxygenation reaction. Even after over a week at room temperature, the conversion of HBPin was still only 29% and **15j** is the major product with 47% conversion and only 19% conversion to **20**. This is in contrast to the magnesium catalyst reported by Hill *et al*. which selectively

forms the hydrodeoxygenation product with a 3:1 HBPin:RNCO ratio. This confirms the selectivity of catalyst **3** towards the monohydroboration product.

3.3.1.4 Stoichiometric Studies

In the catalytic reactions with **3**, a colour change in the solution from yellow to colourless was observed suggesting a new iron species is possibly being formed. This colour change could indicate a change in the oxidation state of the metal centre. In order to investigate the change to the catalyst, a stoichiometric NMR reaction was undertaken. An equimolar volume of HBPin and PhNCO was added to a solution of **3** in C_6D_6. Unlike the catalytic reaction, there was no colour change observed. The ^{1}H and ^{11}B NMR spectra were recorded immediately after the addition of the substrates and 24 h after. The paramagnetically-shifted peaks for **3**, at −54, −33, −11 and 30 ppm in the ^{1}H NMR spectrum are still present after 24 h suggesting that the majority of **3** is unchanged (Figure 13). However, there are also some new paramagnetically-shifted resonances at −63, −38, −20, −10, −7 and 29 ppm, which could indicate that there is a new iron species being formed in the solution, possibly due to the coordination of either the starting materials or the product in a similar way to **19**. The new peaks are different to the peaks observed for the hydroamination reactions (−17, 8, 10 and 17 ppm). There is a resonance at 9.16 ppm present in the ^{1}H NMR spectrum which indicates the presence of **15a** in the reaction and also a resonance at 4.94 ppm indicating the presence of the dihydroboration product **16a**. There are also multiple new peaks in the region of 0.95–1.10 ppm which suggests that there are multiple new species containing a 'BPin' group, possibly due to the formation of a similar compound to the ligand in **19**.

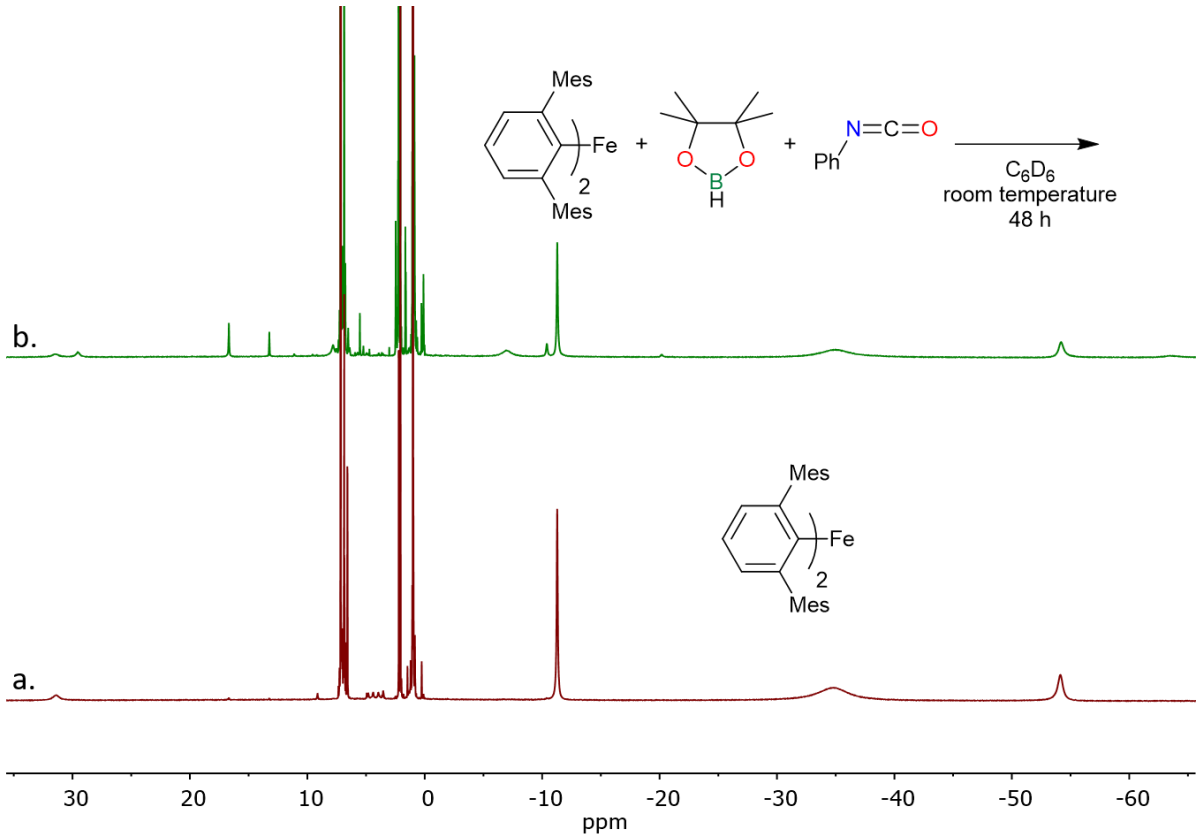


Figure 13. ^{1}H NMR spectra of a stoichiometric reaction between **3**, HBPin and PhNCO in C_6D_6 immediately after adding substrates (a) and after 24 h (b).

The ^{11}B NMR spectrum initially shows the doublet due to the pinacolborane starting material at 28.5 ppm (Figure 14). After 24 h there are two new peaks are observed at 25.9 and 21.8 ppm, which are the same as those observed in the catalytic reactions for the mono- and dihydroboration products **15a** and **16a**. No other peaks were observed in the ^{11}B NMR spectrum. No reaction was observed with the addition of either HBPin or PhNCO separately.

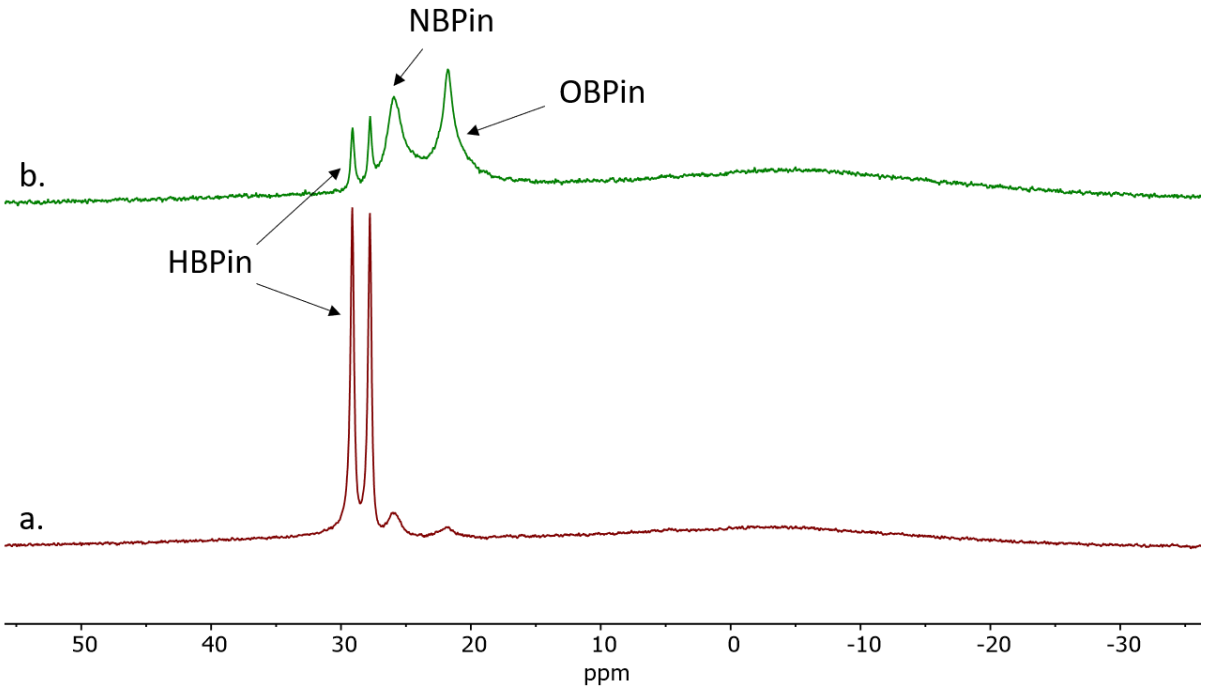


Figure 14. ^{11}B NMR spectra of a stoichiometric reaction between **3**, HBPin and PhNCO in C_6D_6 immediately after adding substrates (a) and after 24 h (b).

3.3.1.5 Posioning experiments

The mechanism of the catalytic hydroboration of isocyanates was investigated by using different poisoning agents. The reaction between HBPin and PhNCO catalysed by **3** was carried out in the presence of 0.1 equivalent of CS_2. This reaction reached 100% conversion after 25 h at room temperature, which is similar to the reaction without any additives (Table 7, Entry 1) so the mechanism is likely to be homogeneous.

The reaction was also carried out in the presence of 1,4-cyclohexadiene which can act as a radical trap. This reaction also reached 100% conversion after 26 h, indicating that the reaction is not radical catalysed (Table 7, Entry 2).

Table 7. Hydroboration of isocyanates mediated by **3** in the presence of additives.[a]

Entry	RNCO	HBPin:RNCO	Additive	t (h)	Conversion (%)[b]	**15**:**16**[b]
1	Ph	1:1	CS_2	25	100	81:19
2	Ph	1:1	1,4-cyclohexadiene	26	100	83:17

[a] Reaction conditions: 10 mg of **3** (5 mol%), 0.6 mL of C_6D_6 at 25 °C. [b] Determined by ^{1}H NMR spectroscopy with TMS as an internal standard.

3.3.1.6 Scale-Up Reactions

The reaction between HBPin and PhNCO was carried out on a larger scale with 30 mg of **3** (5 mol%) in toluene (Figure 15). The solution was stirred at room temperature for 24 h. The solvent was then removed *in vacuo* and the resulting yellow solid was washed with hexane resulting in **15a** as a beige powder with a yield of only 15%. This low yield is likely due to loss of some product due to its high solubility in hexane. Reaction optimisation for the isolation of the product is required to improve the yield.

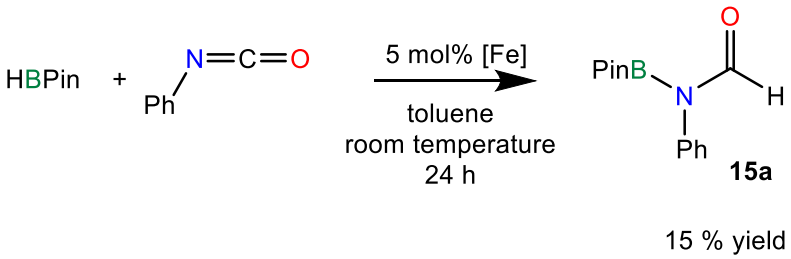


Figure 15. Scaled-up hydroboration of PhNCO with HBPin catalysed by **3** (5 mol%).

3.3.2 Cobalt and Zinc Catalysed Hydroboration of Isocyanates

The hydroboration of PhNCO with HBPin was investigated with Co(2,6-$Mes_2C_6H_3$)$_2$ (**4**). The reactions were carried out on a small scale with a catalyst loading of 5 mol% and monitored using ^{1}H and ^{11}B NMR spectroscopy. The reaction reached 100% conversion after 24 h

(Table 8, Entry 1) which is a similar reaction time to the reaction with **3**. Two new peaks in the ^{11}B NMR spectrum were observed at 25.7 and 21.9 ppm indicating that the products are the same as those observed in the reactions with **3** (**15a** and **16a**). The ratio of **15a**:**16a** is 89:11, which is similar to the ratio observed with precatalyst **3**. After a few hours, there was a small amount of black solid that precipitated in the NMR tube which suggests the possible formation of metal nanoparticles and indicate that the mechanism could be heterogeneous rather than homogeneous.

Table 8. Catalytic hydroboration of isocyanates catalysed by **4** and **5**.[a]

Entry	Catalyst	RNCO	HBPin:RNCO	Time (h)	Conversion (%)[b]	**15**:**16**[b]
1	**4**	Ph	1:1	24	95	89:11
2	**5**	Ph	1:1	24	12	100:0

[a] Reaction conditions: 10 mg of **4** or **5** (5 mol%), 0.6 mL C_6D_6 at 25 °C. [b] Determined by ^1H NMR spectroscopy.

In order to investigate whether the catalysis with **4** is heterogeneous or homogeneous, a Hg(0) poisoning experiment was carried out.[36] The reaction was carried out with the same conditions as described previously, but a drop of Hg(0) was added to the solution after all the reagents had been added (Table 9, Entry 1). The reaction reached 100% conversion after 24 h, indicating that time for completion of the reaction time did not decrease, providing evidence for a homogeneous mechanism. In contrast to the previous reaction without Hg(0) there was no colour change and no visible precipitate. This may indicate that the Hg(0) has prevented the formation of nanoparticles, but that the nanoparticles are not responsible for the catalysis. The catalysis was also carried out in the presence of CS_2 (Table 9, Entry 2). This also did not result in a change to the reaction time lending further evidence to a homogeneous mechanism.

Table 9. Catalytic hydroboration of isocyanates catalysed by **4** in the presence of additives.[a]

Entry	RNCO	HBPin:RNCO	Additive	t (h)	Conversion (%)[b]	**15**:**16**[b]
1	Ph	1:1	Hg(0)	24	100	90:10
2	Ph	1:1	CS_2	24	99	87:13

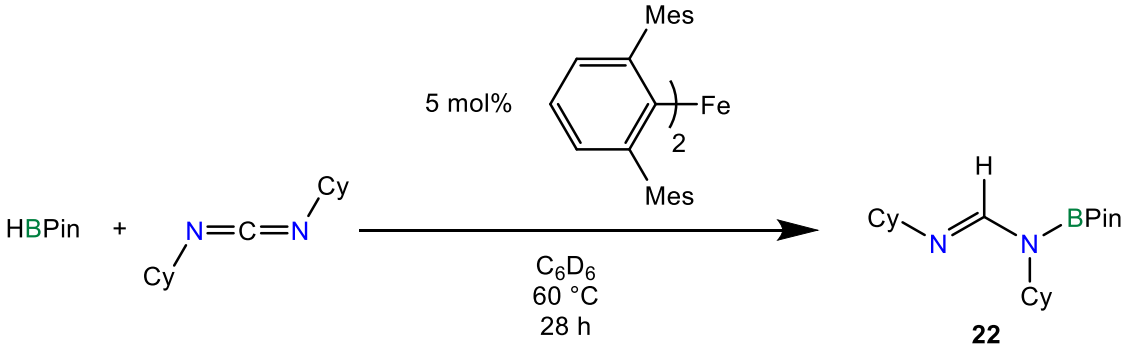
[a] Reaction conditions: 10 mg of **4** (5 mol%), 0.6 mL of C_6D_6 at 25 °C. [b] Determined by ^1H and ^{11}B NMR spectroscopy.

Another test was undertaken in which the reaction was carried out without any additives and once the reaction had reached 100% conversion the reaction mixture was passed through a filter with 0.2 μm pore sizes, resulting in the removal of any visible precipitate.[36] The solution was then returned to the NMR tube and a fresh loading of the substrate was added to the reaction solution. After another 24 h the reaction had again reached 100% conversion and no new precipitate was observed. This test is most useful for determining whether the reaction is catalysed by bulk metal particles. It is not conclusive for determining whether nanoparticles are formed as if they are smaller than 0.2 μm they will pass through the filter (cobalt nanoparticles with diameters as small as 8 nm have been synthesised[37,38]), although it does provides some further evidence towards a homogeneous mechanism.

The reaction was also investigated using Zn(2,6-$Mes_2C_6H_3)_2$ (**5**) as a precatalyst. The reaction proceeded with a much longer reaction time than with **3** or **4**. Only 12% conversion was achieved after 24 h (Table 8, Entry 2). There was also no evidence for the dihydroboration product in the ^1H NMR spectrum. However, this may be due to the slow conversion and if left for longer the monohydroboration product may have undergone a second hydroboration to form the dihydroboration product.

3.3.3 Catalytic Hydroboration of Carbodiimides

The catalytic hydroboration of carbodiimides was investigated using precatalyst **3** (Scheme 12). Small scale reactions were performed in C_6D_6 with a catalyst loading of 5 mol% (Table 10) and were followed using ^{1}H and ^{11}B NMR spectroscopy. These products are thermally stable, so the reactions were amenable to heating to 60 °C in contrast to the reaction conditions necessary for the hydroboration of isocyanates.



Scheme 12. Catalytic hydroboration of CyNCNCy with HBPin in the presence of **3**.

Table 10. Catalytic hydroboration of carbodiimides with HBPin.[a]

Entry	Catalyst	RNCNR	HBPin:RNCNR	t	Conversion (%)[b]
1	**3**	Cy	1:1	28 h	99
2	**3**	Cy	2:1	24 h	100

[a] Reaction conditions: 10 mg of **3** (5 mol%), 0.6 mL C_6D_6 at 60°C. [b] Determined by ^{1}H NMR spectroscopy using TMS as an internal standard with respect to the limiting reagent.

As observed with other catalysts, either the monohydroboration or dihydroboration product could be formed.[24,25,29] The reaction between HBPin and *N,N'*-dicyclohexylcarbodiimide (CyNCNCy) in the presence of **3** was investigated (Table 10, Entry 1). The ^{11}B NMR spectrum (Figure 16) showed a new product, as demonstrated by

a new singlet at 25.5 ppm. This does not indicate whether mono- or dihydroboration has taken place as both products only possess one boron environment. The ^{1}H NMR spectrum, however, indicates the monohydroboration product (**22**) is formed as there is a resonance at 8.31 ppm which can be assigned to the N=C–*H* which has been reported in the literature.[24] The reaction with carbodiimides is much slower than the reaction with isocyanates and required heating to 60 °C before the reaction proceeded. This was also observed for the hydrophosphination of carbodiimides catalysed by this catalyst (see Chapter 2), suggesting that carbodiimides are less reactive towards hydroelementation reactions than isocyanates which has also been observed in the literature.[39] This could be due to the less electrophiic nature of carbodiimides and the more polarised C=O bond in isocyanates compared to the C=N bond in carbodiimides.

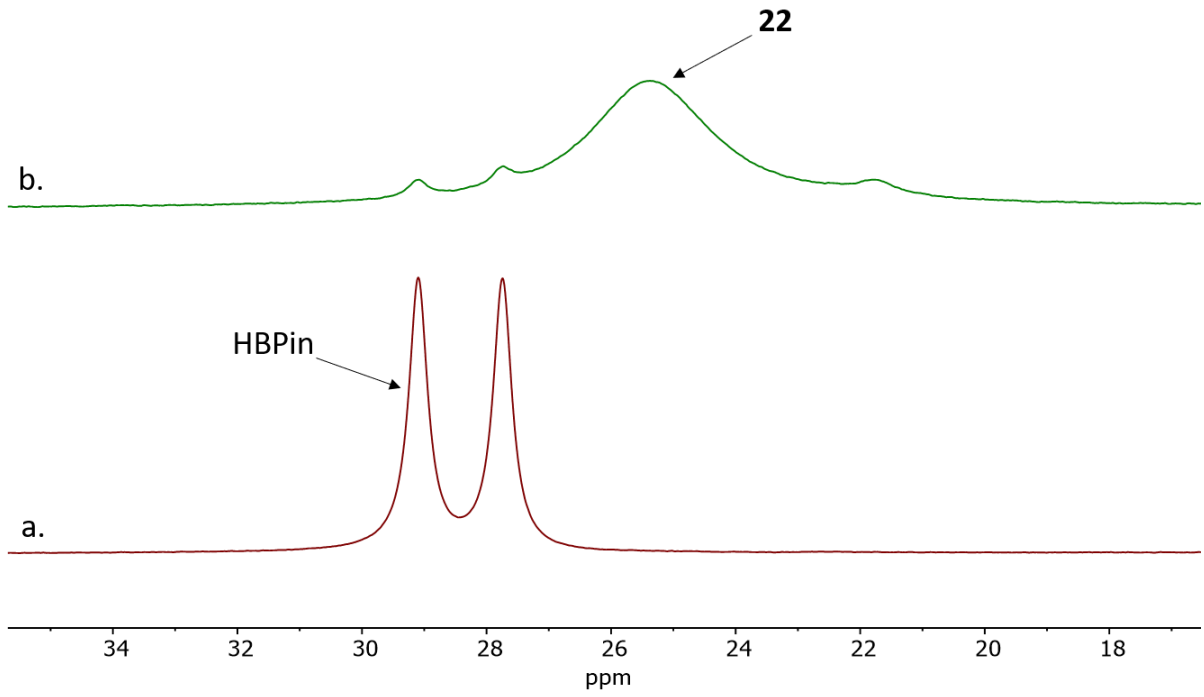


Figure 16. ^{1}H NMR spectra of reaction between HBPin and CyNCNCy in C_6D_6 in the presence of **3** after a) 0 h and b) 28 h.

The reaction was repeated with 2 equivalents of HBPin to investigate whether the dihydroboration product could be formed (Table 10, Entry 2). This resulted in only complete conversion of the CyNCNCy to the product in 24 h and still only one product, as demonstrated by a single resonance at 25.5 ppm in the ^{11}B NMR spectrum after 7 days. This demonstrates that the dihydroboration product is not formed even when using 2 equivalents of HBPin so the catalyst selectively forms the monohydroboration product. This could be due to the monohydroboration product being less activated compared to the original carbodiimide, so a second hydroboration is not favoured. This is also observed with the catalysts reported by Hill *et al*.[24] and Eisen *et al*.[29] that were previously discussed. Crystals suitable for single crystal X-ray diffraction were grown by diffusion of hexane into the C_6D_6 solution. These were found to be the precatalyst **3**. This is a promising result as it gives evidence that the catalyst is able to be recovered from the reaction. This also reinforces the observations from the stoichiometric reaction between **3**, HBPin and PhNCO (section 3.3.1.4) which showed that the precatalyst **3** is mostly unchanged after the addition of the substrates.

3.4 Conclusions

The diaryl *m*-terphenyl complexes M(2,6-$Mes_2C_6H_3)_2$ (**3** (M = Fe), **4** (M = Co) and **5** (M = Zn)) were shown to act as precatalysts for the hydroboration of a range of different aromatic and alkyl isocyanates at room temperature. These are the first examples of transition metal catalysts for this reaction and show a much wider substrate scope compared to previously reported catalysts.[26] This catalysis with **3** favours the monohydroboration of isocyanates and even with an excess of the borane, only a small conversion to the dihydroboration product is observed with aromatic isocyanates and with aliphatic isocyanates the monohydroboration product is formed exclusively. This is a different selectivity to that reported by Hill *et al*. where the dihydroboration of isocyanates was the major product.[26]

The reactions with catalysts **4** and **5** produced the same products as **3** but had much longer reaction times confirming that the iron *m*-terphenyl complexes are much more efficient precatalysts than the cobalt and zinc complexes.

The mechanism of the reaction was investigated with the poisoning experiments which gave evidence for a homogeneous mechanism. A stoichiometric reaction between the catalyst, borane and isocyanate indicated that a new iron species is formed in the reaction which is likely the active species.

The hydroboration of carbodiimides was also shown to be catalysed by **3**, resulting in the selective formation of the monohydroboration product, similar to other group 2 and f-block catalysts for this reaction. The reaction required heating to 60 °C to achieve 99% conversion after 28 h so is slower than the hydroboration of isocyanates, following a similar pattern to the hydrophosphination of carbodiimides with this catalyst.

This work adds to the few reported catalysts for the hydroboration of heterocumulenes which has not been previously well explored in the literature and is the first transition metal example. It shows an efficient method to synthesise organoboron compounds which can be utilised to synthesise a diverse range of organic molecules.

3.5 Experimental Procedures

See Chapter 6 for general experimental.

3.5.1 Catalytic Hydroboration of Isocyanates

3.5.1.1 Iron Catalysed Hydroboration of PhNCO

HBPin (42 µL, 0.292 mmol or 84 µL, 0.584 mmol or 212 µL, 1.46 mmol) and PhNCO (32 µL, 0.292 mmol or 64 µL, 0.584 mmol or 159 µL, 1.46 mmol) were added to a solution of 5 mol% **3** (10 mg, 0.0146 mmol) in C_6D_6 (0.6 mL) in a Young's NMR tube. The reaction was carried out at room temperature and monitored by ^{1}H and ^{11}B NMR spectroscopy. Conversion was quantified by integration of the ^{1}H and ^{11}B NMR spectra using TMS as an internal standard.

3.5.1.2 Standard Procedure for Iron Catalysed Hydroboration of Isocyanates

HBPin (42 µL, 0.292 mmol) and the corresponding isocyanate (0.292 mmol) were added to a solution of 5 mol% **3** (10 mg, 0.0146 mmol) in C_6D_6 (0.6 mL) in a Young's NMR tube. The reaction was carried out at room temperature and monitored by ^{1}H and ^{11}B NMR spectroscopy. Conversion was quantified by integration of the ^{1}H and ^{11}B NMR spectra using TMS as an internal standard.

3.5.1.3 Standard Procedure for Cobalt Catalysed Hydroboration of Isocyanates

HBPin (42 µL, 0.292 mmol) and PhNCO (32 µL, 0.292 mmol) were added to a solution of 5 mol% **4** (10 mg, 0.0146 mmol) in C_6D_6 (0.6 mL) in a Young's NMR tube. The reaction was carried out at room temperature and monitored by ^{1}H and ^{11}B NMR spectroscopy. Conversion was quantified by integration of the ^{1}H and ^{11}B NMR spectra using TMS as an internal standard.

3.5.1.4 Standard Procedure for Zinc Catalysed Hydroboration of Isocyanates

HBPin (42 µL, 0.290 mmol) and PhNCO (32 µL, 0.290 mmol) were added to a solution of 5 mol% **5** (10 mg, 0.0145 mmol) in C_6D_6 (0.6 mL) in a Young's NMR tube. The reaction was carried out at room temperature and monitored by ^{1}H and ^{11}B NMR spectroscopy. Conversion was quantified by integration of the ^{1}H and ^{11}B NMR spectra using TMS as an internal standard.

3.5.1.5 Hydroboration of Isocyanates with 1 mol% catalyst loading

HBPin (42 µL, 0.292 mmol) and ^{n}HxNCO (43 µL, 0.292 mmol) were added to a solution of 1 mol% **3** (2 mg, 0.00292 mmol) in C_6D_6 (0.6 mL) in a Young's NMR tube. The reaction was carried out at room temperature and monitored by ^{1}H and ^{11}B NMR spectroscopy.

Conversion was quantified by integration of the ^{1}H and ^{11}B NMR spectra using TMS as an internal standard.

3.5.1.6 Scaled-Up Catalytic Hydroboration of Isocyanates

In a Schlenk flask 5 mol% of **3** (30.0 mg, 0.0439 mmol), HBPin (248 µL, 0.879 mmol) and PhNCO (96 µL, 0.879 mmol) were dissolved in toluene (3.0 mL) and stirred at room temperature for 24 h. The solvent was removed *in vacuo* and the solid was washed with hexane (5 mL). (**15a**: 34 mg, 15%).

3.5.1.7 Stoichiometric NMR Studies

HBPin (2.1 µL, 0.0146 mmol) and PhNCO (1.6 µL, 0.0146 mmol) were added to a solution of **3** (10 mg, 0.0146 mmol) in C_6D_6 (0.6 mL) in a Young's NMR tube. The reaction was kept at room temperature for 24 h and was monitored by ^{1}H and ^{11}B NMR spectroscopy.

3.5.1.8 Catalytic Hydroboration of Isocyanates in the Presence of Hg(0)

HBPin (42 µL, 0.292 mmol) and PhNCO (32 µL, 0.292 mmol) were added to a solution of 5 mol% **4** (10 mg, 0.0146 mmol) in C_6D_6 (0.6 mL) along with a drop of Hg(0) in a Young's NMR tube. The reaction was carried out at room temperature and monitored by ^{1}H and ^{11}B NMR spectroscopy. Conversion was quantified by integration of the ^{1}H and ^{11}B NMR spectra using TMS as an internal standard.

3.5.1.9 Catalytic Hydroboration of Isocyanates in the Presence of CS_2

HBPin (42 µL, 0.292 mmol) and PhNCO (32 µL, 0.292 mmol) were added to a solution of 5 mol% **3** or **4** (10 mg, 0.0146 mmol) in C_6D_6 (0.6 mL) along with CS_2 (0.05 M in toluene, 29 µL, 0.00146 mmol) in a Young's NMR tube. The reaction was carried out at room

temperature and monitored by ^{1}H and ^{11}B NMR spectroscopy. Conversion was quantified by integration of the ^{1}H and ^{11}B NMR spectra using TMS as an internal standard.

3.5.1.10 Catalytic Hydroboration of Isocyanates in the Presence of 1,4-Cyclohexadiene

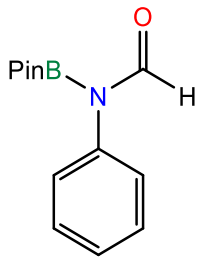
HBPin (42 µL, 0.292 mmol) and PhNCO (32 µL, 0.292 mmol) were added to a solution of 5 mol% **3** (10 mg, 0.0146 mmol) in C_6D_6 (0.6 mL) along with 1,4-cyclohexadiene (6.9 µL, 0.073 mmol) in a Young's NMR tube. The reaction was carried out at room temperature and monitored by ^{1}H and ^{11}B NMR spectroscopy. Conversion was quantified by integration of the ^{1}H and ^{11}B NMR spectra using TMS as an internal standard.

3.5.2 Catalytic Hydroboration of Carbodiimides

HBPin (42 µL, 0.292 mmol or 84 µL, 0.584 mmol) and CyNCNCy (60 mg, 0.292 mmol) were added to a solution of 5 mol% **3** (10 mg, 0.0146 mmol) in C_6D_6 (0.6 mL) in a Young's NMR tube. The reaction was carried out either at 60 °C and monitored by ^{1}H and ^{11}B NMR spectroscopy. Conversion was quantified by integration of the ^{1}H and ^{11}B NMR spectra using TMS as an internal standard.

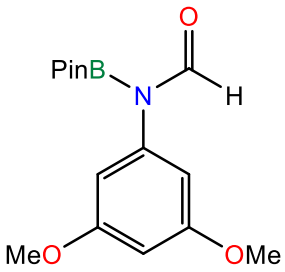
3.5.3 Characterisation of Hydroboration Products

3.5.3.1 PhN(BPin)C(=O)H 15a



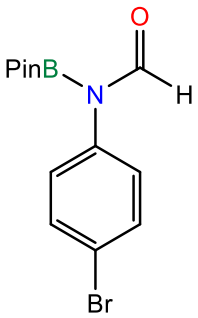
^{1}H NMR (400 MHz, C_6D_6, 25 °C) δ = 9.16 (s, 1H, *H*C=O), 7.22 (d, ^{3}J(H,H) = 7.9 Hz, 2H, Ph^{o}), 7.12 (t, ^{3}J(H,H) = 7.7 Hz 2H, Ph^{m}), 6.97 (t, ^{3}J(H,H) = 7.5 Hz, 1H, Ph^{p}), 0.92 (s, 12H, C*H*$_3$) ppm. ^{13}C{^{1}H} NMR (101 MHz, C_6D_6, 25 °C) δ 164.4 (*C*=O), 139.5 (Ph^{i}), 137.4 (Ph^{o}), 128.8 (Ph^{m}), 126.9 (Ph^{p}), 84.2 (*C*(CH$_3$)$_2$), 23.3 (*C*H$_3$) ppm. ^{11}B{^{1}H} NMR (128 MHz, C_6D_6, 25 °C) δ = 25.7 (BPin) ppm.

3.5.3.2 3,5-(OMe)$_2$C$_6$H$_3$N(BPin)C(=O)H 15b



^{1}H NMR (400 MHz, C_6D_6, 25 °C) δ = 9.18 (s, 1H, *H*C=O), 6.55 (s, 2H, Ph^{o}), 6.40 (s, 2H, Ph^{p}), 3.27 (s, 6H, OC*H*$_3$), 0.99 (s, 12H, CC*H*$_3$) ppm. ^{13}C{^{1}H} NMR (101 MHz, C_6D_6, 25 °C) δ = 161.0 (*C*=O), 141.6 (Ph^{i}), 130.4 (Ph^{m}), 106.5 (Ph^{o}), 99.2 (Ph^{p}), 84.0 (*C*CH$_3$), 54.5 (O*C*H$_3$), 24.0 (C*C*H$_3$) ppm. ^{11}B{^{1}H} NMR (128 MHz, C_6D_6, 25 °C) δ = 25.8 (BPin) ppm.

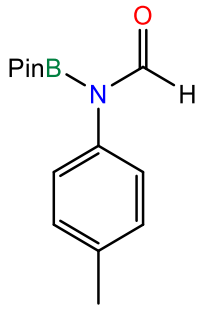
3.5.3.3 4-BrC$_6$H$_4$N(BPin)C(=O)H 15c



^{1}H NMR (400 MHz, C_6D_6, 25 °C) δ = 9.08 (s, 1H, *H*C=O), 7.16 (br s; overlapping with C_6D_6, 2H, Ph^{o}), 6.84 (br s, 2H, Ph^{m}), 0.97 (s, 12H, CC*H*$_3$) ppm. ^{13}C{^{1}H} NMR (101 MHz, C_6D_6, 25 °C) δ = 164.7 (*C*=O), 136.2 (Ph^{i}), 131.9 (Ph^{o}), 129.7 (Ph^{m}), 120.6 (Ph^{p}), 84.5

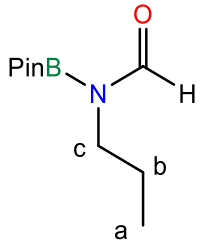
($C(CH_3)_2$), 24.4 ($C(CH_3)_2$) ppm. $^{11}B\{^1H\}$ NMR (128 MHz, C_6D_6, 25 °C) δ = 25.6 (BPin) ppm.

3.5.3.4 *p*-TolN(BPin)C(=O)H 15d



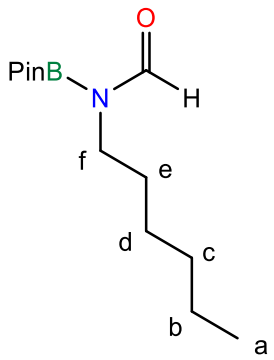
^1H NMR (400 MHz, C_6D_6, 25 °C) δ = 9.19 (s, 1H, *H*C=O), 7.08 (m, 2H, Ph^o), 6.92 (d, ^3J(H,H) = 7.5 Hz, 2H, Ph^m), 2.01 (s, 3H, *p*-CH_3), 0.98 (s, 12H, CCH_3) ppm. $^{13}C\{^1H\}$ NMR (101 MHz, C_6D_6, 25 °C) δ = 164.8 (*C*=O), 155.9 (Ph^i), 136.4 (Ph^p), 129.5 (Ph^m), 125.6 (Ph^o), 84.2 ($C(CH_3)_2$), 24.4 ($C(CH_3)_2$), 20.9 (*p*-CH_3) ppm. $^{11}B\{^1H\}$ NMR (128 MHz, C_6D_6, 25 °C) δ = 25.9 (BPin) ppm.

3.5.3.5 ^{n}PrN(BPin)C(=O)H 15e



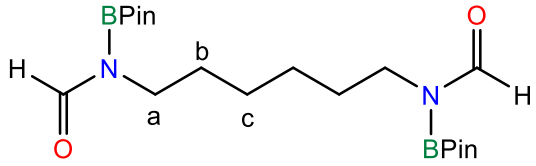
^1H NMR (400 MHz, C_6D_6, 25 °C) δ = 8.80 (s, 1H, *H*C=O), 3.30 (br s, 2H, H^c), 1.54 (q, ^3J(H,H) = 7.0 Hz, 2H, H^b), 0.73 (t, ^3J(H,H) = 7.1 Hz, 3H, H^a), 0.99 (s, 12H, CCH_3) ppm. $^{13}C\{^1H\}$ (101 MHz, C_6D_6, 25 °C) δ = 163.8 (*C*=O), 83.9 (*C*CH_3), 42.1 (C^c), 24.5 (C*C*H_3), 23.5 (C^b), 10.99 (C^a). $^{11}B\{^1H\}$ NMR (128 MHz, C_6D_6, 25 °C) δ = 26.1 (BPin) ppm.

3.5.3.6 ^{n}HexN(BPin)C(=O)H 15f



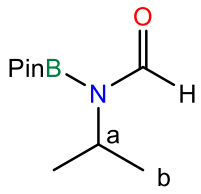
^{1}H NMR (400 MHz, C_6D_6, 25 °C) δ = 8.76 (s, 2H, *H*C=O), 3.36 (m, 2H, H^{f}), 1.55 (m, 2H, H^{e}), 1.16 (m, 6H, $H^{b–d}$), 1.00 (s, 12H, CC*H*$_3$), 0.81 (m, 3H, H^{a}) ppm. ^{13}C{^{1}H} NMR (101 MHz, C_6D_6, 25 °C) δ = 164.23 (*C*=O), 83.9 (*C*CH$_3$), 40.4 (C^{f}), 31.9 (C^{d}), 30.4 (C^{e}), 26.9 (C^{c}), 24.5 (C*C*H$_3$), 23.0 (C^{b}), 14.24 (C^{a}) ppm. ^{11}B{^{1}H} NMR (128 MHz, C_6D_6, 25 °C) δ = 26.1 (BPin) ppm.

3.5.3.7 HC(=O)N(BPin)(CH$_2$)$_6$N(BPin)C(=O)H 15g



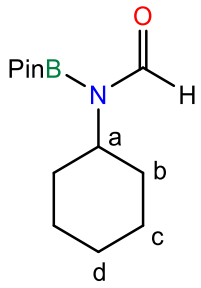
^{1}H NMR (400 MHz, C_6D_6, 25 °C) δ = 9.02 (s, 2H, *H*C=O), 3.44 (t, ^{3}J(H,H) = 7.0 Hz, 4H, H^{a}), 1.55 (quin, ^{3}J(H,H) = 6.6 Hz, 4H, H^{b}), 1.18 (quin, ^{3}J(H,H) = 3.5 Hz, 4H, H^{c}), 0.97 (s, 24H, CC*H*$_3$) ppm. ^{13}C{^{1}H} NMR (101 MHz, C_6D_6, 25 °C) δ = 165.1 (*C*=O), 83.9 (*C*CH$_3$), 40.3 (C^{b}), 30.2 (C^{c}), 26.9 (C^{a}), 24.4 (C*C*H$_3$). ^{11}B{^{1}H} NMR (128 MHz, C_6D_6, 25 °C) δ = 26.1 (BPin) ppm.

3.5.3.8 ^{i}PrN(BPin)C(=O)H 15h



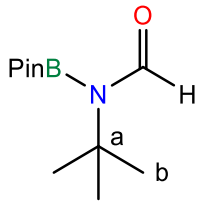
^{1}H NMR (400 MHz, C_6D_6, 25 °C) δ = 9.09 (s, 1H, *H*C=O), 4.64 (sep, ^{3}J(H,H) = 6.9 Hz, 1H, H^{a}), 1.25 (d, ^{3}J(H,H) = 6.8 Hz, 6H, H^{b}), 0.96 (s, 12H, CC*H*$_3$) ppm. ^{13}C{^{1}H} (101 MHz, C_6D_6, 25 °C) δ = 165.5 (*C*O), 83.1 (*C*CH$_3$), 41.8 (C^{a}), 23.9 (C*C*H$_3$), 21.3 (C^{b}) ppm. ^{11}B{^{1}H} NMR (128 MHz, C_6D_6, 25 °C) δ = 26.0 (BPin) ppm.

3.5.3.9 CyN(BPin)C(=O)H 15i



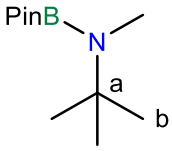
^{1}H NMR (400 MHz, C_6D_6, 25 °C) δ = 9.06 (s, 1H, *H*C=O), 4.20 (m, 1H, H^{a}), 1.96 (q, ^{3}J(H,H) = 12.8 Hz, 2H, H^{d}), 1.62 (d, ^{3}J(H,H) = 11.5 Hz, 4H, H^{b}), 1.12 (m, 4H, H^{c}), 1.00 (s, 12H, CC*H*$_3$) ppm. ^{13}C{^{1}H} (101 MHz, C_6D_6, 25 °C) δ = 83.3 (*C*CH$_3$), 50.4 (C^{a}), 32.0 (C^{d}), 26.6 (C^{b}), 25.7 (C^{c}), 24.4 (*C*H$_3$) ppm. ^{11}B{^{1}H} NMR (128 MHz, C_6D_6, 25 °C) δ = 26.2 (BPin) ppm.

3.5.3.10 ^{t}BuN(BPin)C(=O)H 15j



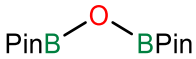
^{1}H NMR (400 MHz, C_6D_6, 25 °C) δ = 9.09 (s, 1H, CO*H*), 1.53 (s, 9H, H^{b}), 1.01 (s, 12H, CC*H*$_3$) ppm. ^{13}C{^{1}H} (101 MHz, C_6D_6, 25 °C) δ = 167.1 (*C*=O), 82.9 (*C*CH$_3$), 55.2 (C^{a}), 30.0 (C^{b}), 24.7 (C*C*H$_3$) ppm. ^{11}B{^{1}H} NMR (128 MHz, C_6D_6, 25 °C) δ = 26.2 (BPin) ppm.

3.5.3.11 ^{t}BuN(BPin)CH$_3$ 20



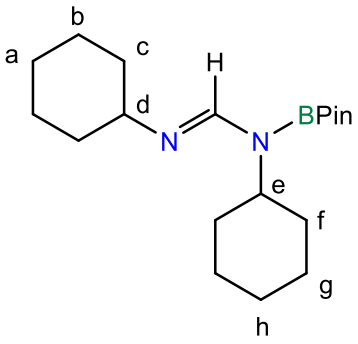
^{1}H NMR (400 MHz, C_6D_6, 25 °C) δ = 2.71 (s, 3H, C*H*$_3$), 1.29 (s, 9H, H^{b}), 1.10 (s, 12H, CC*H*$_3$) ppm. ^{13}C{^{1}H} (101 MHz, C_6D_6, 25 °C) δ = 81.3 (*C*CH$_3$), 52.1 (C^{a}), 30.5 (*C*H$_3$), 29.8 (C^{b}), 24.8 (C*C*H$_3$) ppm. ^{11}B{^{1}H} NMR (128 MHz, C_6D_6, 25 °C) δ = 24.3 (BPin) ppm.

3.5.3.12 O(BPin)$_2$ 21



^{1}H NMR (400 MHz, C_6D_6, 25 °C) δ = 0.95 (s, 12H, CC*H*$_3$) ppm. ^{13}C{^{1}H} (101 MHz, C_6D_6, 25 °C) δ = 82.9 (*C*CH$_3$), 24.7 (C*C*H$_3$) ppm. ^{11}B{^{1}H} NMR (128 MHz, C_6D_6, 25 °C) δ = 21.7 (BPin) ppm.

3.5.3.13 CyN=CHN(BPin)Cy 22



^{1}H NMR (400 MHz, C_6D_6, 25 °C) δ = 8.31 (s, 1H, NC*H*), 4.58 (m, 1H, H^e), 2.98 (m, 1H, H^d), 2.36–1.24 (m, 20H, $H^{a-c,f-h}$) 1.08 (s, 12H, CCH_3) . ^{13}C{^{1}H} (101 MHz, C_6D_6, 25 °C) δ = 150.6 (N=*C*H), 82.8 (*C*CH_3), 65.4 (Cy^d), 51.8 (Cy^e), 36.2 (Cy), 32.1 (Cy), 26.9 (Cy), 26.3 (Cy), 26.1 (Cy), 25.4 (Cy), 24.6 (C*C*H_3). ^{11}B{^{1}H} NMR (128 MHz, C_6D_6, 25 °C) δ = 25.4 (BPin) ppm.

3.6 References

1 G. W. Kabalka, R. J. Newton and J. Jacobus, *J. Org. Chem.*, 1978, **43**, 1567–1569.

2 I. Beletskaya and A. Pelter, *Tetrahedron*, 1997, **53**, 4957–5026.

3 E. Fernandez, M. W. Hooper, F. I. Knight and J. M. Brown, *Chem. Commun.*, 1997, **21**, 173–174.

4 S. N. Mlynarski, A. S. Karns and J. P. Morken, *J. Am. Chem. Soc.*, 2012, **134**, 16449–16451.

5 M. E. D. Hillman, *J. Am. Chem. Soc.*, 1962, **84**, 4715–4720.

6 H. C. Brown, C. Snyder, B. C. S. Rao and G. Zweifel, *Tetrahedron*, 1986, **42**, 5505–5510.

7 K. Hirano, H. Yorimitsu and K. Oshima, *Org. Lett.*, 2007, **9**, 1541–1544.

8 C. E. Garrett and G. C. Fu, *J. Org. Chem.*, 1996, **61**, 3224–3225.

9 S. R. Tamang and M. Findlater, *J. Org. Chem.*, 2017, **82**, 12857–12862.

10 T. C. Morrill, C. A. D'Souza, L. Yang and A. J. Sampognaro, *J. Org. Chem.*, 2002, **67**, 2481–2484.

11 D. Männig and H. Nöth, *Angew. Chem. Int. Ed. English*, 1985, **24**, 878–879.

12 G. Zhang, J. Wu, M. Wang, H. Zeng, J. Cheng, M. C. Neary and S. Zheng, *Eur. J. Org. Chem.*, 2017, 5814–5818.

13 Z. Yang, M. Zhong, X. Ma, K. Nijesh, S. De, P. Parameswaran and H. W. Roesky, *J. Am. Chem. Soc.*, 2016, **138**, 2548–2551.

14 S. Kisan, V. Krishnakumar and C. Gunanathan, *ACS Catal.*, 2017, **7**, 5950–5954.

15 K. Burgess, W. A. Van Der Donk, S. A. Westcott, T. B. Marder, R. T. Baker and J. C.

Calabrese, *J. Am. Chem. Soc.*, 1992, **114**, 9350–9359.

16 C. M. Vogels, P. G. Hayes, M. P. Shaver and S. A. Westcott, *Chem. Commun.*, 2000, 51–52.

17 S. A. Wescott, H. P. Blom, T. B. Marder and R. T. Baker, *J. Am. Chem. Soc.*, 1992, **114**, 8863–8869.

18 Y. Xi and J. F. Hartwig, *J. Am. Chem. Soc.*, 2017, **139**, 12758–12772.

19 A. Bismuto, M. J. Cowley and S. P. Thomas, *ACS Catal.*, 2018, **8**, 2001–2005.

20 S. Pereira and M. Srebnik, *Tetrahedron Lett.*, 1996, **37**, 3283–3286.

21 T. J. Hadlington, M. Hermann, G. Frenking and C. Jones, *J. Am. Chem. Soc.*, 2014, **136**, 3028–3031.

22 C. C. Chong and R. Kinjo, *ACS Catal.*, 2015, **5**, 3238–3259.

23 Z. Huang, D. Liu, J. Camacho-Bunquin, G. Zhang, D. Yang, J. M. López-Encarnación, Y. Xu, M. S. Ferrandon, J. Niklas, O. G. Poluektov, J. Jellinek, A. Lei, E. E. Bunel and M. Delferro, *Organometallics*, 2017, **36**, 3921–3930.

24 C. Weetman, M. S. Hill and M. F. Mahon, *Chem. Eur. J.*, 2016, **22**, 7158–7162.

25 D. Mukherjee, S. Shirase, T. P. Spaniol, K. Mashima and J. Okuda, *Chem. Commun.*, 2016, **52**, 13155–13158.

26 Y. Yang, M. D. Anker, J. Fang, M. F. Mahon, L. Maron, C. Weetman and M. S. Hill, *Chem. Sci.*, 2017, **8**, 3529–3537.

27 M. Rauch, S. Ruccolo and G. Parkin, *J. Am. Chem. Soc.*, 2017, **139**, 13264–13267.

28 Q. Shen, X. Ma, W. Li, W. Liu, Y. Ding, Z. Yang and H. W. Roesky, *Chem. Eur. J.*, 2019, **25**, 11918–11923.

29 H. Liu, K. Kulbitski, M. Tamm and M. S. Eisen, *Chem. Eur. J.*, 2018, **24**, 5738–5742.

30 M. Arrowsmith, M. S. Hill and G. Kociok-Köhn, *Chem. Eur. J.*, 2013, **19**, 2776–2783.

31 H. R. Sharpe, A. M. Geer, W. Lewis, A. J. Blake and D. L. Kays, *Angew. Chem. Int. Ed.*, 2017, **56**, 4845–4848.

32 H. R. Sharpe, A. M. Geer, H. E. L. Williams, T. J. Blundell, W. Lewis, A. J. Blake and D. L. Kays, *Chem. Commun.*, 2017, **53**, 937–940.

33 M. Kamitani, H. Kusaka and H. Yuge, *Chem. Lett.*, 2019, **48**, 898–901.

34 A. J. Ashe, J. W. Kampf and J. R. Waas, *Organometallics*, 1997, **16**, 163–167.

35 A. Harinath, J. Bhattacharjee and T. K. Panda, *Chem. Commun.*, 2019, **55**, 1386–1389.

36 J. A. Widegren and R. G. Finke, *J. Mol. Catal. A Chem.*, 2003, **198**, 317–341.

37 B. Farkaš and N. de Leeuw, *Nanotechnology*, 2020, **31**, 195711.

38 M. Wolf, H. Kotzé, N. Fischer and M. Claeys, *Faraday Discuss.*, 2017, **197**, 243–268.

39 K. Naktode, S. Das, J. Bhattacharjee, H. P. Nayek and T. K. Panda, *Inorg. Chem.*, 2016, **55**, 1142–1153.

Chapter 4

Synthesis and Reactivity of *m*-Terphenyl Complexes Containing Bidentate Ligands

4.1 Introduction

Bidentate ligands are a diverse group of compounds that have a range of different donor atoms and substituents which can alter the sterics and electronic effects of the ligand.[1–4] Perhaps the most ubiquitous bidentate ligands are diphosphines. They are particularly prevalent in catalysis.[5–17] Diphosphines can possess various substituents on the flanking groups or the backbone which can influence the properties of the ligand (Figure 1). The length and rigidity of the backbone can alter the bite angle (θ) of the ligand.

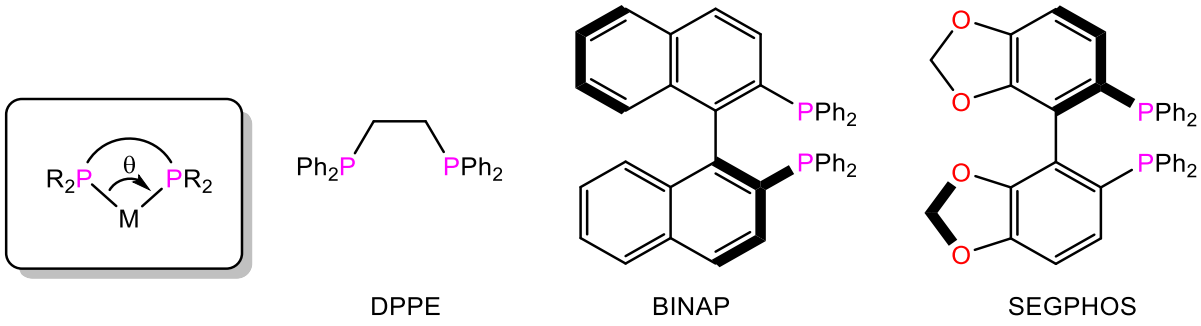
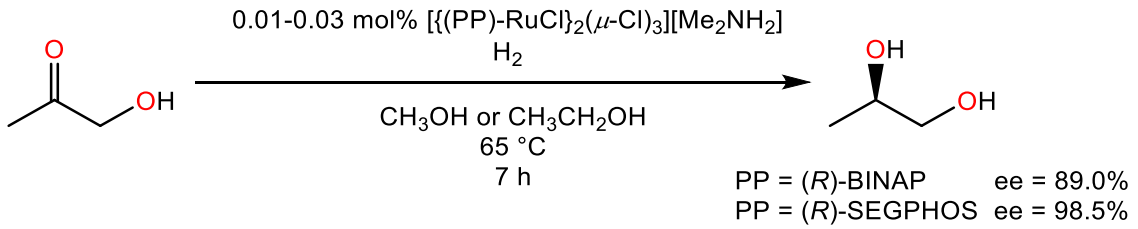


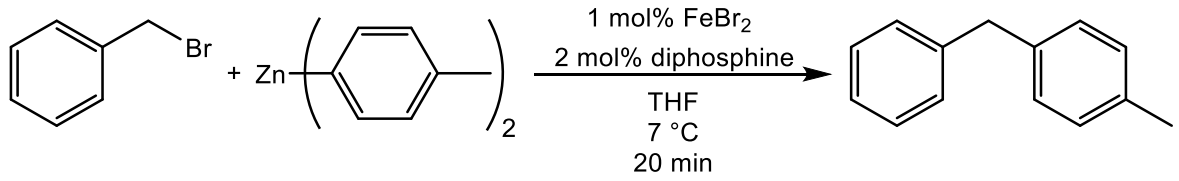
Figure 1. General structure of diphosphines showing the bite angle (R = any alkyl or aromatic group, θ = bite angle) and examples of common diphosphines.

A change in the bite angle of the diphosphine can alter the selectivity of a catalytic reaction. This can be demonstrated with the example of the ruthenium catalysed hydrogenation of ketones. This reaction is catalysed by a BINAP-Ru(II) complex.[18–21] The enantiomeric excess for the hydrogenation of hydroxyacetone to 1,2-propanediol is 89.0% for the *R* isomer (Scheme 1).[21] This enantioselectivity can be improved with the use of SEGPHOS which has a smaller bite angle than BINAP (SEGPHOS: 65.0°, BINAP: 73.5°). This results in an enantiomeric excess of 98.5%. The smaller bite angle means that the metal centre is more sterically encumbered and so the angle at which the substrate can approach the metal centre is more limited resulting in a more selective reaction.[21]



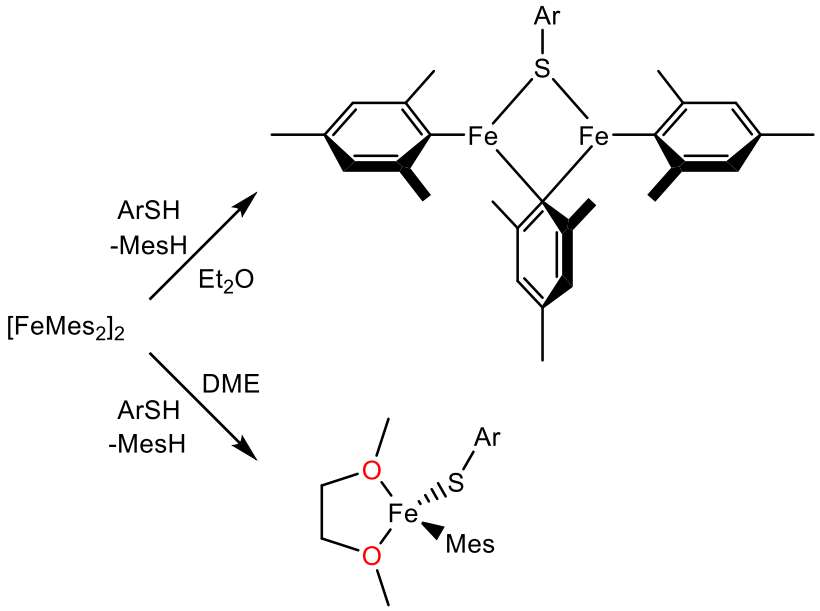
Scheme 1. Catalytic hydrogenation of hydroxyacetone with a diphosphine Ru(II) complex.[21]

Another example of catalysis with diphosphine ligands is the iron-catalysed Negishi coupling (Scheme 2) reported by Bedford and co-workers.[17] The reaction is catalysed by $FeBr_2$ in the presence of a diphosphine. Monodentate ligands such as PPh_3 show no activity, showing that the presence of the bidentate ligand is vital to the catalysis. The activity of the catalysis depends heavily on the structure of the Fe(II) complex that is formed. The ligands that showed the highest activity are DPBZ and DPTH which both formed mononuclear complexes with the formula $FeBr_2$(PP) (PP = diphosphine). The ligands that formed either a polymer (DPPE) or a bis(diphosphine) complex (DMBZ) showed much lower activity than DPBZ or DPTH.[17]



Scheme 2. Iron catalysed Negishi coupling.[17]

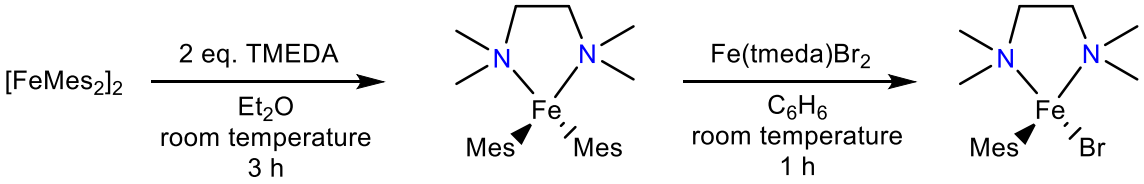
Bidentate ligands can be used in the stabilisation of low coordinate monomeric complexes. This is shown by the bidentate ligand 1,2-dimethoxyethane (DME) which is used to stabilise the complex Fe(SAr)(Mes)(DME) (Ar = 2,6-$Mes_2C_6H_3$ or 2,6-$(2,6\text{-Xyl})_2C_6H_3$).[22] This is synthesised from the addition of the bulky thiol ArSH to $[FeMes_2]_2$ in the presence of DME (Scheme 3). In the absence of DME the dimeric complex $Fe_2Mes_2(\mu\text{-SAr})(\mu\text{-Mes})$ is formed.



Scheme 3. Synthesis of $Fe_2Mes_2(\mu\text{-}SAr)(\mu\text{-}Mes)$ and Fe(SAr)(Mes)(DME) (Ar = 2,6-$Mes_2C_6H_3$ or 2,6-(2,6-Xyl)$_2C_6H_3$).[22]

There are some examples of four-coordinate bidentate complexes containing a bidentate ligand and an aryl ligand.

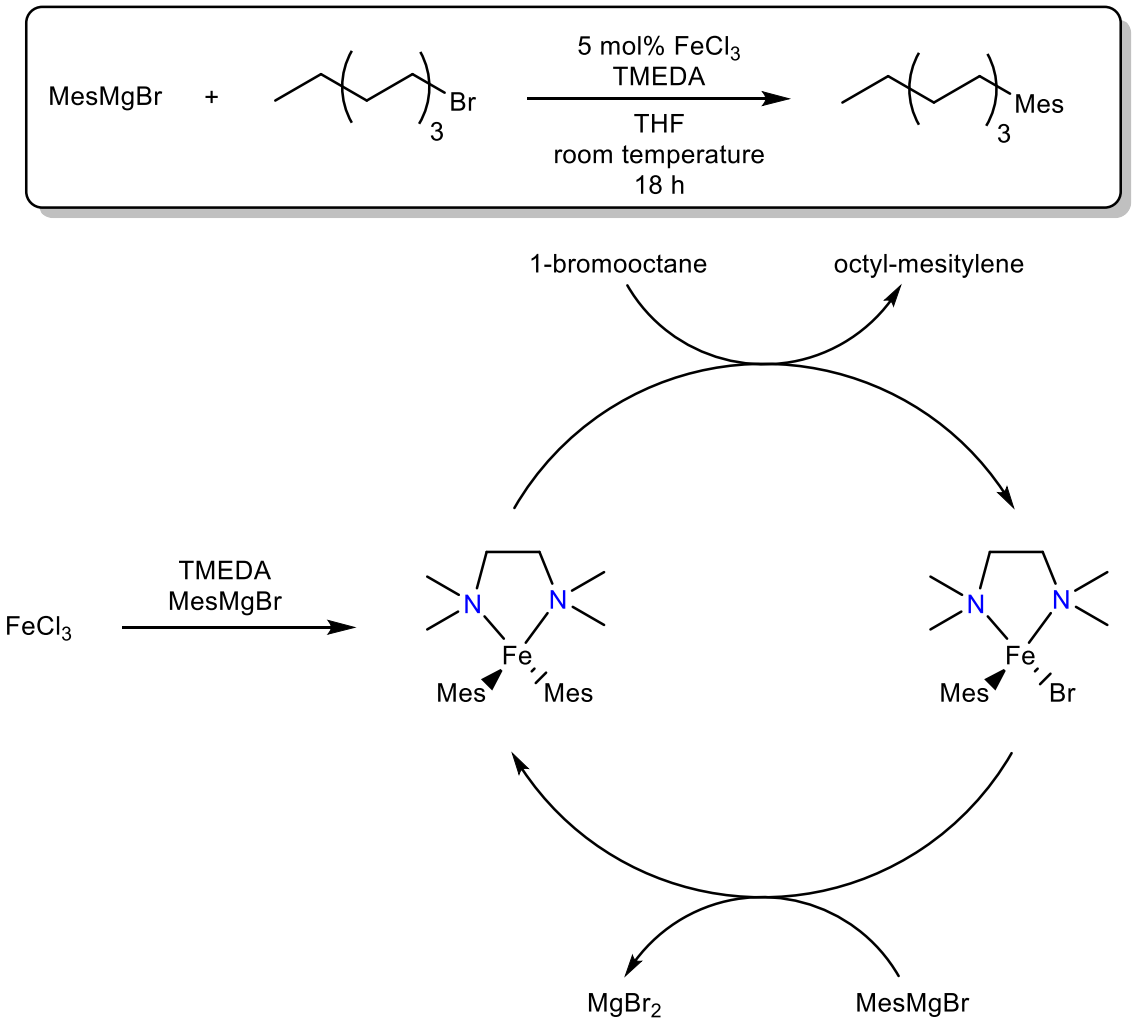
An example of this is the complex $FeMes_2$(tmeda), which can be synthesised *via* the addition of TMEDA to $[FeMes_2]_2$.[23,24] The addition of $FeBr_2$(tmeda) to $FeMes_2$(tmeda) results in the formation of Fe(Mes)Br(tmeda) (Scheme 4).[24] These complexes have a tetrahedral geometry.



Scheme 4. Synthesis of $FeMes_2$(tmeda) and Fe(Mes)(tmeda)Br.[23,24]

These two complexes were shown to be part of the catalytic cycle for the coupling between a MesMgBr and 1-bromooctane (Scheme 5).[24] The reaction is catalysed by $FeCl_3$ and TMEDA in THF at room temperature, with a yield of 32% after 18h. Slow addition of

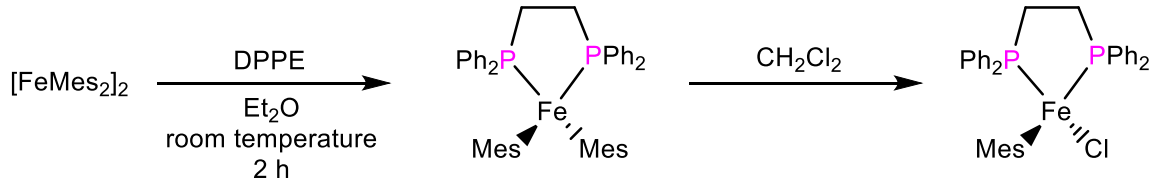
MesMgBr and TMEDA leads to an increase in the yield. Addition of MesMgBr to $FeCl_3$ and TMEDA in the absence of 1-bromooctane resulted in the formation of $FeMes_2$(tmeda). The further reaction of $FeMes_2$(tmeda) with 2 equivalents of 1-bromooctane resulted in the formation of Fe(Mes)Br(tmeda) along with 1-octyl-2,4,6-trimethylbenzene. Subsequent reaction of Fe(Mes)Br(tmeda) with MesMgBr regenerated $FeMes_2$(tmeda). It was proposed that these species are part of the mechanistic cycle and the slow addition of MesMgBr and TMEDA contributes to the formation of $FeMes_2$(tmeda), increasing the yield of the reaction.[24]



Scheme 5. Coupling reaction between MesMgBr and 1-bromooctane catalysed by $FeCl_3$ and TMEDA.[24]

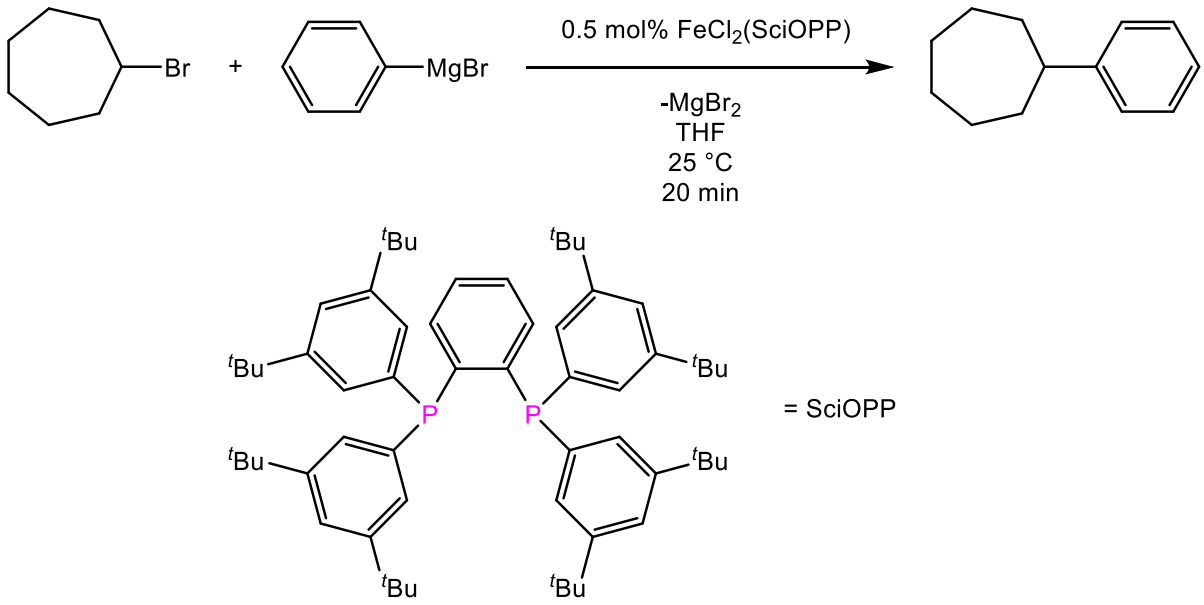
The similar complexes $FeMes_2$(dppe) and Fe(Mes)Cl(dppe) have also been synthesised.[23] $FeMes_2$(dppe) was synthesised by the addition of DPPE to $[Fe(Mes)_2]_2$.[23,25] Following an

attempt to crystallise this complex from dichloromethane, the complex Fe(Mes)Cl(dppe) was isolated, with a tetrahedral geometry (Scheme 6).



Scheme 6. Synthesis of $FeMes_2$(dppe) and Fe(Mes)Cl(dppe).[23,25]

The complexes Fe(Ph)Br(SciOPP) and Fe(Mes)Br(SciOPP) have also been isolated as part of a catalytic cycle (Scheme 7). $FeCl_2$(SciOPP) acts as a precatalyst for the cross-coupling of alkyl halides and Grignard reagents.[26] The species Fe(Ph)Br(SciOPP) was identified *in situ* by Mössbauer spectroscopy,[27] and the similar species Fe(Mes)Br(SciOPP) was identified with the use of MesMgBr.[28] These complexes were also synthesised outside of the catalysis by the addition of ArMgBr (Ar = Ph or Mes) to $FeCl_2$(SciOPP) or $FeBr_2$(SciOPP).[27,28]

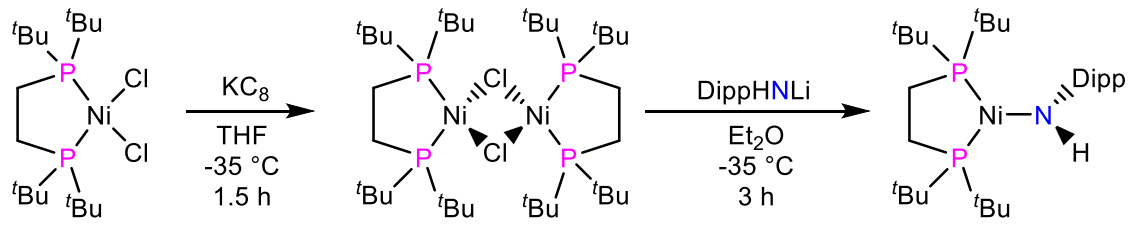


Scheme 7. Cross-coupling of alkyl halide and Grignard reagent catalysed by $FeCl_2$(SciOPP).[26]

These examples highlight the important role these complexes can play in catalysis. Investigating them can give us some insight into the nature of these species and the role they play in catalysis. These complexes show that a four-coordinate complex containing a bidentate ligand, an aryl ligand and a halide can be synthesised, however a complex containing an *m*-terphenyl ligand has not yet been reported. A similar approach to the synthesis of these complexes could be applied to incorporate an *m*-terphenyl ligand. The steric bulk of the *m*-terphenyl may also lead to the possibility of a three-coordinate species containing an *m*-terphenyl ligand and a bidentate ligand, which due to the unsaturated metal centre could have applications as a catalyst.

Hillhouse and co-workers have reported the synthesis of several M(I) complexes containing a bidentate ligand and an anionic ligand.[29–31]

In 2001 the synthesis of the Ni(I) complex Ni(NHDipp)(dtbpe) was reported.[29] First, the Ni(II) complex $NiCl_2$(dtbpe) was reduced with KC_8 to give the Ni(I) dimer [NiCl(dtbpe)]$_2$. The Li salt DippHNLi was then added to the dimer to give Ni(NHDipp)(dtbpe) (Scheme 8).



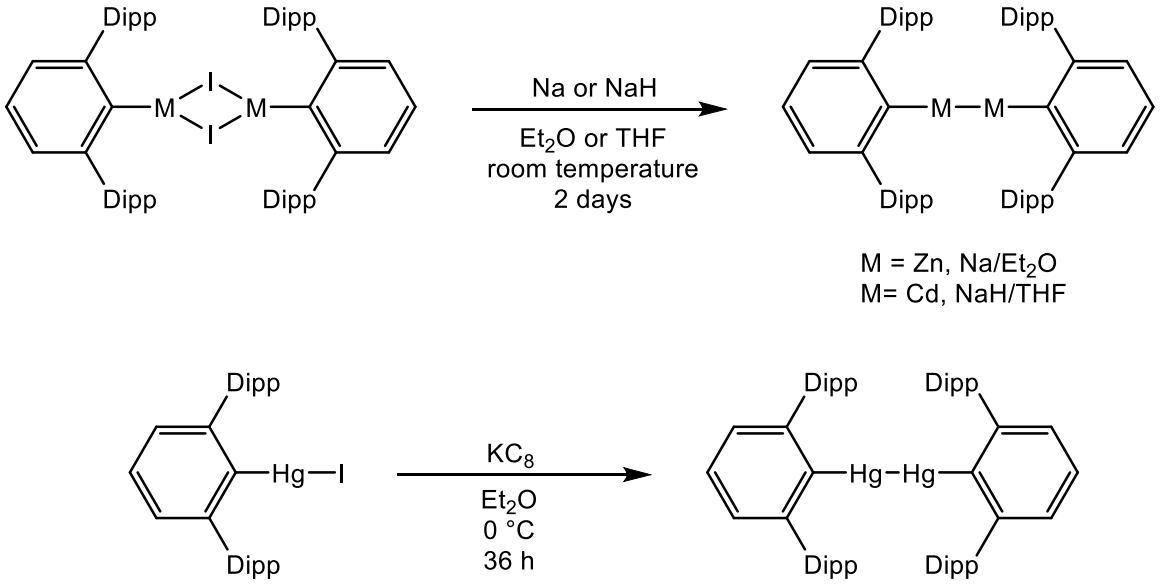
Scheme 8. Synthesis of Ni(NHDipp)(dtbpe).[29]

The similar species Ni(P^{t}Bu$_2$)(dtbpe) and Ni[PH(2,6-Mes$_2$C$_6$H$_3$)](dtbpe) were also synthesised by Hillhouse *et al*. using this method,[30] as well as the silyl complex Ni(SiHMes$_2$)(dtbpe).[31]

It can be envisioned that similar complexes could be synthesised containing an *m*-terphenyl complex through the reduction of the proposed four-coordinate species containing an *m*-terphenyl ligand, a bidentate ligand and a halide. A species containing a

bidentate ligand and an *m*-terphenyl ligand would combine the already established catalytic properties of *m*-terphenyl complexes[32–34] with the ability to selectively tune the selectivity through sterics that bidentate ligands have previously shown.[11,17,21]

A common reducing agent used with *m*-terphenyl complexes is KC_8 which was utilised by Power *et al.* to synthesise a Cr(I) complex containing a quintuple Cr–Cr bond.[35] Power *et al*. also reported the synthesis of three group 12 *m*-terphenyl complexes containing M–M bonds (M = Zn, Cd, Hg). These were synthesised using different reducing agents (Scheme 9).[36–38] The three reducing agents utilised are Na (M = Zn), NaH (M = Cd) and KC_8 (M = Hg). The addition of the reducing agent to either (2,6-(2,6-Dipp)$_2$C$_6$H$_3$)M(μ-I)$_2$M(2,6-(2,6-Dipp)$_2$C$_6$H$_3$) (M = Zn, Cd) or Hg(2,6-(2,6-Dipp)$_2$C$_6$H$_3$)I produces the complexes M$_2$[2,6-(2,6-Dipp)$_2$C$_6$H$_3$]$_2$.



Scheme 9. Reduction of group 12 *m*-terphenyl complexes to form a M–M bond (M = Zn, Cd, Hg).[36–38]

Power *et al*. also reported the synthesis of a monomeric Cr(I) species containing an *m*-terphenyl ligand and a neutral monodentate phosphine ligand (Figure 2).[39] This was synthesised by the reduction of (2,6-Trip$_2$-3,5-^{i}Pr$_2$C$_6$H)CrCl with KC_8 in the presence of

PMe_3. The steric bulk of the *m*-terphenyl ligand ensured that this was a monomeric complex. A similar method could be utilised with a bidentate phosphine.

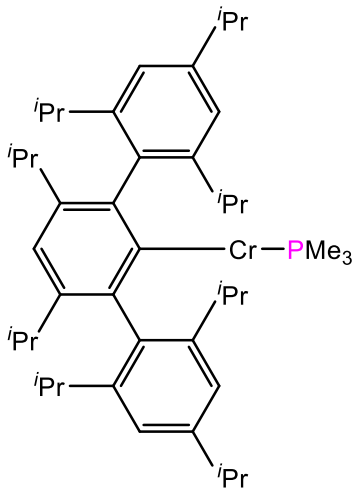


Figure 2. Molecular structure of (2,6-$Trip_2$-3,5-$^i Pr_2$-C_6H)Cr(PMe_3).[40]

Another method that could be used to remove a halide is halide abstraction where the halide is replaced by a weakly coordinating counteranion.[41–50] There are many examples of halide abstracting agents in the literature: Na[BAr^F_4],[51] $AgPF_6$,[44,46] $AgBF_4$,[41] and $NaBPh_4$.[49,50]

Reduction and halide abstraction are both methods that can be utilised in the synthesis of a three-coordinate complex containing a bidentate ligand and an *m*-terphenyl ligand.

4.2 Aims

The aim of this work was to synthesise and characterise a family of four-coordinate monomeric complexes containing a bidentate ligand, an *m*-terphenyl ligand and a halide. The effect of altering both the metal centre and the bidentate ligand employed was investigated. Investigations into the magnetic properties of these complexes was undertaken using Evans method. The reactivity of these complexes towards reduction and halide abstraction was then explored.

4.3 Results and Discussion

4.3.1 Diphosphines

The synthesis of an *m*-terphenyl complex containing the diphosphine ligand 1,2-bis(diphenylphosphino)ethane (DPPE) was initially attempted with a one-pot reaction between $ZnCl_2$, $[Mes_2C_6H_3Li]_2$ (**2**) and DPPE. An equimolar solution of the three reagents in diethyl ether was stirred at room temperature, and it was noted that under the reaction conditions the diphosphine did not fully dissolve. After 24 h, the reaction mixture was filtered, resulting in a very pale-yellow solution, and after storage of the filtrate at room temperature for 24 h, colourless crystals suitable for X-ray diffraction were isolated. Analysis of these crystals demonstrated that they were the polymer $[ZnCl_2(dppe)]_n$ (**23**) (Figure 3), featuring a DPPE ligand bridging two zinc centres, the structure of which was previously observed by Bedford *et al*. in 2019.[17]

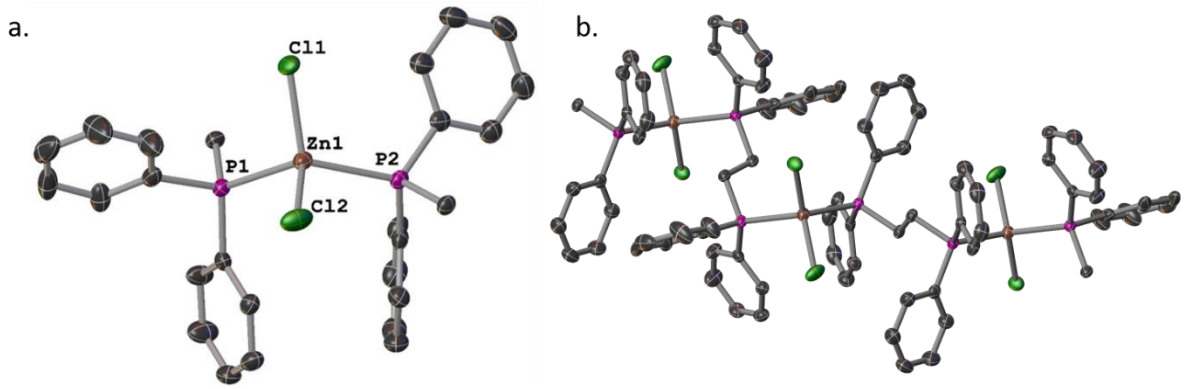
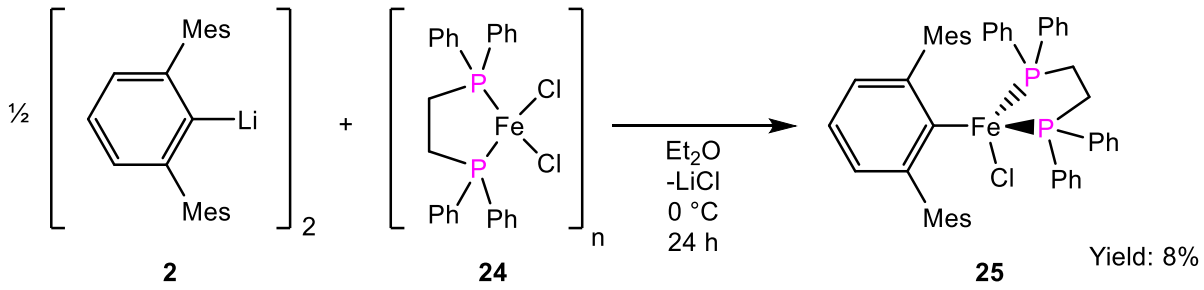


Figure 3. Crystal structure of **23** (a. monomer unit; b. polymer chain), with thermal ellipsoids at 50% probability and hydrogen atoms omitted for clarity (brown = zinc, black = carbon, pink = phosphorus, green = chlorine).

A similar reaction was undertaken using $FeCl_2$ in an attempt to synthesise an iron complex containing DPPE, as iron has a larger atomic radius than zinc (Fe: 1.52 Å; Zn: 1.22 Å)[52] it was postulated that it may be able to accommodate both a coordinating DPPE and an *m*-terphenyl ligand. The synthesis was also altered from the initial one-pot reaction, where the diphosphine complex $[FeCl_2(dppe)]_n$ (**24**) was synthesised initially.[53] A solution of $[Mes_2C_6H_3Li]_2$ (**2**) in diethyl ether was added dropwise at 0 °C to a solution of **24** in diethyl

ether. The reaction mixture was stirred at 0 °C for 4 hours and was then allowed to slowly warm to room temperature (Scheme 10). After stirring the yellow reaction mixture for 24 h, it was filtered, and the solvent removed *in vacuo*. The resulting yellow powder was extracted into hexane and yellow crystals formed in the solution at room temperature suitable for X-ray diffraction. These were demonstrated to be the Fe(II) complex Fe(2,6-$Mes_2C_6H_3$)Cl(dppe) (**25**) (Figure 4).



Scheme 10. Synthesis of **25**.

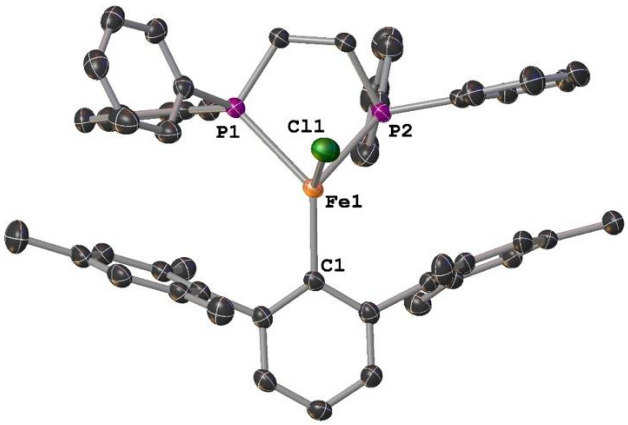


Figure 4. Crystal structure of **25**, with thermal ellipsoids at 50% probability. Hydrogen atoms omitted for clarity (orange = iron, black = carbon, pink = phosphorus, green = chlorine).

The solid-state structure of **25** contains one *m*-terphenyl ligand, one DPPE ligand and a halide coordinated to the iron centre (Figure 4). The halide site exhibits partial occupancy by a chloride and a bromide (Cl:Br ratio of 54:46). Although there are no bromide-containing reagents in this reaction, it is conceivable that the bromide originates from the initial synthesis of the *m*-terphenyl iodide preligand (which utilised MesMgBr). A similar result has been reported by Power and co-workers for [2,6-$Dipp_2C_6H_3$Mn(μ_3-

$Cl)_2Li(THF)]_2$,[54] and previously within our own laboratory for [2,6-$Mes_2C_6H_3Cd(\mu_3$-$Cl)_2Li(THF)]_2$,[55] although this involved Cl/I mixed occupancy, the origin of which has been postulated as an *m*-terphenyl iodide precursor. The crystal structure of **25** displays a distorted tetrahedral geometry with a C–Fe–Cl/C–Fe–Br bond angle of 119.3(3)°/115.02(13)° and a P–Fe–P bond angle of 81.31(2)° (Table 1). The Fe–C bond length is 2.066(2) Å which is longer than the diaryl complex Fe(2,6-$Mes_2C_6H_3)_2$ (2.040(3) Å) and the tetrahedral complex FeMes(dppe)Cl (2.044(5) Å).[23] The Fe–P bond lengths are 2.5332(6) and 2.4843(6) Å which are considerably longer than other iron DPPE containing complexes FeCp(dppe)Cl, Fe(dmpe)Cl_2 and FeMes(dppe)Cl which have Fe–P bond lengths of 2.1963(10), 2.241(1) Å and 2.4598(15) Å respectively.[23,56,57] This could be due to the presence of the *m*-terphenyl ligand which is more sterically hindered than Mes or Cp so the diphosphine is not able to be as close to the metal centre in **25**. The monomeric structure of **25** is in contrast to the halide bridged dimers that are observed for similar four-coordinate complexes containing *m*-terphenyl ligands and halides without the presence of a bidentate ligand.[58]

Table 1. Selected bond lengths (Å) and angles (°) for **25**.

	25
Fe1–C1	2.066(2)
Fe1–P1	2.5332(6)
Fe1–P2	2.4843(6)
Fe1–Cl1	2.4364(13)
P1–Fe1–P2	81.31(2)
P1–Fe1–C1	132.40(6)
P2–Fe1–C1	127.01(6)
C1–Fe1–Cl1	119.3(3)
P1–Fe1–Cl1	91.2(3)
P2–Fe1–Cl1	94.0(3)

Complex **25** has also been characterised by ^{1}H and ^{31}P NMR spectroscopy, and as expected for a paramagnetic species, the ^{1}H NMR spectrum was very broad and showed 10 paramagnetically-shifted peaks between −100 and 100 ppm, and no resonances were observed in the ^{31}P NMR spectrum. This is most likely due to the paramagnetic broadening of the peak for the DPPE ligand upon coordination to the Fe(II) centre which is common in iron diphosphine complexes.[17] Unfortunately, the yield of this compound was very low as only a few crystals were isolated. The ^{1}H NMR spectrum of the remaining yellow hexane solution that did not crystallise showed the presence of a small amount of the Li salt **2** and some paramagnetically-shifted peaks suggesting the presence of an Fe(II) compound.

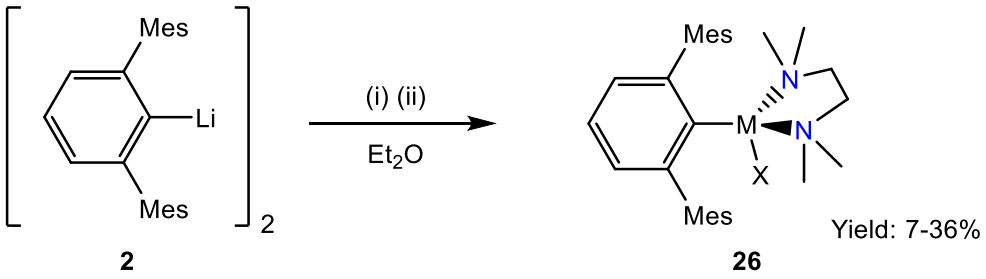
The synthesis of a DPPE-containing Mn complex was also attempted by the reaction of **2** and $MnBr_2$ in diethyl ether at −78 °C, followed by the addition of a suspension of DPPE in diethyl ether at room temperature. After stirring at room temperature for 24 h and filtration, colourless crystals suitable for X-ray diffraction precipitated from a saturated diethyl ether solution at −30 °C, however these were found to be crystals of uncoordinated DPPE.

Due to the difficulty in the isolation and characterisation of these complexes and the issues with the solubility of DPPE, attention was moved to the more soluble nitrogen and oxygen ligands, TMEDA and DME.

4.3.2 TMEDA

Tetramethylethylenediamine (TMEDA) is much smaller than DPPE as it only contains methyl groups instead of phenyl groups so it should coordinate more readily to the metal centre with an *m*-terphenyl ligand. The Mn complex Mn(2,6-$Mes_2C_6H_3$)Br(tmeda) (**26a**) was synthesised by adding a solution of **2** in diethyl ether dropwise to a solution of $MnBr_2$ in diethyl ether at −78 °C, followed by warming to room temperature and addition of one equivalent of TMEDA (Scheme 11). The reaction mixture was stirred at room temperature for 16 hours, followed by filtration and storage of the solution at −30 °C for 48 h afforded colourless crystals of **26a** with a moderate yield of 29%.

Analogous reactions using $FeCl_2$, $CoBr_2(DME)$ and $ZnCl_2$ resulting in the analogous complexes **26b** (M = Fe), **26c** (M = Co) and **26d** (M = Zn). Crystals suitable for X-ray diffraction for these complexes were grown from a saturated diethyl ether solution stored at −30 °C (Figure 5) with yields of 13% (**26b**) and 36% (**26d**).



Scheme 11. Synthesis of TMEDA complexes **26a**–**d** (MX_2 = $MnBr_2$ (**26a**), $FeCl_2$ (**26b**), $CoBr_2(DME)$ (**26c**) and $ZnCl_2$ (**26d**)). (i) MX_2, −78 °C, 2h; (ii) TMEDA, room temperature, 16 h.

The Co(II) complex (**26c**) was isolated in small quantities (7%) as a blue crystalline solid. This low yield meant that only limited analysis was able to be carried out on **26c**. A colourless crystalline solid (**27**) was also obtained from the same reaction mixture in much higher yields than **26c**, which was characterised by ^1H, $^{13}C\{^1H\}$ and ^7Li NMR spectroscopy. The complex displayed a resonance at 2.0 ppm in the ^7Li NMR spectrum and resonances in the ^1H NMR spectrum at 2.22 and 1.86 ppm can be assigned to the C*H*$_3$ and C*H*$_2$ protons in TMEDA respectively. This suggests the presence of a lithium halide salt with TMEDA coordinated to the lithium metal centre, likely $Li(tmeda)_2Br$.

Complexes **26a**–**d** showed similar distorted tetrahedral geometry to **25** and they all have one molecule in the asymmetric unit (Figure 5). The M–C bond length decreases as you move from Mn to Co (Mn–C>Fe–C>Co–C) as would be expected with the decreasing covalent radii of the metal. The M–C bonds are slightly longer compared to the analogous diaryl $M(2,6\text{-}Mes_2C_6H_3)_2$ complexes.[59,60] This could be due to the four-coordinate complex being slightly more sterically hindered which pushes the *m*-terphenyl ligand away. The C–M–X bond angles for M = Mn, Fe and Zn range from 112.71(7)–115.80(16)°, which is larger than the optimal tetrahedral angle of 109.5°. The C–M–X bond angle for **26c** (M = Co) is significantly smaller at 104.49(7). The N–M–N bond angles are in the range

78.52(10)–84.20(8)°, which is significantly smaller than 109.5° as would be expected with the chelating ligand forcing the nitrogen atoms of the TMEDA closer together. The N–Fe–N angle observed for Fe(Mes)(tmeda)Br which is 81.23(11)°[24] is slightly larger than the N–Fe–N angle observed for **26b** (79.44(9) Å).

Complex **26b** consists of two crystallographically distinct molecules and has partial occupancy of the Cl1 position with a bromine (Cl:Br, 54:46). This is the same ratio that is observed in complex **25** suggesting that this does arise from an impurity in one of the starting materials.

Complex **26b** can be compared with the iron DPPE complex **25**. The Fe–C (**25**: 2.066(2) Å; **26b**: 2.0843(3) Å) and Fe–Cl (**25**: 2.4364(13) Å; **26b**: 2.309(5) Å) bond lengths are similar and the Fe–P bond lengths (2.5332(6) Å) are longer than the Fe–N bond lengths (2.208(2) Å) as would be expected due to the increased covalent radius for phosphorus (1.07 Å) compared with nitrogen (0.71 Å).[52] The N–Fe–N bond angle (79.44(9) Å) is smaller compared to the P–Fe–P (81.31(2) Å) bond angle and the C–Fe–Cl bond angle is slightly larger in the DPPE complex **25** compared to **26b**.

Table 2. Selected bond lengths (Å) and bond angles (°) for **26a**–**d**.

	26a M = Mn X = Br	**26b** M = Fe X = Cl	**26c** M = Co X = Br	**26d** M = Zn X = Cl
M1–C1	2.139(3)	2.084(3)	2.028(3)	2.017(2)
M1–N1	2.294(3)	2.208(2)	2.196(2)	2.191(2)
M1–N2	2.271(3)	2.239(2)	2.097(2)	2.155(2)
M1–X1	2.5735(7)	2.309(5)	2.4625(5)	2.3132(7)
N1–M1–N2	78.52(10)	79.44(9)	84.20(8)	82.18(9)
N1–M1–C1	123.84(11)	132.78(10)	131.54(9)	127.48(9)
N2–M1–C1	133.72(11)	123.37(10)	127.56(9)	130.60(9)
C1–M1–X1	113.73(8)	115.80(16)	104.49(7)	112.71(7)
N1–M1–X1	103.94(8)	92.42(15)	101.66(6)	100.89(8)
N2–M1–X1	95.41(9)	104.80(17)	102.52(7)	95.11(8)

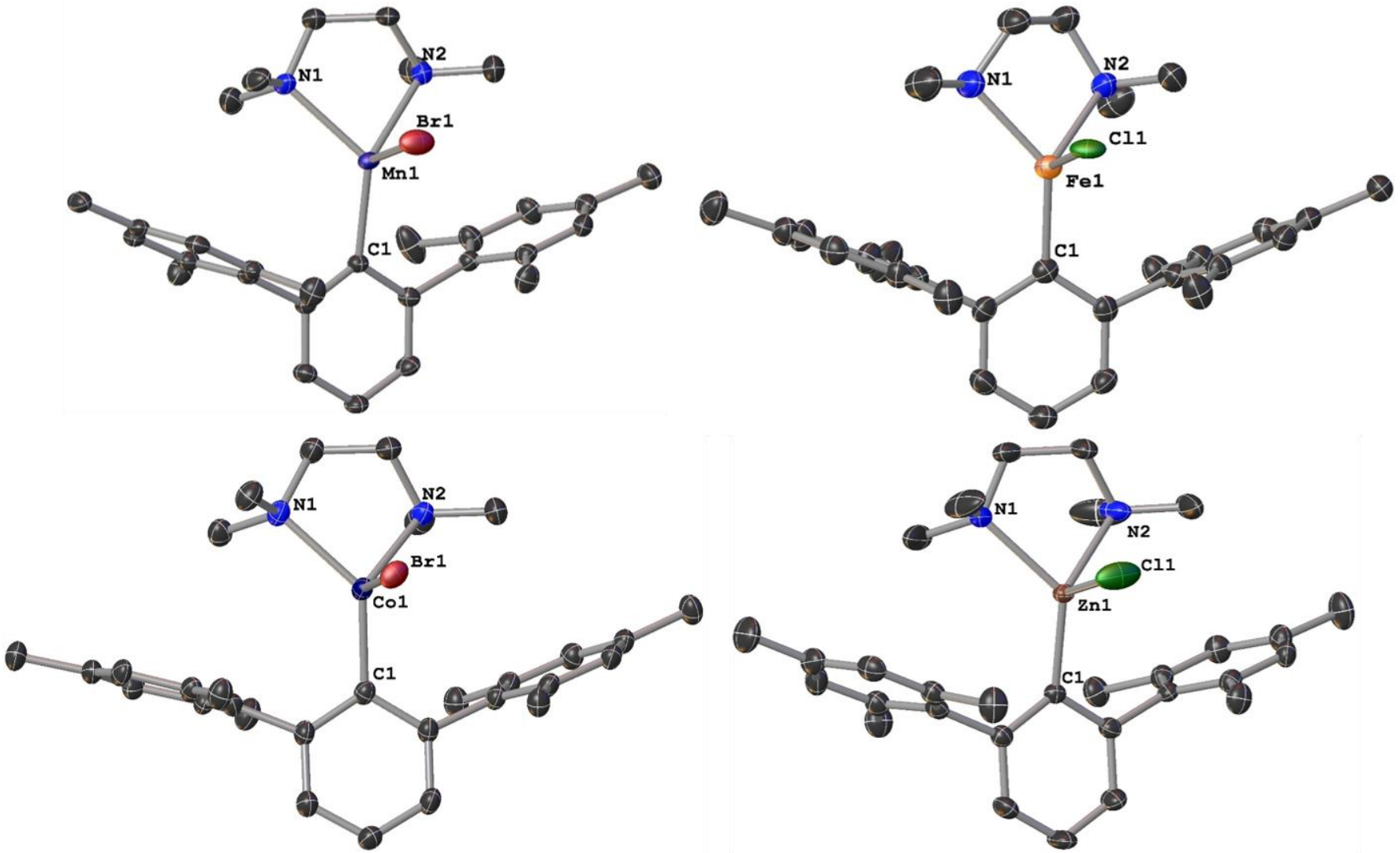


Figure 5. Crystal structures of **26a**–**d** with thermal ellipsoids at 50% probability. Hydrogen atoms omitted for clarity (purple = manganese, orange = iron, dark blue = cobalt, brown = zinc, black = carbon, blue = nitrogen, maroon = bromine, green = chlorine).

Mass spectrometric analysis through APCI was attempted with these complexes, but it was not possible to detect the desired species through this technique. A different ionisation technique may be more successful although there are other reports in the literature of similar complexes containing TMEDA ligands that were not able to be detected by mass spectrometry such as $[Fe_3Cl_5(tmeda)_3][BPh_4]$.[61]

Unlike the other complexes, **26d** provided diamagnetic NMR spectra (Figure 6). The TMEDA peaks appear at 1.60 (CH_3) and 1.75 (CH_2) ppm in the ^1H NMR spectrum, which is shifted significantly upfield from free TMEDA (2.12 (CH_3) and 2.35 (CH_2) ppm) as the protons have become more shielded after coordination to the metal.

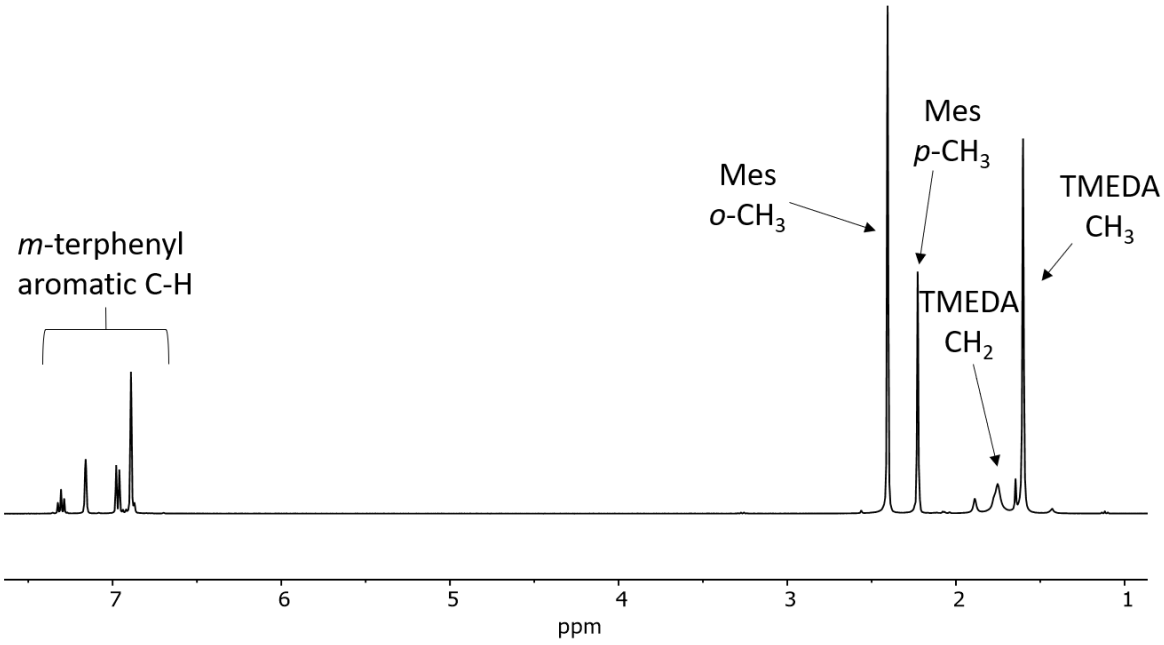


Figure 6. ^1H NMR spectrum of **26d**.

The zinc complex **26d** was also synthesised *via* an alternative method that is analogous to the method used to synthesise the DPPE complex **25**. $ZnCl_2(tmeda)$ (**28**) was synthesised by the reaction between $ZnCl_2$ and TMEDA in THF.[62] The structure was confirmed by ^1H NMR spectroscopy and X-ray crystallography (Figure 7).

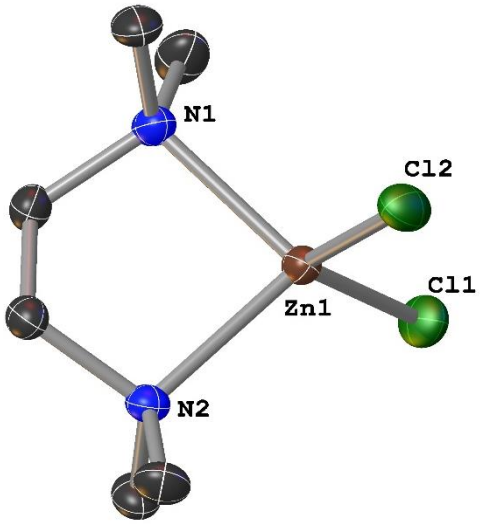
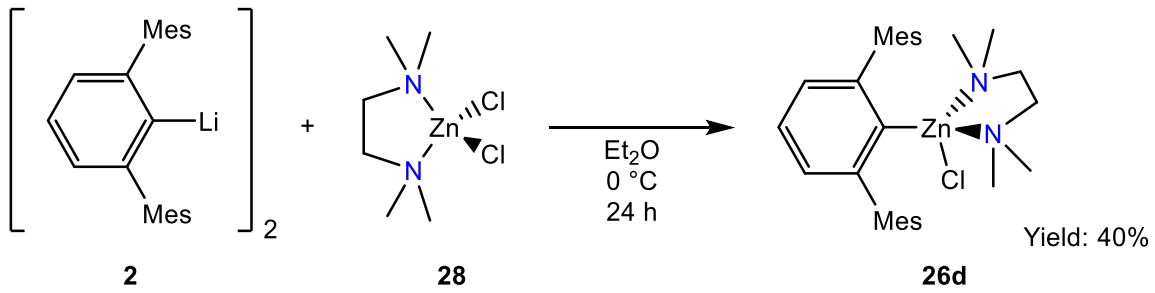


Figure 7. Crystal structure of **28** with thermal ellipsoids at 50% and hydrogen atoms omitted for clarity (brown = zinc, black = carbon, blue = nitrogen, green = chlorine).

Complex **28** was then used to synthesise **26d** by adding a solution of **2** in diethyl ether dropwise to a solution of **28** in diethyl ether at 0 °C (Scheme 12). Colourless crystals were isolated by storing the solution at −30 °C and confirmed to be **26d** by ^{1}H and ^{13}C NMR spectroscopy. A similar yield to the previous method was obtained.

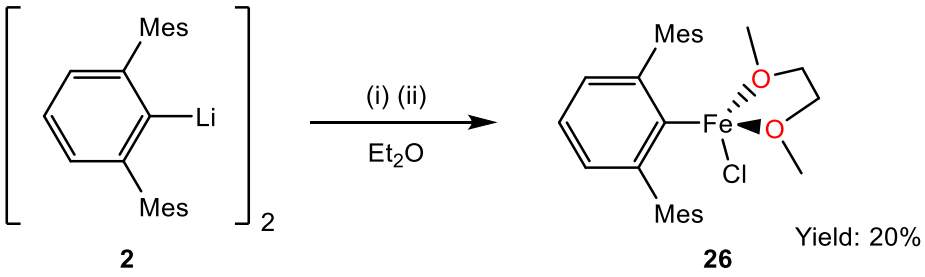


Scheme 12. Alternative method to synthesise **26d**.

4.3.3 DME

In order to extend on the work with TMEDA, the ligand 1,2-dimethoxyethane (DME) was investigated. It is slightly smaller than TMEDA as there is only one methyl group on each of the oxygen atoms compared to the two methyl groups on the nitrogen atoms in TMEDA. The Fe(II) complex Fe(2,6-Mes$_2$C$_6$H$_3$)Cl(dme) (**29b**) was synthesised using a similar

method to the TMEDA complexes where **2** was added dropwise to $FeCl_2$ in diethyl ether at −78 °C. Stirring the solution at this temperature for 2 h, warming to room temperature, followed by addition of one equivalent of DME afforded **29b** with a 20% yield (Scheme 13).



Scheme 13. Synthesis of **29b**. (i) $FeCl_2$, −78 °C, 2h; (ii) DME, room temperature 16 h.

Crystals of **29b** were grown from a saturated diethyl ether solution at −30 °C over 1 week. The crystal was found to be twinned and three separate crystal environments (with ratios of 51:39:10) were identified and the major environment was resolved with two molecules in the asymmetric unit. The complex has a distorted tetrahedral geometry similar to the DPPE (**25**) and TMEDA complexes (**26a**–**d**). It displays Fe–C bond lengths of 2.058(12) and 2.054(13) Å which is similar to the Fe–C bond length in **25** (2.066(2) Å) and **26b** (2.084(3) Å). The Fe–O bond length (2.150(11), 2.150(12) Å) is shorter than the Fe–N bond length (2.208(2) Å) in **26b**. The bond length decreases from Fe–P>Fe–N>Fe–O (**25**>**26b**>**29b**). This trend can be explained by the decreasing covalent radii (P: 1.07 Å; N: 0.71 Å; O: 0.66 Å)[52] and the increasing electronegativity of the atom bonded to the Fe metal centre. There will also be an influence of the sterics of the bidentate ligands on the bond length. The DPPE ligand is the most sterically demanding of these bidentate ligands and the Fe–P bond length for **25** is the longest of these bonds.

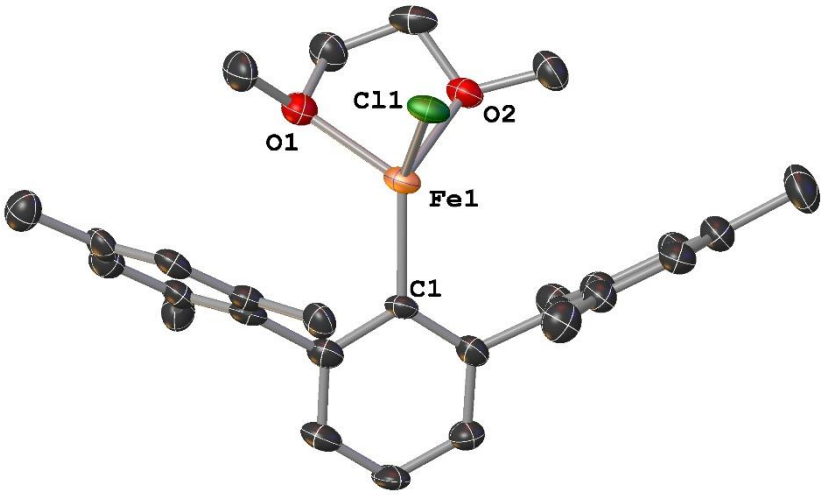


Figure 8. Crystal structure of **29b**, with thermal ellipsoids at 50%. Hydrogen atoms omitted for clarity (orange = iron, black = carbon, red = oxygen, green = chlorine).

Table 3. Selected bond lengths (Å) and angles (°) for **29b**.[a]

	29b
Fe1–C1	2.058(12), 2.054(13)
Fe1–O1	2.150(11), 2.150(12)
Fe1–O2	2.136(9), 2.120(10)
Fe1–Cl1	2.287(4), 2.306(4)
O1–Fe1–O2	77.4(4), 77.3(4)
O1–Fe1–C1	115.5(5), 118.0(5)
O2–Fe1–C1	120.8(4), 121.6(5)
C1–Fe1–Cl1	131.4(4), 124.2(4)
O1–Fe1–Cl1	101.7(3), 105.5(3)
O2–Fe1–Cl1	96.0(3), 99.9(3)

[a] Values provided for both molecules in asymmetric unit

A similar reaction was repeated with $CoBr_2$(DME), and from this green crystals were grown from a saturated diethyl ether solution at −30 °C over 1 week, however they were not the expected analogous cobalt complex, but were instead found to be the bimetallic complex

30 (Figure 9 and Table 4). In the solid state structure of **30**, the DME ligand is coordinated to the Co centre but only through one oxygen atom and it is also coordinated to a lithium atom, likely originating from the Li complex **2**, which is interacting with the aromatic ring of one of the flanking groups (Figure 10). The interaction of lithium with the flanking groups in an *m*-terphenyl ligand has been previously observed by Power *et al*. in the solid state structures of Li(^{t}Bu)Li(2,6-Trip$_2$C$_6$H$_3$)[63] and (2,6-Trip$_2$C$_6$H$_3$)(Me)$_2$Sn–Sn(Li)(Me)(2,6-Trip$_2$C$_6$H$_3$).[64] The Li–O bonds between the Li and the DME ligand are 2.096(4) and 1.971(4) Å, the former is similar to the 2.09(3) Å Li–O bond length in Li(dme)Br$_2$.[61] The Li1–O2 bond length in **30** is slightly shorter than this at 1.863(4) Å. The Co–Br bond length is shorter than in the TMEDA complex **26c** (2.3994(4) Å for **30** compared with 2.4625(5) Å for **26c**).

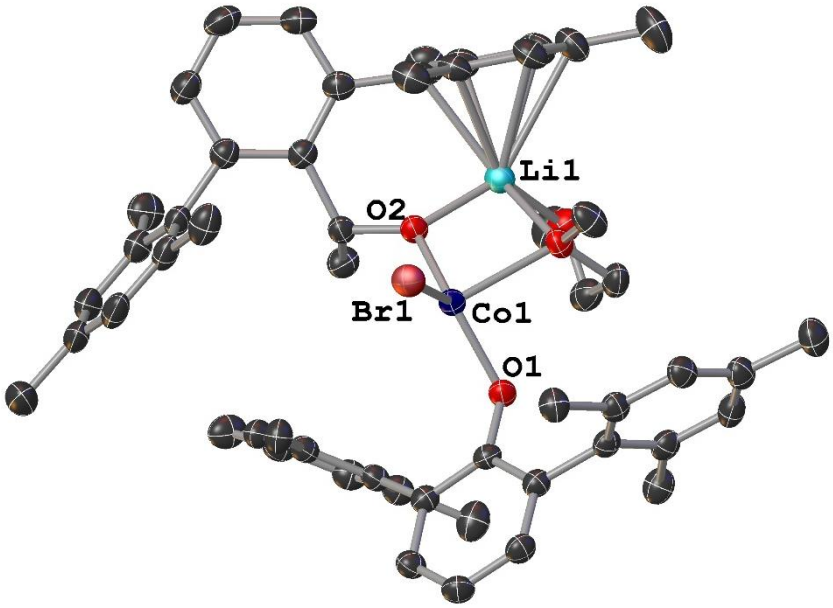


Figure 9. Crystal structure of **30**, with thermal ellipsoids at 50% probability. Hydrogen atoms omitted for clarity (dark blue = cobalt, black = carbon, light blue = lithium, red = oxygen, maroon = bromine).

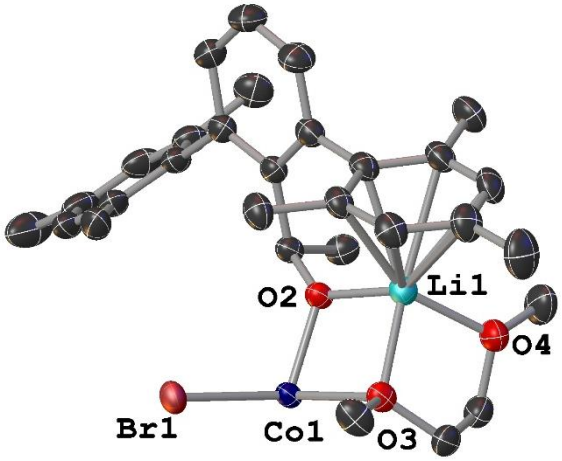


Figure 10. Crystal structure of **30**, with thermal ellipsoids at 50% probability. Hydrogen atoms and second *m*-terphenyl ligand omitted for clarity (dark blue = cobalt, black = carbon, light blue = lithium, red = oxygen, maroon = bromine).

Table 4. Selected bond lengths (Å) and angles (°) for **30**.

	30
Co1–O1	1.8912(16)
Co1–Br1	2.3994(4)
Li1–O2	1.863(4)
Li1–O3	2.096(4)
Li1–O4	1.971(4)
C1–O1	1.340(3)
O1–Co1–O2	136.75(7)

In the solid state structure of **30**, an oxygen atom has been inserted into one of the *m*-terphenyl ligands and formed an alkoxide. Power *et al.* has previously reported the reactivity of diaryl *m*-terphenyl complexes with O_2 which proceed via the insertion of an oxygen atom into the M–C bond in a similar way.[65] It is therefore conceivable that a small amount of O_2 was present in the reaction and a similar insertion occured. The C1–O1 bond length of 1.340(3) Å is similar to that observed for the aryloxide groups in the $Fe(OAr)_2$ complex reported by Power *et al*. (1.3485(15) Å).[65] On the second *m*-terphenyl group there are two extra carbon atoms and an oxygen atom, forming an alkoxide ligand on the

metal. It is possible that this is from a molecule of DME that has been fragmented and inserted into the Co–C bond. This insertion is similar to that observed for the insertion of CO into the Fe–C bond of Fe(2,6-$Dipp_2C_6H_3)_2$ to form a carbonyl complex.[65] The fragmentation of DME to form **30** would result in the cleavage of the C–O which is not commonly observed under mild conditions. This fragmentation would also result in the formation of 'CH_3' and 'OCH_3' fragments so it seems likely that the isolated complex **30** is not the only species that was formed in this reaction and that there are other species present in the reaction solution that did not crystallise. Further work to investigate this reaction could be undertaken by attempting to isolate crystals using different solvents (or other crystallisation methods) to identify different reaction products that may contain these missing fragments. This will help to determine the mechanism of this reaction.

An analogous reaction between $ZnCl_2$, **2** and DME afforded a colourless polycrystalline solid isolated from diethyl ether solution at −30 °C over 1 week. Further attempts to obtain single crystals suitable for X-ray crystallography by crystallisation from toluene or hexane were unsuccessful. The ^{1}H and ^{13}C NMR spectra of the colourless solid in C_6D_6 demonstrated that the resonances for the DME at 2.72 (CH_3) and 2.81 (CH_2) ppm had shifted significantly from free DME (3.12 and 3.33 ppm), indicating that coordination to the metal centre has taken place (Figure 11).

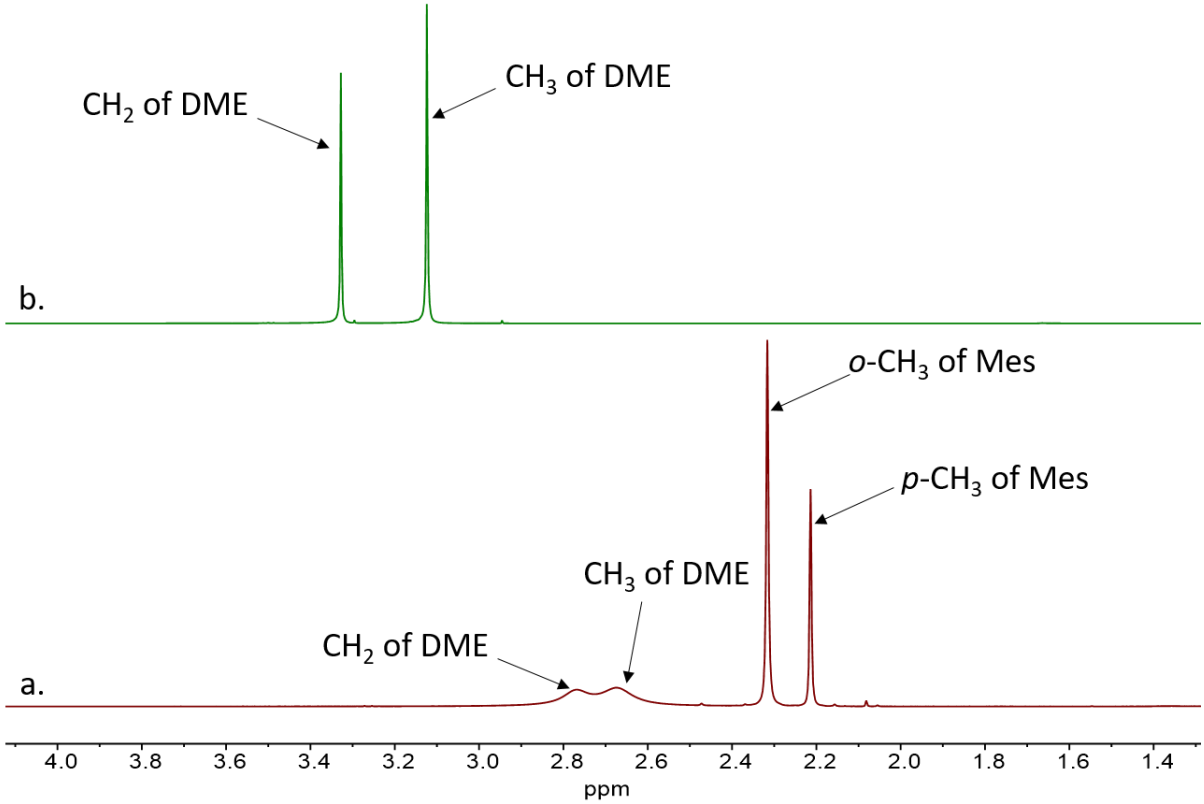


Figure 11. ^{1}H NMR spectra of **29d** (a) and free DME (b) in C_6D_6.

4.3.4 Magnetic Measurements

Evans method[66] was used to determine the magnetic moment of the three paramagnetic Fe(II) compounds **25**, **26b** and **29b** and Mn(II) complex **26a** (Table 3) in C_6D_6. The measurements were repeated once and the average was taken as the magnetic moment. The effective magnetic moment for **25** was measured as 3.61 μ_B, which is significantly smaller than the spin only value for a high spin d^6 complex (4.90 μ_B), but is similar to the magnetic moment for $FeMes_2(dppe)$ (3.4 μ_b) which is attributed to an electron configuration with two unpaired electrons indicating a low spin tetrahedral d^6 complex.[23] A similar observation is made for the Fe(II) DME complex **29b** which has a magnetic moment of 3.12 μ_B.

The effective magnetic moment for **26b** was 4.91 μ_B, which is close to the spin only value for a high spin d^6 complex with four unpaired electrons (4.90 μ_B), and to the diaryl *m*-terphenyl complex $Fe(2,6\text{-}Mes_2C_6H_3)_2$ (4.90 μ_B)[59] and $FeMes_2(tmeda)$ (5.1 μ_B).[23] These

results suggest that the TMEDA ligand is able to stabilise the high spin electron configuration more than the DPPE and DME ligands.

The magnetic moment for the Mn(II) complex **26a** was found to be 3.66 μ_B which is significantly smaller than the spin only value for a high spin d^5 complex with five unpaired electrons (5.92 μ_B) and the observed value for Mn(2,6-$Mes_2C_6H_3)_2$ (5.89 μ_B)[59] and the tetrahedral complex MnCp(tmeda)Cl (5.9 μ_B).[67] This value is similar to the spin only value for three unpaired electrons (3.87 μ_B) which corresponds to an intermediate spin electron configuration for a d^5 complex.

4.3.5 Reactivity of TMEDA complexes

4.3.5.1 Reduction and Halide Abstraction

As most successful complex synthesis occurred with the TMEDA complexes, these complexes were chosen to investigate the possibility of synthesising a three-coordinate species containing an *m*-terphenyl ligand and a bidentate ligand.

A reduction was carried out in an attempt to synthesise an M(I) species. KC_8 was chosen as a reducing agent as this has been shown to reduce other *m*-terphenyl transition metal complexes.[35,39] A suspension of KC_8 in diethyl ether was added to a solution of **26a** in diethyl ether at −30 °C, and after a few minutes a black precipitate had formed. After stirring the reaction mixture at room temperature for 16 h and filtration and storage at −30 °C for 2 weeks, no crystals had precipitated. Removal of solvent and then extraction of the resulting white powder into both toluene and hexane respectively in unsuccessful attempts to crystallise the solid was undertaken. A ^{1}H NMR spectrum in C_6D_6 solution was recorded of the white powder from these crystallisations and was similar to that measured for the starting material **25a**. Crystals from this solution *via* hexane diffusion were shown to be **31** (Figure 12) from singe crystal X-ray diffraction measurements. In the solid state **31** is a Mn(II) bromide bridged dimer containing two TMEDA ligands, indicating that the reduction reaction was unsuccessful. It is also possible that **26a** is not stable in solution

for extended periods, during the attempted crystallisations. It is possible that **26a** is in a Schlenk equilibrium with the homoleptic diaryl and dihalide complexes (Scheme 14).[68,69] Halide abstraction reactions with $NaBAr^{F}_{4}$ and $AgPF_6$ were also attempted and were unsuccessful.

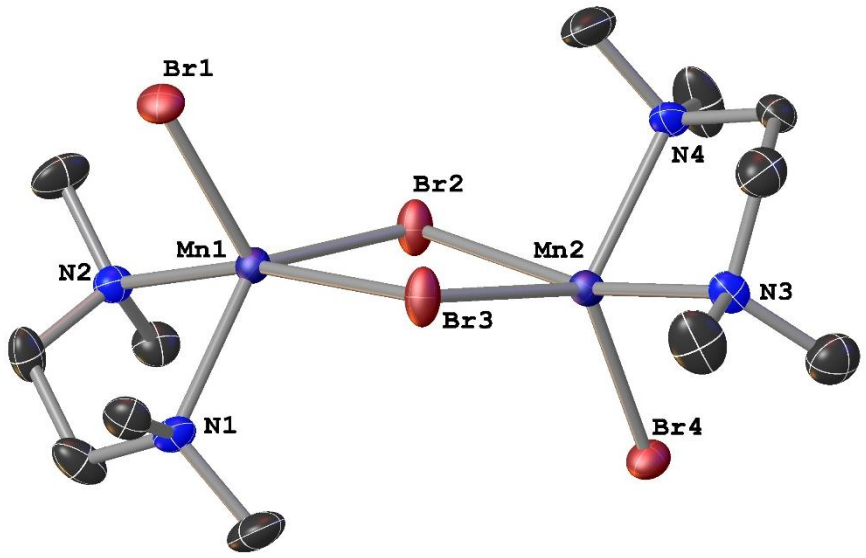
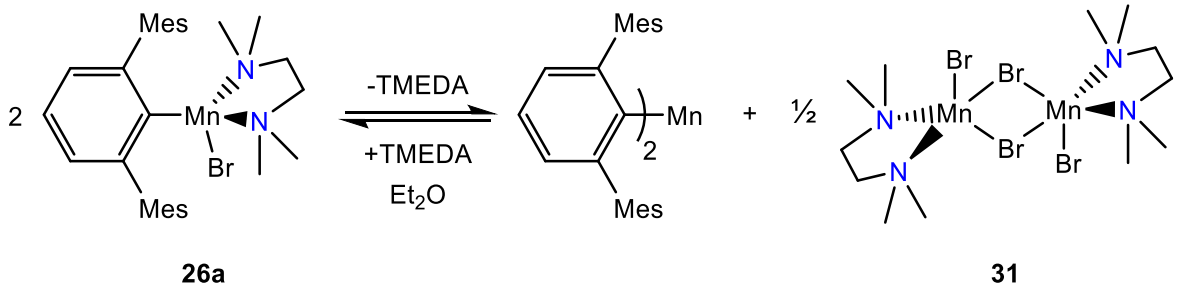


Figure 12. Crystal structure of **31**, with thermal ellipsoids at 50% probability. Hydrogen atoms omitted for clarity (purple = manganese, black = carbon, blue = nitrogen, red = oxygen, maroon = bromine).



Scheme 14. Proposed Schlenk equilibrium between **26a** and **31**.

4.3.5.2 Metathesis Reactions

Power *et al*. have reported the use of $Li[N(SiMe_3)_2]$ in a salt metathesis reaction with $[2,6\text{-}Dipp_2C_6H_3Co(\mu\text{-}Cl)]_2$ to synthesise $Co(2,6\text{-}Dipp_2C_6H_3)[N(SiMe_3)_2]$.[70] A similar salt metathesis reaction was carried out with KO^tBu in an effort to form $M(2,6\text{-}Mes_2C_6H_3)_2O^tBu(tmeda)$ on a small scale with **26d** in C_6D_6 and the reaction was monitored using ^1H NMR spectroscopy (Figure 13). A slight shift upfield in the resonances

for the Mes C*H*$_3$ groups from 2.41 and 2.23 ppm in **26d** to 2.36 and 2.22 ppm was observed. The CH_3 TMEDA peak for **26d** at 1.60 ppm and the ^{t}Bu peak for KO^{t}Bu at 1.16 ppm were no longer present. There are multiple peaks in the range 0.4 to 1.2 ppm that may be assigned to a new ^{t}Bu environment. Unsuccessful attempts to crystallise a product by hexane diffusion into the C_6D_6 solution were undertaken.

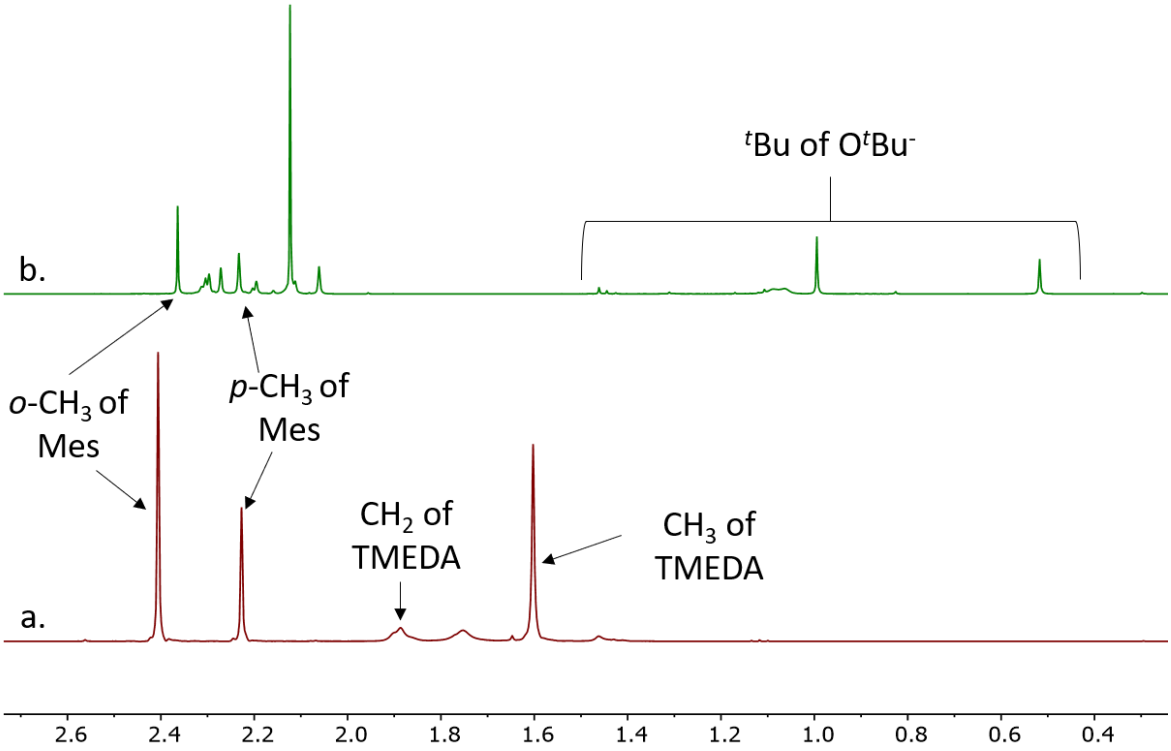


Figure 13. ^{1}H NMR spectra of **26d** (a) and after addition of KO^{t}Bu (b) at room temperature in C_6D_6.

Similarly the reaction between **26d** and Na[N(SiMe$_3$)$_2$] in C_6D_6 was attempted and was followed by ^{1}H NMR spectroscopy, which showed a shift in the aromatic protons for the *m*-terphenyl ligands after 24 h (Figure 14). Figure 15 shows the SiMe$_3$ peaks in the ^{1}H NMR spectra, where the resonance for Na[N(SiMe$_3$)$_2$] (0.12 ppm) is no longer present, but two new resonances are observed at 0.20 and –0.04 ppm. The ^{29}Si NMR spectrum shows a single peak at –1.9 ppm.

The ^{1}H NMR spectrum shows resonances for the CH_2 and CH_3 groups for free TMEDA (δ_H = 2.12 and 2.35 ppm, respectively). The lack of coordination of TMEDA to the metal centre may be due to the steric bulk of N(SiMe$_3$)$_2^-$. The peak at –0.04 ppm has been assigned as

$Zn(2,6\text{-}Mes_2C_6H_3)[N(SiMe_3)_2]$ (**32**) in analogy with $Co(2,6\text{-}Dipp_2C_6H_3)[N(SiMe_3)_2]$ reported by Power *et al.* in 2010,[70] and the second $SiMe_3$ peak at 0.20 ppm has been assigned as $Zn[N(SiMe_3)_2]_2$ (**33**), which has been reported previously.[71,72]

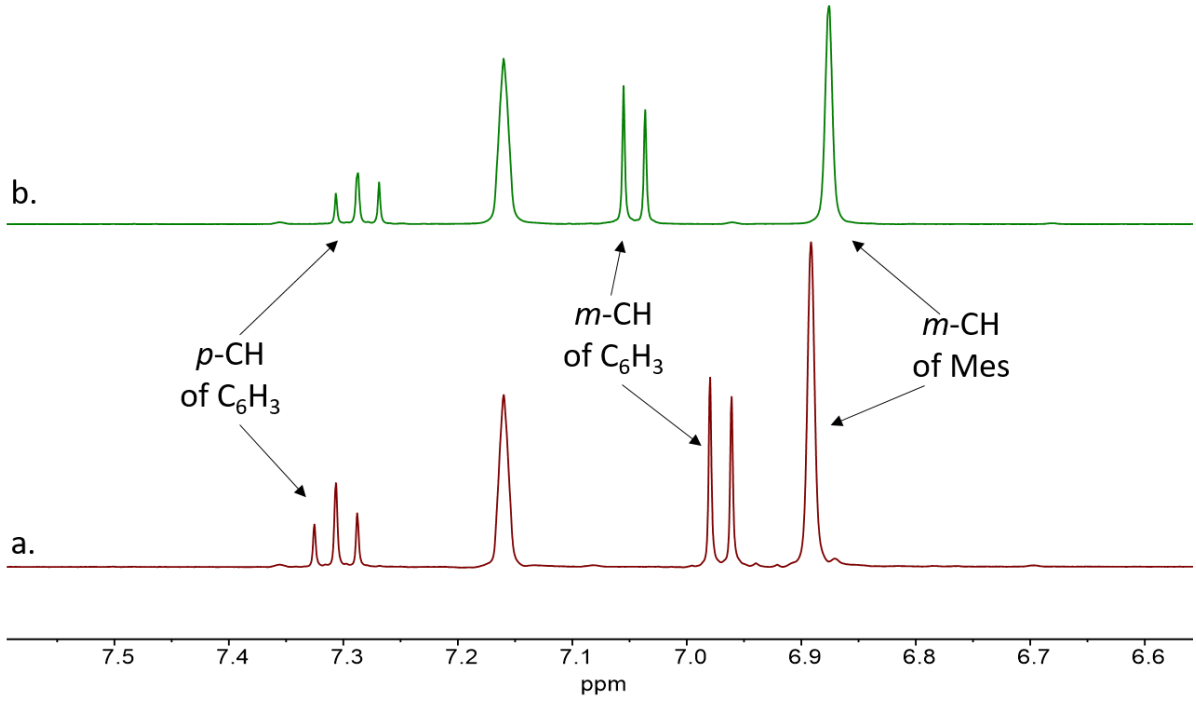


Figure 14. Selected region of ^1H NMR spectra of **26d** (a.) and after addition of $Na[N(SiMe_3)_2]$ (b.) in C_6D_6.

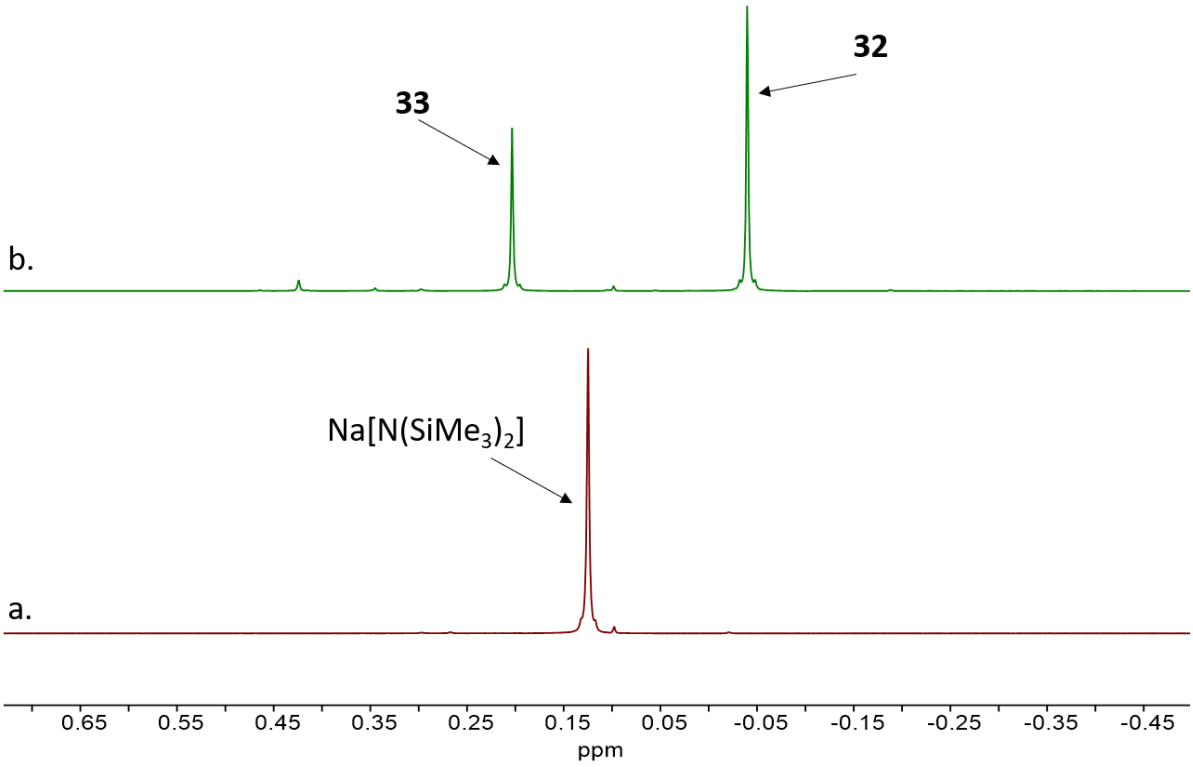
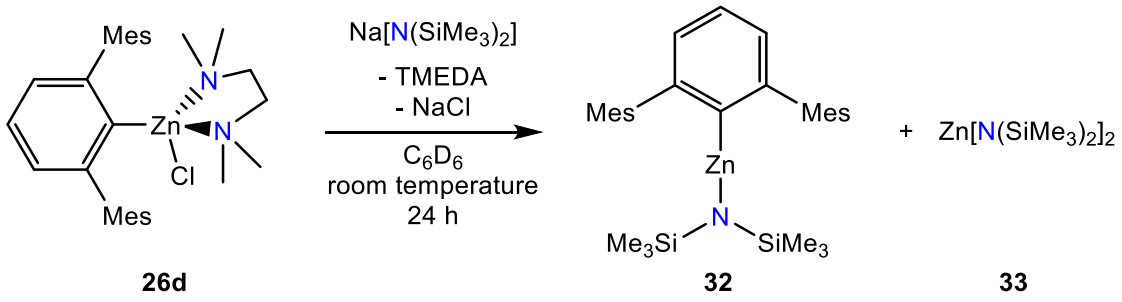


Figure 15. Selected region of ^{1}H NMR spectra of $Na[N(SiMe_3)_2]$ (a.) and after addition of $Na[N(SiMe_3)_2]$ to **26d** (b.) in C_6D_6 showing $SiMe_3$ peaks.



Scheme 15. Synthesis of **32** in C_6D_6 at room temperature.

4.4 Conclusions

A series of four-coordinate complexes containing an *m*-terphenyl ligand, a bidentate ligand (DPPE, TMEDA or DME) and a halide were synthesised and characterised. These complexes all showed a distorted tetrahedral geometry. Attempts to isolate complexes containing the sterically encumbered diphosphine ligand DPPE were unsuccessful for M = Mn and Zn. These reactions resulted in either the formation of the polymer $[ZnCl_2(dppe)]_n$ (**23**) or the

free diphosphine ligand. These issues could be overcome with the use of a less sterically hindered diphosphine such as DMPE which contains methyl groups instead of phenyl groups.

The reactivity of the TMEDA complexes was investigated. Attempts at reducing **26a** with KC_8 were unsuccessful. The dimer $[MnBr(\mu\text{-}Br)(tmeda)]_2$ (**31**) was isolated suggesting the presence of a Schlenk equilibrium between **26a** and **31** which requires further investigation. The use of cyclic voltammetry could aid in the selection of a more suitable reducing agent for these complexes.

A metathesis reaction between **26d** and $Na[N(SiMe_3)_2]$ results in the formation of $Zn(2,6\text{-}Mes_2C_6H_3)[N(SiMe_3)_2]$ (**32**) showing that the TMEDA ligand does not remain coordinated to the metal centre due to the steric bulk of the $N(SiMe_3)_2^-$ ligand.

This work has explored the synthesis of *m*-terphenyl complexes containing bidentate ligands. The use of these ligands has aided in the stabilisation of the monomeric four-coordinate complexes. The presence of the halide leads to the possible reactivity of the complex towards reduction, halide abstraction and salt metathesis reactions. This chapter reports some preliminary efforts to utilise this reactivity although they were mostly unsuccessful. Future work should focus on the exploration of this reactivity with different reducing agents and halide abstraction agents. This proposed three-coordinate complex containing a bidentate ligand and an *m*-terphenyl ligand would have potential applications as a catalyst due to its unsaturated metal centre. The presence of both the *m*-terphenyl ligand and the bidentate ligand could lead to unique applications in catalysis building on the previously reported catalytic properties of *m*-terphenyl complexes and using the bidentate ligand to be able to tune the selectivity of the catalysis. An alternative method to synthesise this proposed complex could involve the reduction of the metal halide adduct before coordination of the *m*-terphenyl in a similar way to the synthesis of the Ni(I) complex Ni(NHDipp)(dtbpe).

4.5 Experimental Procedures

See Chapter 6 for general experimental.

4.5.1 $[ZnCl_2(dppe)]_n$ 23

A solution of $ZnCl_2$ (170 mg, 1.25 mmol), **2** (400 mg, 1.25 mmol) and DPPE (500 mg, 1.25 mmol) in Et_2O (20 mL) was stirred at room temperature for 24 h. The reaction mixture was filtered and colourless crystals formed in the solution suitable for X-ray diffraction after storage of the solution for 3 days at room temperature.

4.5.2 Fe(2,6-$Mes_2C_6H_3$)Cl(dppe) 25

A solution of **2** (91 mg, 0.286 mmol) in Et_2O (10 mL) was added dropwise to a suspension of **24** (150 mg, 0.286 mmol) in Et_2O (10 mL) at 0 °C. The solution was stirred for 4 h at 0 °C and was then allowed to warm to room temperature and stirred for 24 h. The solution was filtered and then the solvent was removed *in vacuo* and the resulting yellow solid was extracted into hexane. Storage of this solution at room temperature for 1 day afforded yellow crystals of **25**; 25 mg, 8%. ^{1}H NMR (400 MHz, C_6D_6, 25 °C) δ = 12.36 (br s), 9.55 (br s), −4.53 (br s), −11.20 (br s), −11.30 (br s), −12.64 (br s), −17.05 (br s), −24.98 (br s), −50.65 (br s), −54.37 (br s) ppm. μ_{eff} (Evans' NMR Method, C_6D_6, 25 °C) = 3.61 μ_B. UV-vis (toluene) strong absorbance between 300 and 350 nm; shoulder at λ_{max} = 365 nm.

4.5.3 Mn(2,6-$Mes_2C_6H_3$)Br(tmeda) 26a

A solution of **2** (200 mg, 0.625 mmol) in Et_2O (20 mL) was added dropwise to a solution of $MnBr_2$ (134 mg, 0.625 mmol) in Et_2O (20 mL) at −78 °C. The solution was stirred at −78 °C for 2 h and was then warmed up to room temperature. TMEDA (0.09 mL, 0.625 mmol) was added to the solution and it was then stirred for 16 h at room temperature. The solution was filtered resulting in a colourless solution which was stored at −30 °C for

2 days, affording colourless crystals of **26a**; 103 mg, 29%. ^{1}H NMR (400 MHz, C_6D_6, 25 °C) δ = 10.66 (br s), 2.33 (br s) ppm. μ_{eff} (Evans' NMR Method, C_6D_6, 25 °C) = 3.66 μ_B. UV-vis (toluene) strong absorbance between 300 and 350 nm.

4.5.4 Fe(2,6-Mes$_2$C$_6$H$_3$)Cl(tmeda) 26b

A solution of **2** (200 mg, 0.625 mmol) in Et_2O (20 mL) was added dropwise to a solution of $FeCl_2$ (79 mg, 0.625 mmol) in Et_2O (20 mL) at −78 °C. The solution was stirred at −78 °C for 2 h and was then warmed up to room temperature. TMEDA (0.09 mL, 0.625 mmol) was added to the solution and it was then stirred for 16 h at room temperature. Filtration afforded a pale-yellow solution which was stored at −30 °C for 1 day affording colourless crystals of **26b**; 42 mg, 13%. ^{1}H NMR (400 MHz, C_6D_6, 25 °C) δ = 69.2 (br s), 50.9 (br s), 38.9 (br s), −0.52 (br s), −5.30 (s), −8.52 (s), −10.24 (s), −17.98 (s) ppm. μ_{eff} (Evans' NMR Method, C_6D_6, 25 °C) = 4.91 μ_B.

4.5.5 Co(2,6-Mes$_2$C$_6$H$_3$)Br(tmeda) 26c

A solution of **2** (200 mg, 0.625 mmol) in Et_2O (20 mL) was added dropwise to a solution of $CoBr_2$(DME) (193 mg, 0.625 mmol) in Et_2O (20 mL) at −78 °C. The solution was stirred at −78 °C for 2 h and was then warmed up to room temperature. TMEDA (0.09 mL, 0.625 mmol) was added to the solution and it was then stirred for 16 h at room temperature. The solution was filtered resulting in a blue solution which was stored at −30 °C for 3 days, which afforded blue crystals (**26c**: 25 mg, 7%) and colourless crystals (**27**: 75 mg).

26c: ^{1}H NMR (400 MHz, C_6D_6, 25 °C) δ = 65.82 (br s), 63.3 (br s), 2.24 (br s), 1.91 (br s), 0.28 (br s), −1.87 (br s), −3.15 (br s) ppm.

27: ^{1}H NMR (400 MHz, C_6D_6, 25 °C) δ = 2.21 (s, 24H, CH_3), 1.85 (s, 8H, CH_2) ppm. ^{13}C{^{1}H} NMR (101 MHz, C_6D_6, 25 °C) δ = 56.6 (CH_2), 46.8 (CH_3) ppm. ^{7}Li{^{1}H} (117 MHz, C_6D_6, 25 °C) δ = 2.02 (s) ppm.

4.5.6 Zn(2,6-$Mes_2C_6H_3$)Cl(tmeda) 26d

Method 1: A solution of **2** (200 mg, 0.625 mmol) in Et_2O (20 mL) was added dropwise to a solution of $ZnCl_2$ (85 mg, 0.625 mmol) in Et_2O (20 mL) at −78 °C. The solution was stirred at −78 °C for 2 h and was then warmed slowly to room temperature. TMEDA (0.09 mL, 0.625 mmol) was added to the solution and then stirred for 16 h. Filtration resulted in a colourless solution which was stored at −30 °C for 2 days, upon which colourless crystals precipitated. 120 mg, 36%.

Method 2: A solution of **2** (190 mg, 0.594 mmol) in Et_2O (10 mL) was added dropwise to a suspension of **28** (150 mg, 0.594 mmol) in Et_2O (10 mL) at 0 °C and then stirred at room temperature for 24 h. The reaction mixture was filtered resulting in a colourless solution which was stored at −30 °C for 4 days upon which colourless crystals precipitated. 125 mg, 40%.

^{1}H NMR (400 MHz, C_6D_6, 25 °C) δ = 7.31 (t, ^3J(H,H) = 7.5 Hz, 1H, *p*-H of C_6H_3), 6.97 (d, ^3J(H,H) = 7.5 Hz, 2H, *m*-H of C_6H_3), 6.89 (s, 4H, *m*-H of Mes), 2.41 (s, 12H, *o*-CH_3 of Mes), 2.23 (s, 6H, *p*-CH_3 of Mes), 1.75 (s br, 4H, CH_2 of TMEDA), 1.60 (s, 12H, CH_3 of TMEDA) ppm. ^{13}C{^{1}H} NMR (101 MHz, C_6D_6, 25 °C) δ = 155.4 (Ph^i of C_6H_3), 150.9 (*o*-*C*Mes of C_6H_3), 146.4 (*o*-*C*CH_3 of Mes), 137.6 (Ph^i of Mes), 135.8 (*p*-*C*CH_3 of Mes), 128.6 (*m*-*C*H of Mes), 127.9 (*m*-*C*H of C_6H_3), 127.1 (*p*-*C*H of C_6H_3), 57.6 (*C*H_2 of TMEDA), 46.9 (*C*H_3 of TMEDA), 22.2 (*o*-*C*H_3 of Mes), 21.1 (*p*-*C*H_3 of Mes) ppm.

4.5.7 $ZnCl_2$(tmeda) 28[62]

TMEDA (0.22 mL, 1.47 mmol) was added to a solution of $ZnCl_2$ (200 mg, 1.47 mmol) in THF (20 mL). The solvent was removed *in vacuo* and the resulting solid was extracted into THF. Colourless crystals formed in the solution at room temperature after 3 days. 283 mg, 76%. ^{1}H NMR (400 MHz, $CDCl_3$, 25 ºC) δ = 2.73 (s, 4H, CH_2), 2.60 (s, 12H, CH_3) ppm. ^{13}C{^{1}H} NMR (101 MHz, C_6D_6, 25 °C) δ = 57.0 (*C*H_2), 47.9 (*C*H_3) ppm. Characterisation matched literature data.[62]

4.5.8 Fe(2,6-$Mes_2C_6H_3$)Cl(dme) 29b

A solution of **2** (200 mg, 0.625 mmol) in Et_2O (20 mL) was added dropwise to a solution of $FeCl_2$ (79 mg, 0.625 mmol) in Et_2O (20 mL) at −78 °C. The solution was stirred at −78 °C for 2 h and then warmed up to room temperature. DME (0.06 mL, 0.625 mmol) was added to the solution and it was then stirred for 16 h at room temperature. The solution was filtered resulting in a pale yellow solution which was stored at −30 °C for 20 days upon which colourless crystals formed; 61 mg, 20%.

^{1}H NMR (400 MHz, C_6D_6, 25 °C) δ = 14.49 (br s), 4.02 (br s), 0.29 (s), −0.49 (br s), −2.68 (br s), −3.06 (br s), −7.93 (br s), −49.52 (br s). μ_{eff} (Evans' NMR Method, C_6D_6, 25 °C) = 3.12 μ_B. UV-vis (toluene) strong absorbance between 300 and 350 nm; shoulder at λ_{max} = 359 nm.

4.5.9 Zn(2,6-$Mes_2C_6H_3$)Cl(dme) 29d

A solution of **2** (200 mg, 0.625 mmol) in Et_2O (20 mL) was added dropwise to a solution of $ZnCl_2$ (85 mg, 0.625 mmol) in Et_2O (20 mL) at −78 °C. The solution was stirred at −78 °C for 2 h and was then warmed up to room temperature. DME (0.06 mL, 0.625 mmol) was added to the solution and it was then stirred for 16 h at room temperature. This was then filtered resulting in a colourless solution, which was stored at −30 °C for 1 day affording colourless crystals; 239 mg, 76%.

^{1}H NMR (400 MHz, C_6D_6, 25 °C) δ = 7.35 (t, ^3J(H,H) = 7.5 Hz, 1H, *p*-H of C_6H_3), 7.08 (d, ^3J(H,H) = 7.5 Hz, 2H, *m*-H of C_6H_3), 6.90 (s, 4H, *m*-H of Mes), 2.32 (s, 12H, *o*-CH_3 of Mes), 2.21 (s, 6H, *p*-CH_3 of Mes), 2.91 (s br, 4H, CH_2 of DME), 2.72 (s br, 6H, CH_3 of DME) ppm. ^{13}C{^{1}H} NMR (101 MHz, C_6D_6, 25 °C) δ = 150.2 (*o*-*C*Mes of C_6H_3), 144.8 (Ph^i of Mes), 136.7 (*o*-*C*CH_3 of Mes), 135.5 (*p*-*C*CH_3 of Mes), 128.4 (*m*-*C*H of Mes), 127.9 (*p*-*C*H of C_6H_3), 125.8 (*m*-*C*H of C_6H_3), 70.3 (*C*H_2 of DME), 59.1 (*C*H_3 of DME), 21.5 (*o*-*C*H_3 of Mes), 21.2 (*p*-*C*H_3 of Mes) ppm.

4.5.10 Synthesis of 30

A solution of **2** (200 mg, 0.625 mmol) in Et_2O (20 mL) was added dropwise to a solution of $CoBr_2$(DME) (193 mg, 0.625 mmol) in Et_2O (20 mL) at −78 °C; this was stirred at −78 °C for 2 h and was then warmed up to room temperature. DME (0.06 mL, 0.625 mmol) was added to the solution and it was then stirred for 16 h. The solution was filtered resulting in a dark blue solution; storage at −30 °C for 1 day afforded a small number of green crystals formed suitable for X-ray diffraction.

4.5.11 Reduction with KC_8

A suspension of KC_8 (13.1 mg, 0.097 mmol) in diethyl ether (10 mL) was added dropwise to a solution of **26a** (50 mg, 0.089 mmol) in diethyl ether (5 mL) at −30 °C and slowly allowed to warm to room temperature. After stirring at room temperature for 24 h the reaction mixture was filtered resulting in a colourless solution. Colourless crystals were grown from diffusion of hexane into a C_6D_6 solution over 1 month and were found to be **29** by X-ray crystallography.

4.5.12 Metathesis Reaction

$Na[N(SiMe_3)_2]$ (3.5 mg, 0.019 mmol) was added to a solution of **26d** (10 mg, 0.019 mmol) in C_6D_6 (0.6 mL). The reaction was monitored at room temperature by ^1H NMR spectroscopy. The formation of Zn(2,6-$Mes_2C_6H_3$)[$(N(SiMe_3)_2]$ (**32**) and $Zn[N(SiMe_3)_2]_2$ (**33**) was observed by ^1H, ^{13}C and ^{19}Si NMR spectroscopy.

32: ^1H NMR (400 MHz, C_6D_6, 25 ºC) δ = 7.29 (t, ^3J(H,H) = 7.6 Hz, 1H, *p*-H of C_6H_3), 7.05 (d, ^3J(H,H) = 7.5 Hz, 2H, *m*-H of C_6H_3), 6.88 (s, 4H, *m*-H of Mes), 2.20 (s, 6H, *p*-CH_3 of Mes), 2.16 (s, 12H, *o*-CH_3 of Mes), −0.04 (s, 18H, Si(CH_3)$_2$ ppm. $^{13}C\{^1H\}$ NMR (101 MHz, C_6D_6, 25 °C) δ = 150.1 (Ph^i of C_6H_3), 143.4 (Ph^i of Mes), 137.1 (*p*-CCH_3 of Mes), 135.6 (*o*-CCH_3 of Mes), 129.5 (*p*-CH of C_6H_3), 129.2 (*m*-CH of Mes), 126.2 (*m*-CH of C_6H_3), 21.3

(*o*-CH_3 of Mes), 21.1 (*p*-CH_3 of Mes), 4.7 (Si(CH_3)$_2$) ppm. ^{19}Si{^{1}H} (79.48 MHz, C_6D_6, 25 °C) δ = −1.9 ppm.

33: ^{1}H NMR (400 MHz, C_6D_6, 25 ºC) δ = 0.20 (s, 36H, Si(CH_3)$_2$ ppm. ^{13}C{^{1}H} NMR (101 MHz, C_6D_6, 25 °C) δ = 5.2 (Si(CH_3)$_2$) ppm.

4.5.13 Evans Method

Magnetic moments were calculated using Evans method at 298 K in C_6D_6.[66] The ^{1}H NMR spectra of the sample is measured in C_6D_6 containing an insert with a 1:1 ratio of C_6D_6:C_6H_6. There is a shift in the frequency of the solvent peaks in the two different environments. The measurements were carried out twice and the average value was used as the magnetic moment. The magnetic moments were calculated using the following equation:

$$X = \frac{3\Delta f}{4\pi f m} + X_0 + \frac{X_0(d_o - d_s)}{m}$$

where,

X = mass susceptibility

f = frequency of spectrometer

Δf = frequency separation between signals

m = mass of sample (in 1 mL solution)

X_0 = mass susceptibility of solvent

d_0 = density of solvent

d_s = density of solution

4.6 References

1 P. E. Goudriaan, P. W. N. M. Van Leeuwen, M. N. Birkholz and J. N. H. Reek, *Eur. J. Inorg. Chem.*, 2008, 2939–2958.

2 J. Meeuwissen, R. J. Detz, A. J. Sandee, B. De Bruin and J. N. H. Reek, *Dalton Trans.*, 2010, **39**, 1929–1931.

3 H. Imoto, M. Konishi, S. Nishiyama, H. Sasaki, S. Tanaka, T. Yumura and K. Naka, *Chem. Lett.*, 2019, **48**, 1312–1315.

4 C. M. Killian, L. K. Johnson and M. Brookhart, *Organometallics*, 1997, **16**, 2005–2007.

5 J. López-Serrano, S. B. Duckett, J. P. Dunne, C. Godard and A. C. Whitwood, *J. Chem. Soc., Dalton Trans.*, 2008, 4270–4281.

6 A. J. Martínez-Martínez, B. E. Tegner, A. I. McKay, A. J. Bukvic, N. H. Rees, G. J. Tizzard, S. J. Coles, M. R. Warren, S. A. Macgregor and A. S. Weller, *J. Am. Chem. Soc.*, 2018, **140**, 14958–14970.

7 M. Kranenburg, Y. E. M. van der Burgt, P. C. J. Kamer, P. W. N. M. van Leeuwen, K. Goubitz and J. Fraanje, *Organometallics*, 1995, **14**, 3081–3089.

8 P. W. N. M. Van Leeuwen, P. C. J. Kamer, J. N. H. Reek and P. Dierkes, *Chem. Rev.*, 2000, **100**, 2741–2769.

9 G. Zassinovich, G. Mestroni and S. Giadiali, *Chem. Rev.*, 1992, **92**, 1051–1069.

10 M. R. Friedfeld, H. Zhong, R. T. Ruck, M. Shevlin and P. J. Chirik, *Science*, 2018, **360**, 888–893.

11 M. K. Cybulski, J. E. Nicholls, J. P. Lowe, M. F. Mahon and M. K. Whittlesey, *Organometallics*, 2017, **36**, 2308–2316.

12 G. M. Lee, C. M. Vogels, A. Decken and S. A. Westcott, *Eur. J. Inorg. Chem.*, 2011, 2433–2438.

13 S. K. Murphy, A. Bruch and V. M. Dong, *Chem. Sci.*, 2015, **6**, 174–180.

14 S. M. Jing, V. Balasanthiran, V. Pagar, J. C. Gallucci and T. V. RajanBabu, *J. Am. Chem. Soc.*, 2017, **139**, 18034–18043.

15 A. Scarso, M. Colladon, P. Sgarbossa, C. Santo, R. A. Michelin and G. Strukul, *Organometallics*, 2010, **29**, 1487–1497.

16 A. B. Chaplin, J. F. Hooper, A. S. Weller and M. C. Willis, *J. Am. Chem. Soc.*, 2012, **134**, 4885–4897.

17 P. P. Wells, H. A. Sparkes, S. A. Davis, J. Callison, O. Hernandez-Fajardo, D. Elorriaga, E. K. Gibson, A. M. Messinis, R. B. Bedford, H. M. O'Brien, D. Gianolio and S. L. J. Luckham, *Nat. Catal.*, 2019, **2**, 123–133.

18 H. Shimizu, I. Nagasaki, K. Matsumura, N. Sayo and T. Saito, *Acc. Chem. Res.*, 2007, **40**, 1385–1393.

19 T. Ohkuma, H. Ooka, S. Hashiguchi, T. Ikariya and R. Noyori, *J. Am. Chem. Soc.*, 1995, **117**, 2675–2676.

20 A. Miyashita, A. Yasuda, H. Takaya, K. Toriumi, T. Ito, T. Souchi and R. Noyori, *J. Am. Chem. Soc.*, 1980, **102**, 7932–7934.

21 T. Saito, T. Yokozawa, T. Ishizaki, T. Moroi, N. Sayo, T. Miura and H. Kumobayashi, *Adv. Synth. Catal.*, 2001, **343**, 264–267.

22 T. Hashimoto, Y. Ohki and K. Tatsumi, *Inorg. Chem.*, 2010, **49**, 6102–6109.

23 E. J. Hawrelak, W. H. Bernskoetter, E. Lobkovsky, G. T. Yee, E. Bill and P. J. Chirik, *Inorg. Chem.*, 2005, **44**, 3103–3111.

24 D. Noda, Y. Sunada, T. Hatakeyama, M. Nakamura and H. Nagashima, *J. Am. Chem. Soc.*, 2009, **131**, 6078.

25 W. Seidel and K.-J. Lattermann, *Zeitschrift für Anorg. und Allg. Chemie*, 1982, **488**, 69–74.

26 T. Hatakeyama, Y. I. Fujiwara, Y. Okada, T. Itoh, T. Hashimoto, S. Kawamura, K. Ogata, H. Takaya and M. Nakamura, *Chem. Lett.*, 2011, **40**, 1030–1032.

27 S. L. Daifuku, J. L. Kneebone, B. E. R. Snyder and M. L. Neidig, *J. Am. Chem. Soc.*, 2015, **137**, 11432–11444.

28 S. L. Daifuku, M. H. Al-Afyouni, B. E. R. Snyder, J. L. Kneebone and M. L. Neidig, *J. Am. Chem. Soc.*, 2014, **136**, 9132–9143.

29 D. J. Mindiola and G. L. Hillhouse, *J. Am. Chem. Soc.*, 2001, **123**, 4623–4624.

30 R. Melenkivitz, D. J. Mindiola and G. L. Hillhouse, *J. Am. Chem. Soc.*, 2002, **124**, 3846–3847.

31 V. M. Iluc and G. L. Hillhouse, *J. Am. Chem. Soc.*, 2010, **132**, 11890–11892.

32 H. R. Sharpe, A. M. Geer, W. Lewis, A. J. Blake and D. L. Kays, *Angew. Chem. Int.*

Ed., 2017, **56**, 4845–4848.

33 H. R. Sharpe, A. M. Geer, H. E. L. Williams, T. J. Blundell, W. Lewis, A. J. Blake and D. L. Kays, *Chem. Commun.*, 2017, **53**, 937–940.

34 H. R. Sharpe, A. M. Geer, T. J. Blundell, F. R. Hastings, M. W. Fay, G. A. Rance, W. Lewis, A. J. Blake and D. L. Kays, *Catal. Sci. Technol.*, 2018, **8**, 229–235.

35 T. Nguyen, A. D. Sutton, M. Brynda, J. C. Fettinger, G. J. Long and P. P. Power, *Science*, 2005, **310**, 844–847.

36 Z. Zhu, R. J. Wright, M. M. Olmstead, E. Rivard, M. Brynda and P. P. Power, *Angew. Chem. Int. Ed.*, 2006, **45**, 5807–5810.

37 Z. Zhu, R. C. Fischer, J. C. Fettinger, E. Rivard, M. Brynda and P. P. Power, *J. Am. Chem. Soc.*, 2006, **128**, 15068–15069.

38 Z. Zhu, M. Brynda, R. J. Wright, R. C. Fischer, W. A. Merrill, E. Rivard, R. Wolf, J. C. Fettinger, M. M. Olmstead and P. P. Power, *J. Am. Chem. Soc.*, 2007, **129**, 10847–10857.

39 R. Wolf, C. Ni, T. Nguyen, M. Brynda, G. J. Long, A. D. Sutton, R. C. Fischer, J. C. Fettinger, M. Hellman, L. Pu and P. P. Power, *Inorg. Chem.*, 2007, **46**, 11277–11290.

40 R. Wolf, M. Brynda, C. Ni, G. J. Long and P. P. Power, *J. Am. Chem. Soc.*, 2007, **129**, 6076–6077.

41 B. M. Mattson and W. A. G. Graham, *Inorg. Chem.*, 1981, **20**, 3186–3189.

42 G. R. Willey, T. J. Woodman and M. G. B. Drew, *J. Organomet. Chem.*, 1996, **510**, 213–217.

43 N. R. Bunn, S. Aldridge, D. L. Kays, N. D. Coombs, A. Rossin, D. J. Willock, J. K. Day, C. Jones and L. L. Ooi, *Organometallics*, 2005, **24**, 5891–5900.

44 A. N. Marziale, E. Herdtweck, S. Schneider and J. Eppinger, *Inorg. Chem.*, 2009, **48**, 3699–3709.

45 S. Gatard, S. Kahlal, D. Méry, S. Nlate, E. Cloutet, J. Y. Saillard and D. Astruc, *Organometallics*, 2004, **23**, 1313–1324.

46 P. Romero, M. Valderrama, R. Contreras and D. Boys, *J. Organomet. Chem.*, 2003,

673, 102–110.

47 I. Krossing, *Chem. Eur. J.*, 2001, **7**, 490–502.

48 A. Kraft, J. Beck and I. Krossing, *Chem. Eur. J.*, 2011, **17**, 12975–12980.

49 P. Sobota, J. Utko, S. Szafert, Z. Janis and T. Glowiak, *Dalton Trans.*, 1996, 3469–347370.

50 M. W. Bezpalko, B. M. Foxman and C. M. Thomas, *Inorg. Chem.*, 2015, **54**, 8717–8726.

51 O. Buttler, A. Al-Fawaz, D. L. Kays, J. K. Day, L. L. Ooi and S. Aldridge, *Zeitschrift fur Anorg. und Allg. Chemie*, 2006, **632**, 2187–2189.

52 B. Cordero, V. Gómez, A. E. Platero-Prats, M. Revés, J. Echeverría, E. Cremades, F. Barragán and S. Alvarez, *Dalton Trans.*, 2008, 2832–2838.

53 R. Langer, F. Bönisch, L. Maser, C. Pietzonka, L. Vondung and T. P. Zimmermann, *Eur. J. Inorg. Chem.*, 2015, **2015**, 141–148.

54 C. Ni, J. C. Fettinger, G. J. Long and P. P. Power, *Dalton Trans.*, 2010, **39**, 10664–10670.

55 B. M. Gridley, T. J. Blundell, G. J. Moxey, W. Lewis, A. J. Blake and D. L. Kays, *Chem. Commun.*, 2013, **49**, 9752–9754.

56 D. Patel, A. Wooles, A. D. Cornish, L. Steven, E. S. Davies, D. J. Evans, J. McMaster, W. Lewis, A. J. Blake and S. T. Liddle, *Dalton Trans.*, 2015, **44**, 14159–14177.

57 M. Di Vaira, S. Midollini and L. Sacconi, *Inorg. Chem.*, 1981, **20**, 3430–3435.

58 A. D. Sutton, T. Ngyuen, J. C. Fettinger, M. M. Olmstead, G. J. Long and P. P. Power, *Inorg. Chem.*, 2007, **46**, 4809–4814.

59 D. L. Kays and A. R. Cowley, *Chem. Commun.*, 2007, 1053–1055.

60 A. Schröder, E. Lork and J. Beckmann, *Main Group Met. Chem.*, 2014, **37**, 155–157.

61 S. C. Davies, D. L. Hughes, J. Leigh, J. R. Sanders and J. S. De Souza, *Dalton Trans.*, 1997, 1981–1988.

62 F. Mongin, N. T. T. Chau, M. Uchiyama, Y. Fort, F. Chevallier, P. C. Gros, S. Komagawa and M. Meyer, *Chem. Eur. J.*, 2010, **16**, 12425–12433.

63 N. J. Hardman, B. Twamley, M. Stender, R. Baldwin, S. Hino, B. Schiemenz, S. M. Kauzlarich and P. P. Power, *J. Organometalic Chem.*, 2002, **643**–**644**, 461–467.

64 B. E. Eichler and P. P. Power, *Inorg. Chem.*, 2000, **39**, 5444–5449.

65 C. Ni and P. P. Power, *Chem. Commun.*, 2009, 5543–5545.

66 D. F. Evans, *J. Chem. Soc.*, 1959, 2003–2005.

67 J. Heck, W. Massa and P. Weinig, *Angew. Chem. Int. Ed.*, 1984, **23**, 722–723.

68 R. Neufeld, T. L. Teuteberg, R. Herbst-Irmer, R. A. Mata and D. Stalke, *J. Am. Chem. Soc.*, 2016, **138**, 4796–4806.

69 R. M. Peltzer, O. Eisenstein, A. Nova and M. Cascella, *J. Phys. Chem. B*, 2017, **121**, 4226–4237.

70 C. Ni, T. A. Stich, G. J. Long and P. P. Power, *Chem. Commun.*, 2010, **46**, 4466–4468.

71 D. Y. Lee and J. F. Hartwig, *Org. Lett.*, 2005, **7**, 1169–1172.

72 D. Rivillo, H. Gulyás, J. Benet-Buchholz, E. C. Escudero-Adán, Z. Freixa and P. W. N. M. Van Leeuwen, *Angew. Chem. Int. Ed.*, 2007, **46**, 7247–7250.

Chapter 5

Global Conclusions

5.1 Global Conclusions

The aim of this thesis was to expand the knowledge around the use of diaryl *m*-terphenyl complexes as precatalysts for hydroelementation reactions. The diaryl *m*-terphenyl complexes M(2,6-$Mes_2C_6H_3)_2$ (M = Fe (**3**), Co (**4**), Zn (**5**)) are precatalysts for a range of hydroamination, hydrophosphination and hydroboration reactions. Fe(2,6-$Mes_2C_6H_3)_2$ was shown to be the most efficient catalyst, with longer reaction times needed for **4** and **5** for the hydroamination and hydroboration of isocyanates compared to **3**.

The hydroamination of isocyanates using precatalyst **3** demonstrated similar reactivity to the previously reported hydrophosphination of isocyanates[1] with the diinsertion of the aromatic isocyanates leading to the formation of biurets. This is the first reported example of the direct transformation of amines to biurets. This was extended even further to the tri- and tetrainsertion of the isocyanate with diisopropylamine to synthesise molecules with multiple urea moieties which have a high capacity for hydrogen bonding and applications in self-assembly. It was possible to tune the selectivity of the reaction through altering the reaction conditions. An excess of the isocyanate favoured the multiple insertions of the isocyanate whereas the use of THF as the solvent favoured the selective formation of the urea. Although **3** was found to not act as a precatalyst for the hydroamination of carbodiimides it was successful for the hydrophosphination of carbodiimides although there was little evidence for the diinsertion of the carbodiimide. This was attributed to the added steric bulk of carbodiimides compared to isocyanates.

The promising activity of these precatalysts was expanded to the hydroboration of isocyanates which has not been well explored in the literature. These are the first examples of transition metal catalysts for this reaction. The monohydroboration product was selectively formed. Even an addition of excess borane did not promote the dihydroboration which is in contrast to the other reported catalysts in the literature and demonstrates the selectivity of **3**. The hydroboration of carbodiimides is also catalysed by **3** and the

monohydroboration product is exclusively formed which may be due to the lower reactivity of the monohydroboration product compared to the carbodiimide so the second hydroboration does not occur.

These investigations demonstrate the versatility of *m*-terphenyl diaryl complexes as catalysts. Although the nature of the active species was not determined initial steps into the exploration of the mechanism were undertaken. Poisoning experiments revealed that the catalysis presented in this thesis is homogeneous and not radical catalysed. Stoichiometric NMR studies revealed the formation of a new iron species which is likely the active catalyst, although all attempts to isolate this species were unsuccessful. A kinetic investigation into these reactions would provide further insight into the mechanism of the catalysis.

A series of four coordinate complexes containing an *m*-terphenyl ligand, a bidentate ligand and a halide of the form M(2,6-$Mes_2C_6H_3$)X(LL) (M = Mn, Fe, Co or Zn; LL = bidentate ligand; X = Cl or Br) were reported. The three bidentate ligands utilised were DPPE, TMEDA and DME. The only *m*-terphenyl complex with DPPE that was able to be synthesised was the Fe(II) complex Fe(2,6-$Mes_2C_6H_3$)Cl(dppe). Attempts to synthesise analogous Mn and Zn complexes were unsuccessful and resulted in either the formation of the polymer $[ZnCl_2(dppe)]_n$ (**23**) or the free diphosphine ligand. These issues could be overcome with the use of a less sterically hindered diphosphine such as DMPE which contains methyl groups instead of phenyl groups and so may be more able to coordinate to the metal centre.

The attempted reduction of Mn(2,6-$Mes_2C_6H_3$)Br(tmeda) using KC_8 afforded $[MnBr(\mu\text{-}Br)(tmeda)]_2$ as the only crystalline product. The reaction between Zn(2,6-$Mes_2C_6H_3$)Cl(tmeda) and Na[$N(SiMe_3)_2$] formed the two-coordinate complex Zn(2,6-$Mes_2C_6H_3$)[$N(SiMe_3)_2$] with concomitant loss of coordinated TMEDA.

This work has undertaken some preliminary efforts to explore the reactivity of these complexes. This proposed three-coordinate complex containing a bidentate ligand and an

m-terphenyl ligand would have potential applications as catalysts due to its unsaturated metal centre. Future work should focus on the exploration of this reactivity with different reducing agents and halide abstraction agents. The use of cyclic voltammetry would aid the selection of a suitable reducing agent.

5.2 References

1 H. R. Sharpe, A. M. Geer, W. Lewis, A. J. Blake and D. L. Kays, *Angew. Chem. Int. Ed.*, 2017, **56**, 4845–4848.

Chapter 6

General Experimental

6.1 General Experimental Procedures

6.1.1 Manipulation of Air Sensitive Compounds

All manipulations were performed in strict anaerobic and anhydrous conditions using standard Schlenk line and glovebox techniques under an atmosphere of nitrogen or argon unless stated otherwise.

6.1.2 Preparation of Solvents and Reagents

Solvents were dried by refluxing over molten potassium (toluene), sodium/benzophenone (THF), calcium hydride (dichloromethane, TMEDA, dimethoxyethane) or sodium potassium alloy (diethyl ether) for a minimum of three days and *iso*–hexane was dried by passage over a drying column with 4 Å molecular sieves. All solvents were stored in ampoules over a potassium mirror (toluene, diethyl ether and *iso*-hexane) or 4 Å molecular sieves (THF, dichloromethane, TMEDA and dimethoxyethane). All solvents were degassed *in vacuo* before use. Benzene–d_6 was dried over molten potassium and degassed with three freeze–pump–thaw cycles prior to use. KC_8 was synthesised following literature procedures.[1] Diphenylamine was sublimed before use. Isocyanates were transferred to the glovebox and molecular sieves were added before use. All other reagents were used as received unless stated otherwise.

6.2 Physical Measurements

6.2.1 NMR Spectroscopy

All NMR spectroscopy was carried out on Bruker DPX300, AV400, AV(III)400, or AV(III)600 spectrometers. Chemical shifts are quoted in parts per million relative to TMS for ^{1}H, $^{13}C\{^{1}H\}$ and $^{29}Si\{^{1}H\}$, LiCl/D_2O solution for $^{7}Li\{^{1}H\}$, $BF_3{\cdot}OEt_2$ for ^{11}B, H_3PO_4 for ^{31}P and $CFCl_3$ for ^{19}F.

6.2.2 DOSY

DOSY experiments were carried out on an AV(III)600 NMR spectrometer. The intensity (I) of a peak in a ^{1}H NMR spectrum is proportional to:

$$e^{-[(\gamma g\delta)^2 D\left(\Delta-\frac{\delta}{3}\right)]}$$

where,

γ = gyromagnetic ratio

g = gradient strength

δ = diffusion gradient pulse length

D = diffusion coefficient

Δ = diffusion delay

The DOSY experiment was measured by varying values of g along 16 spectra. The intensity of each peak was used to plot ln(I) against g^2 from each of the spectra which gives a straight line. The diffusion coefficient can be obtained from the gradient of this line.

6.2.3 Mass Spectrometry

Mass spectrometry measurements for air stable compounds were carried out with the University of Nottingham open access service on a Bruker MicroToF II spectrometer. Air sensitive samples were sealed in glass capillary tubes under an inert atmosphere and were carried out either by Mr Ben Pointer-Gleadhill at the University of Nottingham using a Bruker Impact II spectrometer or at the EPSRC National Mass Spectrometry Facility (Swansea University, UK) using a Finnigan MAT 95 XP or a Thermo ScientificLTQ Orbitrap XL spectrometer.

6.2.4 Infrared Spectroscopy

Infrared spectroscopy was carried out on a Bruker ALPHA FTIR spectrometer. Air sensitive samples were prepared under an inert atmosphere in a solution cell with KBr windows.

6.2.5 UV-Vis Spectroscopy

Sample solutions were prepared under an inert atmosphere in a glovebox. All UV-Vis spectra were acquired on a Perkin Elmer Lambda 16 spectrophotometer in a Young's tap 10 mm quartz cell.

6.2.6 X-Ray Crystallography

Under a flow of nitrogen, crystals suitable for analysis by X-ray diffraction were quickly removed from the crystallisation vessel and mounted on a MiTeGen MicroMount™ with YR-1800 perfluoropolyether oil and cooled rapidly in a cold stream of nitrogen using an Oxford Cryosystems open flow cryostat at 120 K. Single crystal X-ray diffraction data were collected on an Agilent SuperNova diffractometer (mirrormonochromated Cu-Kα radiation source; λ = 1.54184 Å; ω scans), equipped with either an Atlas, AtlasS2 or TitanS2 detector. Cell parameters were refined from the observed positions of all strong reflections in each data set and absorption corrections were applied using a Gaussian numerical method with beam profile correction (CrysAlisPro[2]). The structures were solved by direct methods and all non-hydrogen atoms refined by full-matrix least-squares on all unique F^2 values with anisotropic displacement parameters. Hydrogen atoms were refined with constrained geometries and riding thermal parameters. Platon SQUEEZE[3] was used for **30** to account for the scattering from highly disordered solvent molecules that could not be sensibly modelled. Programs used include CrysAlisPro[2] (control and integration of Supernova), Platon[3] (SQUEEZE), SHELXS[4] (structure solution), SHELXT[5] (structure solution), SHELXL[6] (structure refinement) and OLEX2[7] (molecular graphics). CIF files were checked using checkCIF.[8]

6.3 References

1 H. Podall, W. E. Foster and A. P. Giraitis, *J. Org. Chem.*, 1958, **23**, 82–85.

2 CrysAlisPRO Oxford Diffraction/Agilent Technologies UK Ltd Yarnton England.

3 A. L. Spek, *Acta Crystallogr. Sect. D Biol. Crystallogr.*, 2009, **65**, 148–155.

4 G. M. Sheldrick, *Acta Crystallogr. Sect. A Found. Crystallogr.*, 2008, **64**, 112–122.

5 G. M. Sheldrick, *Acta Crystallogr. Sect. A Found. Crystallogr.*, 2015, **71**, 3–8.

6 G. M. Sheldrick, *Acta Crystallogr. Sect. C Struct. Chem.*, 2015, **71**, 3–8.

7 O. V. Dolomanov, L. J. Bourhis, R. J. Gildea, J. A. K. Howard and H. Puschmann, *J. Appl. Crystallogr.*, 2009, **42**, 339–341.

8 http://checkcif.iucr.org/.

Appendices

Crystallographic Data

	10	**15a**
Identification code	OAJSLA	OAJSLD
Empirical formula	$C_{27}H_{21}N_3O_3$	$C_{13}H_{18}BNO_3$
M_W	435.47	247.09
T (K)	120(2)	120(2)
Crystal system	monoclinic	monoclinic
Space group	C2/c	$P2_1/n$
a (Å)	13.48880(10)	13.9215(3)
b (Å)	13.53150(10)	6.18243(12)
c (Å)	12.61320(10)	16.4441(4)
α (°)	90	90
β (°)	97.3240(10)	110.727(3)
γ (°)	90	90
V (Å^3)	2283.42(3)	1323.72(6)
Z	4	4
D_{calc} (g/cm^3)	1.267	1.240
μ (mm^{-1})	0.678	0.697
F_{000}	912.0	528.0
Crystal size/mm^3	0.631 × 0.502 × 0.27	0.469 × 0.303 × 0.154
λ (Å)	1.54184	1.54184
2θ range for data collection (°)	9.296 to 153.852	7.176 to 146.986
Reflections collected	20927	5363
Independent reflections	2387	2607
R_{int}	0.0239	0.0198
Final GooF	1.144	1.052
R_1, wR_2 [$I>=2\sigma(I)$]	0.0497, 0.1258	0.0348, 0.0840
R_1, wR_2 [all data]	0.0498, 0.1260	0.0389, 0.0874
Min. and max. electron densities (e Å^{-3})	0.31/-0.60	0.25/-0.21

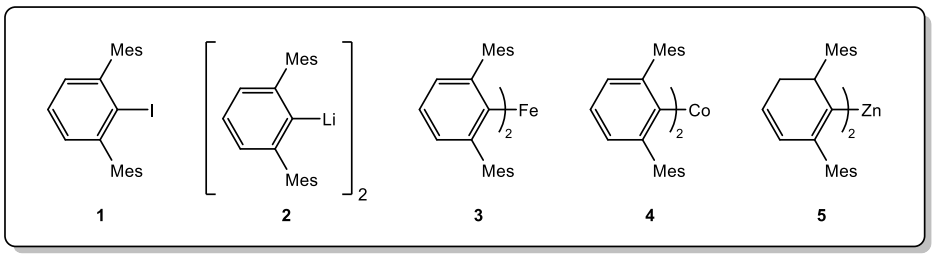
	15g	**17**	**18**
Identification code	OAJSLI	OAJSLL	OAJSLE
Empirical formula	$C_{20}H_{38}B_2N_2O_6$	$C_{18}H_{36}B_2O_6$	$C_{38}H_{29}N_5O_4$
M_W	424.14	370.09	619.66
T (K)	120(2)	120(2)	120(2)
Crystal system	triclinic	monoclinic	triclinic
Space group	P-1	$P2_1/c$	P-1
a (Å)	6.0033(4)	10.5855(3)	11.514(2)
b (Å)	8.3770(5)	10.4037(2)	12.228(2)
c (Å)	12.2109(12)	10.7788(3)	12.288(2)
α (°)	99.232(6)	90	86.344(15)
β (°)	98.584(7)	118.654(3)	62.58(2)
γ (°)	98.782(5)	90	80.578(16)
V (Å^3)	589.44(8)	1041.67(5)	1514.9(6)
Z	1	2	2
D_{calc} (g/cm^3)	1.195	1.180	1.359
μ (mm^{-1})	0.691	0.681	0.728
F_{000}	230.0	404.0	648.0
Crystal size/mm^3	0.249 × 0.082 × 0.061	0.29 × 0.105 × 0.092	0.157 × 0.083 × 0.039
λ (Å)	1.54184	1.54184	1.54184
2θ range for data collection (°)	7.454 to 102.572	9.522 to 144.668	7.328 to 146.622
Reflections collected	4798	26040	9420
Independent reflections	1268	2056	5010
R_{int}	0.0177	0.0356	0.1659
Final GooF	1.072	1.047	1.033
R_1, wR_2 [$I>=2\sigma(I)$]	0.0331, 0.0794	0.0369, 0.1020	0.1307, 0.2845
R_1, wR_2 [all data]	0.0352, 0.0814	0.0381, 0.1033	0.2212, 0.3416
Min. and max. electron densities (e Å^{-3})	0.19/-0.18	0.30/-0.25	0.37/-0.43

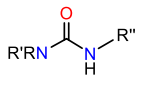
	19	**21**	**23**
Identification code	OAJSLJ	AJSDKN	ZNAJSB
Empirical formula	$C_{60}H_{76}B_2FeN_4O_{16}$	$C_{12}H_{24}B_2O_5$	$C_{26}H_{24}Br_{0.83}Cl_{1.17}P_2Zn$
M_W	1186.71	269.93	571.56
T (K)	120(2)	120(2)	120(2)
Crystal system	monoclinic	monoclinic	monoclinic
Space group	$P2_1/c$	$P2_1/n$	$P2_1/n$
a (Å)	11.58500(10)	6.39980(10)	12.9306(4)
b (Å)	13.2401(2)	20.7501(3)	11.5291(4)
c (Å)	20.6147(3)	11.5743(2)	16.8287(6)
α (°)	90	90	90
β (°)	106.294(2)	94.7830(10)	99.428(3)
γ (°)	90	90	90
V (Å^3)	3035.01(7)	1531.67(4)	2474.91(14)
Z	2	4	4
D_{calc} (g/cm^3)	1.299	1.171	1.534
μ (mm^{-1})	2.575	0.704	5.414
F_{000}	1256.0	584.0	1156.0
Crystal size/mm^3	0.173 × 0.136 × 0.085	0.262 × 0.109 × 0.108	0.154 × 0.093 × 0.051
λ (Å)	1.54184	1.54184	λ = 1.54184
2θ range for data collection (°)	7.95 to 145.596	8.522 to 145.9	8.02 to 149.066
Reflections collected	19910	11567	13320
Independent reflections	5875	2993	4915
R_{int}	0.0211	0.0196	0.0257
Final GooF	1.045	1.063	1.171
R_1, wR_2 [$I>=2\sigma(I)$]	0.0310, 0.0827	0.0468, 0.1274	0.0356, 0.0788
R_1, wR_2 [all data]	0.0341, 0.0848	0.0522, 0.1326	0.0401, 0.0808
Min. and max. electron densities (e Å^{-3})	0.34/-0.33	0.30/-0.21	0.41/-0.34

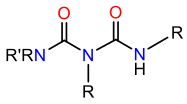
	25	**26a**	**26b**
Identification code	FEAJSC	MNAJSA	FEAJSB
Empirical formula	$C_{50}H_{49}Br_{0.46}Cl_{0.54}FeP_2$	$C_{30}H_{41}BrMnN_2$	$C_{30}H_{41}Br_{0.46}Cl_{0.54}FeN_2$
M_W	820.62	564.50	541.51
T (K)	120(2)	120(2)	120(2)
Crystal system	triclinic	monoclinic	monoclinic
Space group	P-1	$P2_1/n$	$P2_1/n$
a (Å)	11.6387(5)	8.4409(4)	8.44070(10)
b (Å)	12.2509(4)	30.8979(16)	30.7994(5)
c (Å)	17.1728(5)	10.9499(6)	10.8630(2)
α (°)	102.192(3)	90	90
β (°)	101.771(3)	94.196(5)	94.595(2)
γ (°)	112.090(4)	90	90
V (Å^3)	2106.28(14)	2848.1(2)	2814.96(8)
Z	2	4	4
D_{calc} (g/cm^3)	1.294	1.316	1.278
μ (mm^{-1})	4.698	5.543	5.667
F_{000}	856.0	1180.0	1145.0
Crystal size/mm^3	0.363 × 0.148 × 0.134	0.195 × 0.035 × 0.033	0.354 × 0.079 × 0.059
λ (Å)	1.54184	1.54184	1.54184
2θ range for data collection (°)	8.214 to 144.758	8.588 to 145.344	8.656 to 145.88
Reflections collected	21826	22339	21338
Independent reflections	8129	5616	5526
R_{int}	0.0345	0.0642	0.0391
Final GooF	1.060	1.042	1.142
R_1, wR_2 [$I>=2\sigma(I)$]	0.0406, 0.0940	0.0482, 0.1188	0.0484, 0.1022
R_1, wR_2 [all data]	0.0467, 0.0977	0.0608, 0.1287	0.0537, 0.1045
Min. and max. electron densities (e Å^{-3})	0.62/-0.34	0.64/-0.76	0.73/-0.37

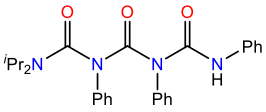
	26c	**26d**	**28**
Identification code	COAJSA	ZNAJSC	ZNAJSA
Empirical formula	$C_{30}H_{41}BrCoN_2$	$C_{30}H_{41}ClN_2Zn$	$C_6H_{16}Cl_2N_2Zn$
M_W	568.49	530.47	252.48
T (K)	120(2)	120(2)	120(2)
Crystal system	triclinic	monoclinic	monoclinic
Space group	P-1	$P2_1/n$	$P2_1/c$
a (Å)	8.1111(4)	10.7081(2)	7.5944(2)
b (Å)	10.8427(7)	24.8304(5)	13.2502(3)
c (Å)	17.2005(11)	10.9003(3)	11.3198(3)
α (°)	74.638(6)	90	90
β (°)	83.180(5)	101.475(2)	103.759(3)
γ (°)	73.094(5)	90	90
V (Å^3)	1394.21(16)	2840.31(11)	1106.39(5)
Z	2	4	4
D_{calc} (g/cm^3)	1.354	1.241	1.516
μ (mm^{-1})	6.637	2.197	7.110
F_{000}	594.0	1128.0	520.0
Crystal size/mm^3	0.198 × 0.138 × 0.104	0.452 × 0.228 × 0.155	0.507 × 0.437 × 0.102
λ (Å)	1.54184	1.54184	1.54184
2θ range for data collection (°)	8.786 to 144.768	7.12 to 146.84	10.456 to 145.448
Reflections collected	12847	42913	11938
Independent reflections	5363	5664	2161
R_{int}	0.0410	0.0318	0.0926
Final GooF	1.081	1.045	1.084
R_1, wR_2 [$I>=2\sigma(I)$]	0.0373, 0.0966	0.0468, 0.1139	0.0393, 0.1055
R_1, wR_2 [all data]	0.0404, 0.1009	0.0505, 0.1170	0.0400, 0.1065
Min. and max. electron densities (e Å^{-3})	0.89/-0.71	1.73/-0.85	0.73/-0.53

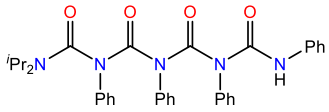
	29b	**30**	**31**
Identification code	FEAJSD	COAJSB	MNAJSE
Empirical formula	$C_{28}H_{32}ClFeO_2$	$C_{54}H_{64}BrCoLiO_4$	$C_{12}H_{32}N_4Mn_2Br_4$
M_W	491.83	922.83	661.93
T (K)	120(2)	120(2)	120(2)
Crystal system	triclinic	tetragonal	monoclinic
Space group	P-1	I-4	$P2_1/n$
a (Å)	13.2798(10)	31.5040(2)	10.42060(10)
b (Å)	14.5250(12)	31.5040(2)	15.4875(2)
c (Å)	15.4432(14)	10.38910(10)	14.4437(2)
α (°)	65.875(9)	90	90
β (°)	72.661(7)	90	92.3990(10)
γ (°)	78.267(7)	90	90
V (Å^3)	2583.7(4)	10311.20(16)	2329.01(5)
Z	4	8	4
D_{calc} (g/cm^3)	1.264	1.189	1.888
μ (mm^{-1})	5.788	3.826	16.864
F_{000}	1036.0	3880.0	1288.0
Crystal size/mm^3	0.745 × 0.313 × 0.201	0.226 × 0.121 × 0.108	0.237 × 0.167 × 0.054
λ (Å)	1.54184	1.54184	1.54184
2θ range for data collection (°)	6.698 to 146.242	7.938 to 144.99	8.374 to 145.748
Reflections collected	26417	46482	9477
Independent reflections	26417	10045	4521
R_{int}	0	0.0311	0.0296
Final GooF	1.041	1.041	1.021
R_1, wR_2 [$I>=2\sigma(I)$]	0.1638, 0.4215	0.0230, 0.0592	0.0368, 0.0942
R_1, wR_2 [all data]	0.2181, 0.4599	0.0238, 0.0599	0.0401, 0.0969
Min. and max. electron densities (e Å^{-3})	2.77/-1.58	0.43/-0.14	1.73/-1.14

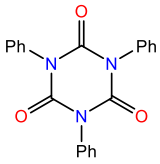

Mes
I
Mes
1
Mes
Li
Mes
2
Mes
Fe
2
Mes
3
Mes
Co
2
Mes
4
Mes
Zn
2
Mes
5

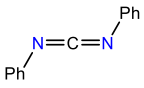

R'RN
R''
6

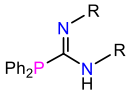

R'RN
R
7

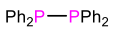

iPr2N
Ph
8g

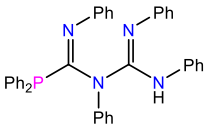

iPr2N
Ph
9g

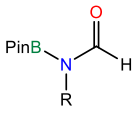

Ph
Ph
Ph
10

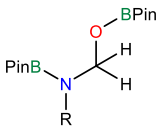

Ph
Ph
11c

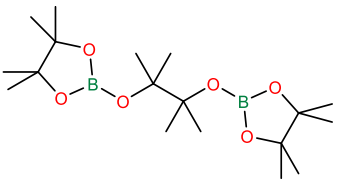

R
Ph2P
R
12

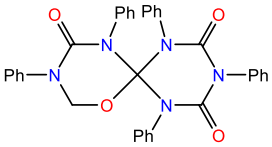

Ph2P—PPh2
13

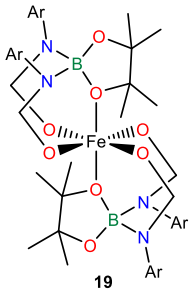

Ph
Ph
Ph2P
Ph
14c

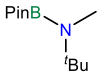

PinB
R
15

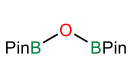

BPin
PinB
R
16

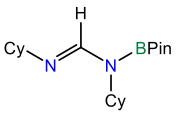

17

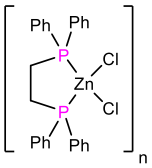

Ph
Ph
Ph
Ph
18

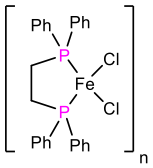

Ar
Fe
Ar
19

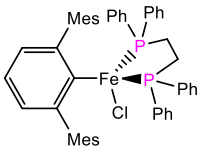

PinB
tBu
20

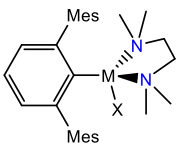

PinB
BPin
21

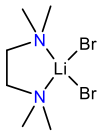

Cy
BPin
Cy
22


Ph
Ph
Zn
Cl
Cl
Ph
Ph
n
23

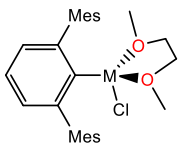

Ph
Ph
Fe
Cl
Cl
Ph
Ph
n
24

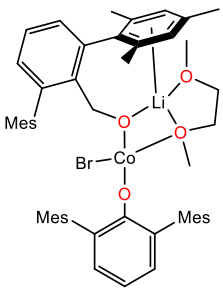

Mes
Ph
Ph
Fe
Cl
Ph
Ph
Mes
25

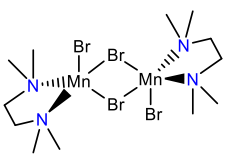

Mes
M
X
Mes
26

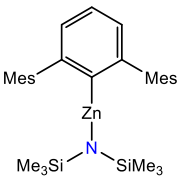

Br
Li
Br
27

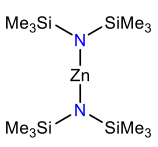

Cl
Zn
Cl
28


Mes
M
Cl
Mes
29


Mes
Li
Br
Co
Mes
Mes
30


Br
Br
Mn
Mn
Br
Br
31


Mes
Mes
Zn
Me3Si
SiMe3
32


Me3Si
SiMe3
Zn
Me3Si
SiMe3
33